



Kent Academic Repository

Sampson, Connor Dereck David (2021) *Examining the Ligand Binding, Transport Cycle, and Lipid Interactions of the DASS Family Secondary Active Transporter, VcINDY*. Doctor of Philosophy (PhD) thesis, University of Kent,.

Downloaded from

<https://kar.kent.ac.uk/88951/> The University of Kent's Academic Repository KAR

The version of record is available from

<https://doi.org/10.22024/UniKent/01.02.88951>

This document version

UNSPECIFIED

DOI for this version

Licence for this version

CC BY-NC (Attribution-NonCommercial)

Additional information

Versions of research works

Versions of Record

If this version is the version of record, it is the same as the published version available on the publisher's web site. Cite as the published version.

Author Accepted Manuscripts

If this document is identified as the Author Accepted Manuscript it is the version after peer review but before type setting, copy editing or publisher branding. Cite as Surname, Initial. (Year) 'Title of article'. To be published in *Title of Journal*, Volume and issue numbers [peer-reviewed accepted version]. Available at: DOI or URL (Accessed: date).

Enquiries

If you have questions about this document contact ResearchSupport@kent.ac.uk. Please include the URL of the record in KAR. If you believe that your, or a third party's rights have been compromised through this document please see our [Take Down policy](https://www.kent.ac.uk/guides/kar-the-kent-academic-repository#policies) (available from <https://www.kent.ac.uk/guides/kar-the-kent-academic-repository#policies>).

**Examining the Ligand Binding, Transport Cycle,
and Lipid Interactions of the DASS Family
Secondary Active Transporter, VcINDY**

Connor Sampson

University of Kent, School of Biosciences

A thesis submitted to the University of Kent for the degree of Doctor of

Philosophy

October 2020

Summary

The rising prevalence of obesity and type 2 diabetes, fuelled by an increase in human life expectancy, places a major burden upon modern healthcare systems. It has been found that these conditions can be effectively prevented in mice by the knockout of a single transport protein, named mINDY. It is therefore hoped that targeting mINDY in humans will have similar effects, providing a solution to this modern health crisis.

mINDY is a member of the Divalent Anion/Na⁺ Symporter (DASS) protein family, and despite their promise as future drug targets, very little is known about their molecular mechanisms. In order to better understand the molecular principles behind the function of these transporters, we examined the bacterial family member known as VcINDY from *Vibrio cholerae*. VcINDY is the best characterised member of the DASS family and shares structural and functional features with the pharmacologically-relevant human homologues, therefore making it an excellent model to probe the underlying mechanistic principles of the wider DASS family.

We applied a range of biochemical and biophysical techniques to the study of VcINDY's substrate interactions and transport cycle in order to build a more complete picture of how the DASS family achieves controlled substrate transport. This resulted in a range of novel findings. Previously unobserved intermediate transport states were uncovered through the use of single residue accessibility assays, whereby the binding of VcINDY's substrates, sodium and succinate, to the transporter each resulted in distinct conformational changes. Clear principles of both cation and anion selectivity, along with a clear order of binding, were established through the use of high throughput thermostability screening. During the course of this high throughput thermostability screening, several new and unexpected small molecule interactors were identified, which may prove useful in future DASS family inhibitor design. Binding affinities for both sodium and succinate were also established for the first time through the use of thermophoresis based binding assays.

The effect of lipids upon VcINDY were also examined through a range of approaches. Aggregation based thermostability measurements demonstrated for the first time not only that VcINDY preferentially interacts with certain lipids, but that the lipid interactions of VcINDY are radically altered in the presence of substrate. This suggests that lipids may play a complex, dynamic, role in the transport cycle of DASS family transporters. In order to further examine the relationship between VcINDY and lipids, methods for the reconstitution of VcINDY into two distinct nanodisc systems were developed; a Membrane Scaffold Protein based nanodisc, and a polymer based native lipid nanodisc, allowing *in vitro* testing of this membrane protein within a lipid environment.

The work presented in this thesis has allowed the creation of a new, far more detailed, mechanistic model for ligand binding and transport by the DASS family, in addition to developing new tools and techniques that will pave the way for further insights in the future.

Acknowledgements

I would like to thank my PhD supervisor, Christopher Mulligan, for providing me with the opportunity to begin this PhD, and the support required to complete it. I would also like to thank all Mulligan Lab members, past and present, for their help and support with this project; in particular Matthew Stewart (aka The Protein Factory), for the batches of generously grown VcINDY he provided me with throughout the course of this project.

Beyond the Mulligan Lab there are many others who deserve acknowledgement. I would like to thank the Colin Robinson Group, who have shown great generosity throughout the years, providing us with equipment, sharing vital facilities such as their HPLC SEC system, and allowing me to use many of their reagents.

I also would like to thank Jose Ortega-Roldan along with his entire lab group for their support, frequent loans of reagents, borrowed equipment, valuable insights, and unwavering friendliness. In particular I would like to thank Alexandra Hendry for the discussion she provided on SMALP purification early in this project.

I would additionally like to thank the Goult Lab for allowing me to use their MST machine and providing training on how to use this key piece of equipment, along with the Kent Fungal Group (KFG) for the repeated loan of their bead-homogeniser and their fluorescent plate readers.

Furthermore, I thank the entire University of Kent School of Biosciences, as I believe there are very few labs within the department which I did not borrow something from. The submission of this thesis marks the end of my seven years within the department, entering as a mere undergraduate student, and soon leaving as a Doctor of Philosophy. I shall miss you all greatly.

Beyond the academic world, I thank my parents, Victoria and Darren Sampson, for their endless support and generosity. I cannot imagine how much more difficult my academic journey would have been without the care they have shown for me over the years. I thank my friends for all the great

times, the opportunity to unwind with Dungeons & Dragons, and their contribution to maintaining my sanity.

Finally, I must thank my extremely patient girlfriend, Ingvild Oset. The love and care she provided were a constant source of strength and motivation.

Declaration

I confirm that this thesis has been composed by myself, and except where stated otherwise through reference or acknowledgement, the work presented herein is entirely my own. No part of this work has been submitted previously in support of an application for a degree or other qualification.

Connor Sampson

Table of Contents

1	INTRODUCTION.....	18
1.1	The Lipid Bilayer and Transport Proteins.....	19
1.2	The Elevator Mechanism – Overview and Classifications.....	25
1.2.1	Fixed Barrier with One Gate.....	26
1.2.2	Fixed Barrier with Two Gates.....	27
1.2.3	Moving Barrier with Two Gates.....	28
1.3	The Elevator Mechanism – The Importance of Lipids.....	31
1.4	The Divalent Anion Sodium Symporter (DASS) Family.....	33
1.5	INDY Proteins – Origins.....	36
1.6	INDY Proteins – Mammalian Health Implications.....	38
1.7	INDY Proteins – Function and mechanism.....	40
1.8	INDY Proteins – Role in Metabolism.....	44
1.9	INDY Proteins – <i>Vibrio cholerae</i>	47
1.10	VcINDY Molecular Function.....	50
1.10.1	Architecture.....	50
1.10.2	Substrate Binding.....	50
1.10.3	Transport.....	52
1.11	Insights Into VcINDY Function Provided by Study of Other Elevator Mechanism Transporters.....	55
1.12	Aims of this work.....	57
2	METHODS.....	59
2.1	Strains and Plasmids.....	60
2.2	Media and Antibiotics.....	61
2.2.1	Lysogeny Broth (LB).....	61
2.2.2	SOC Broth.....	61
2.2.3	PASM5052 Broth.....	61
2.2.4	MDA5052 Broth.....	62
2.2.5	2YT Broth.....	62
2.2.6	TB Broth.....	62
2.2.7	Solid Media.....	63
2.2.8	Antibiotics.....	63
2.3	Production of Styrene Maleic Acid from Styrene Maleic Anhydride - Reflux.....	64
2.4	Production of Styrene Maleic Acid from Styrene Maleic Anhydride – Autoclave.....	65

2.5	General Plasmid Handling.....	66
2.5.1	Plasmid Amplification and Storage.....	66
2.5.2	Plasmid Harvesting.....	66
2.5.3	Transformation of Non-competent Cells.....	66
2.5.4	Transformation of Competent Cells.....	67
2.6	Expression and Purification of VcINDY.....	68
2.6.1	Expression of VcINDY.....	68
2.6.1.1	BL21AI / LB Expression.....	68
2.6.1.2	PASM5052 / Lemo21(DE3) Expression.....	68
2.6.1.3	MDA5052 / Lemo21(DE3) Expression.....	69
2.6.2	Preparation of VcINDY containing Total Membrane Extracts.....	69
2.6.3	Solubilisation of VcINDY (Detergent).....	69
2.6.4	Cobalt Affinity Purification (Detergent).....	70
2.6.5	Solubilisation of VcINDY (SMALPs).....	70
2.6.6	Cobalt Affinity Purification (SMALPs).....	71
2.7	Expression and Purification of TEV Protease.....	72
2.7.1	Expression of TEV Protease.....	72
2.7.2	Purification of TEV protease.....	72
2.8	Expression and Purification of MSP1E3D1.....	74
2.8.1	Expression of MSP1E3D1.....	74
2.8.2	Purification of MSP1E3D1.....	74
2.9	Creation of VcINDY Nanodiscs.....	75
2.10	Protein Handling.....	76
2.10.1	Concentration Determination.....	76
2.10.2	Concentration of Protein Samples.....	76
2.10.3	Buffer Exchange of Protein Samples.....	76
2.10.3.1	Desalting Columns.....	76
2.10.3.2	Dialysis.....	76
2.10.3.3	On Column Exchange.....	76
2.10.3.4	Storage.....	77
2.11	Size Exclusion Chromatography.....	78
2.11.1	Buffer Preparation.....	78
2.11.2	Column Preparation and Storage.....	78
2.11.3	Sample Preparation.....	79
2.11.4	Running Samples.....	79
2.12	Protein Gels.....	80

2.12.1	SDS-PAGE	80
2.12.2	Coomassie Blue Staining	80
2.12.3	Western Blotting	81
2.12.4	Densitometry	81
2.13	PEGylation Assay.....	82
2.13.1	Experimental Procedure	82
2.13.2	Data Analysis.....	82
2.14	CPM Thermoflour Assay.....	84
2.14.1	Substrate Preparation.....	84
2.14.2	CPM Stocks.....	84
2.14.3	Experimental Procedure – Typical Melting.....	84
2.14.4	Data Analysis – Typical Melting	85
2.14.5	Experimental Procedure – Half Life	85
2.14.6	Data Analysis – Half Life	85
2.15	GFP Thermostability Assay.....	86
2.15.1	VcINDY-GFP Preparation.....	86
2.15.2	Experimental Procedure – Temperature Range	86
2.15.3	Experimental Procedure – Fixed Temperature.....	86
2.15.4	Data Analysis – Temperature Range.....	87
2.15.5	Data Analysis – Fixed Temperature	87
2.16	Microscale Thermophoresis (MST)	88
2.16.1	VcINDY Preparation.....	88
2.16.2	Experimental Procedure	88
2.17	Lipid Handling.....	89
2.18	Proteoliposome Reconstitution.....	90
2.19	Transport Assay.....	91
2.19.1	Proteoliposome Preparation.....	91
2.19.2	Experimental Procedure	91
2.19.3	Circular Dichroism (CD)	92
3	RESULTS – VcINDY Solubilisation Techniques.....	93
3.1	The SMALP Native Lipid Nanodisc System Allows <i>In Vitro</i> Examination of VcINDY in a Near Native Environment	94
3.1.1	Introduction	94
3.1.2	The Final Yield Produced From Affinity Purification of VcINDY Is Dependent Upon Both the Composition and Concentration of the SMA Polymer Used For Initial Solubilisation	98

3.1.3	SMALP Solubilised VcINDY Appears Correctly Folded, Monodisperse, and Highly Thermostable	106
3.1.4	SMALPs Have Been Employed Throughout This Thesis for Various Purposes.....	109
3.1.5	Chapter Summary	111
3.2	MSP Based Nanodiscs Allows <i>In Vitro</i> Examination of VcINDY in a Defined Lipid Environment	114
3.2.1	Introduction	114
3.2.2	Troubleshooting and Optimisation of MSP1E3D1 Production	117
3.2.3	Optimisation of TEV Protease Production	127
3.2.4	Optimisation of the Cleavage and Removal of the MSP1E3D1 Construct's His-Tag ..	129
3.2.5	Optimisation of the Reconstitution of VcINDY into MSP1E3D1 Based Nanodiscs	134
3.2.6	Chapter Summary	142
4	Results – Examination of The Mechanism and Interactions of VcINDY.....	145
4.1	Single Residue Accessibility Assays Reveal Substrate Driven Conformational Changes.....	146
4.1.1	Introduction	146
4.1.2	VcINDY Substrate Induced Conformational Changes are Detectable Through Cysteine Accessibility Measurements	149
4.1.3	Monitoring of Single Residue Accessibilities Reveals Novel Conformational Responses to Substrate Addition.....	152
4.1.4	Succinate Induced Accessibility Changes are Replicated by Other Known Substrates, But Not By Similar Non-substrate Molecules	179
4.1.5	VcINDY Substrate Induced Accessibility Changes Are Similar Within Both Detergent and Native Lipid Environments	182
4.1.6	Chapter Summary	184
4.2	High Throughput Thermostability Measurements Reveal the Rules of VcINDY Substrate Binding	189
4.2.1	Introduction	189
4.2.2	Optimisation and Validation of CPM assay for use with VcINDY.....	195
4.2.3	Details of Cation Interactions are Revealed Through Thermostability Measurements	198
4.2.4	High Throughput Thermostability Screening Reveals Clear Rules of Substrate Selectivity.....	202
4.2.5	Native Lipid Nanodisc Solubilised VcINDY Shows Extreme Thermostability Along With Substrate Induced Destabilisation	213
4.2.6	Direct Supplementation of Lipids to Detergent Solubilised VcINDY Results in Poor CPM Thermofluor Output.....	218
4.2.7	Chapter Summary	221
4.3	Aggregation Based Thermostability Measurements Indicate a Complex Relationship Between Substrate Binding and Lipid Interactions.....	228

4.3.1	Introduction	228
4.3.2	The Aggregation Based GFP-TS Thermostability Assay Is Compatible With VcINDY ..	231
4.3.3	GFP-TS is Incompatible With Purified VcINDY Samples	239
4.3.4	The Effects of Lipids Upon VcINDY-GFP Thermostability Are Altered by the Presence of Succinate	242
4.3.5	Chapter Summary	248
4.4	A Thermophoresis Based Binding Assay is Capable of Determining VcINDY's Substrate Binding Affinities	251
4.4.1	Introduction	251
4.4.2	Detergent Solubilised VcINDY is Compatible with MST Binding Affinity Measurements	253
4.4.3	Careful Analysis of VcINDY MST Data is Required In Order To Provide Reliable K_d estimates	256
4.4.4	Succinate Binding is Dependent upon Prior Low Affinity Sodium Binding	261
4.4.5	Preliminary MST Examination of Nanodisc Solubilised VcINDY Indicated Similar Substrate Affinities to Detergent Solubilised VcINDY	265
4.4.6	Preliminary MST Examination of SMALP Solubilised VcINDY Indicates that the SMALP System May be Capable of Isolating Transient Lipid Environments	267
4.4.7	Chapter Summary	269
5	DISCUSSION.....	273
5.1	The methods, and their unique perspectives	274
5.1.1	Cysteine Accessibility Assays.....	274
5.1.2	CPM-based Thermoflour.....	275
5.1.3	GFP-TS Thermostability.....	276
5.1.4	MST Affinity Assays	276
5.1.5	SMALP Solubilisation.....	277
5.1.6	MSP Nanodiscs.....	277
5.2	The New Model of VcINDY Substrate Transport.....	279
5.2.1	Cation Binding.....	279
5.2.2	Anion Binding.....	280
5.2.3	Substrate Release.....	282
5.2.4	Predictions of apo state behaviour	282
5.2.5	VcINDY Transport Mechanism Classification	283
5.3	Unknowns and Future Work	286
5.3.1	Apo State and Unloaded Translocation	286
5.3.2	Binding Site Deconvolution.....	286
5.3.3	Lipid Interaction Exploration.....	288

5.3.4	<i>Vibrio cholerae</i> Pathobiology	290
5.3.5	Concluding Remarks.....	291
6	BIBLIOGRAPHY	293
7	APPENDICES	317
7.1	Appendix 1 – Raw PEGylation Data.....	318
7.2	Appendix 2 – R script used for the fitting of GFP-TS data.....	335

List of Figures

Figure 1.2.1-1 Example phospholipid structure.....	19
Figure 1.2.1-2 The lipid bilayer, and representatives of the various forms of transport protein which exist within it.....	22
Figure 1.2.3-1 Currently known elevator mechanism transporters and their mechanisms, as compiled by Garaeva et al 2020.	29
Figure 1.2.3-1 Metabolic impact of INDY repression in mammalian systems.....	46
Figure 1.2.3-1 Role of VcINDY in Vibrio cholerae infections as elucidated by Kamareddine et al. 2018.	49
Figure 1.10.3-1 VcINDY Structure.	54
Figure 3.1.1-1 SMA polymer composition, showing a styrene – malic acid – styrene monomer sequence.....	97
Figure 3.1.2-1 Solubilisation of VcINDY containing BL21(AI) membranes with varying concentrations of 3:1 SMA.....	98
Figure 3.1.2-2 Optimisation of the solubilisation and purification of VcINDY with SMA.	101
Figure 3.1.2-3 Estimation of SMA / VcINDY ratio for differing VcINDY SMALP preps	103
Figure 3.1.2-4 Solubilisation and purification of VcINDY using differing SMA polymers	105
Figure 3.1.3-1 Characterisation of VcINDY SMALPs.....	108
Figure 3.2.2-1 Optimisation of MSP1E3D1 purification.....	119
Figure 3.2.2-2 Elution fractions of MSP1E3D1 expressed with variations on method 2.....	122
Figure 3.2.2-3 Elution fractions from troubleshooting of MSP1E3D1 expression using the best conditions as determined in Figure 3.6.2-2; 30 µg/mL, 25°C expression, induction OD ₆₀₀ = 1, 6 hours expression time.....	124
Figure 3.2.2-4 One shot optimisation of MSP1E3D1 expression with variants of method 2.	126
Figure 3.2.2-5 Final yield of MSP1E3D1 produced with optimal conditions and fresh BL21(DE3).. ...	126

Figure 3.2.3-1 Location of TEV protease target sequences in expressed constructs.	128
Figure 3.2.3-2 Production of TEV protease.....	128
Figure 3.2.4-1 Initial optimisation of the cleavage and removal of the MSP his-tag.....	131
Figure 3.2.4-2 Optimisation of the removal of the MSP his-tag.....	133
Figure 3.2.5-1 Reconstitution of VcINDY into MSP1E3D1 nanodiscs using varying ratios of VcINDY to MSP	135
Figure 3.2.5-2 HPLC SEC in line 280 nm absorbance readings for varying VcINDY nanodisc reconstitution ratios.	137
Figure 3.2.5-3 Calibration of the superdex 200 increase 10/300 SEC column	141
Figure 3.3.2-1 Principle of the mPEG5K accessibility assay	151
Figure 3.3.3-1 Transport data for the cysteine mutants used for PEGylation assays, performed by Matthew Stewart	154
Figure 3.3.3-2 Cysteine Accessibility Profile for VcINDY _{Cysless} T154C.....	155
Figure 3.3.3-3 Cysteine Accessibility Profile for VcINDY _{Cysless} M157C.....	156
Figure 3.3.3-4 Cysteine Accessibility Profile for VcINDY _{Cysless} T177C.....	157
Figure 3.3.3-5 Cysteine Accessibility Profile for VcINDY _{Cysless} A120C.....	158
Figure 3.3.3-6 Cysteine Accessibility Profile for VcINDY _{Cysless} S381C.....	159
Figure 3.3.3-7 Cysteine Accessibility Profile for VcINDY _{Cysless} T215C.....	160
Figure 3.3.3-8 Cysteine Accessibility Profile for VcINDY _{Cysless} L384C.....	161
Figure 3.3.3-9 Cysteine Accessibility Profile for VcINDY _{Cysless} V388C.....	162
Figure 3.3.3-10 Cysteine Accessibility Profile for VcINDY _{Cysless} E42C.....	163
Figure 3.3.3-11 Cysteine Accessibility Profile for VcINDY _{Cysless} A383C.....	164
Figure 3.3.3-12 Cysteine Accessibility Profile for VcINDY _{Cysless} S430C.....	165
Figure 3.3.3-13 Cysteine Accessibility Profile for VcINDY _{Cysless} F79C.....	166
Figure 3.3.3-14 Cysteine Accessibility Profile for VcINDY _{Cysless} W148C.....	167
Figure 3.3.3-15 Cysteine Accessibility Profile for VcINDY _{Cysless} Y178C.....	168

Figure 3.3.3-16 Cysteine Accessibility Profile for VcINDY _{Cysless} S436C.....	169
Figure 3.3.3-17 Impact of substrates on the accessibility of key VcINDY residues.	172
Figure 3.3.3-18 The effects of substrate addition on the accessibility of substrate responsive cysteine positions within VcINDY.....	174
Figure 3.3.3-20 Single cysteine positions and their substrate response in the PEGylation based accessibility assay.....	178
Figure 3.3.4-1 PEGylation of the VcINDY _{Cysless} M157C single cysteine mutant in the presence of varying substrates.....	181
Figure 3.3.5-1 Observation of substrate induced accessibility shifts for SMALP solubilised VcINDY _{Cysless} M157C and VcINDY _{Cysless} A120C.....	183
Figure 3.4.1-1 Principle of the CPM based thermostability shift assay.	194
Figure 3.4.2-1 Optimisation of CPM based thermostability measurements for use with VcINDY	197
Figure 3.4.3-1 Thermostability based examination of VcINDY cation binding	201
Figure 3.4.4-1 Concentration series of known substrates	203
Figure 3.4.4-2 VcINDY thermostability based substrate screening	205
Figure 3.4.4-3 Sub-comparisons of substrate derived VcINDY thermostabilisation	210
Figure 3.4.4-4 VcINDY thermostability measurements for TCEP and other Miscellaneous substrates	212
Figure 3.4.5-1 Standard CPM thermofluor examination of SMA solubilised VcINDY.....	214
Figure 3.4.5-2 Half-life based CPM thermofluor examination of SMA solubilised VcINDY	217
Figure 3.4.6-1 Lipid supplemented CPM thermofluor examination of DDM solubilised VcINDY.....	220
Figure 3.5.2-1 Initial tests of GFP conjugated VcINDY compatibility with GFP-TS.....	232
Figure 3.5.2-2 Demonstrating suitability of GFP-TS for VcINDY thermostability determination	235
Figure 3.5.2-3 Optimisation and testing of the GFP-TS assay for use with DDM solubilised GFP-VcINDY containing membranes expressed through the PASM5052 expression system.....	238
Figure 3.5.3-1 Attempted GFP-TS for purified VcINDY-GFP.....	241

Figure 3.5.4-1 The impact of lipids on VcINDY thermostability and succinate interaction	247
Figure 3.6.2-1 Demonstration of the compatibility of MST with VcINDY	255
Figure 3.6.3-1 Capillary scans showing the distribution of fluorescence with respect to position across the capillary tube	256
Figure 3.6.3-2 Optimisation of MST for detection of VcINDY succinate binding.....	260
Figure 3.6.4-1 MST readings covering range of sodium and succinate concentrations for his-tag labelled detergent solubilised VcINDY	264
Figure 3.6.5-1 MST binding analysis of detergent and nanodisc solubilised VcINDY	266
Figure 3.6.6-1 MST results, showing the effect of varying succinate concentration in the presence of 150 mM sodium on VcINDY (2:1) SMALPs	268
Figure 4.2.5-1 Proposed updated transport cycle for VcINDY, showing which chapters of this thesis provide supporting information for each step	285

List of Tables

Table 1.2.3-1 Names and functions of human DASS family transporters.....	35
Table 1.2.3-1 Known activities of INDY mutants taken from a range of animal systems.	43
Table 1.10.3-1 Bacterial strains used in this thesis.	60
Table 2.12.1-1 Components of the SDS-PAGE gels used in this thesis.	80
Table 3.6.2-1 Initial expression conditions trialled for the expression of his-tagged MSP1E3D1. ...	117
Table 3.6.5-1 Molecular weights and Stoke’s Radius sizes for the standard proteins in the High and Low molecular weight GE Healthcare Gel Filtration Calibration Kits used to calibrate the superdex 200 increase 10/300 HPLC SEC column.	140
Table 3.1.3-1 Effects of substrate addition on the ability of mPEG5K to label single cysteine mutants at varying positions within the protein.	175
Table 3.3.4-1 Lipid preparations used in the GFP-TS lipid screening experiment.	246

1 INTRODUCTION

1.1 The Lipid Bilayer and Transport Proteins

The basic unit of life is the cell. A cell consists, in the most basic sense, of a barrier separating an inside compartment from the outside world. Without this barrier there would be no sequestering of cellular components, no distinction between the ordered living interior and the surrounding world. It is the most fundamental requirement of life that this barrier must be impermeable to the diffusion of both macromolecules and small molecules, else cells would be unable to generate controlled internal environments and maintain metabolic processes.

This barrier is formed by a lipid bilayer; a flexible impermeable double layer of lipid molecules. These lipid molecules are generally amphipathic cylindrical units, with a hydrophilic head group and hydrophobic tail group (Figure 1.2.1-1). By orienting their head groups to the aqueous solution and their tail groups together they form lipid bilayers; remarkably effective barriers between the intracellular and extracellular worlds.

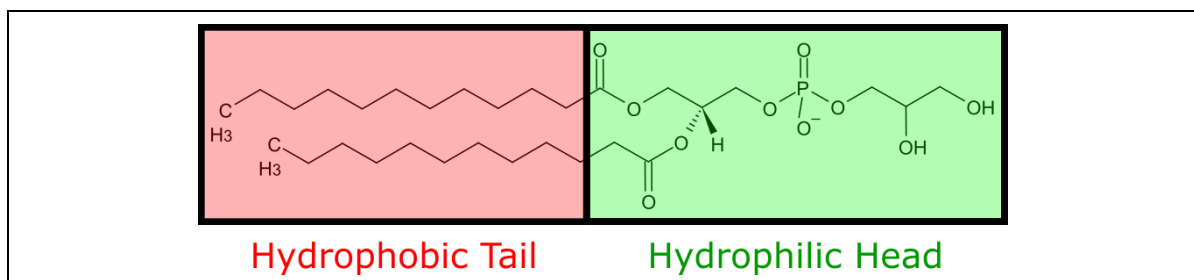


Figure 1.2.1-1 Example phospholipid structure. The hydrophobic tail region is typically embedded within the hydrophobic core of the phospholipid bilayer, while the hydrophilic head group makes contact with the surrounding aqueous environment. 12:0 Phosphatidylglycerol, commonly found within bacterial lipid bilayers, is shown.

In order to cross the lipid bilayer, a molecule must pass through the aqueous external environment, then into the hydrophobic membrane core, and then back out into the largely aqueous intracellular environment; a high energy process inhibitory to the passage of most biologically important molecules.

A cell cannot exist in isolation. In order to thrive a cell must be able to take up energy sources and raw materials, secrete unwanted molecules, and sense the nature of its surrounding environment.

The lipid bilayer is the only contact between the cell and the outside world, meaning that these processes must be mediated through the use of machinery which bridges the bilayer itself.

To this end, a wide range of proteins are embedded in the membrane, including proteins dedicated to tasks such as signalling and maintenance of the membrane itself, although herein we shall focus on those dedicated to transport.

Early studies on the diffusion of substrates across bacterial membranes noted the enzymatic nature of the process, with the saturation of transport rates at high substrate concentrations suggesting the roll of active transporting proteins [1]. These transport proteins are now known to facilitate the controlled movement of molecules across the membrane, achieving this through several broad approaches, as overviewed in Figure 1.2.1-2 and discussed below. These approaches are similar in that they are controlled, selective, and energetically favourable; either transporting molecules down their concentration gradients, or coupling the transport of molecules against their concentration gradients to other energetically favourable processes. Generally, transport proteins can be separated into two main categories; channels and carriers, with carriers being further subcategorised based on their modes of transport.

Channels represent a passive approach to the movement of ions and molecules across the membrane, as exemplified by the potassium channel KcsA. During KcsA mediated potassium diffusion four identical subunits form a homotetramer, interacting to create a central channel through the membrane which is protected from the lipid environment. Passage through this channel is controlled by a selectivity filter; a series of precise coordination positions which the ion must pass through, allowing the rejection of non-potassium ions [2]. While KcsA is capable of undergoing conformational changes which open and close this central channel, ion transport occurs without the need for any major conformational changes; a defining feature of this approach to transport. Channels are therefore very effective mediators of rapid ion diffusion, however they are also limited

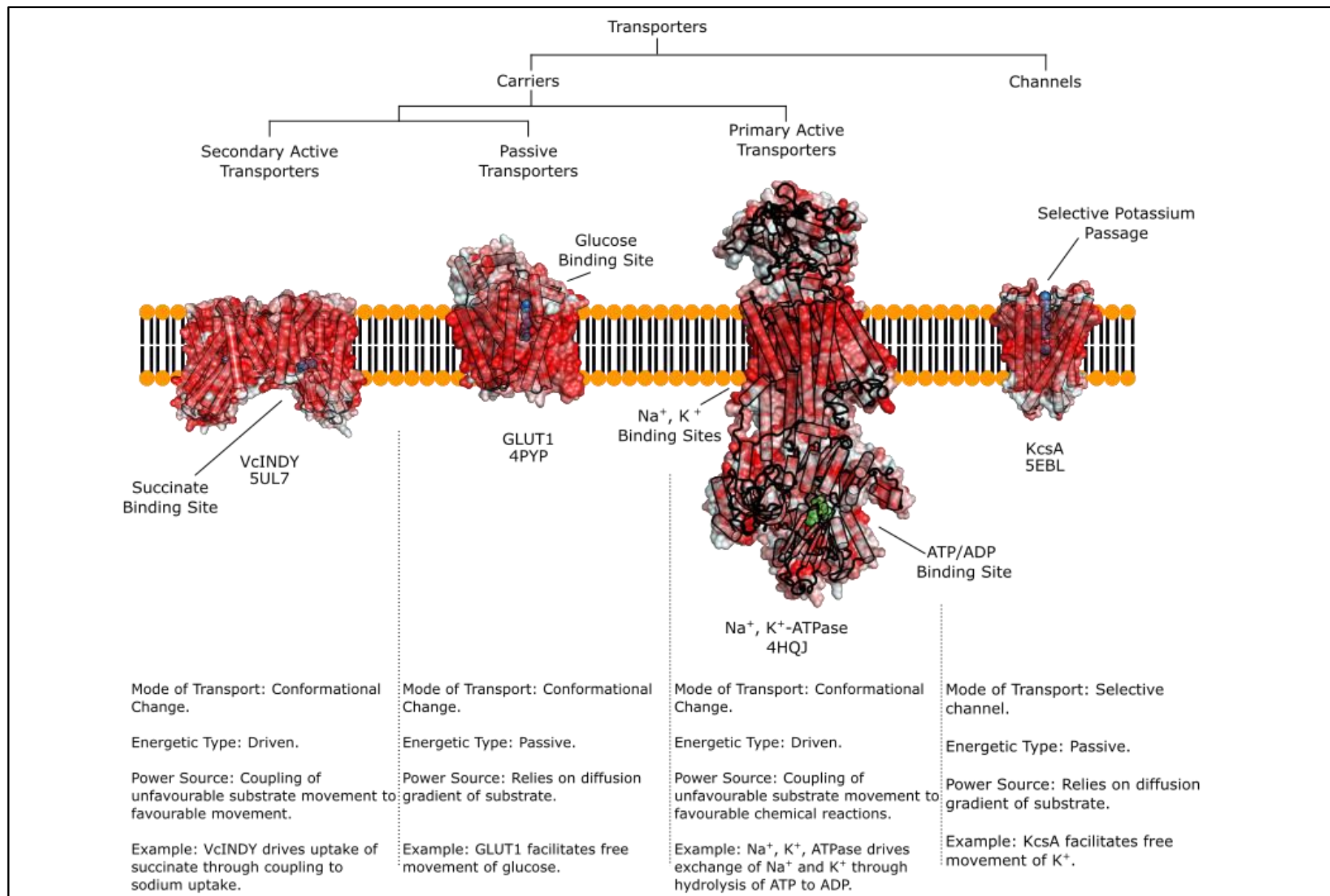


Figure 1.2.1-2 The lipid bilayer, and representatives of the various forms of transport protein which exist within it. General classification of transporter types, with example structures for each. Protein structures are shown with surface rendering and detailing of internal secondary structure features. Proteins are coloured according to hydrophobicity; white = hydrophilic, red = hydrophobic. Blue = transport substrates or competitive inhibitors. Green = other bound substrates. It should be noted that huge heterogeneity of structure and function exists within each mechanistic classification. Structure references, left to right; [3] [4] [5] [6]. Each form of transporter, along with the example presented here, is discussed in the main text.

to a passive transport role; they only allow the movement of substrates according to their concentration gradient, and cannot conduct powered transport.

Carrier transport is the other major approach to the task of shuttling molecules across the lipid bilayer. In this case no open channel is formed through the membrane, with molecular translocation being achieved through alternating access mechanisms. The principles of alternating access are exemplified by the passive carrier GLUT1. GLUT1 contains a central glucose binding site, which may open to either the extracellular or the intracellular side of the bilayer, but not both at the same time. Transport is achieved by the entry of extracellular glucose into this central binding site whilst the protein is in the outward-open / inwards-closed state, followed by spontaneous translocation of the protein to the inwards-open / outwards-closed state, allowing the transported glucose molecule to diffuse into the cell [7]. This process of bridging the bilayer is bidirectional, and will carry glucose both into and out of the cell dependent upon local concentrations. Through the use of this alternating access carrier mechanism, the selective transport of larger molecules can be achieved without the risk of non-specific molecular leakage occurring through large channels.

The alternating access approach to transport also provides an important opportunity; powered, or active transport. The transporters already discussed are passive, allowing the diffusion of their target molecules across the membrane, however, a cell will often require control over this process, such as to sequester molecules of importance, expel unwanted molecules, or manage chemical signalling processes. In order to carry a molecule against its concentration gradient, energy must be used. One approach to this is primary active transport, as exemplified by the Na^+ , K^+ ATPase. The Na^+ , K^+ ATPase uses an alternating access mechanism to move three Na^+ ions to the extracellular side of the membrane, while also moving two K^+ ions to the intracellular side, regardless of local concentration gradients. Primary active transporters carry out these energetically unfavourable transport processes through the direct application of chemical energy; in this case an ATP is used, with the

binding and hydrolysis of this energy rich molecule occurring in a distinct allosteric ATP binding site in order to drive the transport cycle [5].

An alternate, and more indirect, way to achieve active transport is through secondary active transport, as exemplified by VcINDY, the protein upon which this thesis shall focus. VcINDY transports succinate against its concentration gradient not through the direct application of energy, but by coupling succinate movement to the transport of sodium ions in accordance with their concentration gradients. During alternating access transport, VcINDY is able to transition between the outward-open / inwards-closed state and the inwards-open / outwards-closed state either entirely empty of substrates or containing three sodium ions and one succinate ion, meaning that any transport of substrate will include the favourable movement of sodium alongside the unfavourable movement of succinate, resulting in a net energetically favourable process [8][9]. Through this approach secondary active transporters couple the gradients of multiple substrates together in order to achieve the desired direction of transport.

Transport proteins are extremely varied, and while the underlying principles of transport are given here, the molecular mechanisms employed to carry out these principles are diverse. Two secondary active transporters, for example, may have entirely different domain architectures, mechanisms to facilitate alternating access to the binding sites, numbers of substrates, and directions of substrate transport.

Here we shall be looking at the mechanism behind VcINDY's secondary active transport in detail, attempting to understand the molecular mechanisms which allow this protein to carry out its secondary active transport of sodium and succinate.

1.2 The Elevator Mechanism – Overview and Classifications

Active transport is based upon the principle of alternating access. This has been described in 1.1 The Lipid Bilayer and Transport Proteins, however to summarise; in order to function a non-channel transporter must alternate the accessibility of its binding site between the two sides of the membrane. It is vital that the site is only accessible from one side of the membrane at a time, else protein would simply form a channel and no form of energy coupled transport could be applied, as exemplified by CLC family of transport proteins, which contains both H⁺/Cl⁻ exchangers operating through the alternating access mechanism, and Cl⁻ channels which do not conduct powered transport [10].

Alternating access often achieved through a variation of the moving barrier mechanism, whereby movements of the protein result in the opening and closing of the intracellular and extracellular access route to a static binding site (see 1.1 The Lipid Bilayer and Transport Proteins) [11]. Another mechanism of alternating access transport is possible; elevator mechanism transport.

Reyes et al. 2009 published the first known transport mechanism for Glt_{ph}, an aspartate transporter from *Pyrococcus horikoshii*. Previously only the outwards-facing state of this trimeric transporter had been determined, however pre-structure work by *Renae et al. 2004* had performed cross linking of introduced cysteine residues which were 25-30 Å apart according to the then current outwards facing structure [12], suggesting that these positions must be brought into proximity by an unknown conformational state. The use of these previously observed cysteines allowed the trapping and structural determination of the inwards facing state of Glt_{ph} [13]. This revealed a novel transport mechanism distinct from moving barrier transport, in which transport was instead facilitated through translocation of the binding site across the membrane [13]. By 2011 this had been dubbed the elevator mechanism [14], and it would be rapidly discovered within a range of additional protein families (Figure 1.2.3-1A).

All elevator mechanism transporters achieve alternating access through the translocation of their binding sites across the membrane (Figure 1.2.3-1B). In order to facilitate this, at least two domains are present; a scaffold domain, often involved in oligomerisation, and a transport domain. The transport domain carries out the dynamic process, and as such the binding site must be located either entirely within this domain, or at the interface between the two domains [15].

These elevators can be categorised based on two major features of their mechanisms; the number of flexible regions involved in gating, and whether the barrier is fixed or mobile (Figure 1.2.3-1C) [15]. In order to discuss this it is important to emphasise the distinct roles of barriers and gates. The gate is the dynamic region controlling access between the solvent and the binding site, typically closing upon substrate binding in order to ready the protein for substrate translocation. The barrier, on the other hand, is the blocking section of the protein which prevents the leakage of substrates from the inwards to the outwards-facing side of the protein. The gate controls access in and out of binding site and the barrier controls movement across membrane.

1.2.1 Fixed Barrier with One Gate

The Fixed Barrier with One Gate mode of elevator mechanism transport is exemplified by the SLC1 family of sodium dependent amino acid transporters; arguably the best characterised family of elevator mechanism transporters, with which structures and mechanisms available for four members (Figure 1.2.3-1A) [15]. Amongst them is Glt_{ph}, the first identified elevator mechanism transporter [13][16].

The binding site of Glt_{ph} includes residues of two hairpin loops, HP1 and HP2. During the transport cycle HP2 is a substrate responsive region, responsible for the opening and closing of solvent access to the active site in response to substrate binding [17]. Importantly, this same loop acts as the gate in both the inwards and outwards-facing states of the protein [14], hence the classification as a one gate elevator.

The barrier regions of this protein are fixed, with the movement of the binding site across the membrane bringing the substrate past the barrier regions, thus achieving transport [13]. This mode of elevator mechanism transport therefore involves one gate and a fixed barrier (Figure 1.2.3-1C).

It is noteworthy that for all currently confirmed instances of fixed barrier one gate elevator mechanism transport the binding site is fully buried within the transport domain, allowing speculation that this arrangement of substrate binding is required for a single gate mechanism [15].

1.2.2 Fixed Barrier with Two Gates

This approach to the elevator mechanism is best characterised by CNT_{NW}, for which a remarkable array of transport intermediate crystal structures have been established through the generation of binding site mutants [18].

During the transport cycle two gates are used instead of one; i.e. in the outward facing state of CNT_{NW} the helix TM4b moves in order to control solvent access to the binding site, but in the inwards-facing state TM4b is largely static, with movements of the hairpin region HP1 instead regulating solvent access to the binding site [18].

Similarly to Fixed Barrier with One Gate mechanisms, the barrier region is again static, with elevator movement of the binding site allowing substrates to pass [18].

Intriguingly, unlike Fixed Barrier with Two Gates transporters, in all currently confirmed instances of this mechanism the binding site is located at the interface between the transport and scaffold domains, again allowing speculation that this arrangement of substrate binding is required for a two gate mechanism [15] (Figure 1.2.3-1C).

1.2.3 Moving Barrier with Two Gates

As previously discussed, the movement of barrier regions is a typical feature of non-elevator mechanism transporters, allowing the regulation of substrate transfer between the inward and outward facing sides of the proteins while coordinating to prevent uncontrolled movement of substrates across the membrane [11]. Elevator mechanism transporters, by translocating the binding site itself relative to a static barrier region, are able to circumvent the need for moving barriers [15]. This does not mean, however, that proteins do not exist in which both moving barriers and elevator mechanism translocations occur simultaneously. A prominent example of this approach is the bile acid transporter ASBT. Crystal structure determination in the inwards and outwards-facing states for two closely related homologues has demonstrated an elevator mechanism, with the binding site undergoing a translocation of 7.5 Å perpendicular to the membrane, regulated by two gating regions [15][19][20]. Curiously, the barrier region does not appear static, alternating blockage with the transport cycle similarly to a non-elevator mechanism transporter, indicating a hybrid mode of transport [15][19][20].

It is interesting to note that in all currently recorded instances of this mechanism, the binding site is located at the interface of the transport and scaffold domains, and hairpin regions are not required for substrate binding, again suggesting relationship between elevator transporter architecture and mechanism (Figure 1.2.3-1C).

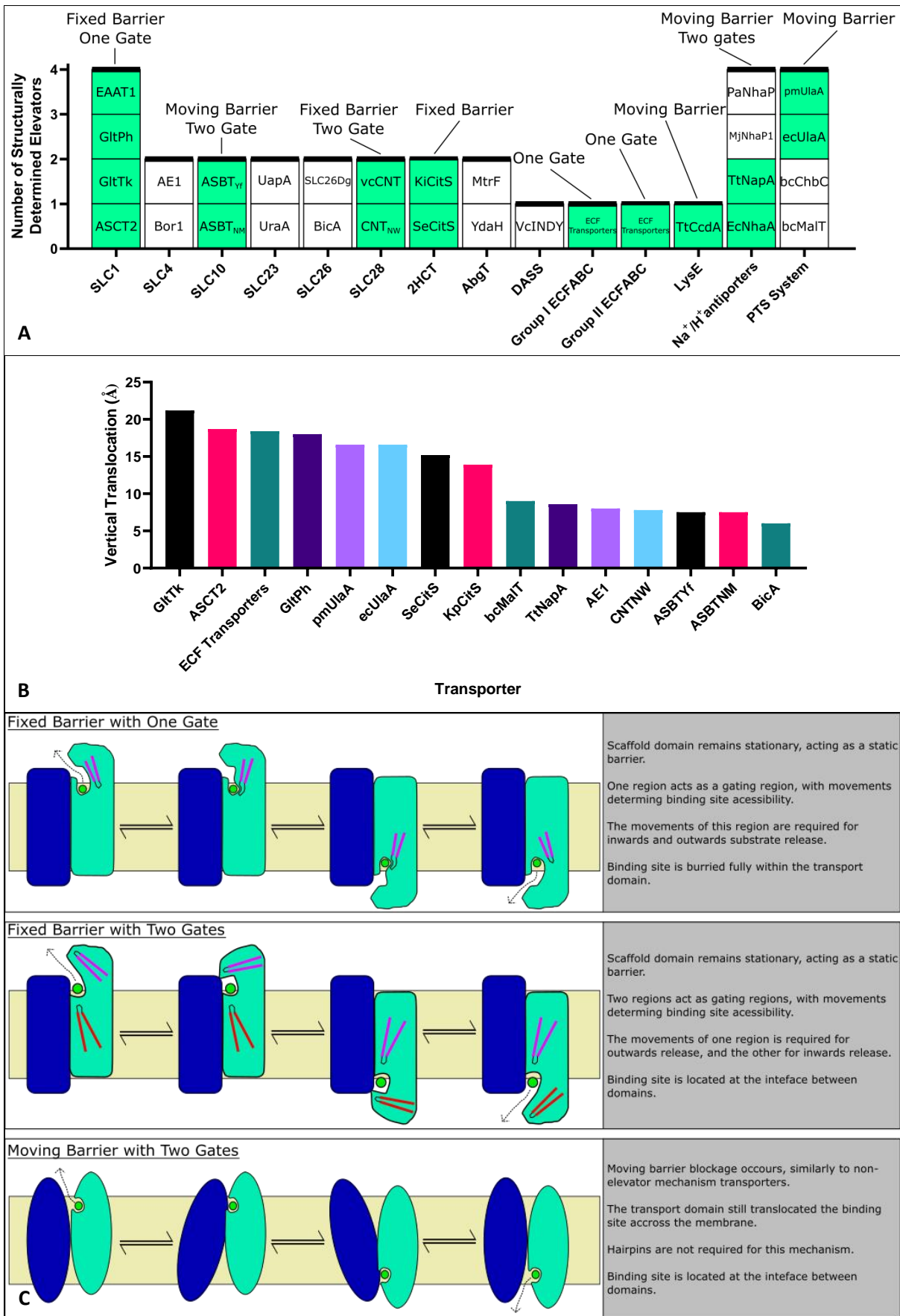


Figure 1.2.3-1 Currently known elevator mechanism transporters and their mechanisms, as compiled by Garaeva et al

2020. A: Known elevator mechanism transporters by family. Transporters for which the form of elevator mechanism

transport has been confidently established are coloured blue. For all elevator mechanisms so far studied in sufficient detail, the form of elevator mechanism transport has been consistent within families. B: Distance translocated by elevator mechanism transporter substrate binding sites relative to a vertical axis perpendicular to the membrane. This movement of the binding site is the defining characteristic of an elevator mechanism transporter [15]. C: Known forms of elevator mechanism transporter [15]. Diagrams show ideal and simplified examples designed to demonstrate the key features of each form of transporter, and as such are not representative of any specific proteins, nor do they take into account oligomeric states or any specific architectures.

1.3 The Elevator Mechanism – The Importance of Lipids

As already much discussed, elevator mechanism transporters rely on large, rigid body, translocations taking place within the lipid bilayer. This necessitates a complex relationship between the moving protein regions and the surrounding lipid bilayer. Unfortunately, these interactions are currently poorly understood.

The SLC1 family of Fixed Barrier One Gate elevator mechanism transporters is best characterised in this context. These transporters are known to be sensitive to the components of the lipid bilayer, with the addition of cholesterol increasing transport activity for both ASCT2 in proteoliposomes [21], and EAAT2 in whole cells [22]. Additionally, studies of ASCT2 have revealed the presence of structural lipids contacting the scaffold domain in multiple locations; including the interface between scaffold and transport domains [23][21][24]. Intriguingly, structural study of the related EAAT1 found an inhibitor to bind at this interface between scaffold and transport domains, occupying a region known to bind cholesterol in ASCT2 [25]. While this evidence is imperfect, relying on comparisons between related proteins, it does strongly indicate a vital role for this interface bound cholesterol in SLC1 transport.

Furthermore, Glt_{ph} transport has been shown to be sensitive to differently methylated PE derivatives, conducting transport at a higher rate in the presence of tri-methyl PE than mono- or di-methyl PE [26]. Interestingly, in this case, specific mutations have been identified which alter these lipid effects, suggesting suggest specific and selective interactions to occur [26].

Studies of the transport cycle have also detected major alterations in the curvature of the membrane to occur during Glt_{ph} transport at significant energetic cost [27][28], which must be satisfied using substrate binding energy [29], tentatively suggesting a coordinated relationship between lipid and substrate interactions to occur during the transport cycle.

Studies of the SLC1 family have therefore done much to hint at the complexity of the relationship between elevator mechanism transporters and lipids, although these interactions are currently

poorly understood. Beyond the SLC1 family, empirical study of elevator mechanism transporter lipid interactions is extremely rare [15], leaving a vast array of questions in need of answering.

1.4 The Divalent Anion Sodium Symporter (DASS) Family

The most numerous member of the Ion Transporter (IT) superfamily, the DASS family possesses a misnomer of a name [30]. This family of secondary active elevator mechanism transporters is found throughout all domains of life, with five members in humans alone [31], named SLC13A1-5.

Generally, these proteins are secondary active transporters, coupling the transport of sodium to the uptake of substrate [31]. It should be noted, however, that the anions they transport include trivalent ions such as citrate, and at least one characterised DASS transporter is capable of cation independent anion transport [32][33][34].

In humans, DASS transporters are responsible for a range of functions, and can be separated into two broad categories; transporters of Krebs cycle intermediates, and transporters of sulphate (Table 1.2.3-1). All human DASS family transporters, however, are entirely dependent on sodium for the uptake of their anionic substrate [35][36][37][38][39][40][41].

The Krebs cycle intermediate transporters consist of SLC13A2 (NaDC-1), SLC13A3 (NaDC-3), and SLC13A5 (NaCT). The former pair exhibit similar functions; expressed in the kidney, they uptake high energy Krebs Cycle intermediates which have previously been removed from the blood, preventing their loss in urine [42][43][44]. Their specificities are complementary to one another, with SLC13A2 able to uptake the dicarboxylic succinate along with the tricarboxylic citrate [36], and SLC13A3 able to uptake such dicarboxylates as succinate, malate, fumarate, oxaloacetate, and α -Ketoglutarate [37][44]. Between these two transporters almost the entire population of Krebs Cycle intermediates is known to be covered. SLC13A3 is also expressed in the intestine, where its dicarboxylate specificity is employed to uptake dietary Krebs' Cycle intermediates [42].

SLC13A5 carries out a distinctly different physiological role, being expressed primarily in the liver with a specificity for citrate and weak succinate uptake [42][39][40][41]. Here SLC13A5 is responsible for the uptake of these high energy metabolites into the tissue of intermediary metabolism, with major implications for the balance of anabolism and catabolism both in the liver and beyond [45].

For a detailed discussion of SLC13A5's role in energy signalling, see 1.6 INDY Proteins – Mammalian Health Implications and 1.8 INDY Proteins – Role in Metabolism.

The sulphate transporters are SLC13A1 (NaSi-1) and SLC13A4 (NaS2). SLC13A1 carries out a similar physiological role to SLC13A2 and SLC13A3, being primarily expressed in the kidneys where it uptakes sulphate ions which have been removed from the blood [35][42], preventing their loss in urine [46]. SLC13A4 is expressed in the brain and placenta, where it carries out physiologically important sulphate transport [42]. This is a particularly vital transporter, as failure of SLC13A4 sulphate transport leads to foetal developmental defects [47].

Our current understanding of human SLC13 transporters at a molecular level is limited despite their important position in human health, as is our understanding of the wider DASS family. At the present time only one member of this family has published crystal structures, the *Vibrio cholerae* succinate transporter known as VcINDY [48][3]. This makes VcINDY a scientifically important member of the DASS family, as its known structure allows detailed mechanistic studies to be performed.

Accordingly, VcINDY is the first and only member of the DASS family for which a transport mechanism has been determined, revealing this family to conduct transport through the elevator mechanism. It is hoped that further study of this bacterial family member will allow the underlining principles of DASS family transport to be determined, producing further insights which can be applied to the human transporters discussed here.

Name (Alternate)	Expressed In	Cation	Anion	Function
SLC13A1 (NaSi-1)	Kidney	Sodium [35]	Sulphate, thiosulphate, selenite [35]	Re-absorption of sulphate from the renal proximal tubule [46]
SLC13A2 (NaDC-1)	Kidney and Small Intestine	Sodium [36]	Succinate, Citrate [36]	(Re-)absorption of Krebs cycle intermediates in expressed tissues [43]
SLC13A3 (NaDC-3)	Kidney	Sodium [37]	Succinate, malate, fumarate, oxaloacetate [37], α - Ketoglutarate [44]	(Re-)absorption of Krebs cycle intermediates in the kidneys [44]
SLC13A4 (NaS2, SUT-1)	Brain, Placenta, Retina	Sodium [38]	Sulphate [38]	Required for sulphate transport, especially across placenta into developing foetus [47]
SLC13A5 (NaCT, mINDY)	Liver, Salivary Gland	Sodium [39][40][41]	Citrate [39][40], weak succinate [41]	Uptake of citrate into hepatocytes, playing a key role in energy signalling [45]

Table 1.2.3-1 Names and functions of human DASS family transporters. It should be noted that the anions and cations listed here do not necessarily represent the extent of substrate flexibility displayed by each protein, but rather substrates so far proven to be transported, as extensive substrate screens have not been performed in all cases. Tissue expression data taken from the Human Protein Atlas [42]

1.5 INDY Proteins – Origins

Indy proteins are a group of homologous transporters within the DASS family which carry out conserved physiological functions. Much of the current interest in INDY proteins and the adoption of this name originated, oddly enough, with the study of learning in flies. During mutagenesis screening carried out by *Bonyton et al 1992* in the hope of discovering novel learning-related genes, two flies demonstrated dramatically increased lifespans [49]. While lifespan was not the focus of this original study, these unusually long-lived flies were later examined in *Rogina et al 2000*, where it was found that each fly possessed a mutation in the same gene. As the original mutagenesis screen had deactivated genes at random, the presence of a shared mutation between the long lifespan flies was highly intriguing. After further examination indicated a causal relationship between this gene and lifespan, it was duly named I'm Not Dead Yet, or INDY for short [50].

This discovery was of great interest to those studying ageing, as until this time only one single gene knockdown had been known to increase lifespan in *Drosophila*; the aptly named *methuselah (mth)* gene [51], although the function of that gene was then unknown. (The *mth* gene was later identified as a G Protein Coupled Receptor from a family common to various species of *Drosophila* [52], and the lifespan extensions were attributed to the role of *mth* in the insulin producing cells of the fly brain [53].) INDY, on the other hand, appeared homologous to mammalian dicarboxylate transporters, making it an appealing target for further study [50].

Just two years later, in 2002, knockouts of the *Caenorhabditis elegans* INDY homologues, ceNaC1 and ceNaC2, were observed to confer lifespan extensions in this very different animal [54], and two years after this a reduction in adiposity in *C. elegans* was also observed [55].

It would be remiss not to comment on the level of controversy which came with these findings. A study by *Toivonen et al* in 2007 boldly claimed to have determined that there was no effect of INDY knockout on lifespan for either *Drosophila* or *C. elegans*, presenting both this lab's inability to replicate either of these lifespan extensions, and a growing body of literature demonstrating

inconsistencies for *Drosophila* INDY knockouts [56]. This raised the question of why different labs were producing such different results.

In 2009, a study by *Wang et al* examined the relationship between INDY mutation and Caloric Restriction (CR) in *Drosophila*, producing findings which shed light on the ongoing controversy. They demonstrated that the effects of INDY knockout were highly interwoven with those of CR; INDY mutants exhibited CR-like phenotypes, and INDY expression was significantly suppressed by CR. Thus, INDY knockouts would not result in clear phenotypic changes for *Drosophila* raised on low energy diets. Furthermore, the relationship between INDY and lifespan was not binary, with suppression of INDY expression increasing lifespan significantly more than complete abolishment of the gene [57].

Following this, the first and last authors of the original 2000 paper which initially discovered the role of INDY in fly lifespan published a new paper in 2013, in which multiple alleles of INDY were examined in multiple genetic backgrounds, correcting for potential issues raised in the combative *Toivonen et al 2007* paper, and finding conclusively that INDY mutations did reliably increase lifespan in the flies [58].

As such, the intriguing impact of these knockouts was securely established in these simple model animals, raising the question; what is the role of INDY homologues mammals?

1.6 INDY Proteins – Mammalian Health Implications

Birkenfeld et al. 2011, provides key insights as to the role of the mammalian homologue, mammalian INDY (mINDY / SLC13A5). Through the careful study of mouse metabolism and phenotype, this paper builds a detailed and fascinating overview of the effects of INDY (mSLC13A5) knockout, including both phenotypic and metabolic observations, however the metabolic findings shall largely be discussed in the following sections. Mammalian INDY is predominantly expressed in the liver, and the knockout of this gene results in the impairment of hepatic citrate transport, along with an increase in plasma citrate concentrations [45]. The phenotypic effects of this slowed citrate uptake are remarkable. Double INDY knockout mice show body weight reductions of around 10% when fed regular diets compared to WT mice, however on high fat diets this increased to around 17%. These differences are even more dramatic when relative body fat levels were examined, showing double knockout mice to produce far lower levels of body fat even whilst fed high fat diets [45].

Further to the reduction in general fat levels, hepatic diacylglycerol (DAG) levels are greatly reduced in double INDY knockout mice, contributing to greatly improved insulin sensitivity and glucose response [45]. INDY knockouts even protect against the reduction in insulin sensitivity which normally comes with ageing [45].

Finally, mitochondrial biogenesis is heightened in double knockout mice, as is the expression of respiratory genes; highly intriguing effects given the role of mitochondria reduction in ageing [45].

These remarkable impacts, resulting in mice resistant to obesity, resistant to type 2 diabetes, and predisposed to healthy ageing, are both phenotypically and genetically similar to those achieved through caloric restriction. Analysis of gene expression demonstrated that 80% of pathways are regulated similarly in INDY knockout and calorically restricted mice, suggesting huge levels of overlap between these two processes. Furthermore, mice undergoing fasting demonstrated a 48% drop in mINDY expression over 36 hours [45], suggesting that mINDY regulation may be a key component of the natural caloric restriction response which its knockout emulates.

Tantalisingly, this relationship between mINDY and diet appears to be conserved in other species of mammal. Rhesus monkey mINDY expression is similarly linked to diet, whereby monkeys fed high fat, high sucrose, diets exhibit 3 to 4 fold increased mINDY expression [59]. While it would be difficult to perform such controlled diet experiments on humans, correlations between human BMI, waist circumference, body fat percentage, and liver fat content with human mINDY (SLC13A5) expression all suggest that this relationship also occurs in our own species [59].

Further to this, mINDY/SLC13A5 targeting is a potentially useful approach to the treatment of hepatoma, with silencing of this gene resulting in greatly reduces levels of cancer cell proliferation and colony formation [60].

Human mINDY is therefore a highly promising therapeutic target for the treatment of human health conditions and the promotion of healthy human ageing. Supporting this possibility, drug inhibition of mINDY has already been carried out in mice, resulting in reductions in hepatic citrate uptake reminiscent of those observed in mouse mINDY knockouts [61], raising the potential of the development of similar treatments for humans.

1.7 INDY Proteins – Function and mechanism

The consistent, caloric restriction like, role of INDY homologues throughout multiple animal systems begs the question; what is the underlying mechanism? To answer this we will first examine the nature of these transporters on a molecular level, and then build a metabolic context.

All of the relevant INDY homologues from the model organisms covered so far have been functionally characterised, allowing comparison of their functional characteristics (Table 1.2.3-1). First, the differences shall be discussed. The majority of characterised DASS transporters are sodium driven, although some are also able to drive transport using lithium. The clear exception to this is the *Drosophila* transporter DrINDY. Strangely enough in this family of secondary active transporters, three separate studies have demonstrated the ability of DrINDY to catalyse succinate transport in the absence of sodium ions, indicating a capacity for unpowered uniporter activity [32][33][34]. Perhaps even more intriguing, the transport of citrate also appears to occur in the absence of sodium [34], but is clearly enhanced in the presence of sodium [32][33], suggesting multiple modes of transport to occur within DrINDY. This ability to conduct anion independent transport, and transport different anions with differing cation dependencies, is observed in none of the other biologically key INDY proteins discussed here.

While studies have sometimes reported large differences in the absolute rates of INDY homologue substrate transport, the K_m values (representing the concentration of substrate required to achieve half maximal transport rate) are normally within an order of magnitude of one another; in the micromolar range. In this case, the human INDY, SLC13A5, is the exception, with estimations of both citrate and succinate K_m ranging into the millimolar range [41].

All of the transporters discussed here are able to transport both citrate and succinate, along with some similar molecules such as fumarate, although their apparent preferences vary. DrINDY and ceNaC1 transport succinate at a higher rate than citrate [32][33][34][55], while ceNaC2, mouse mINDY, and human mINDY transport citrate at a higher rate than succinate [55][45][41]. Human

mINDY demonstrates this preference to such an extent that multiple cell based radioligand transport assays failed to detect any succinate transport [39][40], despite it being clearly detectable through patch clamp assays [41].

These differences in cation coupling, absolute transport rates, K_m , and Krebs's cycle intermediate preference likely represent parameters not vital to the phenotypic role of these homologues. Instead, the common features of INDY homologues must explain their shared role in caloric restriction.

These homologues all transport citrate and succinate, which are key high energy metabolites involved in both Krebs's Cycle metabolism and energy signalling (see 1.8 INDY Proteins – Role in Metabolism). Additionally, they share remarkably similar expression patterns. All the examples discussed here are predominantly expressed in tissues of intermediary metabolism and energy storage, be it DrINDY in the *Drosophila* midgut [32], ceNac2 in the *C. elegans* intestinal tract [55], mouse mINDY in the mouse liver [45], or human mINDY in the human liver (and, interestingly, the human salivary gland [62], where a citrate concentration of roughly 100 μM is found [63]).

Thus, while the INDY homologues vary in the details of their transport, they share strictly conserved roles as importers of high energy molecules in tissues of intermediary metabolism.

Transporter	Host	Relative Transport Rates	Known K_m values	Anion Dependence
DrINDY	<i>Drosophila</i>	Succinate faster than citrate [32][33][34]	Succinate – 39 μ M [32] 40 \pm 4 μ M [33]	Succinate transport cation independent [32][33][34] Citrate transport cation independent [34], but accelerated by sodium presence [32][33]
ceNaC1	<i>C. elegans</i>	Succinate faster than citrate [55]	Succinate – 730 \pm 50 μ M [54]	Sodium dependent [54]
ceNaC2	<i>C. elegans</i>	Citrate faster than succinate [55]	Succinate – 60 \pm 9 μ M [54], 88 \pm 13 μ M [55] Citrate – 76 \pm 14 μ M [55]	Sodium dependent [54]
mINDY	Mouse	Citrate faster than succinate [45]	Citrate – 49 \pm 9 μ M [45], 38 \pm 5 μ M [64], 7.2 (6.5–8.0) μ M [41] Succinate – 105 \pm 9 μ M [45], 37 \pm 6 μ M [64], 5.5 (3.3–9.2) [41]	Strong sodium dependence [64]

mINDY, (SLC13A5)	Human	Citrate, no succinate transport according to radioisotope assays [39][40] Weak succinate transport detected through patch clamping [41]	Citrate – 604 ± 73 μM [40], 3.5 ± 0.2 mM [41] Succinate – 9.3 (7.4–12) mM [41]	Strong sodium dependence [39][40][41].
---------------------	-------	--	---	--

Table 1.2.3-1 Known activities of INDY mutants taken from a range of animal systems. Alternate names are shown in brackets. In many studies definitive V_{max} values are not given, however comparative rates between citrate and succinate are shown, so this qualitative measurement is presented.

1.8 INDY Proteins – Role in Metabolism

The dramatic metabolic and phenotypic changes achieved through the deletion of INDY homologues is grounded in the role of the high energy molecules which they transport. In mouse models, the knockout of mINDY reduces hepatic citrate uptake by approximately 36%, sufficient to alter the hepatic energy landscape [45]. This reduction in intracellular citrate has three main effects (Figure 1.2.3-1).

Firstly, as citrate is a component of the Krebs cycle, shuttled into the mitochondria after conversion into malate [65], a reduction in its availability leads directly to a reduction in Krebs cycle activity, and thus energy generation. This inevitably results in a reduction in the ATP to ADP ratio in the cell, as detected by AMP Kinase (AMPK) [66][67]. AMPK can be considered a general cellular energy regulator, responsible for the detection of ATP/ADP ratio flux and regulation of cellular processes in response. AMPK mediated responses to the lowering of ATP levels include increasing peroxisome proliferator-activated receptor Gamma Coactivator 1-alpha (PGC-1 α) expression through which mitochondrial biogenesis is stimulated [45][67], a suppression of sterol regulatory element-binding transcription factor 1 (SREBP-1c) and acetyl-CoA carboxylase (ACC2) leading to decreased lipogenesis [45][68][67][69], an upregulation of phosphofructokinase (PFK) resulting in an increase in glycolysis [67][70], and further interactions leading to decreases in gluconeogenesis and increase in β -oxidation (fatty acid breakdown) [45].

Secondly, citrate is a key substrate for lipogenesis as it is converted first into Acetyl-CoA, and then into the cholesterol precursor β -Hydroxy β -methylglutaryl-CoA (HMG-CoA) and the lipid precursor Malonyl-CoA [65]. A reduction in the availability of this substrate therefore leads to additional drops in the rate of lipid and cholesterol production.

Thirdly, citrate acts as a signalling molecule independently of its role as a substrate. Through this mechanism, a reduction in citrate levels leads to a downregulation of PFK leading to a reduction in glycolysis [67], an upregulation of Fructose-1,6-Bisphosphatase (F-1,6-BP) leading to an increase in

gluconeogenesis [67], and a downregulation of ACC2 leading to a reduction of lipogenesis [45][67][69].

With these observations, the impact of animal INDY knockouts is well explained. Without lowering the energy intake of an entire organism, cells responsible for secondary metabolism are prevented from taking up a molecule vital for the sensing of energy levels. Without the uptake of citrate, the balance of anabolism and catabolism is shifted towards catabolism in a manner similar to caloric restriction, suppressing the creation of fats and other energy stores while promoting the generation of mitochondria. In this way, healthy ageing, without reductions in insulin sensitivity and with greatly improved mitochondrial count, is encouraged.

Human mINDY is therefore an extremely promising therapeutic target, offering the potential benefits of caloric restriction through simple drug treatment, including the reduction of obesity and diabetes levels. The potential for a human mINDY targeting drug to improve societal health and reduce healthcare burdens is huge.

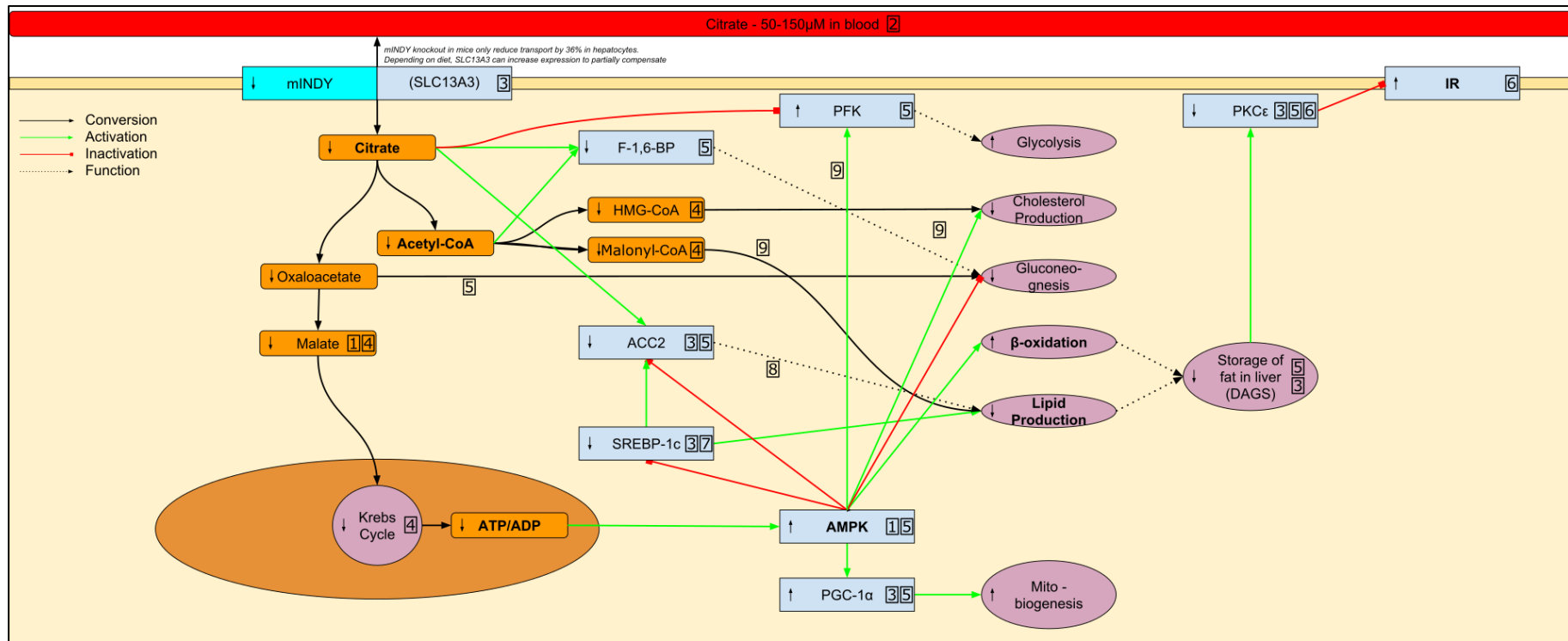


Figure 1.2.3-1 **Metabolic impact of INDY repression in mammalian systems.** A greatly abridged model of metabolism is shown for simplicity, with only the most relevant components included. Knockout of the mINDY (SLC13A5) citrate transporter in hepatocytes leads to reduced uptake of citrate into the cell. Lower intracellular citrate levels lead to a reduction in anabolism and an increase in catabolism through a combination of direct citrate signalling and reduced energy source availability. Abbreviations: F-1,6-BP = Fructose-1,6-Bisphosphatase, PFK = Phosphofructokinase, PKC ϵ = Protein Kinase C ϵ , IR = Insulin Receptor, CoA = Coenzyme A, HMG-CoA = β -Hydroxy β -methylglutaryl-CoA, ACC2 = Acetyl-CoA Carboxylase 2, DAG = Diacylglycerol, SREBP-1c = Sterol regulatory element-binding transcription factor 1, AMPK = 5' adenosine monophosphate-activated protein kinase, ATP = Adenosine Triphosphate, ADP = Adenosine Monophosphate, PGC-1 α = Peroxisome proliferator-activated receptor Gamma Coactivator 1-alpha. Figure references match document references as follows: [4] - [66], [2] - [71], [3] - [45], [4] - [65], [5] - [67], [6] - [72], [7] - [68], [8] - [69], [9] - [70].

1.9 INDY Proteins – *Vibrio cholerae*

Until now we have been discussing animal INDY homologues, however the focus of this project is the *Vibrio cholerae* homologue, VcINDY. This homologue is arguably the most well characterised DASS family transporter and the only member of the family with known structures, making it an ideal testbed for examining the molecular mechanism of DASS family transport.

Given that *Vibrio cholerae* cells do not contain tissues of intermediary metabolism, it is worth considering what role is played by an INDY homologue a bacterial pathogen. VcINDY is primarily a succinate transporter, with a K_m of $1.0 \pm 0.2 \mu\text{M}$ [73], lower than many of the INDY homologues discussed so far (Table 1.2.3-1). It is, however, unable to transport citrate, and while citrate binding has been observed both functionally and in X-ray crystal structures [73][48][3], this interaction appears to be far lower affinity than succinate binding [73].

VcINDY was recently shown to play a key role in managing the lethality of cholera infections, as modelled in an arthropod host, owing to the importance of succinate for disease-host interactions during infection [74]. During infection, the quorum sensing master regulator HapR oversees a large number of responses within *V. cholerae* [75]. Importantly to us, it greatly reduces the transcription of VcINDY, resulting in a greatly reduced level of *V. cholerae* succinate uptake [74].

This reduction in succinate uptake appears to dramatically improve host survival through the prevention of host succinate depletion (Figure 1.2.3-1). In HapR knockout infections, even when the influence of HapR on biofilm formation has already been abolished through the knockout of *vspA*, host survival is dramatically reduced unless host feed is supplemented with additional succinate. Host gut cells deprived of succinate perform increased rates of lipolysis, depleting host triglyceride stores and hastening host death [74].

Once again, the importance of these high energy Krebs Cycle intermediates for the maintenance of cellular energy levels is highlighted, along with the key role played by INDY homologues in the maintenance of this balance, even in such bacterial systems. Additionally, specific targeting of

VcINDY during infection may represent a novel therapeutic route for the treatment of cholera infections, reducing the lethality of the disease in combination with other treatments.

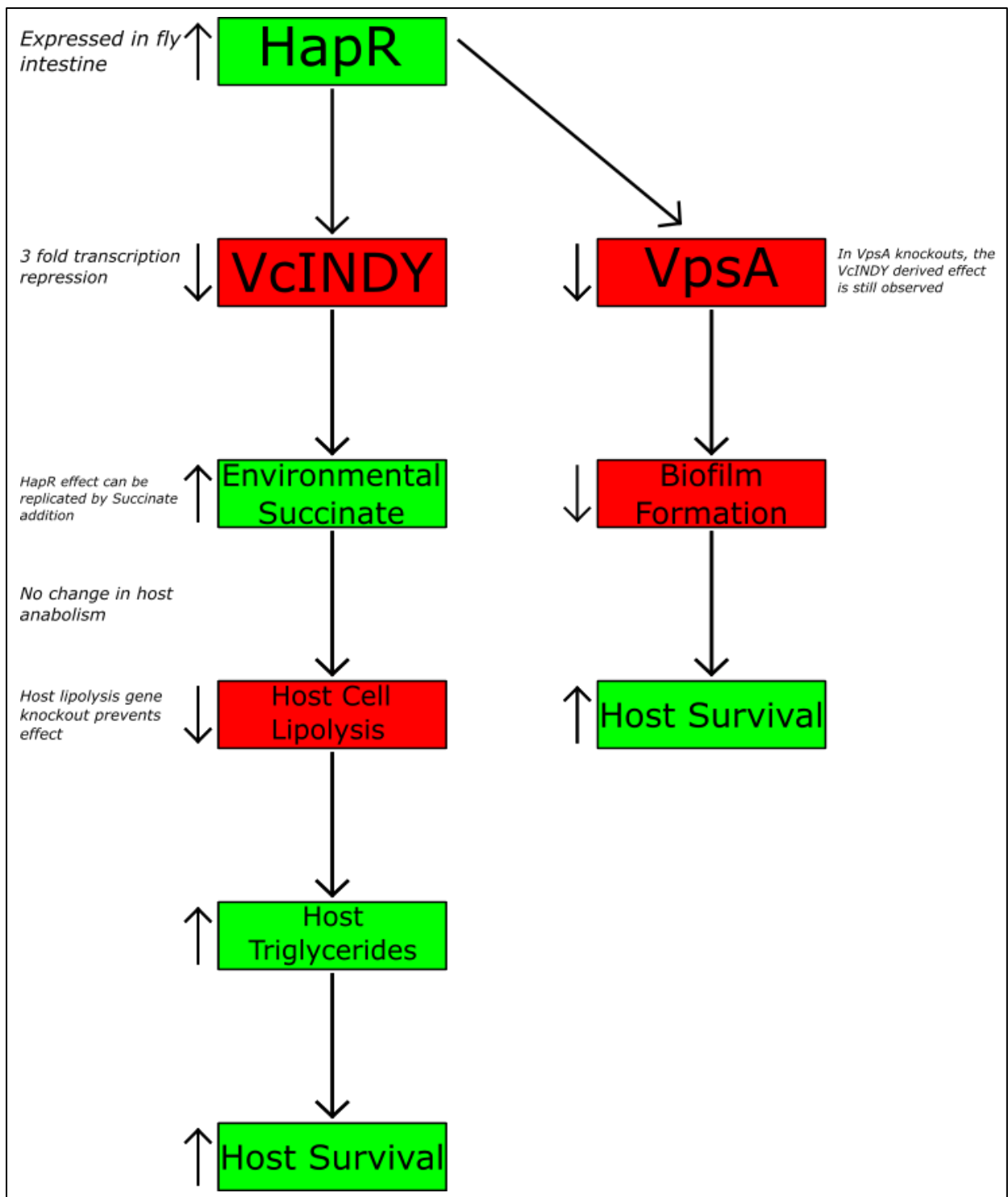


Figure 1.2.3-1 Role of VcINDY in *Vibrio cholerae* infections as elucidated by Kamareddine et al. 2018. During infection of an arthropod host HapR expression is upregulated, resulting in phenotypic changes which suit host gut colonisation, such as biofilm formation through the VpsA pathway. HapR also represses transcription of VcINDY, leading to reduced *V. cholerae* succinate uptake. Reduced succinate uptake maintains host gut succinate levels. If HapR were not to suppress *V. cholerae* succinate uptake this would cause host gut succinate depletion, leading to host cell triglyceride depletion, followed by host death [74].

1.10 VcINDY Molecular Function

VcINDY is a dimeric elevator mechanism sodium coupled secondary active succinate transporter.

1.10.1 Architecture

The structure of VcINDY has been determined through two separate crystallographic studies, both times in the inwards-facing conformation. These studies are largely in agreement, showing VcINDY to be a homodimeric protein, with one anionic binding site per protomer (Figure 1.10.3-1A) [48][3][9][76]. Each protomer consists of two main domains; the scaffold domain and the transport domain. The binding site is mainly contained within the transport domain, with some contacts made to the scaffold domain. Two hairpin regions within the transport domain contribute heavily to the binding site, and these hairpins are a common feature of elevator mechanism transporter structure. It should be noted, however, that the human mINDY, SLC13A5, has been shown to interact with allosteric inhibitors, suggesting the presence of further allosteric binding sites in this family of proteins [77].

1.10.2 Substrate Binding

The binding of anionic substrates is highly charge dependent, with previous work examining the relationship between pH and binding having shown that both succinate and citrate are preferentially bound in their doubly charged states [73], interacting with the two carboxylate binding regions (Figure 1.10.3-1B) [48][3]. The first of these carboxylate binding region consists of the N151 side-chain amide and the T152 side-chain carboxyl, while the second consists of the S377 side-chain hydroxyl, the N378 side-chain amine, and T379 side-chain van der Waals interactions. Due to this focus on the binding of carboxylate regions, with only slight van der Waals interactions with the uncharged backbone of succinate carried out by the T379 side chain, the binding of other similar dicarboxylate molecules is possible; however the exact extent of this binding flexibility is currently unknown [73]. Unlike similar elevator mechanism transporters such as Glt_{Ph} [78], Glt_{Tk} [79], or CitS

[80], this anion binding is achieved without the use of charged binding site residues; instead a combination of polar interactions, oriented helix dipoles, and the positive charge of the co-transported sodium ions themselves are thought to allow the binding of this negatively charged substrate [48][3].

To date only two sodium ion binding sites have been confidently identified, shown by the latest crystal structure to be located behind succinate within the binding pocket so that they likely must enter before succinate is bound (Figure 1.10.3-1A) [48][3]. Sodium 1 is coordinated by the side-chain hydroxyl of S146 and the side-chain carbonyl of N151, along with the main-chain hydroxyls of S146, S150, and G199. Sodium 2 is coordinated by the side-chain hydroxyl of T373 and the side-chain carbonyl of N378, along with the main-chain-carbonyls of T373, A376, and A420. Binding is therefore achieved through the use of pentacoordination sites, a common approach to sodium binding [3].

It should be noted that both of these sodium binding sites had been previously either observed or predicted. A previous, lower resolution, crystal structure demonstrated the presence sodium binding site 1, and correctly predicted the general position of sodium binding site 2 based upon VcINDY's intrinsic structural symmetry (see 1.10.3 Transport) [48].

Additionally, two elevator mechanism transporters of the AbgT family (see 1.2 The Elevator Mechanism – Overview and Classifications), MtrF and YdaH, were shown to have extremely similar architectures to VcINDY, including similarly located substrate binding sites [58]. Comparison of these structures allowed reasonable prediction of the then undiscovered sodium binding site 2, suggesting residues T373, S377, N378, T379, S381, S412, and T421. These residues are in good agreement with the later discovered, and abovementioned, sodium binding site 2, demonstrating the power of this approach.

A third sodium binding site is known to exist, as functional studies based on the electrochemistry of transport have determined that three sodium ions are transported per succinate ion [9], however the location of this site is unknown. The elusive third sodium binding site may remain unfound due

to the inability of current crystal structures to resolve the small region of density which represents the third sodium ion. Alternatively, the third sodium ion simply may not bind to the inwards facing conformation observed in both crystallographic studies, only associating with the protein as it moves into a more occluded state ready for translocation across the membrane.

As with anion binding there is some flexibility in cation binding; it has been observed that lithium ions are capable of facilitating low levels of succinate transport [73], although the molecular details of cation selectivity are currently obscure.

The molecular details of these binding interactions are still poorly elucidated, with major features such as order of binding, binding affinities, and the principles of substrate discrimination still lacking any experimental verification.

1.10.3 Transport

The outwards-facing structure of VcINDY, and therefore the nature of the transport mechanism, was determined through an approach known as repeat-swap homology modelling. Briefly, secondary active transporters often contain inverted repeat architecture, in which large sections of the protein are structurally similar, yet topologically inverted from one another (Figure 1.10.3-1C). These structurally inverted regions often show very little sequence similarity, making them difficult to identify without established protein structures. When these inverted structural repeats are identified, it is possible through computational approaches to swap the conformational arrangements of the inverted repeats. Subtle differences in the structures of each repeat region cause this swapping to result in a new overall protein conformation. After refinement, the new model will represent the inverse orientation to the orientation to the original structure; i.e. if the inward facing structure is initially used, repeat-swap homology modelling will allow an approximation of the outward facing structure to be formed [8].

The application of this approach to VcINDY, along with careful experimental validation, produced a model of the outward facing state which allowed the mechanism of transport to be determined (Figure 1.10.3-1D) [81]. In VcINDY, the alternating access mechanism of transport, whereby access to the binding site alternates between either side of the membrane (see 1.1 The Lipid Bilayer and Transport Proteins), is implemented through the translocation of the binding site across the membrane, along with the entire transport domain in a large rigid body movement [81]. VcINDY is therefore an elevator mechanism transporter (see 1.10.3 Transport).

Currently, very few details are known beyond this basic two state model. We know that substrates bind, the transport domain translocates, substrates release, and the now empty transport domain must translocate back to the start position in order to continue the transport cycle. We do not know whether local conformational changes may occur, how substrates affect the dynamics of this process, or even how the transport of sodium and succinate is coupled to prevent sodium leakage. Furthermore, it is unclear which form of elevator mechanism transport is performed by VcINDY as the movement of gating regions has not yet been identified, preventing the characterisation of this protein as either a One Gate or Two Gate elevator mechanism transporter (see 1.2 The Elevator Mechanism – Overview and Classifications).

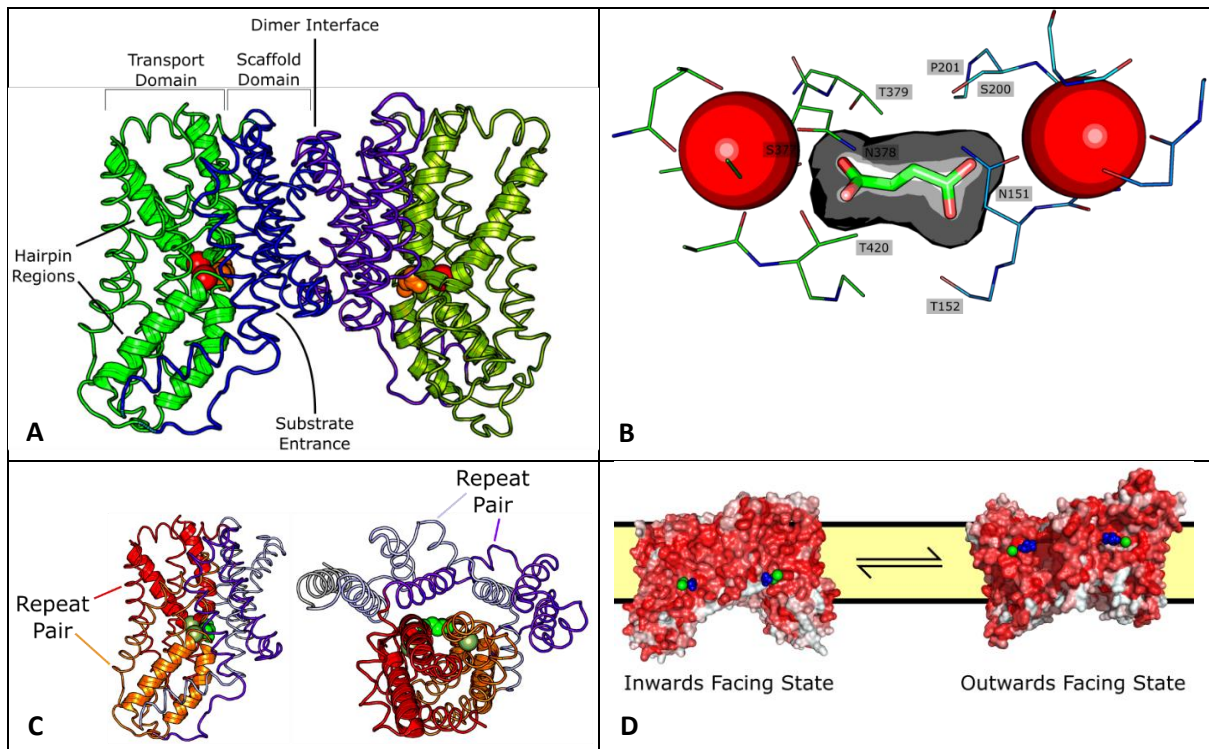


Figure 1.10.3-1 VcINDY Structure. A: Architecture of VcINDY. Domains and protomers are differently coloured for clarity.

The peptide backbone is shown as a ribbon, and the hairpin regions responsible for forming much of the binding sites are shown in cartoon form. Sodium ions are shown in blue, and succinate in orange. Structure PDB ID 5ul7. B: Succinate binding site, with nearby residues labelled. VcINDY's succinate interactions are mainly mediated by two carboxylate binding regions as shown. Bound sodium ions are shown as red spheres. Bound succinate is shown through bold stick representation with its surface area represented in grey. Protein residues are shown as thin sticks, with the two carboxylate binding regions coloured green and blue. Structure PDB ID 5ul7. C: Inverted repeat architecture of a single VcINDY protomer. Two sets of inverted structural repeats form a VcINDY protomer, shown by colour here. A protomer is displayed "side on" and from the extracellular side of the membrane. Purple / violet = Scaffold domain inverted repeat. Red / orange = transport domain inverted repeat. D: Comparison of Inward and Outward facing states for VcINDY with roughly approximated membrane position. Substrates are not visible from this angle, however their positions have been superimposed on the structure for clarity. Colours; Red = Hydrophobic residue, White = Hydrophilic residue, Blue = Succinate (IFS) or Citrate (OFS), Green = Sodium. IFS Structure PDB ID 5ul7. OFS model from Mulligan et al 2016 [81].

1.11 Insights Into VcINDY Function Provided by Study of Other Elevator Mechanism

Transporters

The DASS family, of which VcINDY is a member, is poorly characterised, especially in comparison to the extensively studied SLC1 family (Figure 1.2.3-1A). As such, comparisons to better characterised elevator mechanism transporters such as CitS and GlT_{Ph} will occur frequently throughout this thesis. Based on comparisons with other elevator mechanism transporters, some speculation can be performed before experimentation begins.

Firstly, speculation as to transport mechanism. Currently all known Two Gate elevators position their substrate binding sites at the interface between scaffold and transport domains, while all One Gate elevators contain the binding site fully within the transport domain [15]. VcINDY positions its binding site at the interface between domains, indicating that VcINDY is likely to be a Two Gate mechanism transporter. As there appears to be no barrier movement in current VcINDY structures (see 1.2 The Elevator Mechanism – Overview and Classifications) this would suggest VcINDY to be a Fixed Barrier Two Gate elevator mechanism transporter.

Secondly, speculation as to lipid interactions. These interactions have been studied little for elevator mechanism transporters, especially outside the SLC1 family, and not at all for VcINDY. What little is known, however, suggests a major role for lipids in the transport cycle (see 1.3 The Elevator Mechanism – The Importance of Lipids). Given that the SLC1 and DASS family must both achieve transport in similar lipid environments using similar elevator mechanisms, it appears likely that they must both undertake some level of lipid interaction in order to achieve transport function. Thus, while details are scarce, it can at least be predicted that VcINDY will have some major lipid interactions throughout its transport cycle.

Thirdly, speculation as to the applicability of VcINDY study to the wider DASS family, and therefore to the function of the human mINDY / SLC13A5. For each family in which the form of elevator mechanism transport has been categorised thus far, the major functional mechanisms have been

consistent between members; i.e. the number of gating regions used and the nature of the barrier regions do not vary within families (Figure 1.2.3-1A) [15]. While exceptions to this pattern will likely emerge in time as the diversities of different protein families is further explored, it does at least lend confidence that major mechanistic features of VcINDY will be applicable to the medically important SLC13A5, greatly increasing the importance of this work.

1.12 Aims of this work

This work will apply a diverse range of techniques to the examination of VcINDY *in vitro* in an attempt to gain a deeper understanding of its mechanism, and in doing so provide a basis by which other members of the DASS family may be understood.

In order to do this, three general approaches shall be utilised.

Firstly, accessibility assays shall be employed to probe the dynamics of the elevator motions of VcINDY. By focusing on residues which are only solvent accessible in either the inward- or outward-facing conformation of the protein it will be possible to detect the conformational preferences of the protein in the absence and presence of substrates. Additionally, these assays will allow detection of local conformational responses in addition to the large rigid body translocation expected, possibly providing further insights as to the movements of this transporter.

Secondly a range of binding assays shall be applied to VcINDY. As previously mentioned, no binding assay has yet been established for VcINDY. Previous work has largely relied upon transport measurements, where the processes of substrate binding, translocation, and substrate release are interwoven. Specialised binding assays will allow the isolation and examination of the binding process itself. These assays will include high throughput approaches, allowing extensive characterisation of binding interactions, assays with high tolerance of additives, allowing the effects of lipid supplementation to be probed, and high precision assays, allowing binding affinities to be confidently established for the first time.

Finally, the role of lipids shall be examined. This shall be examined partially through the lipid supplementation of detergent solubilised protein, providing a simple system in which the exploration of lipid interactions can be carried out. Additionally, two different nanodisc systems shall be applied to VcINDY, one allowing the creation of native lipid nanodiscs and the other allowing the creation of defined lipid nanodiscs. These nanodiscs shall form the basis of new experimental systems in which multiple aspects of VcINDY lipid interaction can be examined in detail.

Through these approaches it is hoped that a far more detailed picture of VcINDY's molecular function may be established, both increasing the current knowledge of this particular transporter, and informing future study of the medically relevant human members of the DASS family.

2 METHODS

2.1 Strains and Plasmids

Bacterial strains and plasmids used are summarised in Table 1.10.3-1

Bacterial Strain	Species	Genotype	Source and Catalogue Number
BL21-AI	<i>E. coli</i>	$F^- ompT hsdS_B (r_B^-, m_B^-) gal dcm araB::T7RNAP-tetA$	ThermoFisher C607003
BL21(DE3)	<i>E. coli</i>	$fhuA2 [lon] ompT gal (\lambda DE3) [dcm] \Delta hsdS$ $\lambda DE3 = \lambda sBamHI \Delta EcoRI-B int::(lacI::PlacUV5::T7 gene1) i21 \Delta nin5$	ThermoFisher EC0114
Lemo21	<i>E. coli</i>	$fhuA2 [lon] ompT gal (\lambda DE3) [dcm] \Delta hsdS/$ pLemo(CamR) $\lambda DE3 = \lambda sBamHI \Delta EcoRI-B$ $int::(lacI::PlacUV5::T7 gene1) i21 \Delta nin5$ pLemo = pACYC184-PrhaBAD-lysY	New England Biolabs C2528J
NEB Turbo	<i>E. coli</i>	$F' proA+B+ lacIq \Delta lacZM15 / fhuA2 \Delta(lac-proAB)$ glnV galK16 galE15 R(zgb-210::Tn10)TetS endA1 thi-1 $\Delta(hsdS-mcrB)5$	New England Biolabs C2984H

Table 1.10.3-1 Bacterial strains used in this thesis.

2.2 Media and Antibiotics

2.2.1 Lysogeny Broth (LB)

LB broth was made using 10 g tryptone, 5 g yeast extract, and 10 g NaCl per litre. It was autoclaved as a completed broth.

2.2.2 SOC Broth

SOB broth was made using 20 g tryptone, 5 g yeast extract, 0.58 g NaCl, 0.2 g KCl, 2 g MgCl₂, 2.4 g MgSO₄ per litre, adjusted to pH 7.5 using NaOH, and autoclaved. 1 M glucose was separately prepared and autoclaved. 2 % v/v glucose solution was added to the SOB broth to produce SOC broth.

2.2.3 PASM5052 Broth

PASM5052 was made according to the MemStar system [82]. The following component solutions were used; MgSO₄ (1 M MgSO₄, filter sterilised), 20x NPS (100 mM PO₄, 25mM SO₄, 50 mM NH₄, 100 mM Na, 50 mM K, filter sterilised), 50x 5052 (0.5% glycerol, 0.05% glucose, 0.2% lactose, filter sterilised), 1000x trace metals (0.1 M FeCl₃, 1 M CaCl₂, 1 M MnCl₂, 1 M ZnSO₄, 0.2 M CoCl₂, 0.1 M CuCl₂, 0.1 M NiCl₂, 0.1 M Na₂MoO₄, 0.1 M Na₂SeO₃, 0.1 MH₃BO₃, 50 mM HCl, all components added from individual pre-autoclaved stocks), B₁₂ (100 µM Vitamin B₁₂, autoclaved), 17aa (1% w/v glutamic acid monosodium salt, aspartic acid, lysine monohydrochloride, arginine monohydrochloride, histidine monohydrochloride monohydrate, alanine, proline, glycine, threonine, serine, glutamine, asparagine, valine, leucine, isoleucine, phenylalanine, tryptophan, dissolved in this order and filter sterilised), methionine (25 mg/ml methionine, autoclaved). On the day of use, the following volumes of these solutions were added to 900 ml of autoclaved dH₂O; 2 ml MgSO₄, 0.2 ml 1000x trace metals, 20 ml 50x 5052, 50 ml 20x NPS, 1 ml B₁₂, 20 ml 17aa, 20 ml methionine.

2.2.4 MDA5052 Broth

The following component solutions were used; MgSO₄ (1 M MgSO₄, filter sterilised), 50x 5052 (0.5% glycerol, 0.05% glucose, 0.2% lactose, filter sterilised), 20x M (50 mM PO₄, 50 mM NH₄Cl, 5mM Na₂SO₄, filter sterilised), 1000x trace metals (0.1 M FeCl₃, 1 M CaCl₂, 1 M MnCl₂, 1 M ZnSO₄, 0.2 M CoCl₂, 0.1 M CuCl₂, 0.1 M NiCl₂, 0.1 M Na₂MoO₄, 0.1 M Na₂SeO₃, 0.1 M H₃BO₃, 50 mM HCl, all components added from individual pre-autoclaved stocks), 17aa (1% w/v glutamic acid monosodium salt, aspartic acid, lysine monohydrochloride, arginine monohydrochloride, histidine monohydrochloride monohydrate, alanine, proline, glycine, threonine, serine, glutamine, asparagine, valine, leucine, isoleucine, phenylalanine, tryptophan, dissolved in this order and filter sterilised), methionine (25 mg/ml methionine, autoclaved), 18aa (70% v/v 17 aa, 30 % v/v methionine), 25% aspartate (25% w/v aspartate, 8% w/v NaOH volume, pH adjusted to pH 7, filter sterilised). On the day of use the following volumes of these solutions were added to 900 ml of autoclaved dH₂O; 2 ml MgSO₄, 0.2 ml 1000x trace metals, 20 ml 50x 5052, 40 ml 25x M, 20 ml 18 AA, 4 mL 25% aspartate.

2.2.5 2YT Broth

2YT broth was made using 16 g tryptone, 10 g yeast extract, and 5 g NaCl per litre. It was autoclaved as a complete broth.

2.2.6 TB Broth

TB broth was made using 12 g tryptone, 24g yeast extract, and 5g glycerol per litre, made up to 90% volume with dH₂O and autoclaved. 20 ml 1M KH₂PO₄ and 80 ml 1M K₂HPO₄ per litre were filter sterilised and added to form the final broth.

2.2.7 Solid Media

Agar plates were made by mixing liquid media with 15 g agar per litre before autoclaving.

2.2.8 Antibiotics

The following 1000x stock solutions were filter sterilised and added to broth and solid media at 0.1 % v/v when required; 50 mg/ml Kanamycin in dH₂O, 100 mg/mL Ampicillin in dH₂O, and 25 mg/mL Chloramphenicol in ethanol.

2.3 Production of Styrene Maleic Acid from Styrene Maleic Anhydride - Reflux

Styrene Maleic Acid (SMA) was produced through the hydrolysis of Styrene Maleic Anhydride as detailed by *S. Lee et al 2016* [83]. 25 g of Styrene Maleic Anhydride copolymer was transferred to a 500 mL round bottomed flask and dissolved in 250 mL 1M NaOH. 0.5 g of anti-bumping granules were added before heating the solution under reflux at a steady boil for 2 hours, then allowing the solution to cool whilst still under reflux. The refluxed polymer was then transferred into two 400 mL polypropylene centrifuge tubes. Concentrated HCl was gradually added, causing precipitation of the polymer, until the pH of the solution reached <5. The tubes were then filled to 400 mL using ddH₂O and centrifuged at 11,000 xg for 15 minutes at room temperature. The supernatant was then discarded. The pellet was resuspended in ddH₂O and re-pelleted through centrifugation three times in order to thoroughly wash the polymer. In the same centrifuge tube, 125 mL 0.6 M NaOH was added and the pellet dissolved either using a magnetic stirrer, or a shaking incubator at 37°C 180 rpm. Once resuspended concentrated HCl was again added gradually until a pH <5 was reached and precipitation was observed. Water was added up to the capacity of the centrifuge tubes and the pelleting/ddH₂O resuspension/pelleting cycle washing cycle repeated three more times. Finally the polymer was re-dissolved in 0.6 M NaOH and adjusted to a pH of ~ 8 using NaOH and HCl. The solution was transferred to a 1 L round bottom flask, frozen at -80°C overnight, and freeze dried.

2.4 Production of Styrene Maleic Acid from Styrene Maleic Anhydride – Autoclave

Styrene Maleic Acid (SMA) was produced through the hydrolysis of Styrene Maleic Anhydride in an approach derived from *A Kopf et al 2019* [84]. 1 g of Styrene Maleic Anhydride copolymer was dissolved in 10 ml of dH₂O along with 1 molar equivalent of NaOH and transferred to a duran bottle. This was placed in a standard benchtop autoclave for three runs. Between runs the pH was recorded, with a reduction of pH indicating that hydrolysis was occurring. If the pH became acidic before the final run, additional NaOH was added to return weakly alkaline conditions. The solution was mixed well between runs, breaking up any residue adhered to the bottle. After three runs the solution was allowed to cool to room temperature. SMA was precipitated through the cautious addition of 4 mL 1M HCl and pelleted through centrifugation at 4000 xg for 10 minutes. The pellet was washed through two cycles of resuspension in 15 mL 10 mM HCl and pelleting, followed by resuspension in 15 mL H₂O and pelleting. The polymer was resuspended in 10 mL dH₂O and made soluble through adjustment of the pH to 8 with NaCl. The resultant solution was frozen overnight at -80 °C and freeze dried.

2.5 General Plasmid Handling

2.5.1 Plasmid Amplification and Storage

NEB Turbo cells were used for plasmid amplification and storage. A single colony containing the plasmid of interest was used to inoculate a 5 ml LB containing the appropriate antibiotic and grown at 37 °C 190 rpm overnight. The next day 0.6 ml of culture was mixed with 0.4 ml 50% glycerol and stored at -80°C. When needed, cells could be aseptically scrapped from the frozen sample and used to inoculate a new 5 mL overnight culture without defrosting the frozen stock.

2.5.2 Plasmid Harvesting

Plasmids were harvested using standard QIAGEN QIAprep Spin Miniprep Kits and stored at -20°C.

2.5.3 Transformation of Non-competent Cells

For non-competent BL21-AI, BL21(DE3), and NEB-Turbo cells a low efficiency freeze-thaw transformation method could be used for the introduction of plasmid DNA from high concentration stocks. A 5 ml LB culture was grown overnight at 37 °C 190 rpm with the appropriate antibiotic content for plasmid maintenance, of which 500 µl was used to inoculate a 5 ml LB day culture. This was grown for 1h at 37°C 190 rpm before harvesting by centrifugation at 4000 rpm for 10 minutes. Cell pellets were resuspended in 600 µl ice cold 50 mM CaCl₂, divided into 6 x 100 µl aliquots and kept on ice. 100 ng plasmid DNA, ideally in a volume of approximately 1 µl, was added to each aliquot to be transformed and the vortexed. Cells were snap frozen using a dry-ice/ethanol mixture for 1.5 minutes, then thawed at 37 °C for 2 minutes. 200 µl SOC was added and the cells incubated for 1 hour at 37 °C 190 rpm before plating on pre-warmed selective LB agar plates containing the appropriate antibiotic. Cells were allowed to grow overnight at 37 °C.

Lemo21(DE3) cells were transformed similarly, but with the addition of 25 µg/ml Chloramphenicol in all growth media.

2.5.4 Transformation of Competent Cells

For competent cells a simpler heat shock transformation method could be used. An aliquot of competent cells were allowed to thaw on ice, and 1-2 µl DNA (either plasmid or ligation reaction) was added. This was mixed through pipetting and incubated on ice for 30 minutes before a 1.5 minute heat shock at 42 °C. 200 µl SOC was added and the cells incubated at 37 °C for one hour before plating on pre-warmed selective LB agar plates containing the appropriate antibiotic. Cells were allowed to grow overnight at 37 °C.

2.6 Expression and Purification of VcINDY

2.6.1 Expression of VcINDY

n.b. Volumes can vary between expressions depending on purpose, but a typical example is used below.

2.6.1.1 BL21AI / LB Expression

5 ml LB containing 50 µg/ml Kanamycin was inoculated with BL21-AI cells containing the plasmid of interest and grown overnight at 37 °C 190 rpm. All 5 ml was used to inoculate a 150 ml secondary LB-Kan culture, which was then grown for 2-4 h at 37 °C. Six 500 ml LB-Kan cultures were inoculated with 10 ml secondary culture and grown until $OD_{600} \approx 0.8$. Flasks were cold shocked in ice water for 20 minutes, before inducing with 0.1 mM IPTG and 0.1% L-arabinose, followed by incubation overnight at 19 °C. OD_{600} readings were used in morning to confirm expression as VcINDY over-expression is bacteriostatic under these conditions.

2.6.1.2 PASM5052 / Lemo21(DE3) Expression

VcINDY was expressed using the MemStar system [82]. 150 ml LB containing 50 µg/ml Kanamycin and 25 µg/ml Chloramphenicol were inoculated with Lemo21(DE3) cells containing the plasmid of interest and grown overnight at 37 °C 190 rpm. 1 L of freshly prepared modified PASM5052 media [85] containing 50µg/ml Kanamycin, 25 µg/ml Chloramphenicol, and 0.25mM L-Rhamnose was inoculated with 20 mL of the overnight culture. Cultures were grown at 37 °C 190 rpm until $OD_{600} \approx 0.5$, at which point expression was induced beyond the auto-induction occurring within the media through the addition of 0.4 mM IPTG before overnight incubation at 25 °C 190 rpm.

2.6.1.3 MDA5052 / Lemo21(DE3) Expression

VcINDY was expressed using the MemStar system [82]. 150 ml LB containing 100 µg/ml Kanamycin and 25 µg/ml Chloramphenicol were inoculated with Lemo21(DE3) cells containing the plasmid of interest and grown overnight at 30 °C 190 rpm. 1 L of freshly prepared modified MDA5052 media containing 100µg/ml Kanamycin, 25 µg/ml Chloramphenicol, and 0.25mM L-Rhamnose was inoculated with 20 mL of the overnight culture. Cultures were grown at 37 °C 220 rpm in 2.5 L Tunair full baffle shake flasks with filter caps until $OD_{600} \approx 0.5$, at which point expression was induced beyond the auto-induction occurring within the media through the addition of 0.4 mM IPTG before overnight incubation at 25 °C 190 rpm.

2.6.2 Preparation of VcINDY containing Total Membrane Extracts

Cells were harvested through centrifugation at 4000 xg for 20 minutes at 4 °C and resuspended in 16.6 mL INDY Lysis Buffer (50 mM Tris pH 7.5, 200 mM NaCl, 10 % glycerol) per litre of original culture and per OD_{600} unit of original culture, with protease inhibitors (1 mg/mL Pefabloc / 4-(2-Aminoethyl)-benzenesulfonyl fluoride hydrochloride (AEBSF), 0.05 mg/ml Leupeptin) and 1 mg/mL DNase I, plus 0.5 mM TCEP for Cysteine mutants. Lysis was achieved using either cell disruption at 25 kPSI, or sonication for 3 seconds on and 7 seconds off over 10 minutes. Lysate was clarified through centrifugation at 21,000 xg for 20 minutes at 4 °C and the pellet discarded. Membranes were pelleted through centrifugation at 130,000 xg for 2 hours at 4 °C and the supernatant discarded.

2.6.3 Solubilisation of VcINDY (Detergent)

n.b. For Cysteine mutants, all solutions contained 0.5 mM TCEP.

Membranes were resuspended in Buffer A (50 mM Tris pH 8, 100 mM NaCl, 5% glycerol) and homogenised using a glass tissue homogeniser. Once homogenised, membrane samples were made

up to a final volume of 50 mL for every 3 L of original cell culture, with the addition of DDM to a final concentration of 3%. Samples were solubilised for 40 minutes at 4 °C with agitation, after which insoluble material was removed through centrifugation at 120,000 xg for 30 minutes and the pellet discarded.

2.6.4 Cobalt Affinity Purification (Detergent)

Due to the high levels of purity achievable using cobalt affinity purification, his-tagged VcINDY was purified using Clontech TALON Metal Affinity Resin. For every 3 L of original culture 300 µL of resin was incubated with the solubilised membrane fraction overnight at 4 °C. The mixture was added to a gravity flow column, retaining the VcINDY bound talon resin and allowing the flow-through to be collected. The resin was then washed with 20 CV (column volumes) Wash Buffer 1 (Buffer A + 10 mM Imidazole + 0.1% DDM), followed by 20 CV Wash Buffer 2 (Buffer A + 20 mM Imidazole + 0.1% DDM).

Due to the positioning of a trypsin cut site between VcINDY and the his-tag in our construct it is possible to elute through a 1 h incubation at 4 °C with 1.5 ml Elution Buffer 1 (Buffer A + 10 µg/ml Trypsin + 0.1% DDM), and wash with 1.5 ml Elution Buffer 2 (Buffer A + 0.1% DDM). This trypsin elution provides high purity tag free samples.

If the his-tag is required for future experiments elution is instead achieved through replacing the trypsin component of Elution Buffer 1 with 400 mM Imidazole (pH 8).

2.6.5 Solubilisation of VcINDY (SMALPs)

Membranes were resuspended in Buffer A (50 mM Tris pH 8, 100 mM NaCl, 5% glycerol) and homogenised using a glass tissue homogeniser. Once homogenised membrane samples were made up to a final volume of 50 ml for every 3 L of original cell culture, with the addition of either 2:1 or 3:1 SMA to a final concentration of 3%. Samples were solubilised for one hour at room temperature

with agitation, after which insoluble material was removed through centrifugation at 120,000 xg for 30 minutes and the pellet discarded.

2.6.6 Cobalt Affinity Purification (SMALPs)

For every 3 L of original culture 300 µL of resin was incubated with the solubilised membrane fraction overnight at 4 °C. The mixture was added to a gravity flow column, retaining the VcINDY bound talon resin and allowing the flow-through to be collected. The resin was then washed with 40 CV (column volumes) Wash Buffer (Buffer A + 5mM Imidazole).

For trypsin elution the resin is incubated for one hour at 4 °C with 1.5 ml Elution Buffer 1 (Buffer A + 10 µg/ml Trypsin), eluted and washed with 1.5 ml Elution Buffer 2 (Buffer A). This trypsin elution provides high purity tag free samples.

If the his-tag is required for future experiments elution is instead achieved through replacing the trypsin component of Elution Buffer 1 with 400 mM Imidazole (pH 8) in Elution Buffer 1. Increased yields could be achieved by rebinding the flow-through to the resin overnight and repeating the purification process two more times.

2.7 Expression and Purification of TEV Protease

2.7.1 Expression of TEV Protease

n.b. Volumes can vary between expressions depending on purpose, but a typical example is used below.

A 100 mL LB culture containing 100 µg/ml ampicillin was inoculated with BL21(DE3) cells containing the plasmid pRK793 (Addgene plasmid # 8827 ; <http://n2t.net/addgene:8827> ; RRID:Addgene_8827) and grown overnight at 37 °C 190 rpm [86]. 10 mL of overnight culture was used to inoculate each 1 L LB culture containing 100 µg/ml ampicillin. These were grown at 37 °C 190 rpm until $OD_{600} \approx 0.5$, at which point expression was induced through the addition of 0.4 mM IPTG before overnight incubation under the same conditions.

2.7.2 Purification of TEV protease

Cells were harvested through centrifugation at 4000 xg for 20 minutes at 4°C and resuspended in 15 mL TEV Lysis Buffer (20 mM Tris pH 7.4, 300 mM NaCl, 10% glycerol) per litre of original culture, with protease inhibitors (1 mg/mL Pefabloc, 0.05 mg/mL Leupeptin) and 1 mg/mL DNase I. Lysis was achieved through sonication for 3 seconds on and 7 seconds off over 10 minutes. Lysate was clarified through centrifugation at 10,000 xg for 20 minutes at 4 °C and the pellet discarded. Imidazole was added to the supernatant to a final concentration of 20 mM along with 1 mL nickel resin per litre of original culture before incubation at 4 °C with agitation for 30 minutes. The mixture was added to a gravity flow column, retaining the TEV bound nickel resin and allowing the flow-through to be collected. The resin was then washed with 20 CV (column volumes) of TEV Purification Buffer (20 mM Tris pH 7.4, 300 mM NaCl, 20% glycerol) + 50 mM imidazole, followed by elution with 1 CV additions of TEV Purification Buffer + 250 mM imidazole until $A_{280} \leq 0.2$. Elution samples were pooled and dialysed overnight against a 250 fold greater volume of TEV Dialysis Buffer (20 mM Tris pH 7.4,

300 mM NaCl, 5 mM DTT, 30 % glycerol). Final concentration was estimated through Coomassie Blue gel staining alongside known BSA standards. Aliquots were created and stored at -80°C.

2.8 Expression and Purification of MSP1E3D1

2.8.1 Expression of MSP1E3D1

n.b. Volumes can vary between expressions depending on purpose, but a typical example is used below.

A 30 mL LB culture containing 30 µg/ml kanamycin was inoculated with BL21(DE3) cells containing the plasmid pMSP1E3D1 (Addgene plasmid # 20066 ; <http://n2t.net/addgene:20066> ; RRID:Addgene_20066) and grown overnight at 37 °C 190 rpm [87]. 30 mL of overnight culture was used to inoculate each 1 L TB culture containing 30 µg/ml kanamycin. These were grown at 37 °C 220 rpm in 2.5 L Tunair full baffle shake flasks with filter caps until OD₆₀₀ ≈ 2.2 – 2.5, at which point expression was induced through the addition of 1 mM IPTG, followed by 4 hours expression under the same conditions.

2.8.2 Purification of MSP1E3D1

Cells were harvested through centrifugation at 4000 xg for 20 minutes at 4°C pellet frozen overnight. Pellets were then thawed and resuspended in 30 mL MSP Lysis Buffer (20 mM NaPhosphate pH 8, 1% Triton-X-100) per litre of original culture, with protease inhibitors (1 mg/ml? Perfabloc, 0.05 mg/mL Leupeptin) and 1 mg/mL DNase I. Lysis was achieved through sonication for 3 seconds on and 7 seconds off over 10 minutes. Lysate was clarified through centrifugation at 22,000 xg for 30 minutes and the pellet discarded. 1 mL of nickle resin was added per litre of original culture before incubation at 4 °C with agitation overnight. The mixture was added to a gravity flow column, retaining the MSP1E3D1 bound nickel resin and allowing the flow-through to be collected. The resin was then washed with 4 column volumes (CV) of MSP Purification Buffer (40mM Tris-HCl pH8, 300 mM NaCl) + 1% Triton-X-100, followed by 4 CV MSP Purification Buffer + 50 mM NaCholate, 4 CV MSP Purification Buffer + 20 mM Imidazole, 4 CV MSP Purification Buffer + 50 mM Imidazole, and 8 ½ CV fractions of MSP Purification Buffer + 300 mM Imidazole. Fractions are pooled and dialysed overnight against a 500 fold greater volume of MSP Dialysis Buffer (50mM Tris-HCl pH7.5,100mM

NaCl, 0.5 mM EDTA). Final concentration was estimated through A_{280} readings. Aliquots were created and stored at -80°C .

2.9 Creation of VcINDY Nanodiscs

This process is not yet fully optimised and as such a general method cannot be given. For a discussion of approaches and the progress made thus far see (3.2.5 Optimisation of the Reconstitution of VcINDY into MSP1E3D1 Based Nanodiscs)

2.10 Protein Handling

2.10.1 Concentration Determination

Extinction coefficients and molecular weights were estimated using the ProtParam tool found upon the ExPASy server [88]. The absorbance of protein solutions at 280 nm were measured using a spectrophotometer and used to estimate concentration according to the Beer-Lambert law.

2.10.2 Concentration of Protein Samples

Protein samples were concentrated using Pierce™ Protein Concentrators PES, 100 K MWCO or 10 K MWCO, 2-6 mL when required according to manufacturer's instructions.

2.10.3 Buffer Exchange of Protein Samples

2.10.3.1 Desalting Columns

For volumes of < 1 mL Thermo Scientific™ Zeba™ Spin Desalting Columns, 7K MWCO, were used according to manufacturer's instructions.

2.10.3.2 Dialysis

Larger volume protein samples were loaded into 10K MWCO Thermo Scientific™ SnakeSkin™ Dialysis Tubing and stirred overnight at 4 °C in a 5000 x greater volume of the desired buffer unless specified otherwise.

2.10.3.3 On Column Exchange

Buffer exchange could also be achieved during the purification process by changing the wash buffer 2 and elution buffer composition, allowing the protein to be purified into any buffer required.

2.10.3.4 Storage

In order to avoid sample damage arising from freeze thaw cycles, protein samples were typically aliquoted into volumes ranging from 10 to 100 μL and snap frozen in a mixture of dry ice and ethanol before storage at $-80\text{ }^{\circ}\text{C}$. Samples were used on the same day as thawing and not refrozen.

2.11 Size Exclusion Chromatography

An ÄKTA Pure protein purification system with a Superdex® 200 10/300 GL column was used for size exclusion chromatography, allowing high level purification of protein samples and assessment of the homogeneity of purified proteins through examination of the in line A₂₈₀ trace.

2.11.1 Buffer Preparation

All solutions to be run through the SEC column were made using ddH₂O. Filtering and degassing of solutions was achieved by attaching *Nalgene™ Rapid-Flow™ Sterile Disposable Bottle Top Filters with SFCA Membranes* to Duran bottles containing a magnetic stirrer atop a magnetic stirring plate at 4 °C. A pump was attached to the filter top in order to draw buffers through the filter and lower air pressure inside the bottle. Once filtered, buffers would be stirred for approximately thirty minutes under this reduced pressure in order to remove dissolved gasses. Detergents were gently mixed into buffers *after* the degassing process.

2.11.2 Column Preparation and Storage

All runs used a pre-column pressure alarm of 2.0 MPa to prevent damage to the column. The SEC column was stored in 20% ethanol. Before use the column was first equilibrated into ddH₂O using a volume of 50 mL at a flow rate of 0.25 mL/min, followed by equilibration into the desired running buffer using a volume of 50 mL at a flow rate of 0.5 mL/min. When transitioning from detergent containing buffers to non-detergent containing buffers an additional wash step of 500 mL ddH₂O at 0.5 mL/min was used in order to remove residual detergent from the column before equilibration into the desired non-detergent containing buffer. Before storage the column was first equilibrated into ddH₂O using a volume of 50 mL at a flow rate of 0.5 mL/min, followed by equilibration into 20% ethanol using a volume of 50 mL at a flow rate of 0.25 mL/min for storage.

2.11.3 Sample Preparation

Protein samples were concentrated to < 1 ml and centrifuged at 140,000 xg 4 °C for 20 minutes to remove potential aggregates before running on the SEC column.

2.11.4 Running Samples

Unless stated otherwise SEC Buffer (25 mM Tris pH 8, 100 mM NaCl, 5% Glycerol) containing an additional 0.15% n-decyl- β -D-maltoside (DM) for detergent solubilised samples was used. With the column pre-equilibrated into SEC buffer, samples were manually loaded into a 1 mL sample loop. At a flow rate of 0.5 mL/min 5mL of SEC Buffer was used to wash the sample fully onto the column, followed by 35 mL to achieve elution. This process was monitored through in line A_{280} readings. 1 mL fractions were collected. Fractions containing the protein of interest could be pooled post-run and concentrated to produce a useful high purity sample.

2.12 Protein Gels

2.12.1 SDS-PAGE

SDS-PAGE Gels:

SDS-PAGE gels were made according to the following recipe:

	Resolving	Stacking
30% (w/v) acrylamide/0.8% (w/v) bisacrylamide	2.65 mL	0.65 mL
1.875M Tris pH 8.8	1 mL	0
1M Tris pH 6.8	0	0.625 mL
10% SDS	50µl	50µl
H ₂ O	1.45 mL	3.675 mL
10% APS	50 µL	50 µL
TEMED	5 µL	5 µL

Table 2.12.1-1 Components of the SDS-PAGE gels used in this thesis.

Protein samples were mixed in a 3:1 ratio with 4 x SDS-PAGE sample buffer (50 mM Tris pH 7.2, 5% SDS, 0.4% bromophenol blue, 40% glycerol). VcINDY samples were loaded without boiling due to the fragile nature of this protein. Other protein samples were heated to 95 °C for 10 minutes prior to loading. SDS-PAGE gels were run at 180 V for one hour in SDS-PAGE running buffer (3% Tris, 15% glycine, 1 % SDS).

2.12.2 Coomassie Blue Staining

Gels were stained with agitation either for one hour or overnight in Coomassie Blue Stain (40% methanol, 8% acetic acid, 0.2% Coomassie Brilliant Blue R-250), and destained with agitation in destain solution (10% ethanol, 10% acetic acid) until protein bands became clearly visible, before transfer to water and imaging.

2.12.3 Western Blotting

PVDF membrane was activated through soaking in methanol, followed by five minutes soaking in transfer buffer (0.2 M glycine, 10 % methanol, 40 mM Tris pH 8.3) along with blotting paper and the gel itself. Transfer was carried out using a semi-dry blotting system at 9V for 20 minutes.

Once transfer was complete, the membrane was blocked through a one hour incubation with 5 % milk powder TBST (20 mM Tris, 14 mM NaCl, 0.1 % Tween 20, final solution adjusted to pH 7.6 with HCl) and incubated with a primary tetrahis antibody (Qiagen tetrahis antibody) in primary hybridation buffer (0.05 % tetrahis antibody, 1% milk powder, 1 x TBST) with agitation at 4 °C overnight.

Next morning the membrane was washed with TBST for 1 x 15 minutes and 2 x 5 minutes. Secondary antibody binding was achieved through incubation in secondary hybridation buffer (0.02 % Promega Goat Anti-Mouse IgG Polyclonal Antibody (HRP (Horseradish Peroxidase))), 1% milk powder, 1 x TBST) for one hour, followed by washing with TBST for 1 x 15 minute and 6 x 5 minute. Blots were visualised in a Bio-Rad ChemiDoc™ XRS+ system using the Pierce supersignal ECL kit following manufacturer's instructions.

2.12.4 Densitometry

Densitometry was carried out using the ImageJ [89] image analysis software.

2.13 PEGylation Assay

2.13.1 Experimental Procedure

Zeba™ Spin Desalting Columns, 7K MWCO, 0.5 mL were used to desalt protein samples into Conjugation Buffer (50 mM Tris pH 7, 5% Glycerol) containing 0.15% DM for detergent solubilised samples before use. Typical 50 µL reaction mixtures contained 0.5 mg/mL VcINDY mutant, 5% glycerol, 50 mM Tris pH 7, 150 mM of either NaCl or KCl, any substrate of interest, and 0.15% DM for detergent solubilised samples. Reactions were started by the addition of 0.4 mM mPEG5K and fractions of the reaction mixture were quenched at set timepoints through by mixing with Quench Buffer (100 mM methyl-MTS, 2 x SDS-PAGE sample buffer) in a 1 : 1 ratio.

Quenched samples were loaded directly onto an SDS-PAGE gel and run as normal. After Coomassie blue staining, resultant band intensities were quantified through densitometry.

2.13.2 Data Analysis

At each timepoint the proportion of VcINDY which was PEGylated was calculated as:

$$\frac{[VcINDY + PEG Band Intensity]}{[VcINDY Band Intensity] + [VcINDY + PEG Band Intensity]}$$

This controlled for differences in gel loading and staining efficiency, allowing the rate of PEGylation to be accurately visualised. The proportions of PEGylated VcINDY could be averaged between multiple experiments, even between labs operating on different continents, to produce relatively clear data. The proportions of PEGylated VcINDY remaining after 60 minutes could be compared between different conditions through t-tests in order to detect significant changes in the rate of PEGylation.

Due to the differences in PEGylation rates found when carrying out the experiment on different days, emerging from a range of technical factors including the difficulty of accurately controlling the low levels of mPEG5K, normalisation of datasets allows the removal of a great deal of noise, resulting in clearer data analysis and more powerful statistical testing. Datasets were normalised so that the level of PEGylation under the conditions of 150 mM Na and no anion substrate was 1 at all timepoints, allowing clear visualisation of the differences in the rates of PEGylation between the various conditions tested. While this approach removes the absolute rate of PEGylation from datasets and plots only differences in PEGylation rates between conditions, these differences are the only feature of the dataset which is required for further analysis. As with the non-normalised data, normalised proportions of unPEGylated VcINDY remaining after 60 minutes could be compared between different conditions through t-tests in order to detect significant changes in the rate of PEGylation.

2.14 CPM Thermoflour Assay

2.14.1 Substrate Preparation

A stock solution concentration of 60 mM was chosen as a compromise between achieving the highest possible stock concentrations and accounting for substrates with low solubilities. If possible, the stock solution was made using ddH₂O and adjusted to pH 7.5 using concentrated HCl or KOH so that the pH of the final experimental mixture was not affected. When potential substrates were not sufficiently water soluble either DMSO or ethanol was used for stock solution creation, and a higher concentration of HEPES buffer was used in the final reaction solution to prevent changes to final pH. These stock solutions were aliquoted and frozen until use.

2.14.2 CPM Stocks

5 mg/mL 7-Diethylamino-3-(4'-Maleimidylphenyl)-4-Methylcoumarin (CPM) stocks were made in DMSO, aliquoted, and stored at -80°C until use. On the day of use an aliquot would be thawed and diluted 25x into the appropriate assay buffer.

2.14.3 Experimental Procedure – Typical Melting

The experiments were carried out as described by *Crichton et al.* [90] with minor modifications. VcINDY was buffer exchanged into CPM assay buffer (20 mM HEPES pH 7.5, 50 mM NaCl, with an additional 1% DDM for detergent solubilised samples). In thin walled optical cap PCR tubes 2 µg of protein was diluted in CPM assay buffer containing the substrate of interest to a final volume of 45 µL and incubated on ice for 10 minutes before the addition of 5 µL CPM dilute and a further 15 minute incubation on ice with occasional mixing. Samples were loaded into a Thermo Fisher QuantStudio 3 qPCR system running the following programme; cool to 5°C at 1.6 °C/s, rise to 95 °C

with a step and hold of 5 seconds, measure fluorescence using an excitation filter of 470 ± 15 nm and an emission filter of 520 ± 15 nm.

2.14.4 Data Analysis – Typical Melting

Melting temperature was determined as the point of maximal change in fluorescence, as indicated by the peak derivative. Multiple runs showed high levels of repeatability and allowed samples from separate days to be easily compared. Substrate derived stabilisation was calculated as the difference between the average melting temperature without the substrate and the average melting temperature with the substrate. When substrates were added from DMSO or ethanol based stock solutions the melting temperatures were compared to VcINDY melting in the presence of either ethanol or DMSO without substrate, controlling for the effect of these solvents on VcINDY stability.

2.14.5 Experimental Procedure – Half Life

Samples were prepared in the same way as a typical melt experiment. Instead of a melt curve, however, the QuantStudio 3 software was programmed to carry out a series of 10 minute hold steps at 40°C followed by another series at 95°C , taking a fluorescence reading at every step. These readings could be exported and used to form decay graphs.

2.14.6 Data Analysis – Half Life

Half life melt data were normalised so that the fluorescence upon complete denaturation was 1, and initial fluorescence was 0. The time at which this normalised fluorescence reached 0.5 was determined by calculating a linear regression between the final reading before 0.5 and the final reading after 0.5. Due to the level of noise and variation in this dataset multiple repeats were required for validation of changes observed.

2.15 GFP Thermostability Assay

Experimental procedures were carried out similarly to Nji et al. [91], but data analysis was carried out substantially differently.

2.15.1 VcINDY-GFP Preparation

GFP-tagged VcINDY was grown according to the Lemo21(DE3) / PASM5052 approach. Samples of purified GFP tagged VcINDY were produced as normal, using the imidazole elution approach in order to avoid removal of the GFP tag. Membranes containing GFP tagged VcINDY were harvested and solubilised with DDM as normal, before aliquoting and snap freezing.

2.15.2 Experimental Procedure – Temperature Range

GFP-TS can be carried out using solubilised membranes without the need to purify the GFP-tagged protein; in the case of Lemo21(DE3) / PASM5052 production DDM solubilised membranes were diluted to 80 mL GFP-TS buffer (150 mM NaCl, 20 mM Tris HCl pH 7.5, 1% DDM, 1% β -OG) per original litre of culture. When using purified protein, GFP-tagged VcINDY was diluted to 0.01 mg/mL in GFP-TS buffer.

For temperature range experiments 150 μ L samples were heated for 10 minutes at 4, 20, 30, 60, 60, 70, 80, and 100°C before pelleting of aggregates at 18,000 xg for 30 min at 4°C. Supernatant was transferred to a clear bottomed 96 well plate and pellets resuspended in 150 μ L GFP-TS buffer before transfer to the same plate. Fluorescent intensity was measured using either a BMG LABTECH FLUOstar Omega or CLARIOstar Plus.

2.15.3 Experimental Procedure – Fixed Temperature

Fixed temperature experiments were carried out similarly to temperature range experiments, however samples were all heated to the same temperature of $T_m + 5^\circ\text{C}$.

2.15.4 Data Analysis – Temperature Range

Due to the loss of GFP fluorescence with heating raw fluorescence readings were not used to determine melting temperature. Instead the proportion of GFP fluorescence in the supernatant verses the pellet was compared at each temperature, controlling for loss of GFP fluorescence. The resultant supernatant fluorescence data were fitted to a sigmoidal dose response curve in R using the nls() function [92]. The equation itself was as follows, where x equals the current temperature and Tm equals the melting temperature:

$$[\textit{Fluorescence Remaining}] = b + \frac{a - b}{1 + \frac{Tm^s}{x^s}}$$

Typically a temperature range was carried out in triplicate, with each replicate independently fitted, allowing for statistical error to be determined for melting temperatures. For the full programme, see 7.2 Appendix 2 – R script used for the fitting of GFP-TS data.

2.15.5 Data Analysis – Fixed Temperature

Fixed temperature experiments analysed the proportion of GFP fluorescence in the supernatant verses the pellet similarly to temperature range experiments. T testing was used to determine significant differences between conditions.

2.16 Microscale Thermophoresis (MST)

MST was carried out using the NanoTemper Monolith NT.115 and was generally used according to manufacturer's instructions.

2.16.1 VcINDY Preparation

Either GFP-tagged or fluorescently labelled VcINDY was used for MST experiments. GFP-tagged VcINDY was grown according to the Lemo21(DE3) / PASM5052 approach. Purified samples of GFP tagged VcINDY were produced as normal, using imidazole elution in order to avoid removal of the GFP tag. Non-GFP tagged VcINDY fluorescent labelling was achieved by purifying Lemo21(DE3) / PASM5052 produced VcINDY using the imidazole elution approach to preserve the his tag. This purified his-tagged VcINDY was then labelled using the Monolith His-Tag Labeling Kit RED-tris-NTA according to manufacturer's instructions.

2.16.2 Experimental Procedure

MST compatible substrate stock solutions are produced by dissolving substrates in the assay buffer itself and adjusting pH with either KOH or HCl so that the addition of substrate stock solution to samples will result in no chemical changes other than the introduction of the substrate itself. Prior to use a 10 μ L serial dilution of the stock solution is created, diluting with the assay buffer itself. GFP-tagged VcINDY is diluted to 40 nM and fluorescently labelled VcINDY is diluted to 500 nM. 10 μ L diluted VcINDY stock is added to each 10 μ L serial dilution sample, mixed gently, and incubated at room temperature for five minutes before loading into capillary tubes and insertion into the NanoTemper Monolith NT.115. Standard binding affinity protocols in the MO.Control software were used. Data analysis is discussed in detail in 4.4.3 Careful Analysis of VcINDY MST Data is Required In Order To Provide .

2.17 Lipid Handling

Regardless of final application, the same general method for preparation of lipid stocks in desired buffers was used. A round bottomed flask was washed with dH₂O followed by ethanol, and dried under a stream of N₂. Lipids dissolved in chloroform were then added to the flask and dried under the N₂ stream until no chloroform was visible, followed by an additional 30 minutes of drying to ensure no chloroform remained. The lipids were then solubilised with pentane, and once more dried under the N₂ stream until no pentane was visible, followed by an additional 30 minutes of drying to ensure no pentane remained. Lipids were finally solubilised in the desired buffer using a bath sonicator. Resuspended lipid samples were snap frozen in a dry ice / ethanol mixture and thawed three times before aliquoting and storage at -80 °C until use.

2.18 Proteoliposome Reconstitution.

n.b. Typical volumes are given, but actual volumes used varied dependent on experimental requirements.

VcINDY liposomes were produced using the rapid dilution method. 25 µg VcINDY solubilised in Decyl β-D-maltopyranoside (DM) containing buffer and 8 mg lipid were diluted into 2ml of reconstitution buffer (20 mM Tris pH 7.5, 150 mM NaCl, 5% glycerol, 0.1% DM). This mixture was incubated on ice for 10 minutes before rapid dilution into 65 mL Inside Buffer (20 mM Tris pH 7.5, 1 mM NaCl, 199 KCl). The proteoliposomes were harvested by centrifugation at 160,000 xg at 4 °C for 3 hours. The resultant pellet was resuspended in 1ml Inside Buffer before snap freezing in a dry ice / ethanol mixture and thawing three times. The final proteoliposomes was either used immediately or stored at -80°C.

2.19 Transport Assay

Typical volumes are given, but actual volumes used varied dependent on experimental requirements.

2.19.1 Proteoliposome Preparation

1 mL proteoliposomes were passed through a 400 nm filter 11 times using an extruder in order to produce proteoliposomes of uniform size. The proteoliposomes were then pelleted through centrifugation at 140,000 xg at 4 °C for 30 minutes and resuspended in 100 µL Inside Buffer (20 mM Tris pH 7.5, 1 mM NaCl, 199 KCl), giving a lipid concentration of 80 mg/mL. From this point onwards the proteoliposome solution was not placed on ice.

2.19.2 Experimental Procedure

[³H]-succinate was diluted in Transport Buffer (20 mM Tris pH 7.5, 100 mM KCl, 100 mM NaCl, 1 µM Valinomycin, 0.9 µM succinate) to a final concentration of 100 nM, and the resultant Hot Transport Buffer incubated at 30 °C on a heating block. To begin the reaction 10 µL of VcINDY proteoliposome solution was added to 1.5 ml Hot Transport Buffer and immediately mixed through vortexing. 200 µL samples were taken at predetermined timepoints and added to 2 mL ice cold Quench Buffer (20 mM Tris pH 7.5, 200 mM ChCl). This quenched reaction was then immediately added to a 0.2 µM nitrocellulose membrane mounted on a vacuum manifold, removing the buffer solution and retaining the proteoliposomes. Once the timecourse was finished the membranes were placed into Liquid Scintillation Counting vials, and an unused membrane was inserted into an additional vial along with 50 µL of the transport buffer to allow maximum counts to be calculated. 3 mL of Liquid Scintillation Cocktail was added to each vial and 15 minutes given to allow the membranes to dissolve. The vials were then transferred to a Hidex 300 SL scintillation counter for quantification of beta radiation emission.

2.19.3 Circular Dichroism (CD)

Protein was buffer exchanged into CD Buffer (50 mM Tris pH 8, 100 mM NaCl) with the addition of 0.1% DDM for detergent solubilised samples and diluted to 300 μ L 0.1 mg/mL. The sample was loaded into a glass cuvette and placed into a Jasco J-715 CD circular dichrometer for measurement. Readings were taken for buffer only samples to allow the effect of buffer components to be removed from final readings. For spectra measurements, a range of 197 to 260 nm was used due to significant buffer interference at lower wavelengths, and three were readings averaged to reduce noise in the final data. For melting experiments a wavelength of 222 nm was monitored as an indicator of the transition from alpha helix to random coil.

3 RESULTS – VcINDY Solubilisation Techniques

Chapters 3.1 and 3.2 can be considered technical sections of this thesis. They discuss two approaches to the detergent free solubilisation of VcINDY, namely Styrene Maleic Acid Lipid Particles (SMALPs) and Membrane Scaffold Protein (MSP) nanodiscs. These detergent free VcINDY preparations will be used throughout this thesis.

Chapters 4.1, 4.2, 4.3, and 4.4 focus instead on the application of different experimental techniques to the study of VcINDY in order to further our understanding of the molecular mechanisms behind its function.

3.1 The SMALP Native Lipid Nanodisc System Allows *In Vitro* Examination of VcINDY in a Near Native Environment

3.1.1 Introduction

Styrene Maleic Acid (SMA) is a co-polymer formed of repeating units of styrene and malic acid in a defined ratio (Figure 3.1.1-1); most commonly 2:1 or 3:1. When added to lipid membranes this polymer spontaneously enters the hydrophobic core of the bilayer, wherein membrane deformations caused by its presence result in membrane disruption and the formation of aqueous pores. The polymer molecules then line these pores, placing themselves at the interface between the bilayer core and the surrounding aqueous solution. As this process continues, discrete discs are formed, consisting of circular sections of lipids contained by a belt of SMA polymer [93]. If proteins are contained in the membrane they will also be solubilised into these discs. These nanodiscs, containing both proteins and their native lipid contacts within a SMA polymer belt, are known as Styrene Maleic Acid Lipid Proteins (SMALPs).

SMALPs owe their existence to the repurposing of cosmetic pharmaceutical techniques. In 2005 the newly founded Marvin Cosmetics Ltd. was addressing the issue of solubilising hydrophobic substances, particularly for topical use. The existing emulsions were considered oily and unpleasant, driving the search for an alternative delivery method. The same year a patent was filled for the use of styrene-malic acid polymers, allowing the creation of discrete lipid discs in which hydrophobic substances could be solubilised [94]. This patent was immediately followed by another relating to the same 2:1 and 3:1 ratio SMA polymers, in which the process for the creation of native lipid nanodiscs containing proteins is detailed; the prepared SMA polymer powder is added directly to a biological membrane, allowing the solubilisation of the entire compliment of proteins and lipids into discrete nanodiscs, from which the target protein can be purified by standard affinity chromatography [95]. This process is essentially unchanged in current publications [83].

The feature of this nanodisc system which makes it of such great use to membrane protein research is its ability to co-isolate lipids and proteins directly from their native membranes. Membrane proteins, by definition, make extensive contact with the lipids within cell membranes, and are often surrounded by specific lipids with which they interact [96]. The lipid content of this protein induced micro-environment may vary substantially from the lipid content of the total membrane [96].

SMALPs appear able to preserve this native lipid microenvironment. Existing work has found distinct lipid compositions within SMALPs containing three distinct membrane proteins, with clearly altered lipid ratios both compared to each other and compared to the total membrane from which they were isolated [96][97][98]. Given that the process SMALP solubilisation itself appears to be non-selective for lipid type [99], this strongly indicates that SMALPs are able to generate nanodiscs with lipid contents representative of the local microenvironment of individual proteins, even when the exact nature of that environment may be unknown to the experimenter. It may be cautioned, however, that changes in the overall total membrane composition have been known to result in alterations SMALP lipid content [97], suggesting that while there is a protein-lipid selectivity, this process is likely manifested as a protein specific shift in local lipid concentrations, not an absolute protein specific determination of local lipid concentrations. The importance of the nature of the lipid environment for elevator mechanism transporter function is discussed in 1.3 The Elevator Mechanism – The Importance of Lipids.

Since the early demonstrations of the power and potential of native lipid nanodiscs for the study of membrane proteins, a wide range of alternative polymers have been developed through the modification and substitution of functional groups in the SMA polymer. While the work in this thesis will focus only on 2:1 and 3:1 ratio SMAs, it is important to recognise that that a diverse range of alternate polymers exists, with varying properties such as pH tolerance, ion tolerance, disc size, solubilisation ability [100], and thermostability [101]. This range of polymers could, if the application of SMA to VcINDY does not yield satisfactory results beyond this thesis, provide many interesting alternatives for the future solubilisation of VcINDY. For example, DIBMALPs produce 30 nm

nanodiscs and with little impact on acyl chain dynamics [102], far larger and unrestrictive than the 10 nm discs associated with traditional SMALPs [103]. The field of polymer development is rapidly advancing at the present time, and it is expected that once this thesis is complete, an alternative polymer such as DIBMALPs will be established as a far more suitable alternative to the SMALPs used herein [100]. This will be an area for future experimentalists to monitor closely.

SMALPs have proven to be compatible with a wide, ever growing, range of processes including x-ray crystallography [104], cryo-EM [105], Hydrogen-Deuterium eXchange Mass Spectroscopy (HDX-MS) [97], lipidomics (selected examples include [97][96][99][98][106]), all manner of thermostability assays [107][108][109][101][110][103][98][111], fluorescent binding assays [111], radioligand binding assays [107][108], the detection of protein-protein interactions [112], and various activity assays [103][106]. This is by no means a complete list, as dozens of SMALP publications are emerging each year, but rather an example of the widely compatible nature of this system [100]. A particular advantage of this nanodisc system, and one source of this wide compatibility, is that it does not introduce unwanted peptides into the experimental system, unlike MSP nanodiscs (see 3.2.1 Introduction), removing a major barrier imposed by traditional nanodisc systems.

Here, we shall attempt to apply this solubilisation technique to a DASS family transporter for the first time, using the traditional SMA polymer with 2:1 and 3:1 subunit ratios. Once a native lipid nanodisc is created it shall be quality control tested using Circular Dichroism (CD) to confirm maintenance of the secondary structure, and HPLC SEC to confirm sample heterogeneity. The use of SMALPs in PEGylation based accessibility assays and CPM based thermostability assays, along with their impact on GFP-TS thermostability assays, can be found in their respective sections (see 4.1.5 VcINDY Substrate Induced Accessibility Changes Are Similar Within Both Detergent and Native Lipid Environments and 4.2.5 Native Lipid Nanodisc Solubilised VcINDY Shows Extreme Thermostability Along With Substrate Induced Destabilisation).

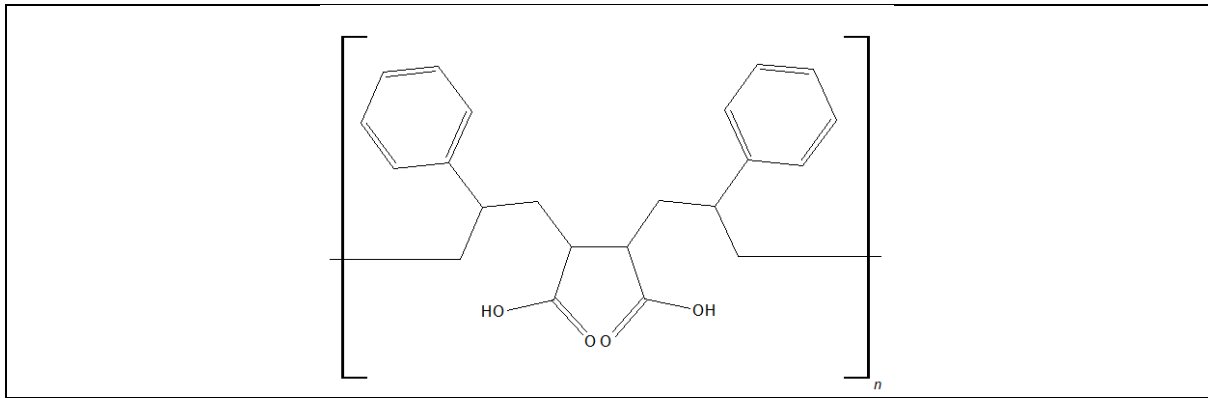


Figure 3.1.1-1 SMA polymer composition, showing a styrene – malic acid – styrene monomer sequence.

3.1.2 The Final Yield Produced From Affinity Purification of VcINDY Is Dependent Upon Both the Composition and Concentration of the SMA Polymer Used For Initial Solubilisation

As an initial test of compatibility, BL21(AI) membranes containing expressed VcINDY were solubilised using varying concentrations of 3:1 SMA. The remaining insoluble fraction was separated through ultracentrifugation, and the resultant samples were examined through both total protein Coomassie Blue staining and his-tag specific western blotting (Figure 3.1.2-1). This resulted in successful solubilisation of VcINDY, as a band of the expected MW was observed during western blotting of the soluble fractions. Increasing the concentration of SMA used to achieve solubilisation incrementally from 1 % to 6 % appeared to result in increasing solubilisation of VcINDY, as the intensity of the western blot detected VcINDY band decreased in the insoluble fraction and increased in the soluble fraction. Examination of the Coomassie blue total protein stained gels revealed that while most membrane proteins achieved almost full solubilisation at high SMA concentrations, being almost entirely present within the soluble fraction, three distinct protein bands appeared more resistant to total solubilisation, remaining partially within the pellet fraction even at 6 % SMA solubilisation. Comparison to the VcINDY western blots indicates that one of these total-solubilisation resistant proteins is VcINDY.

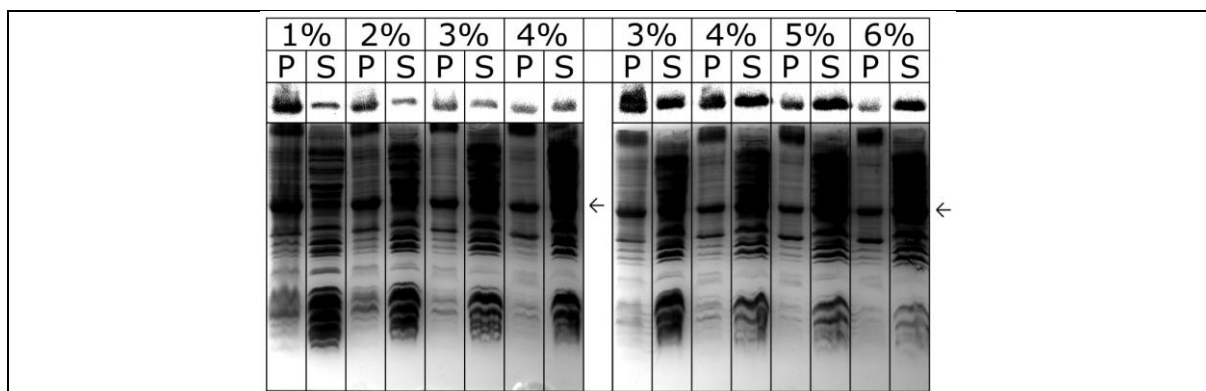


Figure 3.1.2-1 Solubilisation of VcINDY containing BL21(AI) membranes with varying concentrations of 3:1 SMA.

Percentage weight per volume SMA used for solubilisation is indicated. Arrow indicates height of VcINDY band. P = Pellet (insoluble fraction), S = Supernatant (solubilised fraction). Western blot specific to his-tagged proteins, and therefore VcINDY, is shown along with a total protein Coomassie Blue stain of the same samples.

In order to examine whether this population of non-SMA-solubilised VcINDY could be recovered through repeat cycles of 3% SMA solubilisation, VcINDY containing BL21(AI) membranes were solubilised with SMA before separation of the insoluble fraction through ultracentrifugation and attempted re-solubilisation of the remaining insoluble fraction. In this manner the membrane was solubilised thrice with SMA, and finally once with DDM. The resultant soluble fractions were purified through cobalt affinity purification as normal (see 2.6.6 Cobalt Affinity Purification (SMALPs)) (Figure 3.1.2-2A). This provided two interesting results. Firstly, repeat rounds of SMA solubilisation did not solubilise any additional VcINDY into SMALPs; it appears that there is a population of VcINDY within the membrane which is in some manner resistant to SMA solubilisation. This population is, however, able to be solubilised through treatment with detergent.

Secondly, the level of SMALP solubilised VcINDY compared to DDM recovered VcINDY in this solubilisation series is unusually low given that 3% SMA should have already solubilised almost half the available VcINDY, according to the previous solubilisation trials (Figure 3.1.2-1& Figure 3.1.2-2B). The previous experiment relied upon western blot-based detection of VcINDY, in contrast to the current experiment which relied upon the affinity purification of solubilised VcINDY. As such it is possible that DDM solubilised VcINDY is more readily purifiable than SMA solubilised VcINDY.

In order to examine this possibility, the affinity purification of a VcINDY-GFP conjugate solubilised using 3% SMA was monitored through the detection of GFP's distinct fluorescent signal (Figure 3.1.2-2B). Of the VcINDY-GFP which was correctly inserted into the membrane, roughly half was solubilised, in agreement with western blot data (Figure 3.1.2-1). Of the solubilised VcINDY, only around 15 % was extracted through cobalt based affinity purification, indicating that SMALP solubilised VcINDY was not binding effectively to the cobalt affinity resin. Binding levels were so low that the flowthrough from affinity purification attempts could be re-incubated affinity resin multiple times, continuing to extract comparable levels of VcINDY-GFP on each round of binding.

In order to better examine the relationship between initial SMA concentrations and final purification yield, VcINDY containing BL21(AI) membranes solubilised with either 1%, 3%, or 5% SMA were purified, with four cycles of rebinding to the affinity resin (Figure 3.1.2-2C). Interestingly, 1% SMA solubilisation resulted in the highest yield of purified VcINDY, producing in the highest concentration of purified VcINDY for all four cycles of resin binding, despite being the concentration known to solubilise VcINDY least efficiently. Additionally, increasing the incubation time of the solubilised membrane samples with the cobalt affinity resin resulted in increased yields of purified VcINDY in all cases.

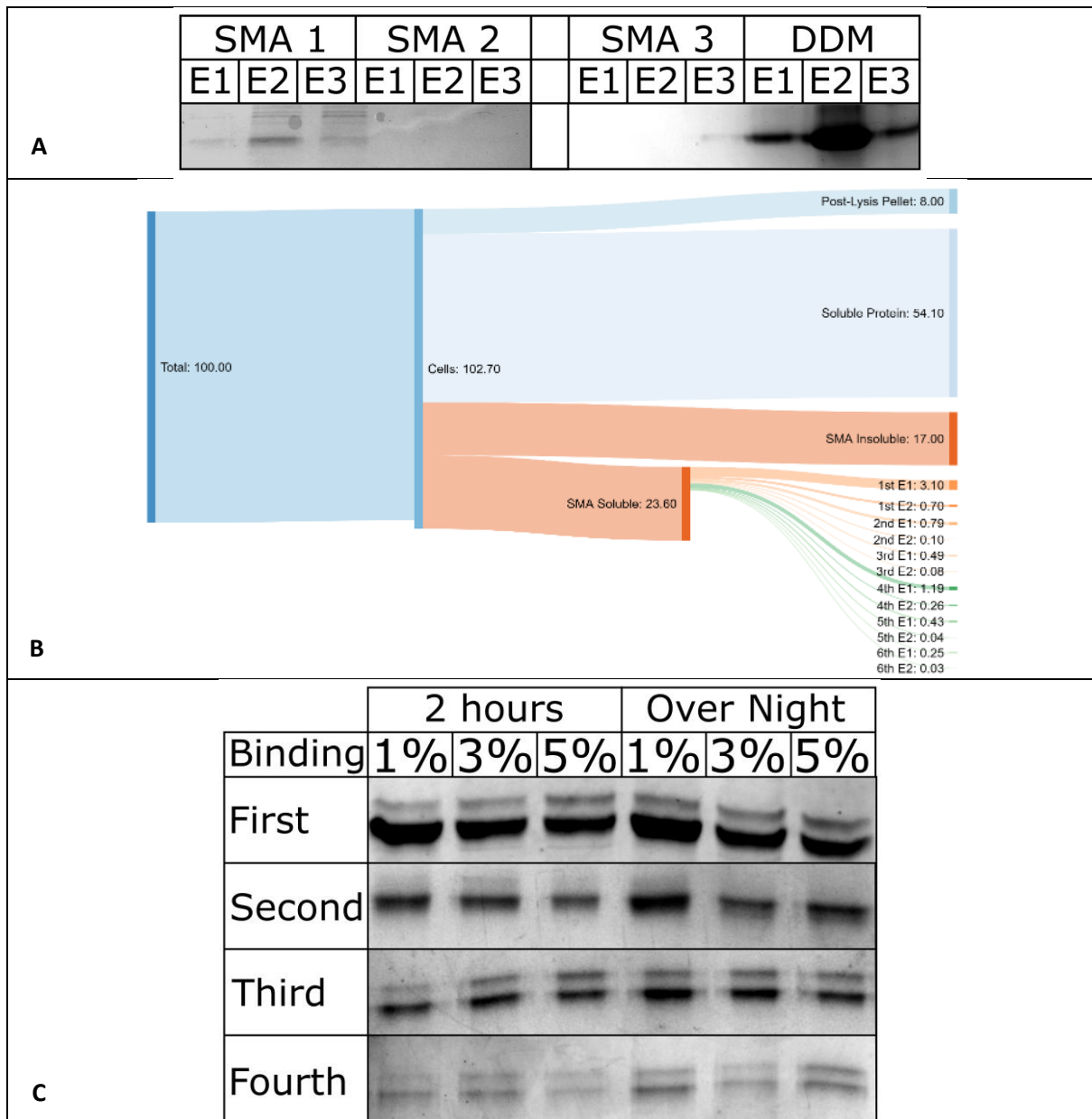


Figure 3.1.2-2 Optimisation of the solubilisation and purification of VcINDY with SMA. **A:** Repeat solubilisation and purification of a single VcINDY containing BL21(AI) membrane. The elution fractions from repeated solubilisation and purification of the insoluble membrane fraction with three cycles of 3:1 SMA, followed by DDM detergent, shown upon Coomassie Blue stained gels. **B:** Purification of VcINDY-GFP using 3:1 SMA. Total VcINDY-GFP content at each stage of the purification is shown, as determined by fluorescence measurements and corrected for solution volume. **C:** Purification of VcINDY following solubilisation with various concentrations of SMA and multiple rounds of binding to cobalt affinity resin, shown upon Coomassie Blue stained gels. Incubation time with cobalt affinity resin is indicated for each solubilisation concentration, along with the number of bindings the affinity resin.

In order to examine why this may be, the ratio of SMA to VcINDY present in samples of purified VcINDY was estimated. This was done using UV-vis spectroscopy as follows: VcINDY's 280 nm extinction coefficient could be estimated through the ExPASy ProtParam server from its sequence as $57075 \text{ M}^{-1} \text{ cm}^{-1}$ [88]. Using this value, examination of VcINDY's absorbance spectra allowed the 260 nm coefficient to be estimated as $59113 \text{ M}^{-1} \text{ cm}^{-1}$ (Figure 3.2.2-2A). For SMA, a standard curve could be constructed from known dilutions, allowing the 260 nm and 280 nm extinction coefficients to be estimated as $12353 \text{ M}^{-1} \text{ cm}^{-1}$ and $507 \text{ M}^{-1} \text{ cm}^{-1}$ respectively for concentrations below $100 \mu\text{M}$ (Figure 3.2.2-2B). Using these values, measurements of 260 and 280 nm absorbances can be used to estimate SMA to VcINDY ratios for mixed samples through the solving of simple simultaneous equations. This methodology was applied to the purified VcINDY containing SMALPs produced using 1 %, 3 %, and 5 % 3:1 SMA, demonstrating them to contain VcINDY to SMA molar ratios of approximately 5.0, 7.0, and 9.5 respectively (Figure 3.2.2-2C). This indicates that the increased initial concentration of SMA, while allowing for a more effective solubilisation of VcINDY, leads to higher concentrations of SMA throughout the purification and into the final product, possibly interfering with binding to the affinity resin. As such, excess SMA should be minimised.

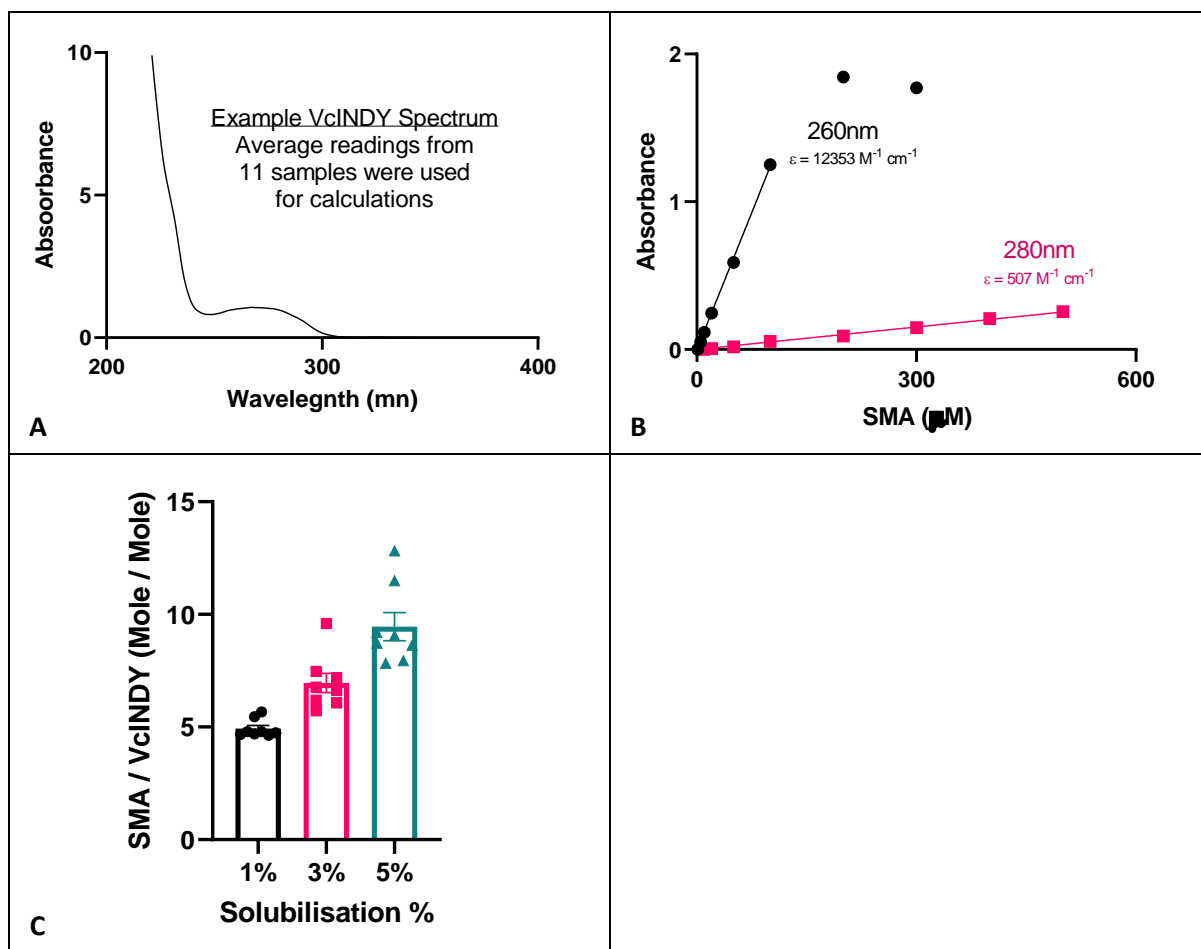


Figure 3.1.2-3 Estimation of SMA / VcINDY ratio for differing VcINDY SMALP preps. **A:** Example absorbance spectrum for detergent solubilised VcINDY. **B:** Standard curves for 3:1 SMA absorbance using weight average molecular weight for SMA, note the saturation of absorbance at 260 nm occurring at concentrations far in excess of those found in SMALP samples. **C:** Estimated molar ratios of 3:1 SMA / VcINDY. Ratios are shown for final elutions following solubilisation with varying SMA % weight/volume concentrations.

After the generous gift of 2:1 SMA from Dr. Alice Rothnie (Aston University), this alternative polymer could be tested. VcINDY containing BL31(AI) membranes were solubilised using 3 % 2:1 SMA, 3 % 3:1 SMA, or 5 % DDM, before purification and comparison of the final yield (Figure 3.1.2-4).

Solubilisation using the 2:1 SMA polymer lead to a yield of purified VcINDY comparable to that achieved through DDM solubilisation, and far higher than that generated through 3:1 SMA solubilisation, indicating the 2:1 polymer to be far more suitable for use with VcINDY than the 3:1 polymer. While the exact reasons for this difference are unclear, further examination of this system is beyond the scope of this thesis now that a useful yield of SMALP solubilised VcINDY can be produced.

VcINDY can therefore be solubilised into both 2:1 and 3:1 SMA polymer SMALPs, and while the 2:1 ratio polymer allows far more efficient purification, it is entirely possible to produce usable levels of VcINDY SMALPs using the 3:1 ratio polymer so long as low polymer concentrations are used for the initial solubilisation of VcINDY.

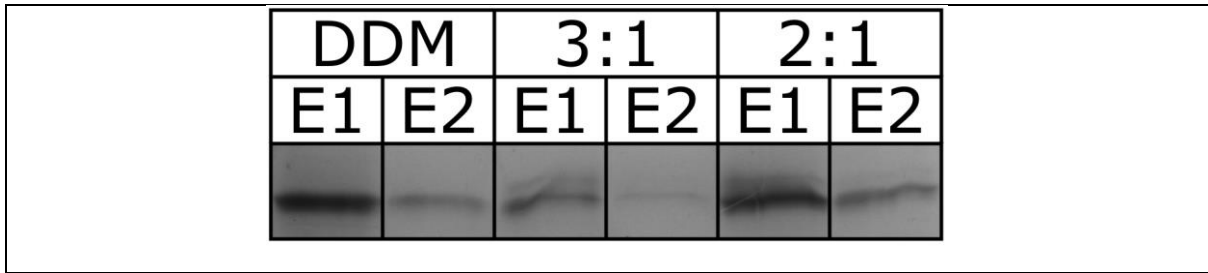


Figure 3.1.2-4 Solubilisation and purification of VcINDY using differing SMA polymers. Affinity purification elution

fractions for VcINDY solubilised using 5% DDM detergent, 3% 3:1 SMA, or 3% 2:1 SMA, shown upon Coomassie Blue stained gels.

3.1.3 SMALP Solubilised VcINDY Appears Correctly Folded, Monodisperse, and Highly Thermostable

Before the newly produced VcINDY SMALPs could be used, quality control and characterisation of these novel nanoparticles was required.

In order to establish the presence of a homogenous species, representing correctly folded VcINDY embedded in a SMALP, and rule out the possibility that the produced SMALPs population consisted entirely of aggregates, HPLC SEC was performed (Figure 3.1.3-1A). Three main observations were made. Firstly, the presence of a clear, sharp, peak indicated the presence of a major homogenous population. Secondly, this main peak elutes slightly before detergent solubilised VcINDY, indicating a larger particle size for SMALP solubilised VcINDY within lipid nanodiscs, compared to the detergent solubilised VcINDY within micelles. Thirdly, there is a large shoulder eluting prior to the main peak, much of which begins to elute at the void volume, indicating the presence of a significant quantity of very large molecules and/or aggregated material.

As this SEC column was later calibrated for estimation of Stoke's Radii (see 3.2.5 Optimisation of the Reconstitution of VcINDY into MSP1E3D1 Based Nanodiscs), the Stoke's Radii of DDM and SMA solubilised VcINDY can be estimated as 5.2 nm and 6 nm respectively. This additional 0.8 nm radius indicates sufficient room for lipid inclusion within the disc.

Next, in order to confirm that VcINDY's secondary structure is correctly maintained within SMALPs, far-UV CD was carried out. Due to difficulties in accurately determining the concentrations of both detergent and SMA solubilised VcINDY, the resulting spectra were not expected to be of identical magnitude; therefore the far-UV spectra, once corrected for buffer effects, were normalised to equal magnitude (Figure 3.1.3-1B). This resulted in near identical spectra, showing the two troughs within the 200 – 230 nm range characteristic of α -helix containing proteins, indicating clearly that the secondary structure of VcINDY is maintained similarly for both DDM and SMA solubilisation.

The stability of VcINDY within SMALPs was also tested through CD, following the reduction in signal at 222 nm, representing the transition from α -helix to random coil spectra (Figure 3.1.3-1C).

Detergent solubilised VcINDY is observed to undergo the transition to random coil, with an estimated secondary structure melting temperature of 78.89 ± 5.92 (95% C.I.). SMA solubilised VcINDY, however, only undergoes moderate alterations in signal, indicating melting to not occur within the temperature range observed, denoting a high level of SMA thermostability, innkeeping with data gathered through CPM-thermofluor (see 4.2.5 Native Lipid Nanodisc Solubilised VcINDY Shows Extreme Thermostability Along With Substrate Induced Destabilisation).

The ability to carry out substrate binding and substrate dependent conformational change was demonstrated through the established cysteine accessibility assay elsewhere in this thesis (see 4.1.5 VcINDY Substrate Induced Accessibility Changes Are Similar Within Both Detergent and Native Lipid Environments).

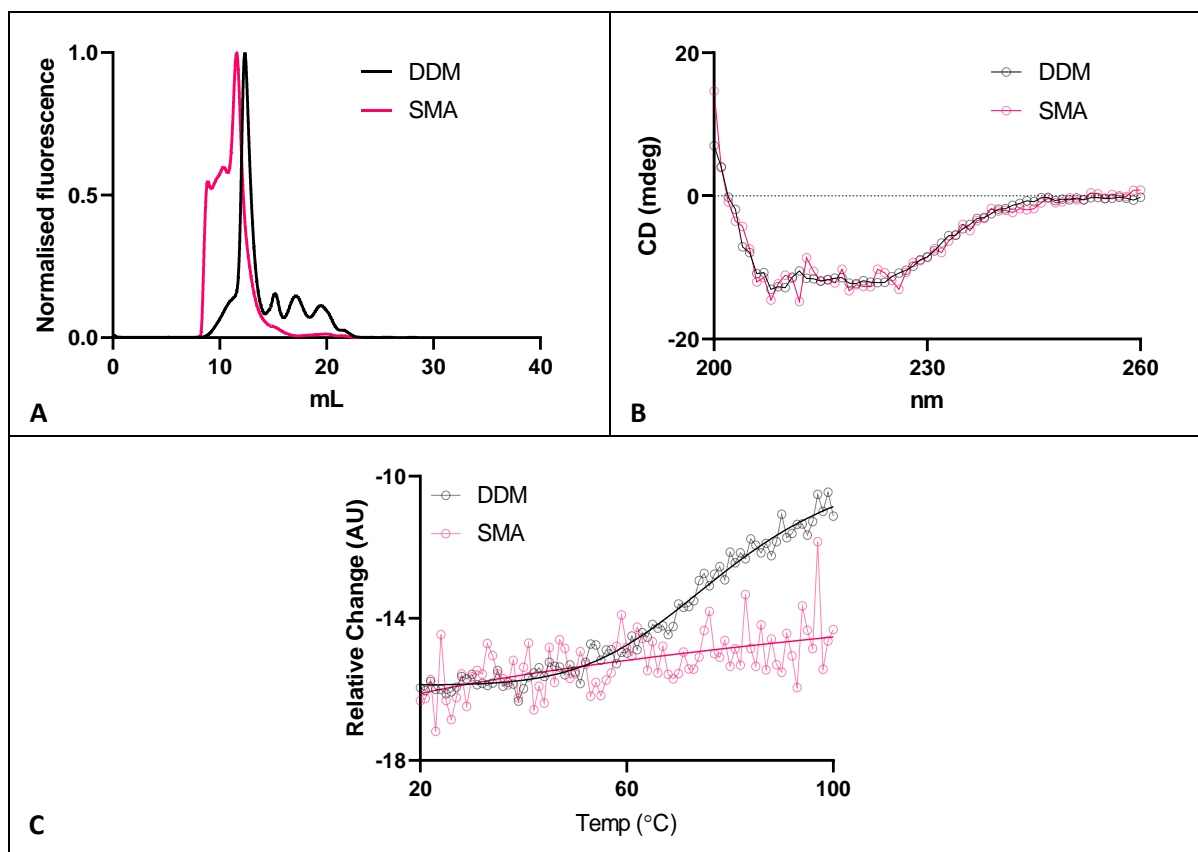


Figure 3.1.3-1 Characterisation of VcINDY SMALPs. A: In line 280 nm absorbance readings for HPLC SEC runs, showing affinity purified samples of VcINDY solubilised with either DDM or 3:1 SMA, normalised to maximum fluorescence. B: Far UV circular dichroism of DDM detergent and 3:1 SMA solubilised VcINDY. The SMA solubilised VcINDY spectra is corrected for magnitude due to uncertainties surrounding its concentration. Average results from 3 scans shown. C: Secondary structure thermal denaturation of DDM and 3:1 SMA solubilised VcINDY observed through the change of CD signal at 222 nm. Starting magnitude for SMA solubilised VcINDY is normalised for ease of comparison. Values are fitted to four parameter sigmoidal melt curves, with 95 % C. I. shown for DDM solubilised VcINDY.

3.1.4 SMALPs Have Been Employed Throughout This Thesis for Various Purposes

SMALPs have been used throughout this thesis. A brief summary of the major findings are presented here for the reader merely interested in SMALPs themselves. For fuller discussions and the relevant data, please view the relevant section.

In 4.1.5 VcINDY Substrate Induced Accessibility Changes Are Similar Within Both Detergent and Native Lipid Environments, the accessibility of key residues in the presence and absence of substrates was compared between DDM and 3:1 SMA solubilised VcINDY. It was observed that the level of mPEG5K label required to label introduced cysteine residues in SMALP solubilised VcINDY was higher than that required to label DDM solubilised VcINDY, but the substrate induced accessibility changes were identical between the differently solubilised forms of VcINDY.

In 4.2.5 Native Lipid Nanodisc Solubilised VcINDY Shows Extreme Thermostability Along With Substrate Induced Destabilisation, the thermostability of SMALPs was found to be extreme, able to withstand hours at near boiling temperatures before melting of VcINDY's tertiary structure occurred, in sharp contrast to the lower thermostability of DDM solubilised VcINDY. Additionally, it was observed that the addition of succinate to SMALP solubilised VcINDY resulted in a reduction in thermostability. Work examining lipid-substrate relationships (see 4.3.4 The Effects of Lipids Upon VcINDY-GFP Thermostability Are Altered by the Presence of Succinate) suggested that this reduction in thermostability was likely due to succinate binding disrupting protein-lipid interactions within the SMALPs themselves, as the succinate bound protein preferentially binds alternative lipids to the succinate free protein.

In 4.4.6 Preliminary MST Examination of SMALP Solubilised VcINDY Indicates that the SMALP System May be Capable of Isolating Transient Lipid Environments, the properties of VcINDY SMALPs produced in the presence of succinate were found to differ from VcINDY SMALPs produced in the absence of this substrate. This demonstrated an ability of SMALP nanoparticles to retain information regarding the substrate binding state of VcINDY at the point of solubilisation, likely through the

isolation of transient, substrate dependent, VcINDY lipid interactions. This suggests that SMALPs may be a useful tool for the examination of dynamic lipid interactions, and raises a number of future research questions.

3.1.5 Chapter Summary

The solubilisation of VcINDY via the SMALP system has been trialled for the first time, allowing useful yields of native lipid nanodisc solubilised VcINDY to be produced, providing a viable alternative to detergent or MSP nanodisc based *in vitro* examination of this protein.

SMA appears unable to achieve 100% solubilisation of VcINDY despite repeated treatments, with a SMA resistant population of VcINDY appearing to be only solubilisable through detergent extraction. This SMA resistant population likely consists of dense protein patches containing insufficient lipid content to allow SMA access [113], as has been observed for a range of proteins in a variety of cell types [110][111]. It is likely that the introduction of additional lipids could allow the dispersal and SMA solubilisation of these dense VcINDY patches [113], however the introduction of additional lipids is likely to alter the lipid compositions of the produced SMALPs [97]. This approach is therefore not recommended, due to the possibility of creating non-native lipid nanodiscs, thereby forfeiting one of the great advantages of the SMALP system [96].

The initial concentration of SMA used to solubilise VcINDY was found to greatly impact both purification efficiency, and the final product. Higher initial concentrations of SMA resulted in greater solubilisation of VcINDY, but significantly reduced purification yield and increased SMA concentration in the final purified product. The exact reasons for this are unclear, although previous literature has recommended the use of buffer exchange to remove excess SMA from solubilised membranes prior to the addition of affinity resin, demonstrating recognition of the deleterious interactions between excess SMA and affinity resins [106].

Existing literature has widely recognised the weak interactions between some SMALP solubilised proteins and his-tag affinity binding resins [114], and many studies have adopted approaches to compensate for this. Batch binding to affinity resin is common, either for two hours [83][98], or overnight [115][106][107][83][111], supporting the observation made here that greater incubation times resulted in greater purification yields. Furthermore, in this project only 10 mM imidazole was

used when washing the resin bound VcINDY SMALPs in order to remove non-specific protein interactions, compared to 20 mM used for DDM solubilised VcINDY. This lower concentration was adopted in order to preserve weak interactions between SMALP solubilised VcINDY and the affinity resin, and similar low imidazole washes can be observed in the literature, employing 10 mM [116], 5 mM [106], or even 0 mM imidazole [115].

2:1 SMA solubilisation resulted in far higher yields of purified VcINDY than 3:1 SMA solubilisation. It has previously been observed that while both of these polymers are similarly able to solubilise membrane proteins, use of the latter polymer consistently results in poorer purification yields [110]. Previously it has been unclear whether this difference in purification efficiency was due to differences in affinity resin binding, or SMALP stability [110]. Herein we have demonstrated SMALP solubilised VcINDY to exhibit extreme levels of thermostability, a general behaviour which occurs for both polymers (data not shown), therefore indicating that the discrepancy in purification efficiencies between these two polymers is likely due to differences in their interactions with affinity resins, and not due to SMALPs denaturing over the course of the purification process.

The HPLC SEC UV absorbance trace generated for SMALP solubilised VcINDY is very similar to that reported in previous literature, in which negative stain EM examination of the resultant fractions indicated that the high MW peaks eluting before the main nanodisc peak consisted of large membranous particles, generated by non-uniform SMA solubilisation [117]. The presence of these large membranous species after purification is a possible explanation for the poor SMALP purification efficiencies. It is evident that these impurities can be removed through the use of HPLC SEC based purification, although this process generally results in a much-reduced yield. The impact of these membranous particles upon apparent protein function in biochemical assays is unclear, although they do not appear to have interfered with the assays carried out within this thesis, in which SMALP solubilised VcINDY behaves largely similarly to detergent solubilised VcINDY, with the exception of thermostability assays, which are discussed elsewhere.

Beyond the matters of purification, VcINDY SMALPs appeared to be an effective nanodisc system of great use. In this chapter and elsewhere in this thesis VcINDY SMALPs have been shown through HPLC SEC to contain an appropriately sized homogenous species, through calibrated SEC to possess ample room for lipid content, through CD to have similarly formed secondary structures to detergent solubilised VcINDY, and through an accessibility assay to perform the same dynamic substrate responses as detergent solubilised VcINDY. They have been effectively employed either to confirm the validity of detergent based measurements, as in the case of PEGylation based accessibility assays (see 4.1.5 VcINDY Substrate Induced Accessibility Changes Are Similar Within Both Detergent and Native Lipid Environments), or to demonstrate the importance of lipids and thus open new avenues of research, as in the case of CPM thermofluor leading to GFP-TS (see 4.2.5 Native Lipid Nanodisc Solubilised VcINDY Shows Extreme Thermostability Along With Substrate Induced Destabilisation and 4.3 Aggregation Based Thermostability Measurements Indicate a Complex Relationship Between Substrate Binding and Lipid Interactions). Furthermore, by analysing SMALPs through the high precision technique MST, the ability of the SMALP system to isolate functionally important transient lipid environments is explored (see 4.4.6 Preliminary MST Examination of SMALP Solubilised VcINDY Indicates that the SMALP System May be Capable of Isolating Transient Lipid Environments).

SMALPs have therefore been successfully applied to VcINDY, providing a simple and highly compatible nanodisc system for the examination of this elevator mechanism transporter.

3.2 MSP Based Nanodiscs Allows *In Vitro* Examination of VcINDY in a Defined

Lipid Environment

3.2.1 Introduction

The importance of lipids in the study of membrane proteins has already been well introduced in this thesis, with examples of the practical difficulties involved (see 4.2.6 Direct Supplementation of Lipids to Detergent Solubilised VcINDY Results in Poor CPM Thermofluor Output), discussions of the crucial roll played by lipids in elevator mechanism transport (see 1.3 The Elevator Mechanism – The Importance of Lipids), and novel observations indicating a complex but obscure relationship to exist between VcINDY and the membrane (see 4.2.6 Direct Supplementation of Lipids to Detergent Solubilised VcINDY Results in Poor CPM Thermofluor Output, 4.3.4 The Effects of Lipids Upon VcINDY-GFP Thermostability Are Altered by the Presence of Succinate, and 4.4.6 Preliminary MST Examination of SMALP Solubilised VcINDY Indicates that the SMALP System May be Capable of Isolating Transient Lipid Environments). As such multiple approaches to examining VcINDY lipid relationships have already been presented. These include lipid supplementation of detergent solubilised samples and the formation of native lipid nanodiscs known as SMALPs. This chapter introduction shall avoid, wherever possible, repeating information presented elsewhere, and will focus on this particular system.

The MSP nanodisc system owes its existence to the ApoA1 protein. This protein is the major component of high-density lipoproteins (HDLs); naturally occurring lipoprotein structures involved in the trafficking of cholesterol in humans. It represents a natural approach to the solubilisation of lipids for transport in an aqueous environment [118]. Consisting of a series of amphipathic helical repeats with a modest cytoplasmic domain, this protein can be expressed and reconstituted in vitro. By employing purified ApoAI with careful control over the conditions and lipid content it was possible to create “discoidal micelles”; discrete soluble discs of lipid bilayer surrounded by a belt of ApoA1 [119].

These discs, while heterologous and unsuitable for use in biophysical studies, provided tantalising evidence that a functional nanodisc system could be created and used to achieve the solubilisation of membrane proteins [120]. Accordingly, *T. Bayburt et al 2002* created the Apo-AI derivative Membrane Scaffold Protein (MSP), allowing the creation of far more homogenous discoidal micelles [121]. With these tools, the reconstitution of other membrane proteins into discoidal micelles, or simply “nanodiscs” becomes possible, allowing soluble lipid protein structures to be produced.

Further modifications of the MSP sequence have been made over the years, resulting in a range of available MSP proteins [120]. For the work in this thesis the MSP derivative MSP1E3D1 shall be used. MSP1E3D1 is modified in two ways from the original MSP protein; a deletion of the non-protein/lipid interface residues 1-11, and the addition of three 22 amino acid alpha helices [87]. This derivative was chosen for use as the additional alpha helices result in the formation of larger nanodiscs, around 12 nm in diameter, in contrast to the 9.7 nm nanodiscs of MSP1 [122]. The use of a larger nanodisc reduces the risk of VcINDY being bound too tightly by the MSP scaffold to behave in a physiological manner.

The process of generating MSP based VcINDY nanodiscs differs greatly from that of SMALPs. Reconstitution of a membrane protein into SMALPs merely requires a lipid membrane containing the protein of interest to be incubated with the SMA polymer of choice, leading to the spontaneous formation of native lipid nanodiscs [83]. Nanodisc reconstitution requires pure, detergent solubilised, membrane proteins to be mixed with experimentally determined ratios of lipids and MSP, before the detergent is gradually removed, forcing the constituents to form defined nanodiscs [120]. A great advantage of this approach is the ability to define the lipid content of the nanodisc, thereby allowing detailed investigation of the relationship between proteins and lipids.

A prominent example of the power of these nanodiscs for the examination of elevator mechanism transporters comes from work upon Glt_{Ph} . The protomers of this trimeric symporter were expected to operate independently, however detergent solubilised structures predominantly showed the

protomers to occupy the same state. Structures gathered in nanodiscs, however, demonstrated a range of conformational ensembles, including those with differently oriented protomers [27].

Accordingly, it is clear that the transition from detergent to nanodisc in some way alters the dynamics of this transporter, with the nanodiscs most likely to represent the native behaviour.

With the key role played by lipids in elevator mechanism transporter function discussed in 1.3 The Elevator Mechanism – The Importance of Lipids, the ability of this nanodisc system to provide customisable lipid environments, in a manner known to have significant impacts upon elevator mechanism transporters [27], will allow key questions raised by GFP-TS (see 4.4.7 Chapter Summary) to be answered.

The aim of this chapter is simply to create a functional MSP based nanodisc system for VcINDY, a process requiring the expression of two proteins (MSP1E3D1 and TEV protease) and multiple layers of careful optimisation [120]. Once these are created it is hoped that nanodiscs containing varying defined lipid environments can be applied to the high resolution MST binding assay (see 4.4.1 Introduction) in order to assess the roll of lipids in substrate binding. The questions of whether the low succinate affinity so far observed (see 4.4.7 Chapter Summary) is representative of the physiological nature of the protein, and how the interplay between substrate and lipid preferences affect binding affinity can be definitively answered using the tools developed in this chapter.

3.2.2 Troubleshooting and Optimisation of MSP1E3D1 Production

Expression and purification of MSP derivatives for the purpose of nanodisc formation is a common process, and such many labs already have well established protocols. Two expression protocols were initially trialled for the expression of his-tagged MSP1E3D1, protocol 1 and 2 (Table 3.2.2-1), and the resultant protein purified through nickel affinity chromatography (see 2.8.2 Purification of MSP1E3D1). Examination of the final elution products through Coomassie blue stained gels revealed Condition 2 to produce significantly more MSP (Figure 3.2.2-1A) than Condition 1, however the yield was poor, and due to the low levels of target protein the final elutions contained high levels of contaminant resulting from non-specific protein interactions with the nickel resin. As such, neither condition produced useful levels of MSP1E3D1.

	1	2
Strain	BL21(DE3)	BL21(DE3)
Media	2YT	TB
Incubator shaker speed	210 rmp	210 rpm
Growth temperature pre induction	37°C	37°C
Induction OD ₆₀₀	3.0-4.0	2.2-2.5
IPTG concentration	1 mM	1 mM
Growth temperature post induction	28°C	37°C
Expression time	4 hours	4 hours

Table 3.2.2-1 Initial expression conditions trialled for the expression of his-tagged MSP1E3D1.

Due to this poor yield, two rapid optimisation experiments were carried out. In the first experiment, a 1 L culture was grown according to the current best conditions, and aliquoted to allow a range of purification conditions to be trialled, quickly determining the optimal purification conditions for this protein.

For this purification optimisation the possibility of large quantities of the expressed MSP entering insoluble inclusion bodies was examined through the solubilisation of the post lysis and clarification cell pellet with 6 M Guanidine Hydrochloride (Gdm HCl) supplemented buffer. The Gdm HCl concentration was maintained in all buffers until the protein was bound to the affinity column, at which point the sample was washed into non-denaturing buffer to allow refolding. Comparison of MSP1E3D1 purified from the soluble fraction, and from the Gdm HCl solubilised pellet, showed that while solubilisation of possible inclusion bodies from the pellet allowed additional protein, likely MSP1E3D1, to be recovered, the MSP1E3D1 recovered from the pellet was of far lower yield and purity than that purified from the soluble fraction (Figure 3.2.2-1B). As such, it appears that the majority of the available MSP1E3D1 is not entering the pellet, and the solubilisation of inclusion bodies does not greatly improve final yields.

Nickel and cobalt based affinity resins were examined, along with the time of sample incubation with the resin. Increasing the incubation time of the solubilised membrane with the affinity resin resulted in the recovery of additional MSP1E3D1 for both nickel and cobalt based resins (Figure 3.2.2-1C and Figure 3.2.2-1D respectively), with both a change from flowthrough (no prior incubation) to 30 minute incubation, and a change from 30 minute incubation to 16 hour incubation, resulting in higher concentrations of protein being recovered into the final elutions. In the case of all incubation times trialled, nickel resins allowed the recovery of higher quantities of protein than cobalt resins (Figure 3.2.2-1E).

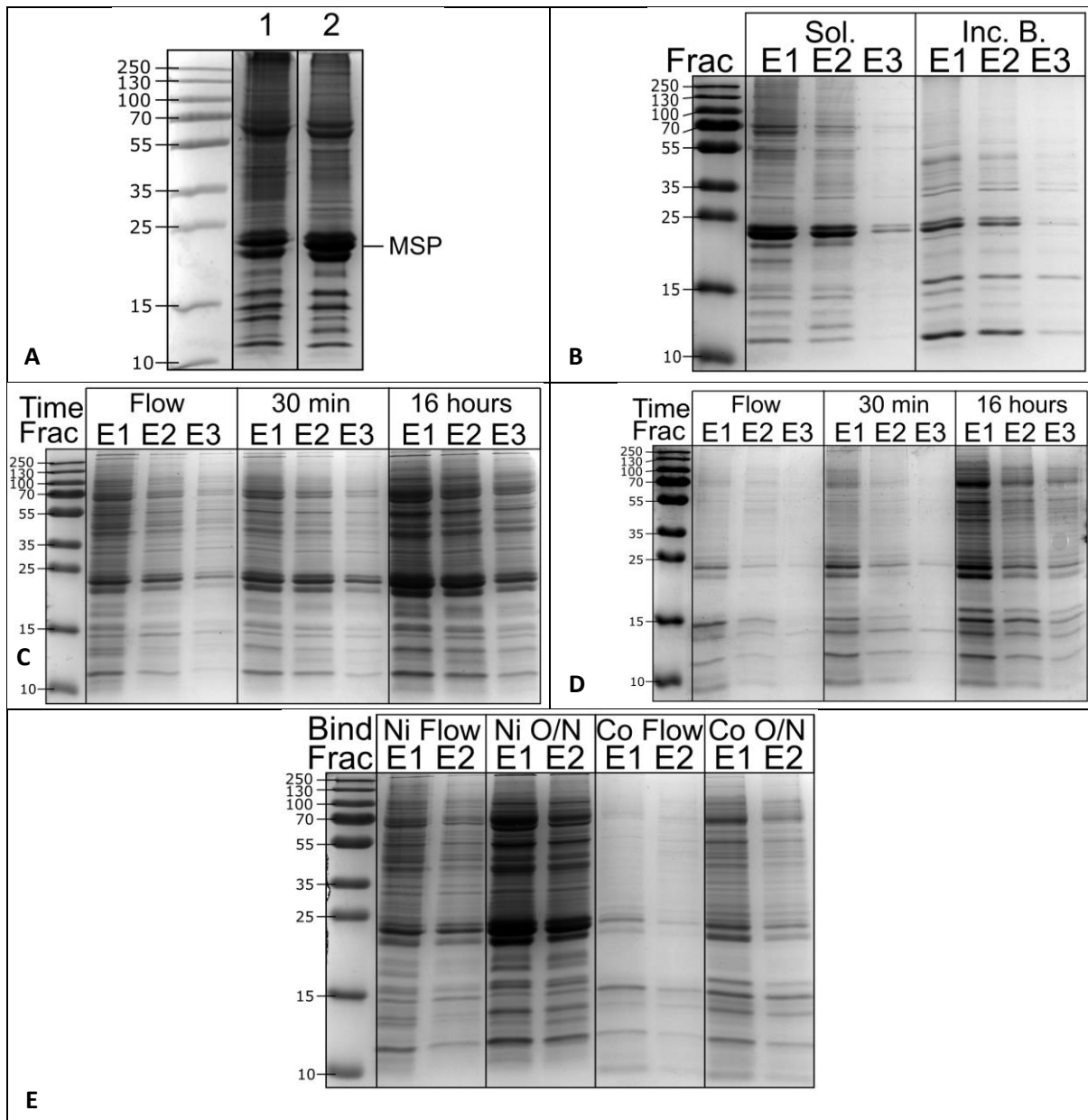
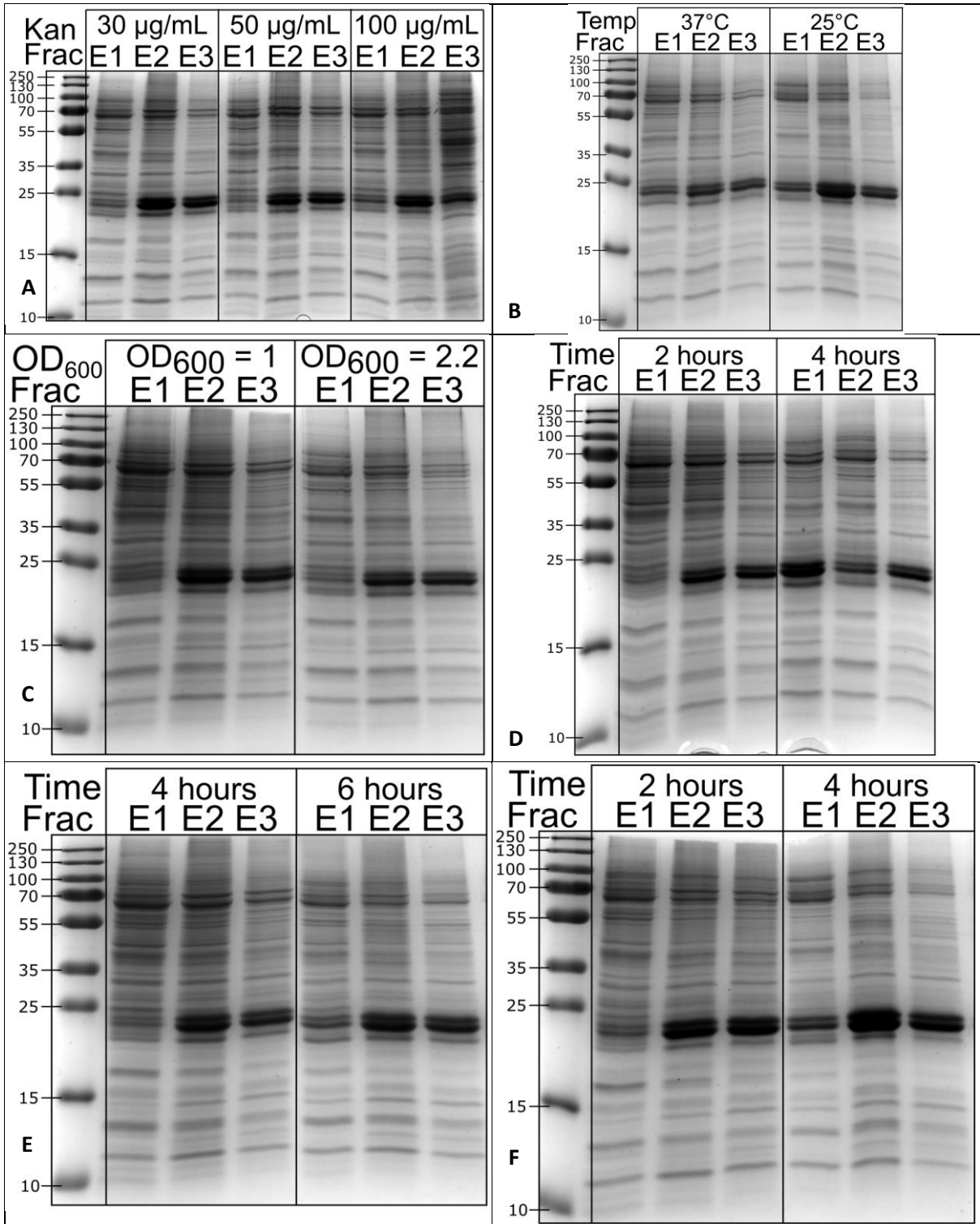


Figure 3.2.2-1 Optimisation of MSP1E3D1 purification. **A:** Elution of MSP1E3D1 purified according to the two sets of conditions detailed in Table 3.2.2-1. Condition 2 forms the basis for further optimisation attempts. **B:** Elution of MSP1E3D1 purified either from the soluble fraction resulting from the clarification of cell lysate, or from the Gdm HCl solubilised inclusion bodies from the same cell batch, expressed through condition 2. **C:** Elution of MSP1E3D1 expressed through condition 2 and purified using nickel sepharose resin. Time of incubation of the clarified lysate with resin is shown, with “flow” indicating the lysate to be passed over a gravity flow column with no prior incubation with resin. **D:** Elution of MSP1E3D1 expressed through condition 2 and purified using cobalt sepharose resin. Time of incubation of clarified lysate with resin is shown, with “flow” indicating the lysate to be passed over a gravity flow column with no prior incubation with resin. **E:** Elution of MSP1E3D1 expressed through condition 2 and purified using either nickel or cobalt resin, both with no resin incubation prior to addition to the gravity flow column and overnight pre-incubation of the clarified lysate with resin.

With purification optimised, a range of expression conditions were trialled in small scale cultures and the yield examined through purification, according to the optimal conditions established above. Lowering Kanamycin concentration from 100 µg / mL to 50 µg / mL, and again to 30 100 µg / mL resulted in incremental increases in final MSP1E3D1 yield, likely do to reducing pressure upon the expressing cells (Figure 3.2.2-2A).

Varying combinations of growth temperatures (37°C and 25°C), induction OD_{600S} (3.5 and 1), and expression times (2, 6, and 6 hours) were compared in order to allow a quick exploration of the effects of these factors (Figure 3.2.2-2B-G). It was consistently observed that growth at 25°C resulted in higher MSP1E3D1 yields levels than 37°C (Figure 3.2.2-2B), indicating that the slowed expression rates encouraged by a lower incubation temperature were beneficial to production of this protein. The lower expression OD₆₀₀ of 1.0 appeared to consistently allow higher yields of MSP1E3D1 than 3.5 (Figure 3.2.2-2C), as it seemed the expression of this protein was not toxic to cell growth and therefore cell count could continue to increase even whilst expression continued. Finally, increasing expression times from 2 to 4 hours, and from 4 to 6 hours consistently resulted in a higher yield of MSP1E3D1 at both 37°C (Figure 3.2.2-2D & Figure 3.2.2-2E), and 25°C (Figure 3.2.2-2F & Figure 3.2.2-2G), as production continued to outpace degradation in this slowly expressing system.

As an alternative approach, the MDA5052 system used for VcINDY expression (see 2.6.1.3 MDA5052 / Lemo21(DE3) Expression), employing Lemo(DE3) cells in a complex, defined, autoinducing media, was trialled as this system is known to be effective for difficult to express proteins [82], however this resulted in very poor yields compared to the BL21(DE3) approach examined thus far (Figure 3.2.2-2H).



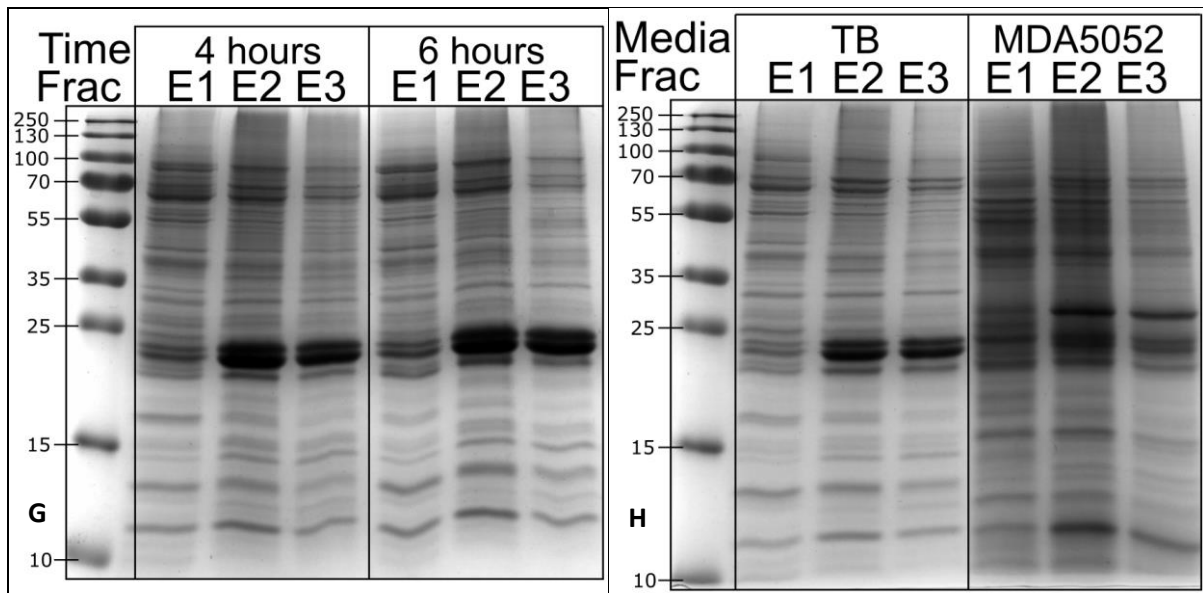


Figure 3.2.2-2 Elution fractions of MSP1E3D1 expressed with variations on method 2. **A:** Elution fractions for MSP1E3D1 expressed according to condition 2, in the presence of varying concentrations of kanamycin. **B:** Elution fractions for MSP1E3D1 expressed according to condition 2, grown at either 37 °C or 25 °C. **C:** Elution fractions for MSP1E3D1 expressed according to condition 2, whereby expression was induced either at OD600 = 1.0 or 2.2. **D:** Elution fractions for MSP1E3D1 expressed according to condition 2, whereby cells were harvested either 2 or 4 hours post induction of expression using IPTG. **E:** Elution fractions for MSP1E3D1 expressed according to condition 2 with the modification of inducing expression at OD600 = 1.0 , whereby cells were harvested either 4 or 6 hours post induction of expression using IPTG. **F:** Elution fractions for MSP1E3D1 expressed according to condition 2 with the modification of cells being incubated at 25 °C , whereby cells were harvested either 2 or 4 hours post induction of expression using IPTG. **G:** Elution fractions for MSP1E3D1 expressed according to condition 2 with the modifications of inducing expression at OD600 = 1.0 and the cells being incubated at 25 °C, whereby cells were harvested either 4 or 6 hours post induction of expression using IPTG. **H:** Elution fractions for MSP1E3D1 expressed either according to condition 2, or through the Lemo21(DE3) MDA5052 expression system used for the expression of VcINDY elsewhere in this thesis.

The results of these two experiments indicated that MSP1E3D1 was produced at a low, non-toxic, rate in *E. coli*, resulting in modest yields. This differed sufficiently from existing reports of MSP production that it became clear that something in the current expression system was behaving in an unexpected manner. Two possibilities were considered; either the hard water content of Kent was not being properly removed by the lab purification equipment, and thus the “ddH₂O” contained unexpected ions, or that there was a problem with the BL21(DE3) cell stock. Thus, new test cultures were grown using the current optimal conditions (30 µg/mL Kanamycin, induction OD₆₀₀ = 1, expression 25°C, expression time 6 h).

The change to ultra-pure water had no impact (Figure 3.2.2-3A), however the newly sourced BL21(DE3) cells produced vastly more MSP1E3D1 (Figure 3.2.2-3B). The source of the strange expression behaviour was, therefore, found to be a faulty glycerol stock.

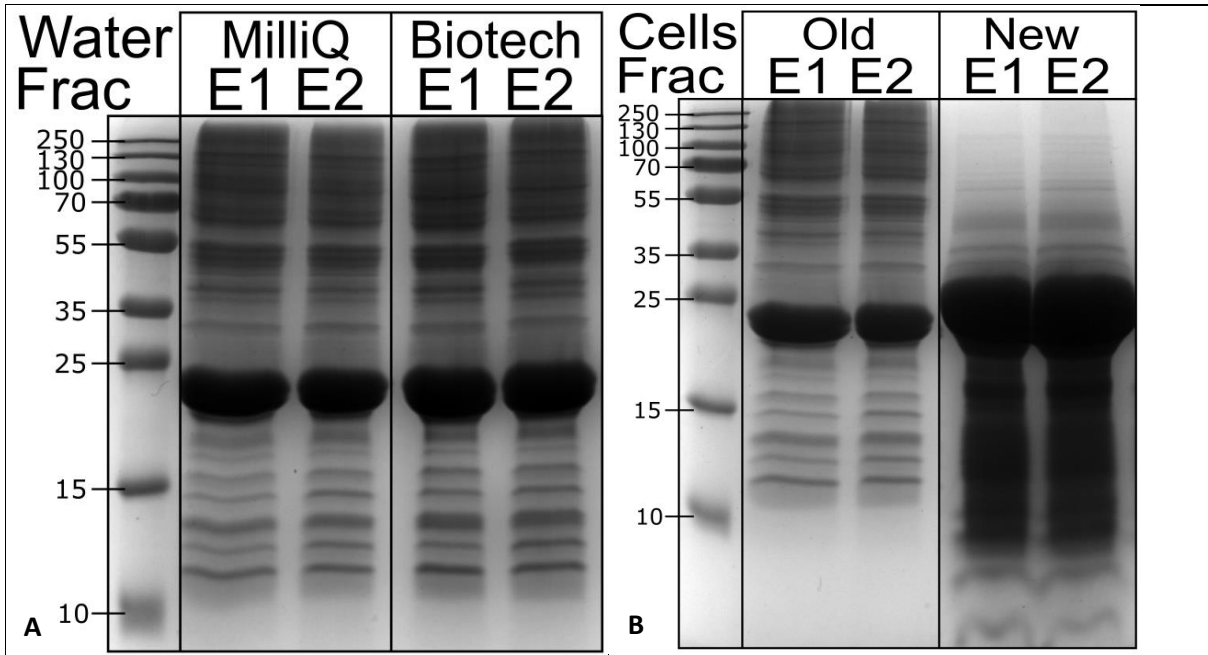


Figure 3.2.2-3 Elution fractions from troubleshooting of MSP1E3D1 expression using the best conditions as determined

in Figure 3.2.2-2; 30 $\mu\text{g}/\text{mL}$, 25°C expression, induction $\text{OD}_{600} = 1$, 6 hours expression time. **A:** Elution fractions for MSP1E3D1 grown in media containing either the MilliQ purified water used throughout this thesis, or with ultrapure biotech grade water. **B.** Elution fractions for MSP1E3D1 expressed using either the original BL21(DE3) stock used thus far, or a new stock of BL21(DE3).

Moving forwards, the purification optimisation data was perfectly usable, and would continue to define the purification conditions used. The expression, however, would need to be re-tested. Now the expression levels exhibited by the fresh BL21(DE3) stock were sufficient for a Coomassie blue stain of clarified lysate to clearly observe any change in expression. Again, a combination of conditions were examined in order to allow swift one shot optimisation of expression, effectively establishing the optimal set of conditions for expression (Figure 3.2.2-4). The highest expression of MSP1E3D1 clearly occurred with an induction OD_{600} of 2.2, an expression time of 4 hours, and an expression temperature of 37 °C.

Now, with expression and purification optimised, the protein could be produced in large quantities without difficulty. Large scale expression using this system produced ~127 mg of MSP1E3D1 from 6 L of original culture, giving a yield of ~21 mg / L (Figure 3.2.2-5).

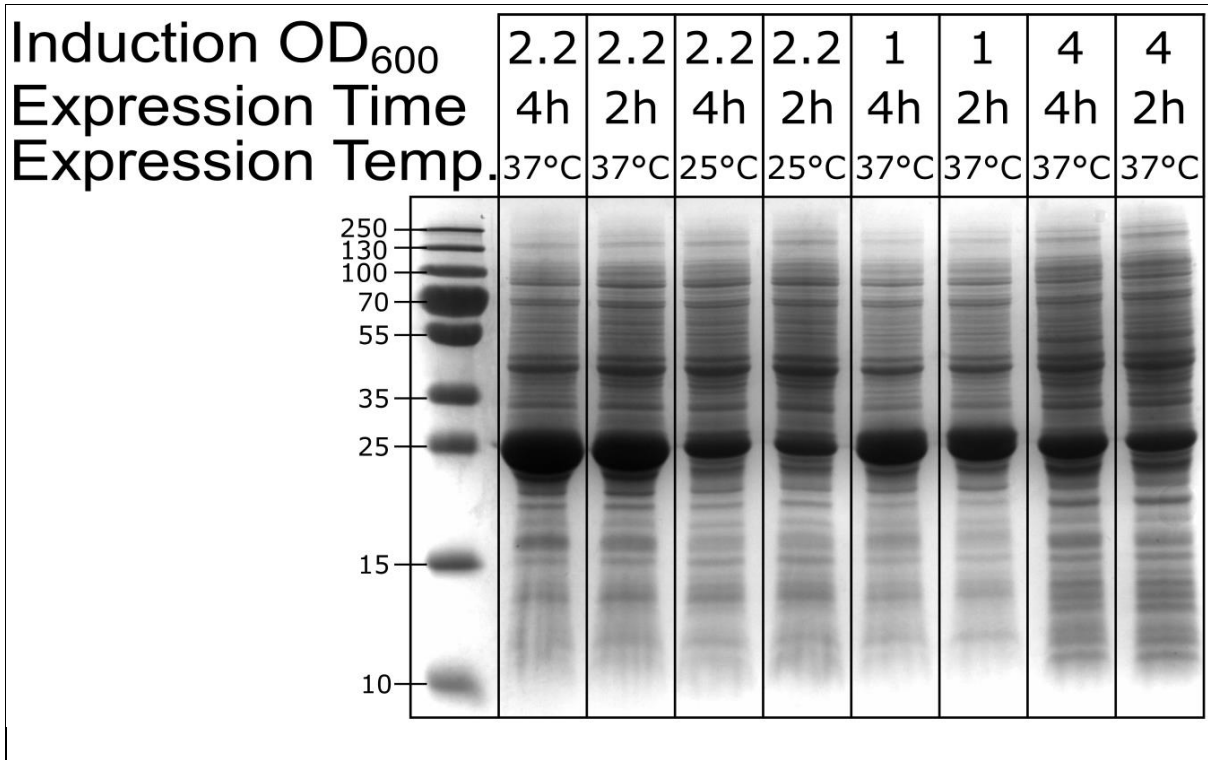


Figure 3.2.2-4 One shot optimisation of MSP1E3D1 expression with variants of method 2. Due to the high expression levels purification was not required for screening. Instead Coomassie blue stained clarified lysate is shown.

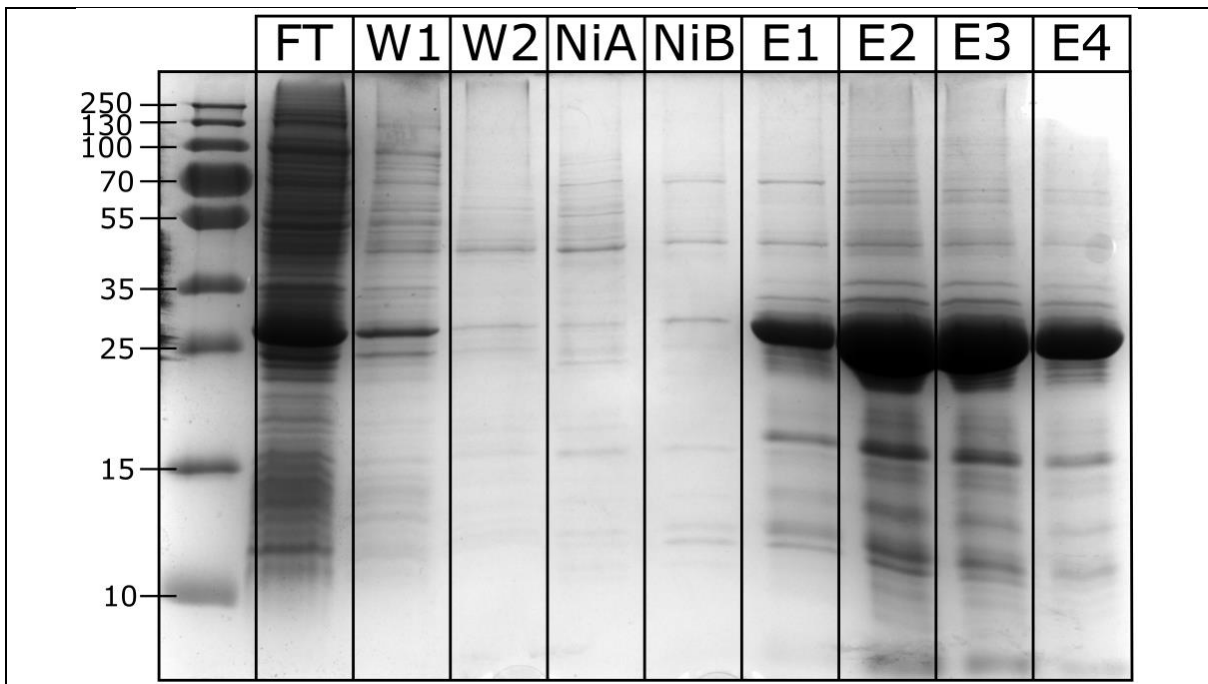


Figure 3.2.2-5 Final yield of MSP1E3D1 produced with optimal conditions and fresh BI21(DE3). The results of nickel Sepharose affinity purification are shown. Fractions: FT = Flowthrough. W1 = Wash 1. W2 = Wash 2. NiA = Nickle buffer A. NiB = Nickle buffer B. E1-4 = Elution fraction 1-4.

3.2.3 Optimisation of TEV Protease Production

Now that MSP1E3D1 could be produced at acceptable levels, the next component of the nanodisc process could be optimised. The current MSP1E3D1 construct contains an N-terminal his tag, used for purification of the protein. In order to be compatible with later steps in the nanodisc creation process (see 3.2.5 Optimisation of the Reconstitution of VcINDY into MSP1E3D1 Based Nanodiscs), this his tag must be removed through the cleavage of a TEV protease recognition site (Figure 3.2.3-1A) [87].

In order to achieve this, TEV protease was produced recombinantly. When expressed alone in *E. coli*, TEV protease folds poorly, rendering the majority of produced protein insoluble and unusable [123]. In order to compensate for this, TEV protease is expressed linked to Maltose Binding Protein (MBP), which acts as a folding chaperone. The construct used here contains a TEV cleavage site between MBP and TEV, allowing specific *in vivo* cleavage to separate these two proteins, providing a pure product (Figure 3.2.3-1B) [123][124].

In order to swiftly optimise the expression of TEV protease, existing protocols were compared through the growth of small scale 10 mL cultures, cell pelleting, resuspension and lysis in 1 mL of lysis buffer, and examination of the clarified lysate by Coomassie blue staining (see **METHODS** for details). All cultures were LB broth + 100 µg / mL ampicillin, grown until an OD₆₀₀ of 0.6 at which point expression was induced through IPTG addition, and expression continued overnight. Differing IPTG concentrations, 0.4 mM vs 1.0 mM, pre-induction growth temperatures, 37 °C vs 25 °C, and post-induction growth temperatures, 37 °C vs 25 °C, were trialled. It was observed that the highest expression of TEV protease was achieved using 0.4 mM IPTG and a constant concentration of 37 °C (Figure 3.2.3-2A).

Using these conditions, large scale expression allowed ~136 mg to be produced from 6 L (Figure 3.2.3-2), giving a final yield of ~22.7 mg/L.

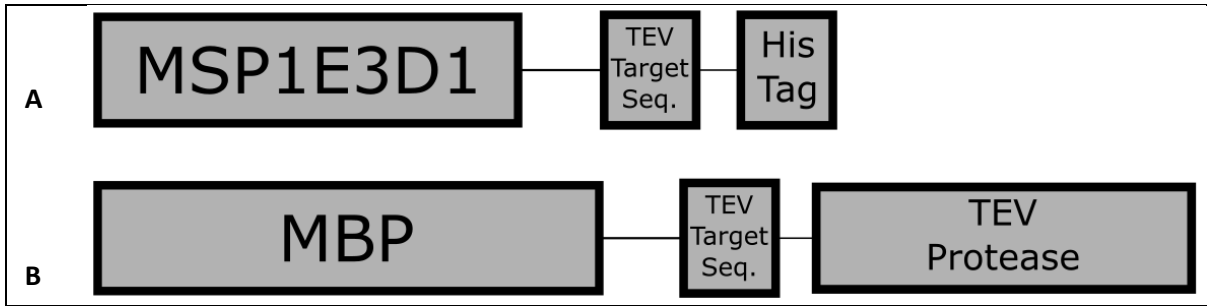


Figure 3.2.3-1 Location of TEV protease target sequences in expressed constructs. **A:** MSP1E3D1, showing the TEV target sequence located to allow cleavage and removal of the his-tag [87]. **B:** TEV protease expression construct, showing the TEV target sequence located to allow *in vivo* cleavage and removal of the MBP expression chaperone [123][124].

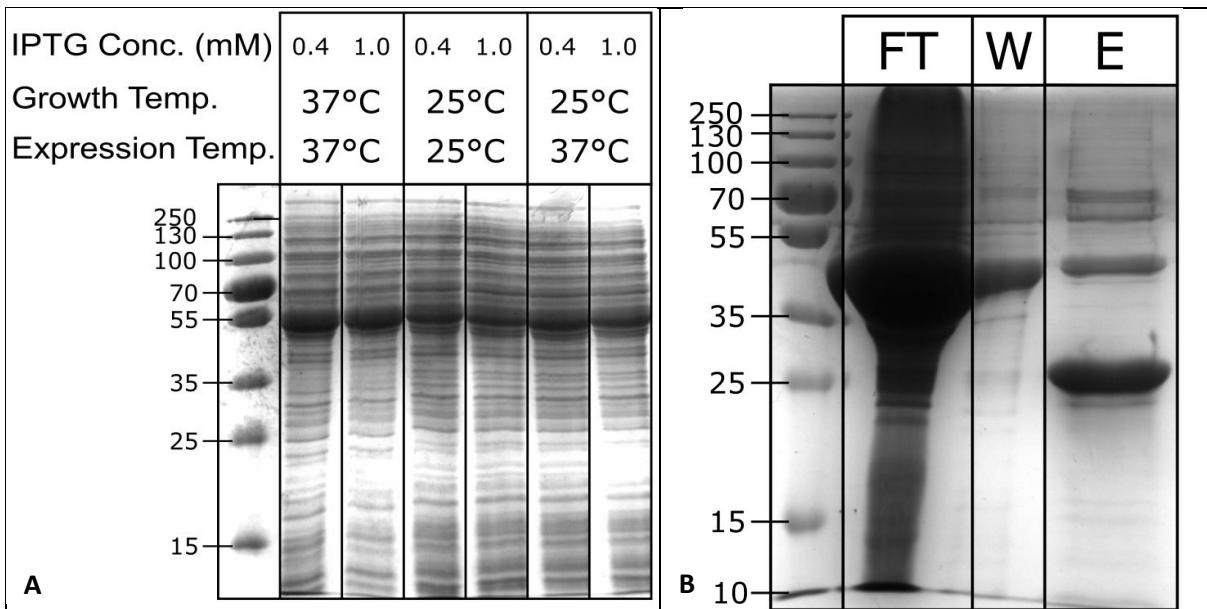


Figure 3.2.3-2 Production of TEV protease. **A:** Clarified lysates for BL21(DE3) cells expressing TEV protease with varying incubation temperatures and concentrations of IPTG used to induce expression. While TEV Protease and MBP are produced at an equimolar ratio, the far larger MBP protein stains to a greater intensity. MBP intensity is, therefore, a useful measure of TEV expression levels. **B:** Nickel sepharose based affinity purification of TEV protease produced under the best established conditions. Labels: FT = Flowthrough. W = Wash. E = Elution.

3.2.4 Optimisation of the Cleavage and Removal of the MSP1E3D1 Construct's His-Tag

Now that MSP1E3D1 and TEV protease are able to be produced in sufficient quantities, the removal of the his-tag from MSP1E3D1 by TEV protease must be optimised. Step 1 of this process is to ensure sufficient cleavage takes place. Literature conditions for this process vary from 18 h at 28°C with a 1:30 ratio of TEV to MSP1E3D1 [87][125] to 1.5 h at room temperature with a 1:150 ratio of TEV to MSP1E3D1 [126]. Here, 3 hours at room temperature was trialled with varying ratios. Due to the drop in molecular weight associated with the removal of the his-tag, the process was assessed through Coomassie blue stained gels. The addition of TEV protease resulted in some cleavage of MSP1E3D1 in all conditions (Figure 3.2.4-1A). Low levels of TEV protease, such as 1:200, resulted in only partial cleavage under these conditions, demonstrated by the separation of MSP1E3D1 into two bands, one of the original MW, and new, lower MW, band representing MSP1E3D1 without the his tag region. Increasing the levels of TEV protease used to a ratio of 1:50 TEV to MSP1E3D1 or higher resulted in almost complete cleavage of the MSP1E3D1 his tag, and depletion of the band representing uncleaved MSP1E3D1. As such, a TEV protease to MSP1E3D1 ratio of 1:50 will be used as standard from hereon.

Step 2 of this process is to ensure the cleaved his-tag is effectively removed. This is performed through reverse affinity chromatography, as the cleaved protein mixture is passed over an affinity column, sequestering the cleaved tag and allowing his-free MSP1E3D1 to flow through. Initially, cleaved MSP1E3D1 was incubated for one hour with nickel affinity resin in the presence of 50 mM Tris pH 7.0 and 200 mM NaCl before purification (see 2.8.2 Purification of MSP1E3D1) (Figure 3.2.4-1B). While this approach effectively removed the cleaved his tag from the flowthrough, the majority of cleaved MSP1E3D1 was also lost from the flowthrough, largely entering the elution fractions along with the cleaved his-tag. This is likely due to interactions between these amphipathic helices causing his-free MSP1E3D1 molecules to co-purify with the few remaining uncleaved MSP1E3D1 molecules.

In order to compensate for this a rapid optimisation experiment was performed. Previous literature supports either the substitution of the nickel based resin for cobalt based resin [126], or supplementation with the detergent choline [87][125]. Cobalt and nickel-based resins were directly compared (Figure 3.2.4-1C), showing that while nickel resin lead to both MSP1E3D1 itself and the cleaved his-tag occurring predominantly in the wash and elution fractions, cobalt resin led to both MSP1E3D1 itself and the cleaved his tag occurring predominantly in the flowthrough elution fractions. As such, neither resin provided the desired separation of MSP1E3D1 and cleaved his tag under these conditions.

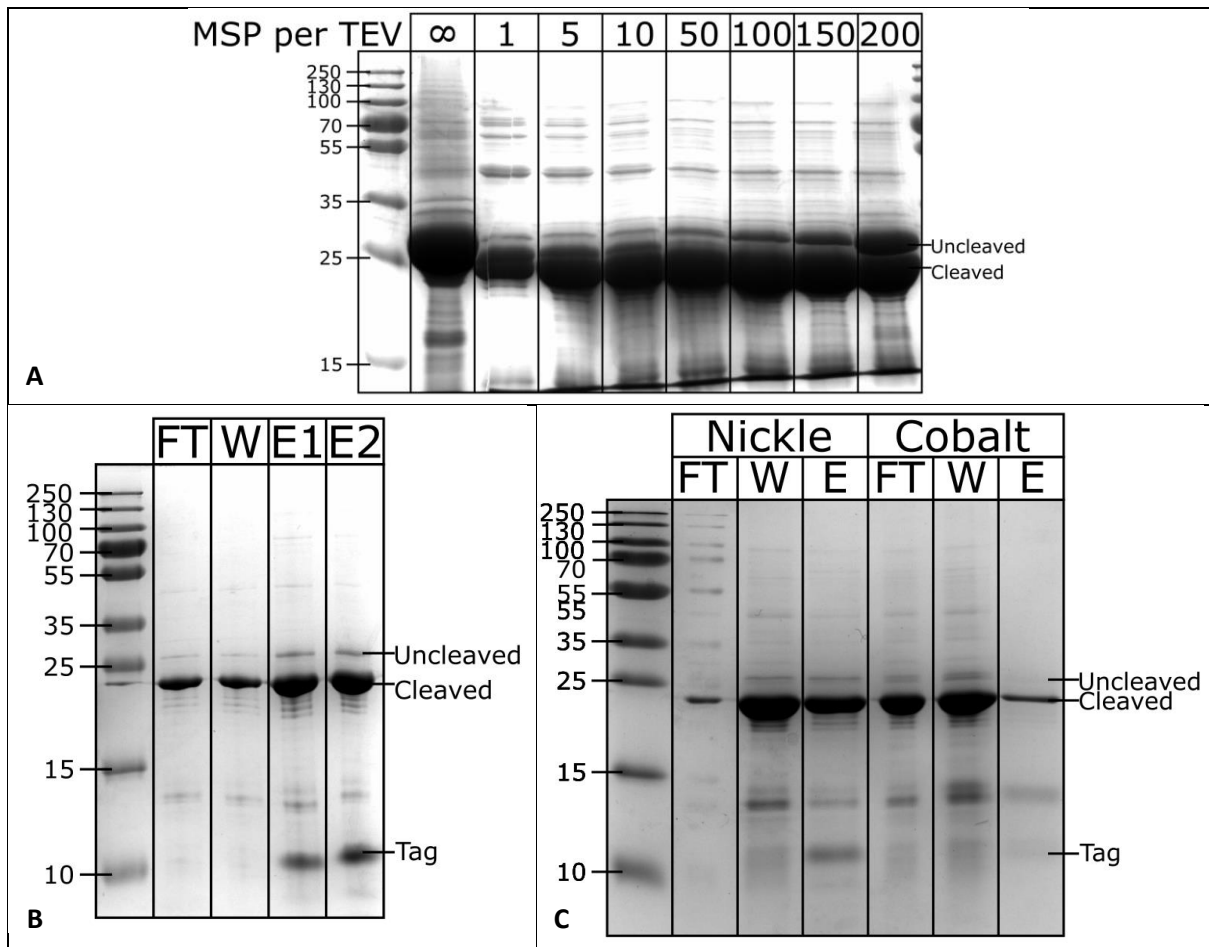


Figure 3.2.4-1 Initial optimisation of the cleavage and removal of the MSP his-tag. **A:** Trial digestions for various ratios of TEV protease to MSP1E3D1, including a zero TEV control. Digestion is carried out over 3 hours at room temperature. Digestion can be observed through the reduction in molecular weight after the removal of the his-tag. **B:** Initial attempt at removal of the cleaved his-tag from MSP1E3D1 through reverse affinity purification, using a one hour incubation with nickel-based affinity resin with no additives. **C:** Comparison of nickel and cobalt based resins for the removal of the cleaved his-tag from MSP1E3D1 through reverse affinity purification.

The effects of the addition of 10% glycerol to the buffers in order to break hydrophobic interactions, or 50 mM cholate to fully coat the hydrophobic patches upon the MSP molecules, were trialled for both affinity resin types. For cobalt based purification, the introduction of 10% glycerol increased the proportion of the cleaved his-tag found within the elution fraction, and the introduction of 50 mM cholate increased the proportion of MSP1E3D1 found within the flowthrough fraction (Figure 3.2.4-2A). Both supplements therefore improved the level of separation between MSP1E3D1 and the cleaved his-tag during cobalt based reverse affinity purification, but failed to provide sufficiently high levels of separation. For nickel based purification, the introduction of 10% glycerol increased the proportion of MSP1E3D1 found within the flowthrough and increased the proportion of cleaved his-tag found within the elution fraction, while the addition of 50 mM cholate provided similar effects, but of a far higher magnitude (Figure 3.2.4-2B). Nickel based reverse affinity purification in the presence of 50 mM cholate therefore allowed effective separation of MSP1E3D1 and the cleaved his-tag, with the majority of MSP1E3D1 being found in the flowthrough and wash fractions, whilst almost all of the cleaved his-tag was found in the elution fraction. As such, nickel-based resin with the supplementation of 50 mM cholate is chosen for future use in this process.

During this optimisation a wash of 2 column volumes (2CV) has been used. For the final adaptation to this process, the wash volume is increased to 5 incremental 2CV additions to ensure all possible cleaved MSP is recovered. With this final modification, the process is ready to be used in large scale processing of MSP, providing high levels of separation as the vast majority of MSP1E3D1 is found within the flowthrough and wash fractions, while almost all the cleaved his-tag is found within the elution fractions (Figure 3.2.4-2C).

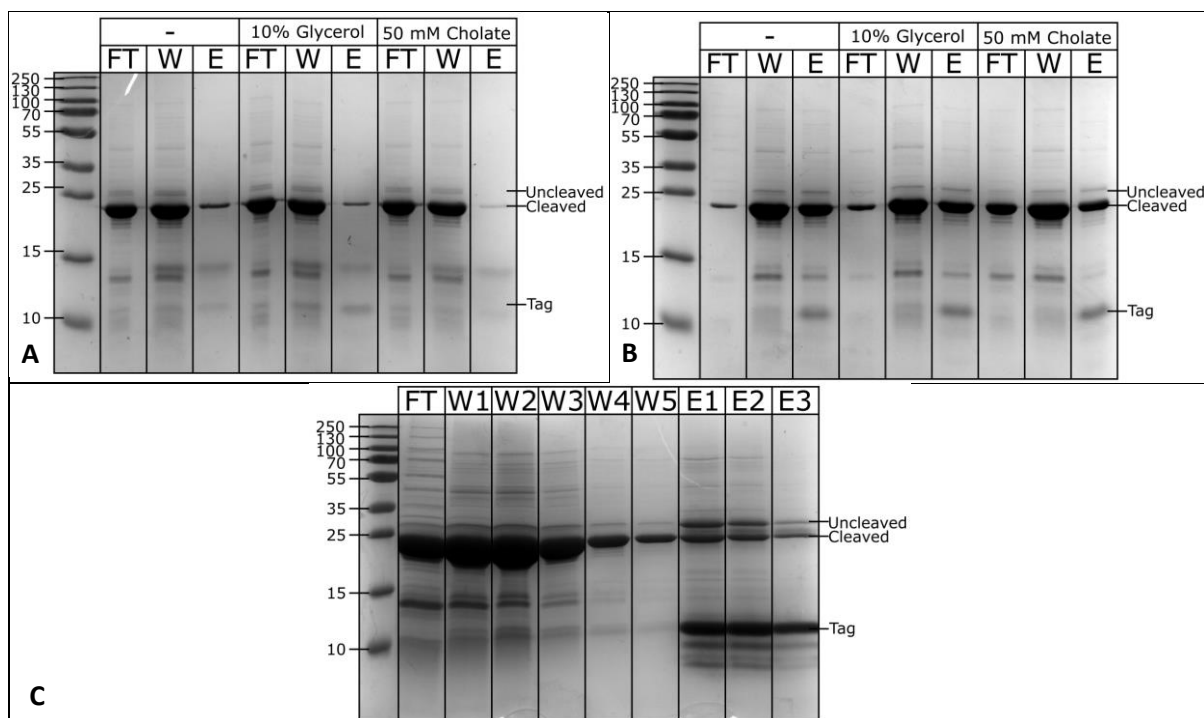


Figure 3.2.4-2 Optimisation of the removal of the MSP his-tag. **A:** Effect of the addition of 10% glycerol or 50 mM cholate to cobalt based reverse affinity purification removal of cleaved his-tag from MSP. **B:** Effect of the addition of 10% glycerol or 50 mM cholate to nickel based reverse affinity purification removal of the cleaved his-tag from MSP. **C:** Final reverse affinity purification based removal of cleaved his-tag from MSP1E3D1 using nickel resin with 50 mM cholate supplementation and additional wash steps. Labels: FT FT = Flowthrough. W = Wash. E = Elution.

3.2.5 Optimisation of the Reconstitution of VcINDY into MSP1E3D1 Based Nanodiscs

The first parameter of this process which must be optimised is the ratio of VcINDY to MSP1E3D1.

Previous work on the related elevator mechanism transporter Glt_{Ph} found the optimal ratio to be 3:5 [27], however protocols provided by another laboratory for VcINDY specific work suggested a 1:25 ratio to be optimal. In the face of such uncertainty a screen of possible ratios was carried out, namely 1:2, 1:5, 1:10, and 1:25.

The reconstitution method used here is a biobead based method. VcINDY, MSP, and Lipids are mixed at the desired molar ratio and allowed to equilibrate at 4°C for one hour, before the addition of 0.25 g/mL biobeads, followed by another 3 hours of incubation at 4°C to allow detergent removal. After this, the hopefully reconstituted VcINDY nanodiscs are incubated with nickel affinity resin and separated from empty nanodiscs through standard affinity purifications.

These test ratios of VcINDY to MSP1E3D1 were examined with a fixed VcINDY to Lipid ratio of 1:500, using *E. Coli* Total Lipid Extract (see Table 4.3.4-1). It was observed that the level of VcINDY found in the flowthrough, likely aggregate unable to bind to the resin, compared to the level of VcINDY co-eluting with MSP1E3D1, likely indicating nanodiscs, varied greatly with differing MSP1E3D1 to VcINDY ratios (Figure 3.2.5-1A-D). 1:2 resulted in by far the most lost VcINDY, while 1:5 appeared to result in the highest level of VcINDY incorporation into possible nanodiscs, with almost all VcINDY remaining soluble and co-eluting with MSP1E3D1 under this condition. The lower ratios, 1:10 and 1:25, while also showing little lost VcINDY in the flowthrough, showed lower levels of incorporation of VcINDY into the elution fractions, especially the 1:25 ratio. As such the 1:5 ratio of VcINDY to MSP1E3D1 was carried forward as the optimal ratio.

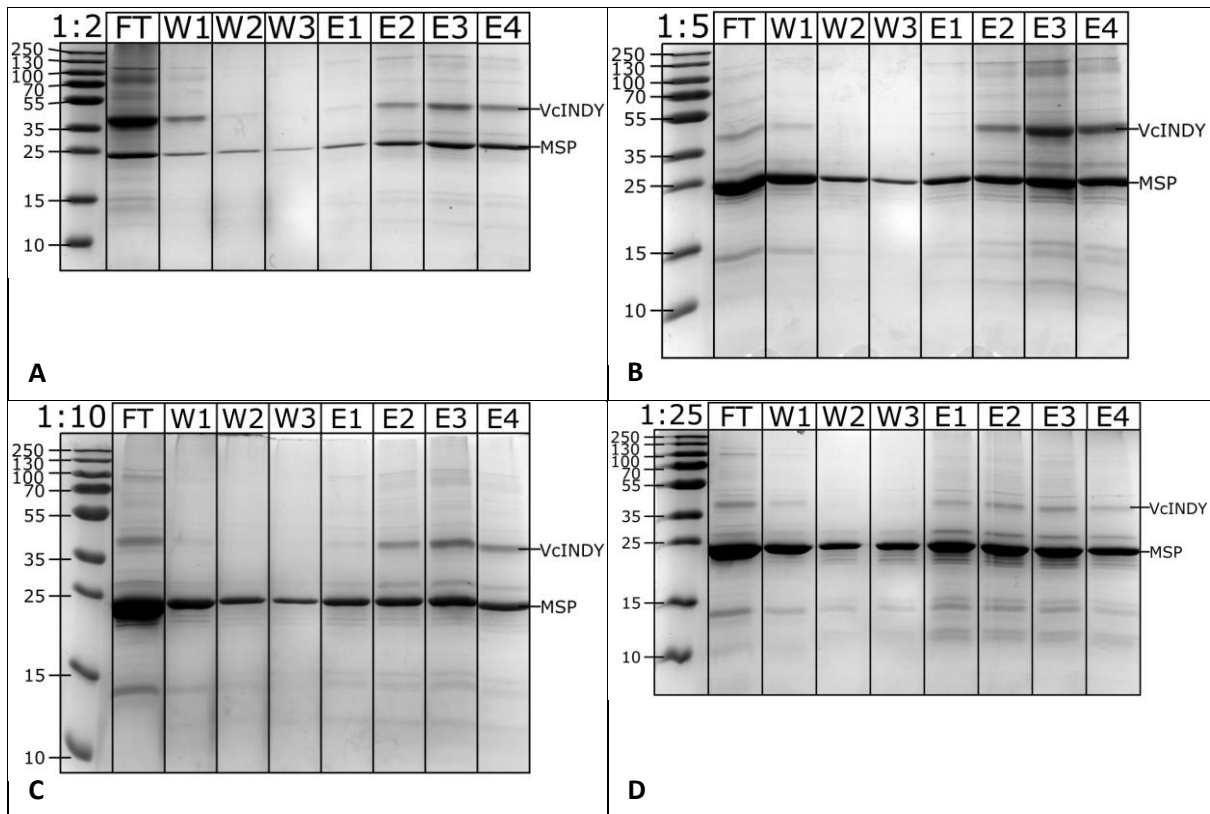


Figure 3.2.5-1 Reconstitution of VcINDY into MSP1E3D1 nanodiscs using varying ratios of VcINDY to MSP. All

reconstitutions are performed with a VcINDY to TLE ratio of 1:500. Reconstitutions were carried out through one step removal of detergents with Biobeads. Reconstituted VcINDY nanodiscs were incubated with nickel affinity resin and purified, removing empty nanodiscs and aggregates. The ratio of VcINDY to MSP for each experiment is indicated.

Now that a good reconstitution efficiency had been achieved, with sufficient yields of VcINDY remaining solubilised in the absence of detergent, the homogeneity of the produced nanodiscs had to be examined and optimised. Putative nanodiscs produced through VcINDY to MSP1E3D1 ratios of 1:25 and 1:5 were analysed through HPLC SEC with inline UV A_{280} detection. This resulted in two overlapping peaks in both instances, around 10.5 mL and 12 mL (Figure 3.2.5-2A), not the single peak desired, indicating that optimisation of the VcINDY to lipid ratio, currently 1:500, was required.

A lower lipid concentration was trailed, with a VcINDY to MSP to Lipid ratio of 1:5:100, producing highly efficient reconstitution as followed by Coomassie blue stained gels. This new ratio resulted in a clear change to the absorbance trace generated through SEC analysis (Figure 3.2.5-2A), with a clear reduction of the 12 mL peak intensity in comparison to the 10.5 mL peak. Examination of fractions produced by this run through Coomassie blue stained SDS-PAGE shows the band representing VcINDY disappearing from later peak fractions while MSP remains (Figure 3.2.5-2B), indicating that the 12 mL peak observed in these traces is in fact empty nanodiscs.

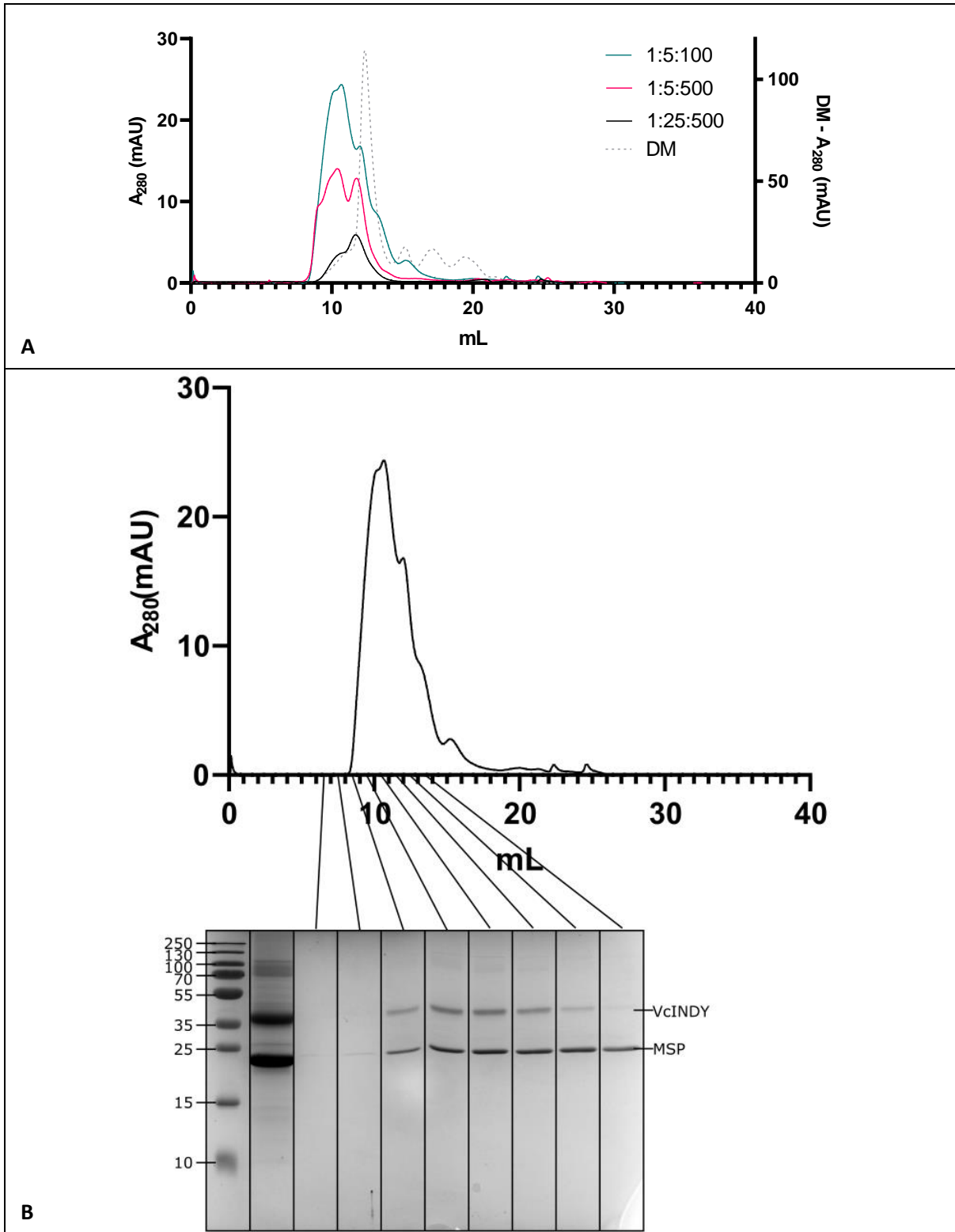


Figure 3.2.5-2 HPLC SEC in line 280 nm absorbance readings for varying VcINDY nanodisc reconstitution ratios. **A:**

Putative VcINDY nanodiscs created using differing reconstitution ratios of VcINDY : MSP1E3D1 : TLE lipids are shown. A

reference detergent (DM) solubilised WT VcINDY trace is displayed on a second axis for comparison. **B:** The 280 nm

absorbance spectrum of putative VcINDY nanodiscs reconstituted using the 1:5:100 ratio of VcINDY : MSP1E3D1 : TLE, with

elution fractions shown through Coomassie blue staining.

In order to confirm this observation, the SEC column, a Superdex 200 Increase 10/300 GL, was calibrated against known commercial standards (Table 3.2.5-1). While SEC calibration is often viewed as a technique for the estimation of protein molecular weight, it is more accurately a technique for determining the frictional coefficient of molecules. While molecular weight and frictional coefficient will correlate for uniformly shaped proteins, these two parameters deviate substantially for proteins of differing shapes [127]. The frictional coefficient may not seem of great use, however for practical purposes this value can be substituted with the Stokes Radius; the radius of a smooth sphere possessing the same frictional coefficient as the molecule in question [127]. As such, calibrating the column according to known Stokes Radius values will allow rough estimation of the sizes of molecules run on the SEC column, remembering that the values found will not account well for features such as ellipticity and will include any hydration shells.

The calibration run was effective, with all standards resolved into clear peaks (Figure 3.2.5-3A), allowing calibration curves to be plotted and equations to be derived for both estimated molecular weight (Figure 3.2.5-3B & Figure 3.2.5-3C) and Stokes Radius (Figure 3.2.5-3D & Figure 3.2.5-3E).

Applying this to the data already gathered it is seen that the 10.5 mL peak has a Stokes Radius of around 7 nm, while the 12 mL peak has a Stokes Radius of around 5.5 nm (Figure 3.2.5-3F). Common literature estimations of empty MSP1E3D1 size to range from 5.5 to 6.0 nm, as determined through Analytical Ultracentrifugation (AUC)[128][129] and Small Angle X-Ray Scattering (SAXS) [130]. These values agree well with the Stoke's Radius estimates made here, strongly indicating the second peak to represent empty nanodiscs (Figure 3.2.5-3F). Observing the relative height of this putative empty nanodisc peak compared to the putative VcINDY containing nanodisc peak in the 1:25:500 reconstitution sample compared to the 1:5:500 reconstitution sample, it is seen that a reduction of excess MSP1E3D1 leads to a reduction in the formation of empty nanodiscs compared to nanodiscs containing VcINDY; a reasonable observation which supports this identification of the peaks.

The yield and quality of reconstituted VcINDY nanodiscs has therefore been greatly improved over the rounds of optimisation carried out herein, with a VcINDY to MSP to TLE ratio of 1:5:100 providing the highest level of incorporation of VcINDY into homogenous nanodiscs, however future work should be carried out in order to further improve the heterogeneity of the reconstituted samples through fine tuning of the constituent ratios and alterations in the reconstitution method itself.

Protein	Mw (kDa)	Stokes Radius (nm)
Thyroglobin	669 ¹	8.5 ¹
Ferritin	440 ¹	6.1 ¹
Aldolase	158 ¹	4.81 ¹
Conalbumin	75 ¹	3.64 ²
Ovalbumin	44 ¹	3.05 ¹
Carbonic Anhydrase	29 ¹	2.3 ²
Ribonuclease A	13.7 ¹	1.64 ¹

Table 3.2.5-1 Molecular weights and Stoke's Radius sizes for the standard proteins in the High and Low molecular weight

GE Healthcare Gel Filtration Calibration Kits used to calibrate the superdex 200 increase 10/300 HPLC SEC column. ¹

Values taken from the GE Healthcare Gel Filtration Calibration Kit Manual. ² Values absent from GE Healthcare documentation taken instead from Sigma Aldrich documentation of the equivalent product.

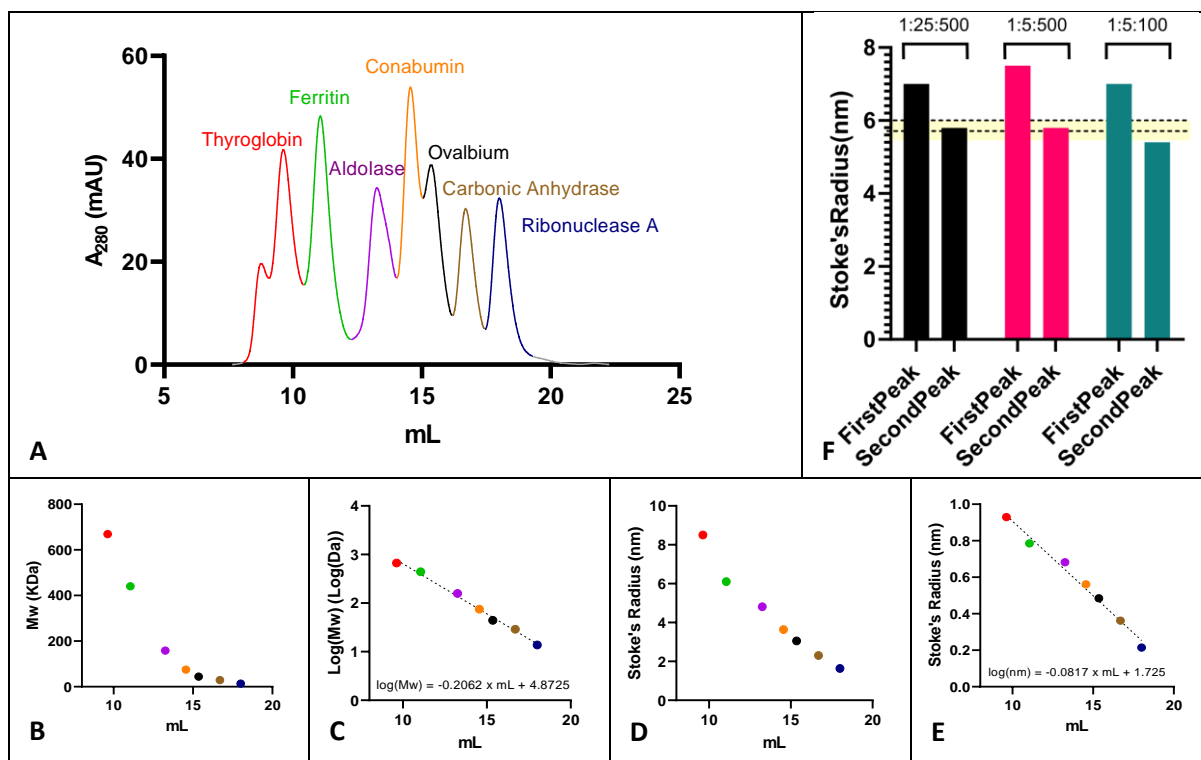


Figure 3.2.5-3 Calibration of the superdex 200 increase 10/300 SEC column. **A:** Initial calibration run. The following proteins were loaded onto the column simultaneously, and their resultant absorbance peaks are labelled; 3 mg/mL Thyroglobin, 0.3 mg/mL Ferritin, 3 mg/mL Aldolase, 3 mg/mL Conalbumin, 3 mg/mL Ovalbumin, 3 mg/mL Carbonic Anhydrase, 3 mg/mL Ribonuclease A. **B:** Known molecular weights of standard proteins against retention volume as determined in part A of this figure. **C:** Logarithmic fitting of molecular weight and retention volume, producing a standard curve applicable to similarly shaped globular proteins. **D:** Known Stokes Radii of standard proteins against retention volume as determined in part A of this figure. **E:** Logarithmic fitting of Stokes Radii and retention volume, producing a standard curve for estimation of Stokes Radii of unknown molecules. **F:** Estimated Stokes Radii of major peaks produced by VcINDY nanodisc reconstitutions with varying VcINDY : MSP : TLE ratios, in order of elution. Literature estimations of empty MSP1E3D1 sizes are indicated by horizontal lines and a highlighted range [128][129][130].

3.2.6 Chapter Summary

The creation of MSP based nanodiscs required the expression and purification of two proteins, MSP1E3D1 and TEV protease. High throughput troubleshooting work was carried out upon MSP1E3D1 production, greatly improving the existing purification protocol and discovering issues with the laboratory stocks of BL21(DE3) cells. Further high throughput optimisation allowed a final yield of 21 mg / L to be achieved using simple TB media. The other protein, TEV Protease, benefited from lessons learnt in MSP1E3D1 optimisation, being expressed with the fresh BL21(DE3) cells throughout its own optimisation process, allowing yields of 23 mg / L to be achieved using simple 2YT media.

Next, MSP1E3D1 needed to be processed ready for use. During nanodisc reconstitution VcINDY containing nanodiscs are separated from empty nanodiscs through affinity purification using VcINDY's his-tag, making it vital that the MSP1E3D1 his-tag is cleaved by TEV Protease and removed from solution through reverse affinity purification. The enzymatic cleavage itself proved to be a robust and simple process, performing effective cleavage with a TEV protease to MSP1E3D1 ratio of 1:50, similar to the 1:30 ratios used in previous publication [87][125]. Balancing the removal of the his-tag from cleaved MSP1E3D1 solutions with retention of the his-free form of MSP1E3D1, however, required careful optimisation. In agreement with previous literature, the addition of 50 mM cholate, a mild detergent, was found to break non-specific interactions between the amphipathic MSP1E3D1 helices, greatly aiding the efficiency and effectiveness of the process and allowing high levels of separation to be achieved [87][125], although it is noteworthy that the addition of 10 % glycerol also aided the efficiency of this process, and while not as effective as cholate addition, the addition of glycerol is a potentially useful alternative in cases for which detergent addition is undesirable.

Optimisation of nanodisc reconstitution took place in two stages. In the first stage SDS-PAGE gels were used to follow the quantity of VcINDY maintained in solution in the absence of detergents and

associated with MSP1E3D1, finding the VcINDY to MSP ratio of 1:5 to be optimal. In the second stage, calibrated HPLC SEC in line 280 nm absorbance was used to optimise the heterogeneity of the VcINDY containing nanodisc samples. Through adjustment of reconstitution ratios, including reduction in excess MSP and lipids, the proportion of VcINDY containing, homogenous, nanodiscs could be greatly increased, with a VcINDY to MSP1E3D1 to TLE ratio of 1:5:100 as the best known condition thus far.

Unfortunately, due to the COVID-19 pandemic, further optimisation was not possible. Next objectives would be to continue to alter the current ratios in order to improve the homogeneity of the SEC A_{280} trace, as well as optimise the reconstitution process. The current process uses a single addition of 0.25 g/mL bio-beads to remove detergent over three hours, although previous work has found sequential smaller bio-beads to be effective, and it has been noted in literature sources that careful control of the bio-bead ratio is important for effective nanodisc formation [87][126].

The nanodiscs produced herein were briefly trialled in MST (see 4.4.1 Introduction) where they showed similar affinity to DDM detergent solubilised VcINDY, however due to the aforementioned lab shutdown experiments examining the effects of defined lipid environments on stability (examined through CPM thermofluor), affinity (examined through MST) and dynamics (examined through cysteine accessibility assays) could, sadly, not be carried out.

In this chapter, therefore, the groundwork has been laid for working with VcINDY within controlled nanodisc environments. The production of two proteins, MSP1E3D1 and TEV protease, has been optimised, along with the cleavage and removal of the MSP1E3D1 his-tag, the determination of suitable VcINDY to MSP1E3D1 ratios for efficient reconstitution, and a greatly improved VcINDY to TLE ratio has been established for the formation of homogenous nanodisc samples. The tools and techniques required to finish the optimisation of this nanodisc system are fully established herein, and will allow future experimentalists to rapidly begin using VcINDY nanodiscs in order to answer a wide range of questions as to the functional nature of this elevator mechanism transporter.

4 Results – Examination of The Mechanism and Interactions of VcINDY

4.1 Single Residue Accessibility Assays Reveal Substrate Driven Conformational Changes

4.1.1 Introduction

Cysteine is a uniquely useful amino acid for biochemical research. Accounting for around 1% of naturally occurring residues, this amino acid is sparingly used in nature [131]. When it does occur it follows distinct patterns of conservation, with cysteine residues typically possessing either extremely high or extremely low levels of conservation, representing the tight evolutionary control over the placement of this key residue [132].

Chemically, the large atomic radius of sulphur along with the low dissociation energy of the S-H bond, combined with the moderate pKa of ~6, allow nucleophilic and redox-active functions to be performed and controlled in a manner unmatched by other residues [133][134]. This allows cysteine to take up a diverse range of roles, including metal binding, catalytic nucleophile action, redox catalysis, regulation, and structural disulphide formation [134].

It is no coincidence, therefore, that this uniquely active residue is of great value to biochemical techniques. The field of bioconjugation focuses on the covalent modification of protein residues through a multitude of approaches, many of which which are better reviewed elsewhere [135][136][137][138]. Within this field, cysteine is a particularly useful target. Firstly, as mentioned above, it is amenable to reaction with a range of diverse chemical labels. Secondly, due to its low abundance many proteins will have only a few native cysteines, which can be removed through mutagenesis to produce cysteine free backgrounds upon which new cysteines can be introduced. Through this approach, a single, controllable, chemical target can be placed anywhere on the protein without fear of unwanted side reactions with other native residues.

Any chemical reaction with this single cysteine residue will, of course, depend on the position of the cysteine within the protein; if a residue is buried within the tertiary structure, reactive molecules may be unable to interact with it. This simple fact allows accessibility assays to be performed,

whereby the observation of cysteine labelling can report on whether the cysteine residue is solvent accessible. The means of labelling vary throughout the existing literature; with multiple approaches to the detection of solvent accessible cysteines having been developed. Perhaps the most prominent example of this general method, known as site-directed alkylation, can be observed in work carried out on the LacY transporter. On this transporter, dozens of positions have been examined in multiple studies, with multiple techniques applied. Fluorescent labelling with tetramethylrhodamine-5-maleimide (TMRM) followed by detection of fluorescent intensity produced accessibility data broadly in keeping with that gathered through radiolabelling with radioactive N-[ethyl-1-¹⁴C]ethylmaleimide (NEM) [139], followed by detection of radioactive signal [140]. Both studies observed clear substrate induced accessibility changes, indicating shifts to the inward and outward facing states, dependent upon the substrates added [139][140]. A further study employing the TMRM labelling approach confirmed that the accessibilities observed, along with the changes in accessibility induced by the addition of substrate, were identical for both detergent and nanodisc solubilised LacY [141], indicating the method of solubilisation to not greatly impact these assays. The method of detection, therefore, may vary but the technique of examining cysteine accessibility to gather structural and dynamic data is both consistent and powerful.

Another notable approach to cysteine accessibility assays is the inactivation of the protein through cysteine specific binding, followed by activity assays to detect the level of inactivation. This has been used to detect a substrate dependent shift to the outward facing state for the Tyt1 transporter through the monitoring of transport inactivation [142], and the reciprocal effects of cocaine and ibogaine on the LeuT transporter's conformation through the monitoring of substrate binding [143]. Accessibility may also be detected through is the labelling of accessible cysteines with a non-fluorescent dye, followed by denaturation and the labelling all free, previously inaccessible, cysteines with a fluorescent dye so that a reduction in fluorescence indicates an increase in accessibility, as has been performed successfully for the LeuT transporter [144].

In all the cases discussed above, substrate additions have resulted in accessibility changes, transitioning the transporters involved to either their inward- or outward-facing states. VcINDY dynamics are poorly understood, and as such the effects of substrate binding on the dynamics of this elevator mechanism transporter are currently unknown. Given the remarkable record of cysteine accessibility assays for detecting these nuances of transporter behaviour, we developed an assay to probe VcINDY's conformational dynamics based upon the binding of the cysteine specific maleimide Poly(ethylene glycol) methyl ether (mPEG5K), detected through the increase in mass gained upon the binding of this 5 kDa tag.

4.1.2 VcINDY Substrate Induced Conformational Changes are Detectable Through Cysteine Accessibility Measurements

mPEG5K is a well-characterised cysteine modifying compound with two main caveats. Firstly, the bulky nature of this compounds means that it is sterically unable to bind to cysteine residues which are partially blocked by the tertiary structure. Secondly, the reaction between mPEG5K and cysteine is slow, with a timescale of minutes, not seconds [145]. For our purposes, however, these are advantageous features. The inability of this compound to react with partially occluded cysteine residues makes it an effective reporter on their changing accessibilities, and the slow reaction allows us to easily quench mPEG5K reactions through the addition of a faster, competing, cysteine reactive compound.

A cysteine-free VcINDY mutant background is used for these experiments, with non-native cysteines introduced at locations of interest. The criteria for the selection of cysteine locations were threefold; low evolutionary conservation, predicted alteration in accessibility based on existing inward- and outward-facing models [81], and the ability of the single cysteine mutant to carry out transport as determined through radio-succinate transport assays, indicating their ability to sample all states required for transport.

The VcINDY_{Cysless}M157C mutant was known from previous work to be succinate responsive (unpublished data), and as such was used for proof of principle experiments.

DM solubilised VcINDY_{Cysless}M157C was incubated in the presence of mPEG5K at room temperature in order to allow labelling to occur. Throughout the reaction, samples were quenched through the addition of a large excess of methyl-MTS (MMTS) in a denaturing SDS-PAGE sample buffer, rapidly reacting with all cysteine residues as yet unmodified by mPEG5K and preventing further PEGylation, therefore capturing timepoints. As mPEG5K is a 5 kDa mass tag, PEGylation can be observed on a standard Coomassie Blue stained SDS-PAGE gel as an increase in MW. Through the use of such a gel, a 5 kDa higher MW band can be seen to form over the course of the experiment as VcINDY becomes

PEGylated over time. The proportion of VcINDY remaining in the low MW unPEGylated band can be compared to the proportion which has entered the high MW PEGylated band through densitometry, allowing the rate of reaction to be assessed.

The expected high MW band was observed to form during the hour-long experiment, increasing in density over time and confirming the labelling process to work as intended (Figure 4.1.2-1A). By 1 hour, around 60% of VcINDY had been PEGylated, indicating that the experiment was operating at a rate which could easily detect both increases and decreases in the rate of PEGylation.

For the remainder of this chapter, SDS-PAGE gel images can be found in 7.1 Appendix 1 – Raw PEGylation Data, with each gel clearly identifiable by the number indicated here.

Now it has been observed that this system can detect mPEG5K conjugation over time, the suitability of this system for observing substrate induced changes must be confirmed. As VcINDY_{Cysless}M157C is known to be succinate responsive, a succinate titration was carried out in order to demonstrate dose dependency (Figure 4.1.2-1B – Appendix 1 #157-R-1, #157-R-2-Chris). Increasing concentrations of succinate were observed to result in increasingly suppressed levels of PEGylation, demonstrating a clear dose dependency, and confirming the ability of this system to report on varying degrees of substrate interaction. It is worth noting that of the two replicates in this figure, one was carried out by Dr. Christopher Mulligan at the NIH in the USA, while the other was carried out by myself at the University of Kent in the UK; representing a high level of intercontinental repeatability.

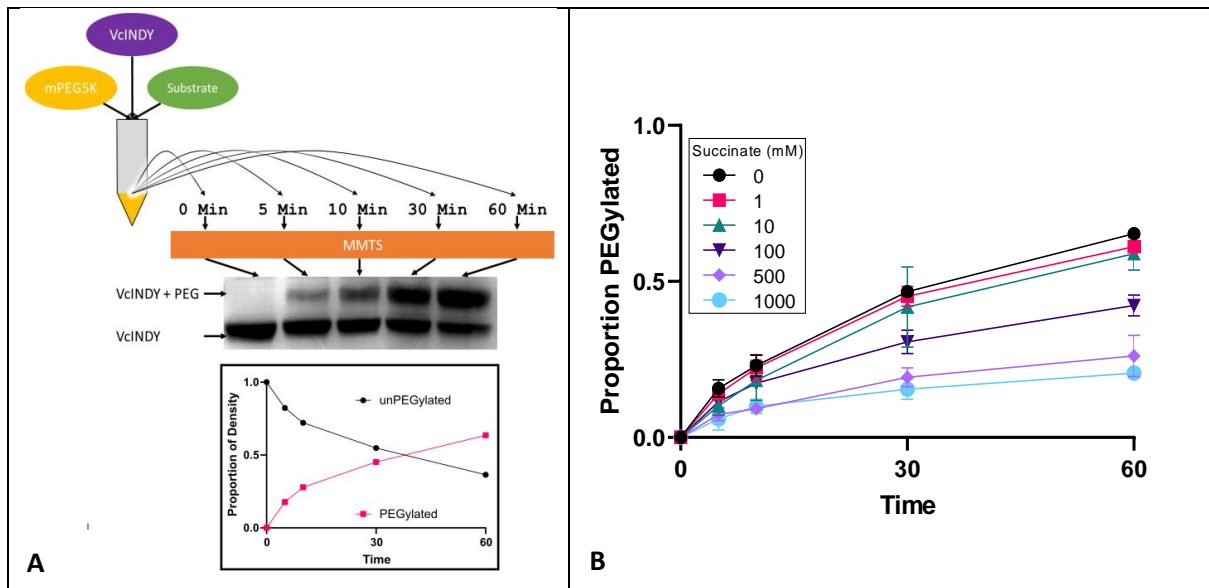


Figure 4.1.2-1 Principle of the mPEG5K accessibility assay. A: Experimental overview, showing how a single cysteine VcINDY mutant, along with any desired substrate, is mixed with the slow reacting mass tag mPEG5K and allowed to undergo a labelling reaction until quenching is performed in a denaturing buffer containing an excess of the fast cysteine reacting MMTS. This results in a series of timepoints which can be visualised through Coomassie Blue stained SDS-PAGE and quantified through densitometry, quantifying the proportion of the protein which has reacted with the 5 kDa mPEG5k mass tag at each timepoint. **B:** Dose dependent effect of Succinate on the labelling of VcINDY_{Cysless}M157C PEGylation in the presence of 150 mM sodium. The proportion of VcINDY_{Cysless}M157C reacted with the mPEG5k mass tag at each timepoint is indicated.

4.1.3 Monitoring of Single Residue Accessibilities Reveals Novel Conformational Responses to Substrate Addition

Now that an accessibility assay has been established and shown to be substrate responsive, the impacts of substrate addition can be examined. VcINDY conducts substrate transport through an elevator mechanism, in which transition from the inward- to the outward-facing state is predicted to be facilitated by a rigid body movement of the transport domain relative to the membrane, carrying the binding site along with it (see 1.10.3 Transport). This raises the question; are the dynamics of the transition between these two states affected by substrate binding in a way that alters their equilibrium? Does the binding of substrates cause VcINDY to favour the inward-facing state, the outward-facing state, or some intermediate state?

In order to test this, 15 functional single cysteine mutants were used, each of which fulfilled the criteria described in 4.1.2 VcINDY Substrate Induced Conformational Changes are Detectable Through Cysteine Accessibility Measurements. These were proven to be functional through radioligand transport assays, in which the uptake of radiolabelled succinate into proteoliposomes was measured compared to empty liposome negative controls (Figure 4.1.3-1). In all cases, inclusion of VcINDY single cysteine mutants in the liposomes resulted in increased levels of radiosuccinate compared to the empty liposomes, and therefore increased final proteoliposome radiation levels. This proof of activity was vital, demonstrating not only that these mutants were correctly folded, but also that they were capable of transitioning through all conformational states required for transport to occur.

The accessibilities of these introduced cysteines was examined under four conditions: sodium only (150 mM sodium), sodium + succinate (150 mM sodium, 1 mM succinate), substrate free (150 mM potassium), and succinate only (150 mM potassium, 1 mM succinate). The resultant datasets are summarised in Figure 4.1.3-2 to Figure 4.1.3-16 so that the underlying data may be seen. These datasets will form the basis of further discussion and analysis throughout this section.

In Figure 4.1.3-2 to Figure 4.1.3-16 the normalised inaccessibility graph represents the data in a more useful but far less intuitive manner than raw proportion PEGylated. A significant proportion of random variation between replicate runs is due to variation in the rate of PEGylation between days, and if possible this should be corrected for. For our purposes, the absolute rate of PEGylation, as shown by the raw data graph, is not of importance. Our hypothesis, that the addition of substrates may alter the accessibility of certain residues, only requires us to examine the difference in PEGylation rates between varying conditions within each run. As such, the runs may be normalised to produce “PEGylation rate relative to sodium only condition”, with the sodium only condition chosen as the benchmark as it is most often a medium rate condition, and thus demonstrates the least extreme variation with respect to other conditions. Due to the initially low values for the of proportion PEGylated VcINDY causing difficulty in normalising such data, the depletion of non-PEGylated VcINDY is followed instead. This results in the creation of the “Relative Inaccessibility” metric, equalling $[\text{Proportion Non-PEGylated}]/[\text{Proportion Non-PEGylated for the Na only condition from the same experiment}]$.

This is presented alongside the simple increase in PEGylated VcINDY over time so that the two extremes of the data processing may be seen; the most intuitive, albeit noisy, graph alongside the most noise free and statistically useful, albeit unintuitive, graph from which p values are calculated.

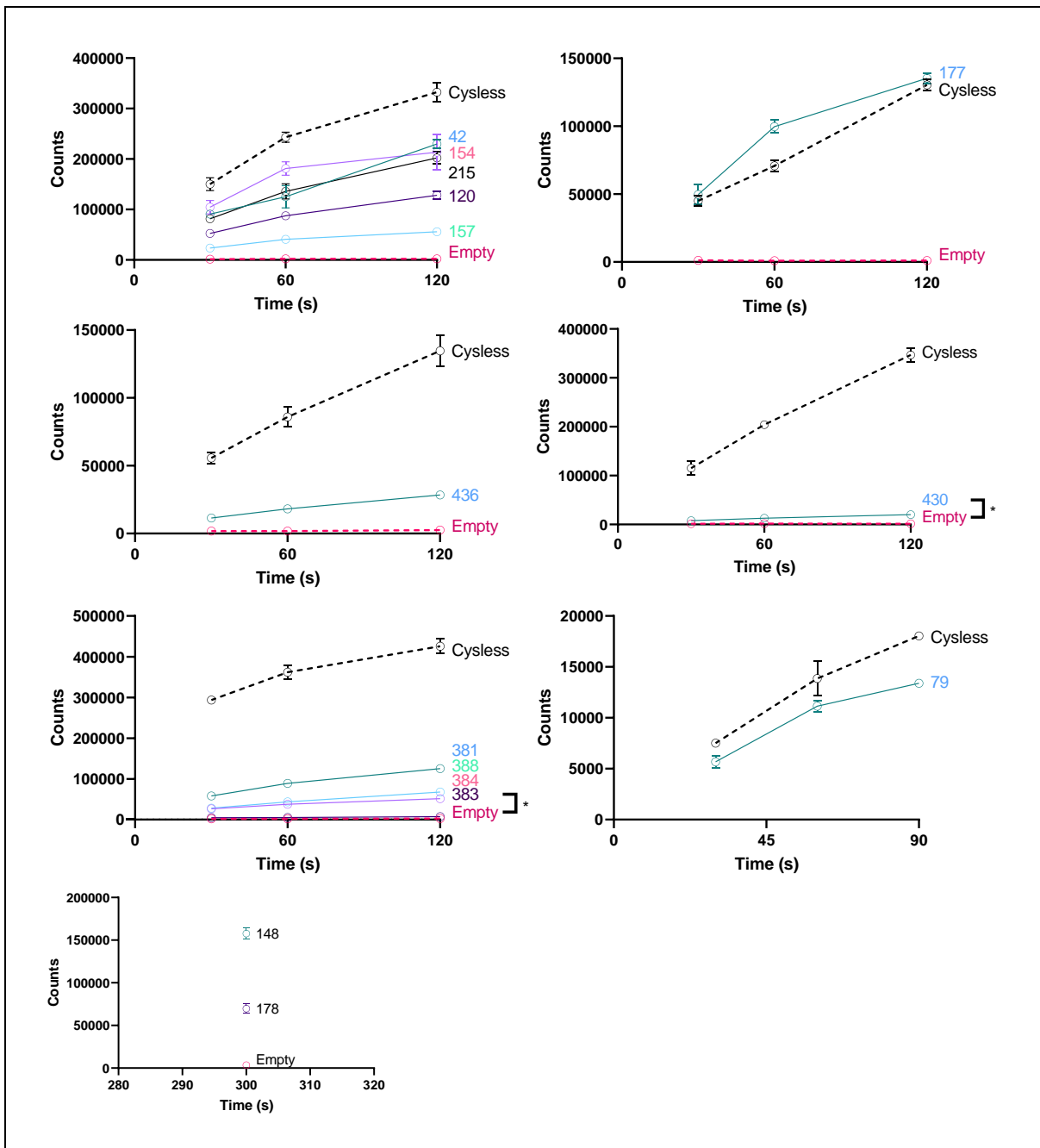


Figure 4.1.3-1 Transport data for the cysteine mutants used for PEGylation assays, performed by Matthew Stewart.

VcINDY containing proteoliposomes were exposed to $[H^3]$ -radiosuccinate in the presence of an inward facing sodium gradient. Transport was allowed to continue for the time indicated before quenching and removal of external radiosuccinate. The level of radiosuccinate sequestered into the proteoliposomes by VcINDY transport activity is recorded through use of a β -radiation detecting scintillation counter. Cysless is the VcINDY cysteine free background upon which these mutants are created. Empty shows liposomes with no VcINDY, indicating background levels of radiation gained in the experiment. In every case except 79C, radiation levels at the final timepoint were significantly ($p < 0.05$) higher than in empty liposomes, confirming transport. In the case of 79C the clear accumulation of radiation over time, in contrast to the constant level of radiation observed for empty proteoliposomes, is clear evidence of transport.

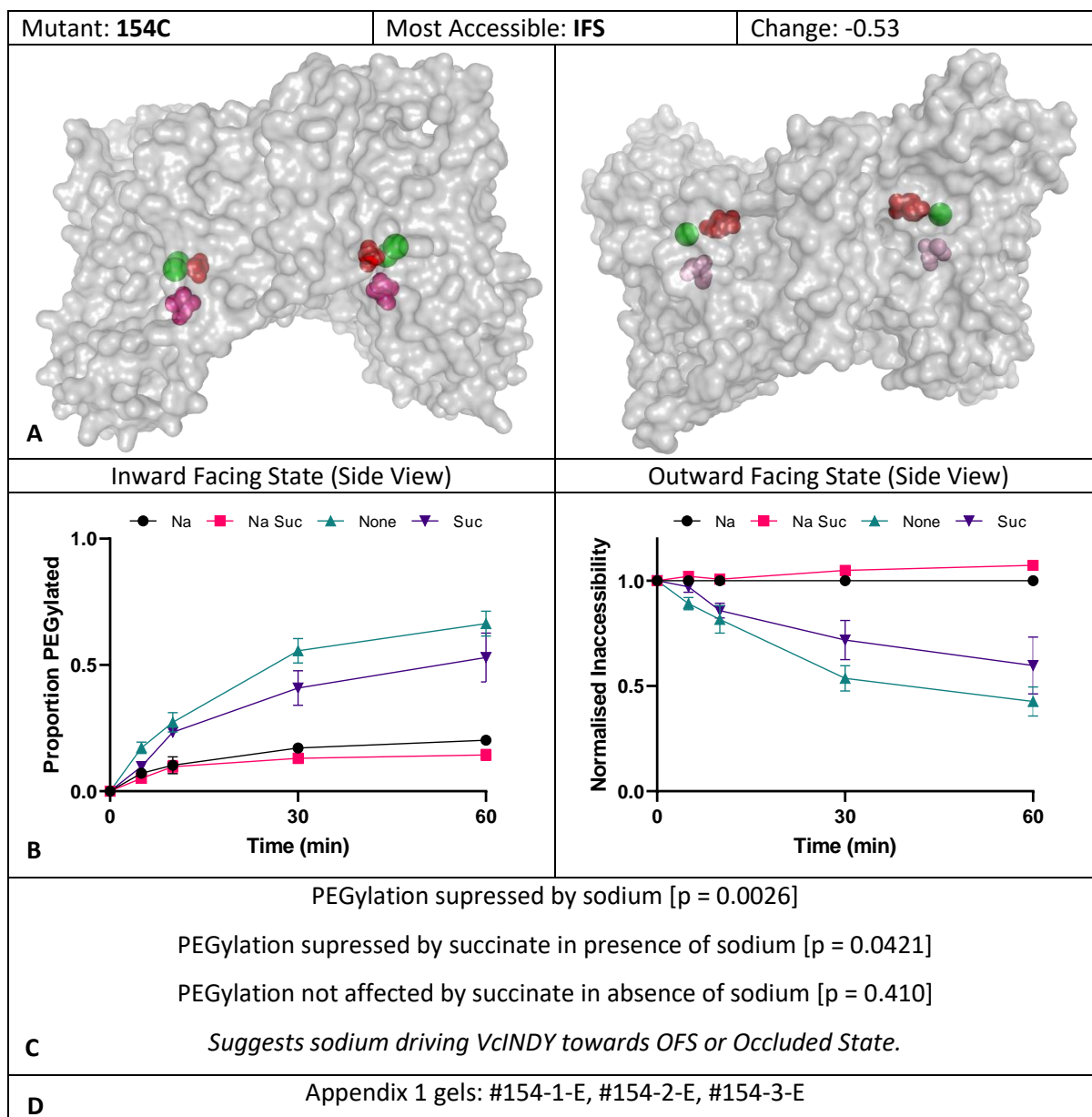


Figure 4.1.3-2 Cysteine Accessibility Profile for VcINDY_{Cysless}T154C. Title Annotations: Position of the introduced cysteine mutant is indicated, along with a prediction of the conformation in which this residue is most accessible based upon manual structure examination. The computationally estimated relative solvent accessibility change from the Inward-Facing State to the Outward-Facing State, with positive values indicating greater accessibility in the IFS, as predicted by Dr. Vanessa Leone, NIH (Unpublished Data), is also shown. **A:** Introduced cysteine residue highlighted on the latest inward facing crystal structure [3], and the predicted outward-facing structure [81]. **B:** Level of PEGylation as a function of time, quantified through densitometry. This is displayed as the average proportion of VcINDY PEGylated at each timepoint, and the relative accessibility metric (discussed in main text). **C:** Simple t-test results for the effects of substrate addition as monitored through the relative accessibility metric. **D:** Reference numbers of the associated gels, which can be found in Appendix 1.

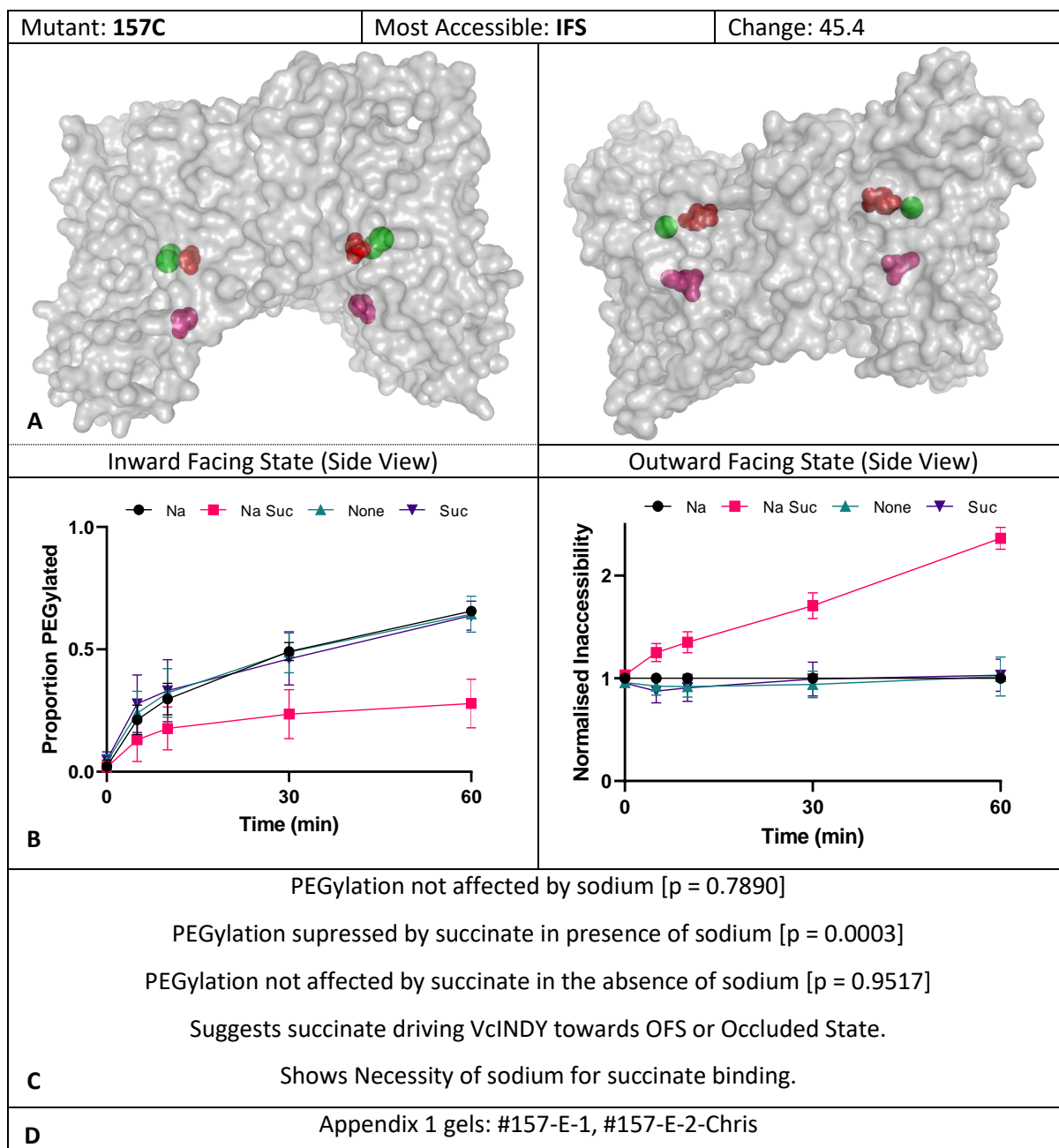


Figure 4.1.3-3 Cysteine Accessibility Profile for VcINDY_{Cysless}M157C. *Title Annotations:* Position of the introduced cysteine mutant is indicated, along with a prediction of the conformation in which this residue is most accessible based upon manual structure examination. The computationally estimated relative solvent accessibility change from the Inward-Facing State to the Outward-Facing State, with positive values indicating greater accessibility in the IFS, as predicted by Dr. Vanessa Leone, NIH (Unpublished Data), is also shown. **A:** Introduced cysteine residue highlighted on the latest inward facing crystal structure [3], and the predicted outward-facing structure [81]. **B:** Level of PEGylation as a function of time, quantified through densitometry. This is displayed as the average proportion of VcINDY PEGylated at each timepoint, and the relative accessibility metric (discussed in main text). **C:** Simple t-test results for the effects of substrate addition as monitored through the relative accessibility metric. **D:** Reference numbers of the associated gels, which can be found in Appendix 1.

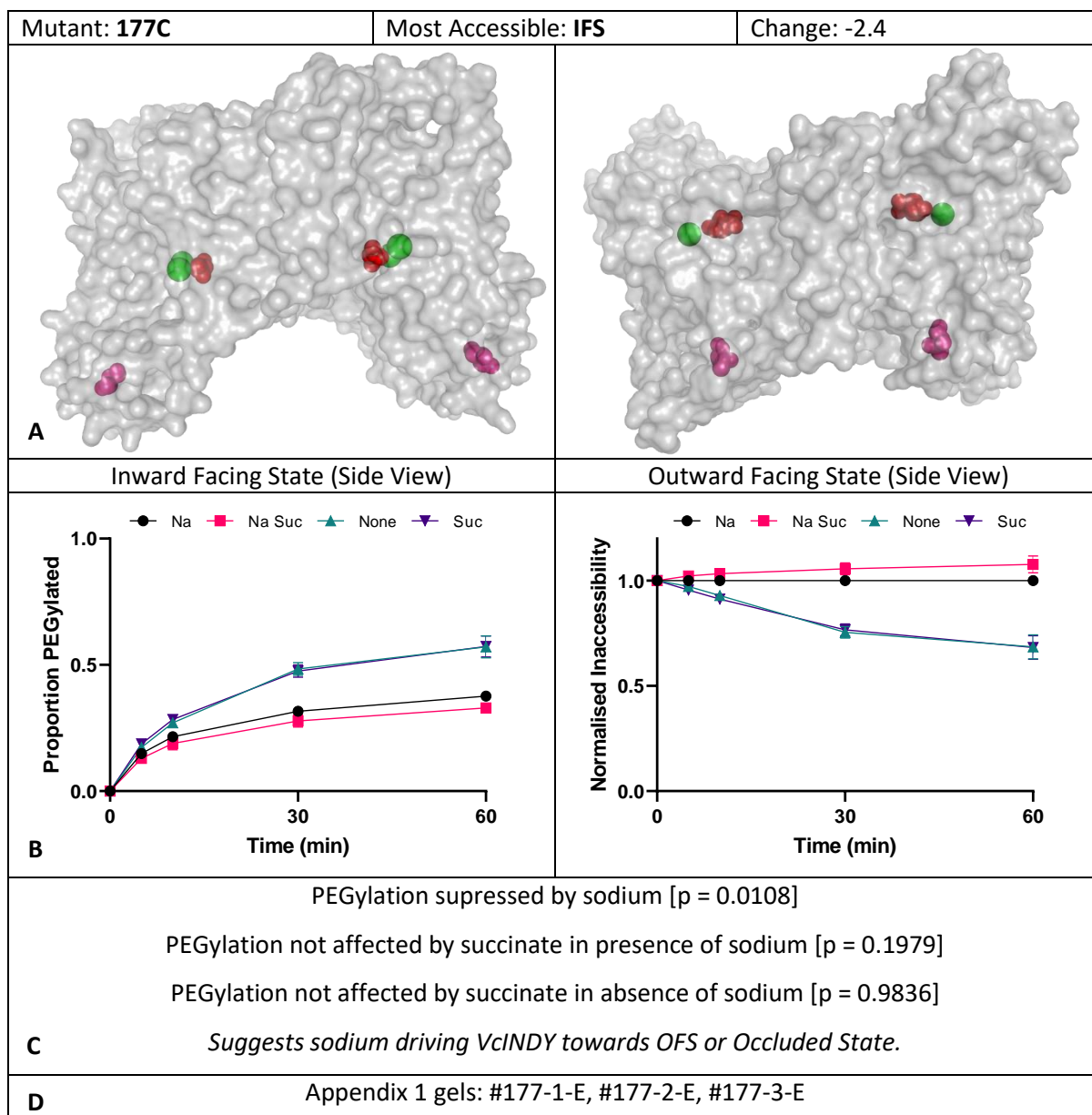


Figure 4.1.3-4 Cysteine Accessibility Profile for VcINDY_{Cysless}T177C. Title Annotations: Position of the introduced cysteine mutant is indicated, along with a prediction of the conformation in which this residue is most accessible based upon manual structure examination. The computationally estimated relative solvent accessibility change from the Inward-Facing State to the Outward-Facing State, with positive values indicating greater accessibility in the IFS, as predicted by Dr. Vanessa Leone, NIH (Unpublished Data), is also shown. **A:** Introduced cysteine residue highlighted on the latest inward facing crystal structure [3], and the predicted outward-facing structure [81]. **B:** Level of PEGylation as a function of time, quantified through densitometry. This is displayed as the average proportion of VcINDY PEGylated at each timepoint, and the relative accessibility metric (discussed in main text). **C:** Simple t-test results for the effects of substrate addition as monitored through the relative accessibility metric. **D:** Reference numbers of the associated gels, which can be found in Appendix 1.

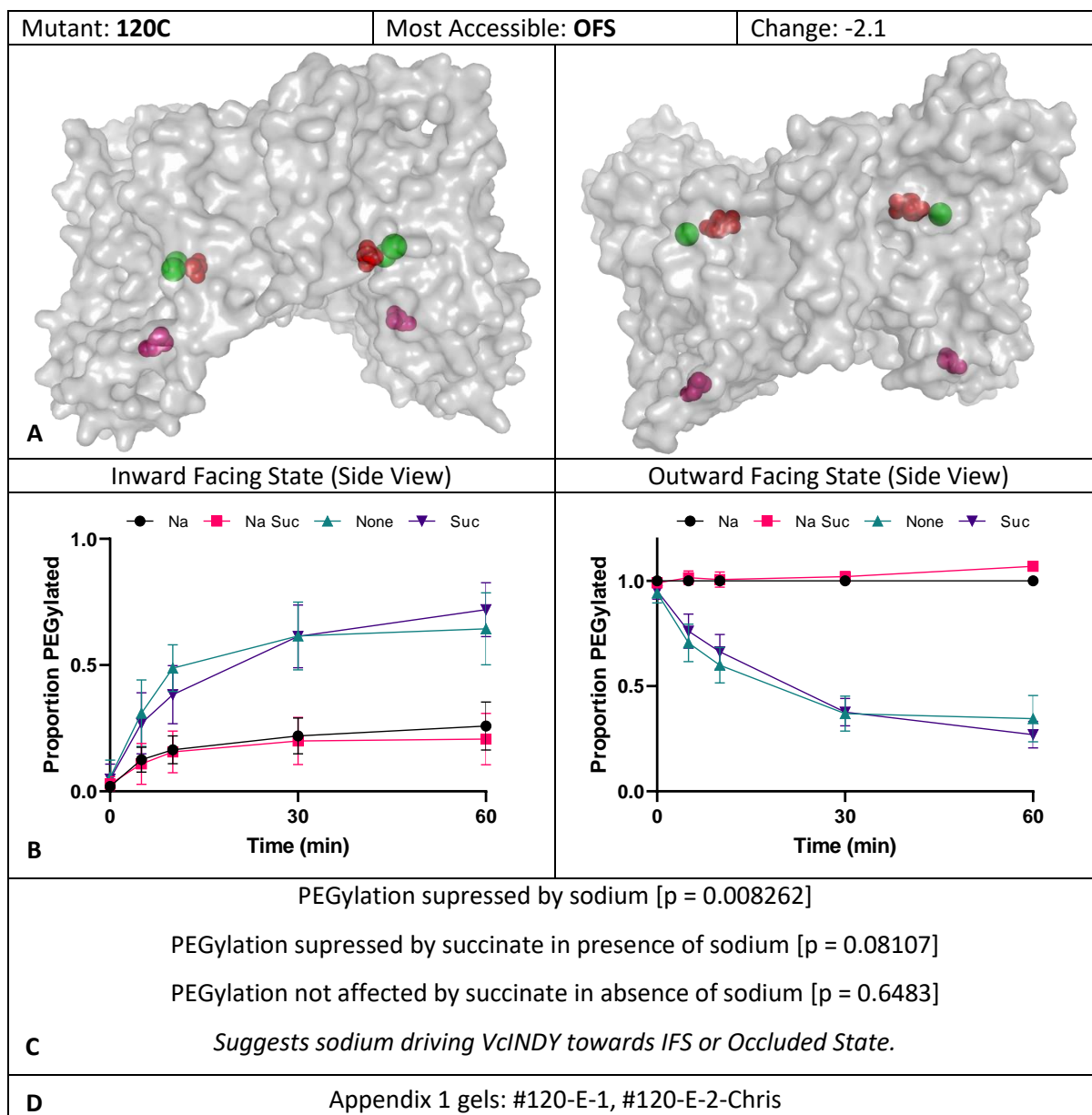


Figure 4.1.3-5 Cysteine Accessibility Profile for VcINDY_{Cysless}A120C. Title Annotations: Position of the introduced cysteine mutant is indicated, along with a prediction of the conformation in which this residue is most accessible based upon manual structure examination. The computationally estimated relative solvent accessibility change from the Inward-Facing State to the Outward-Facing State, with positive values indicating greater accessibility in the IFS, as predicted by Dr. Vanessa Leone, NIH (Unpublished Data), is also shown. **A:** Introduced cysteine residue highlighted on the latest inward facing crystal structure [3], and the predicted outward-facing structure [81]. **B:** Level of PEGylation as a function of time, quantified through densitometry. This is displayed as the average proportion of VcINDY PEGylated at each timepoint, and the relative accessibility metric (discussed in main text). **C:** Simple t-test results for the effects of substrate addition as monitored through the relative accessibility metric. **D:** Reference numbers of the associated gels, which can be found in Appendix 1.

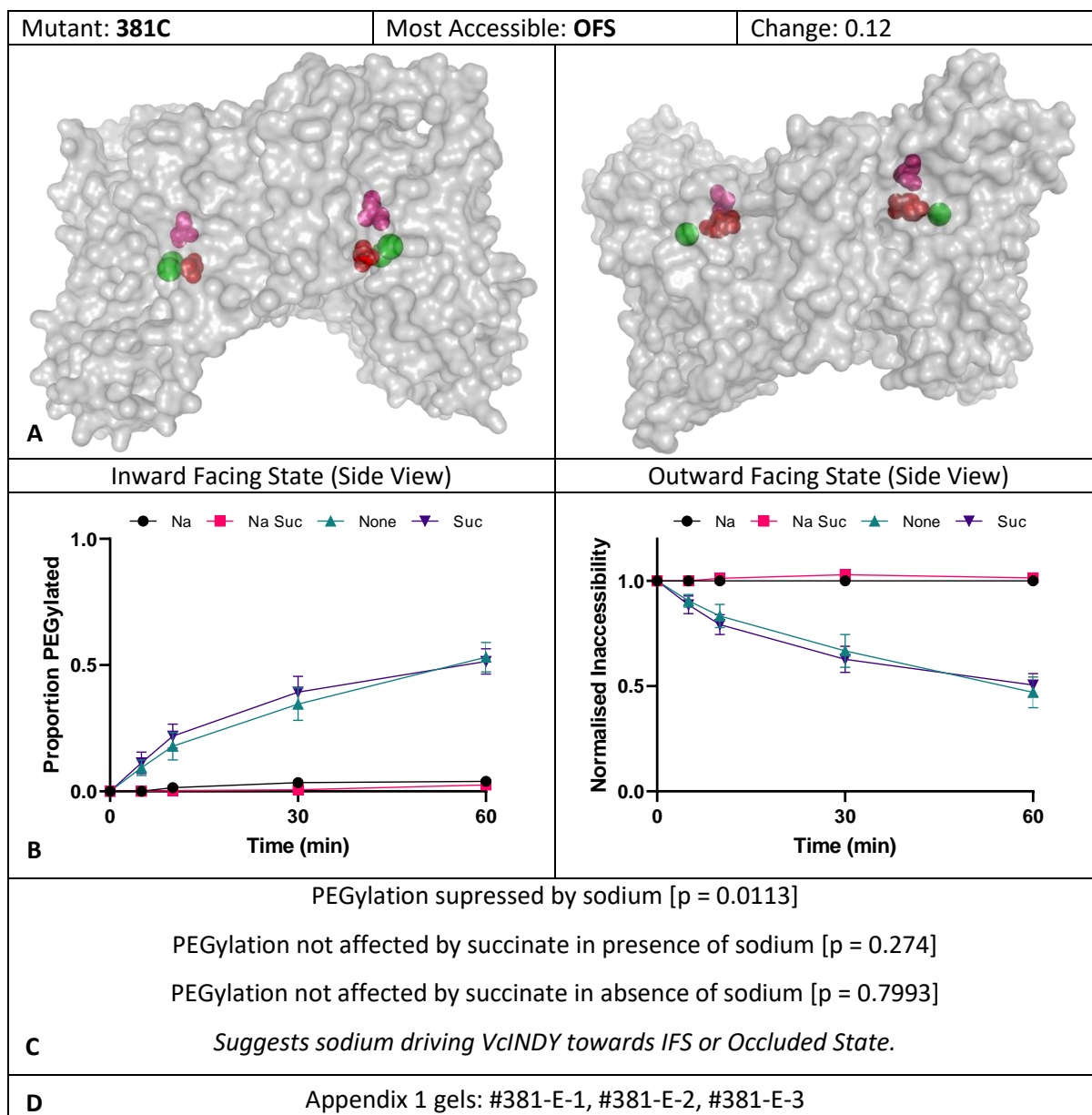


Figure 4.1.3-6 Cysteine Accessibility Profile for VcINDY_{Cysless}381C. Title Annotations: Position of the introduced cysteine mutant is indicated, along with a prediction of the conformation in which this residue is most accessible based upon manual structure examination. The computationally estimated relative solvent accessibility change from the Inward-Facing State to the Outward-Facing State, with positive values indicating greater accessibility in the IFS, as predicted by Dr. Vanessa Leone, NIH (Unpublished Data), is also shown. **A:** Introduced cysteine residue highlighted on the latest inward facing crystal structure [3], and the predicted outward-facing structure [81]. **B:** Level of PEGylation as a function of time, quantified through densitometry. This is displayed as the average proportion of VcINDY PEGylated at each timepoint, and the relative accessibility metric (discussed in main text). **C:** Simple t-test results for the effects of substrate addition as monitored through the relative accessibility metric. **D:** Reference numbers of the associated gels, which can be found in Appendix 1.

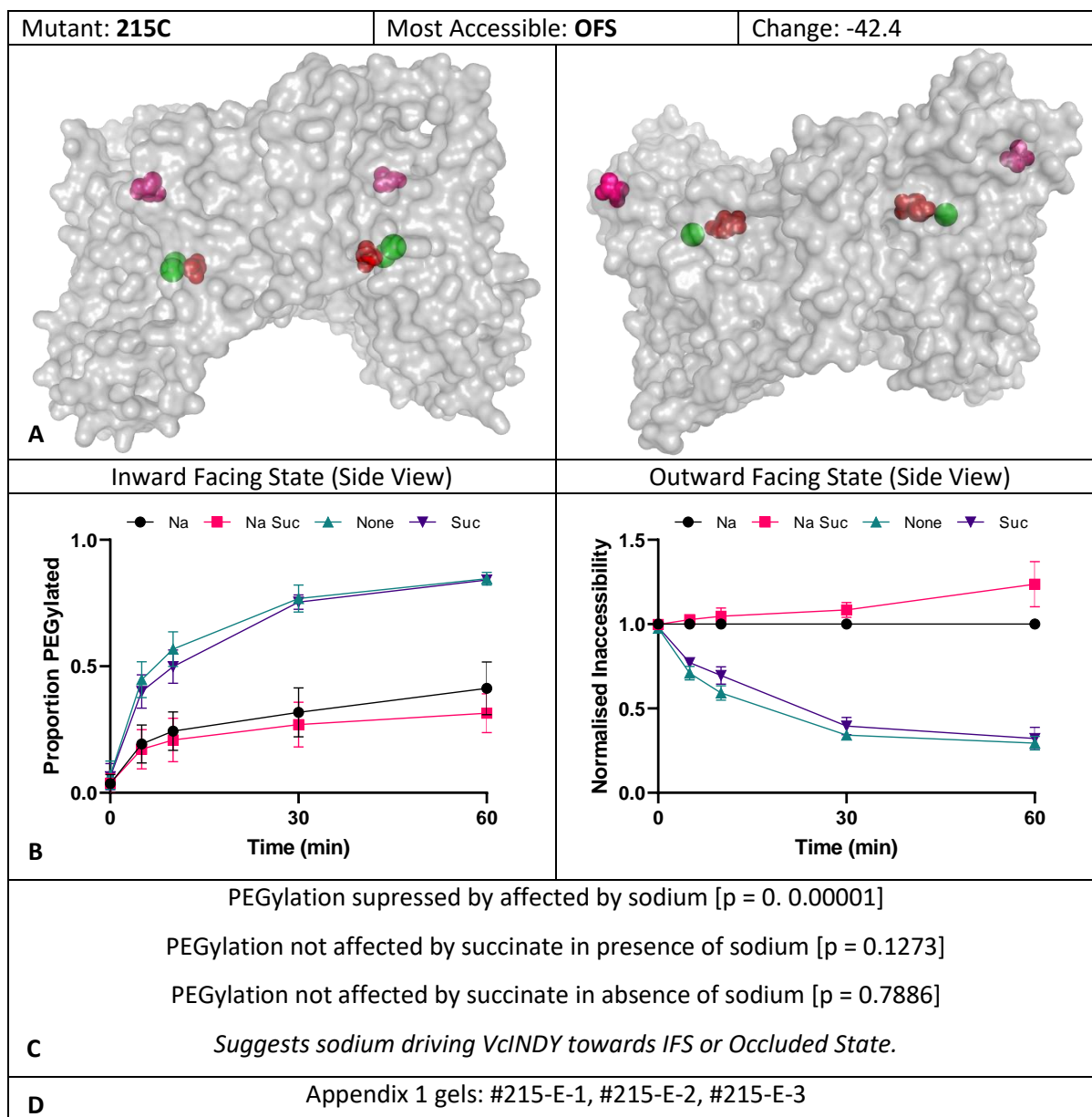


Figure 4.1.3-7 Cysteine Accessibility Profile for VcINDY_{Cysless}T215C. Title Annotations: Position of the introduced cysteine mutant is indicated, along with a prediction of the conformation in which this residue is most accessible based upon manual structure examination. The computationally estimated relative solvent accessibility change from the Inward-Facing State to the Outward-Facing State, with positive values indicating greater accessibility in the IFS, as predicted by Dr. Vanessa Leone, NIH (Unpublished Data), is also shown. **A:** Introduced cysteine residue highlighted on the latest inward facing crystal structure [3], and the predicted outward-facing structure [81]. **B:** Level of PEGylation as a function of time, quantified through densitometry. This is displayed as the average proportion of VcINDY PEGylated at each timepoint, and the relative accessibility metric (discussed in main text). **C:** Simple t-test results for the effects of substrate addition as monitored through the relative accessibility metric. **D:** Reference numbers of the associated gels, which can be found in Appendix 1.

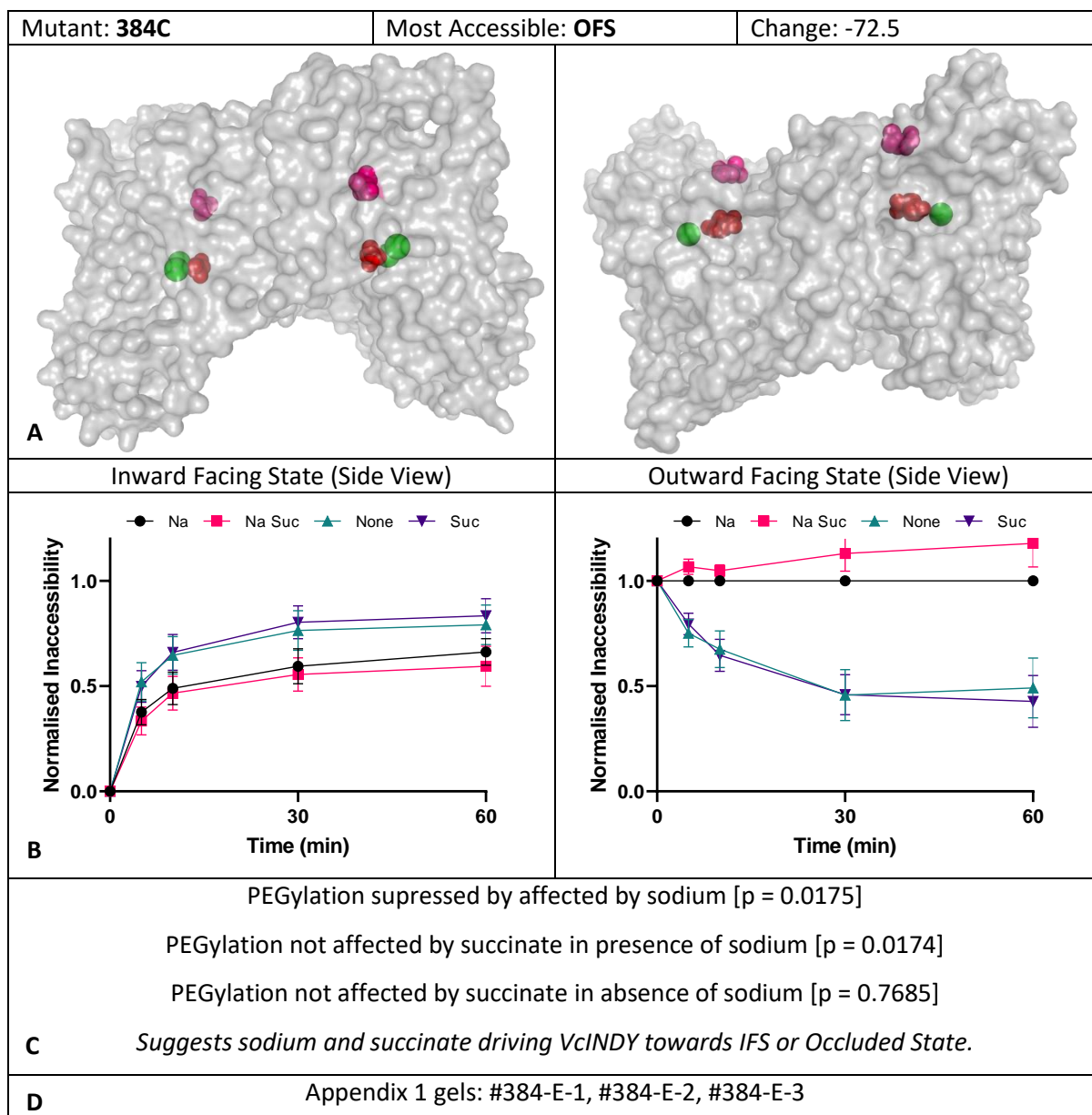


Figure 4.1.3-8 Cysteine Accessibility Profile for VcINDY_{CyslessL384C}. Title Annotations: Position of the introduced cysteine mutant is indicated, along with a prediction of the conformation in which this residue is most accessible based upon manual structure examination. The computationally estimated relative solvent accessibility change from the Inward-Facing State to the Outward-Facing State, with positive values indicating greater accessibility in the IFS, as predicted by Dr. Vanessa Leone, NIH (Unpublished Data), is also shown. **A:** Introduced cysteine residue highlighted on the latest inward facing crystal structure [3], and the predicted outward-facing structure [81]. **B:** Level of PEGylation as a function of time, quantified through densitometry. This is displayed as the average proportion of VcINDY PEGylated at each timepoint, and the relative accessibility metric (discussed in main text). **C:** Simple t-test results for the effects of substrate addition as monitored through the relative accessibility metric. **D:** Reference numbers of the associated gels, which can be found in Appendix 1.

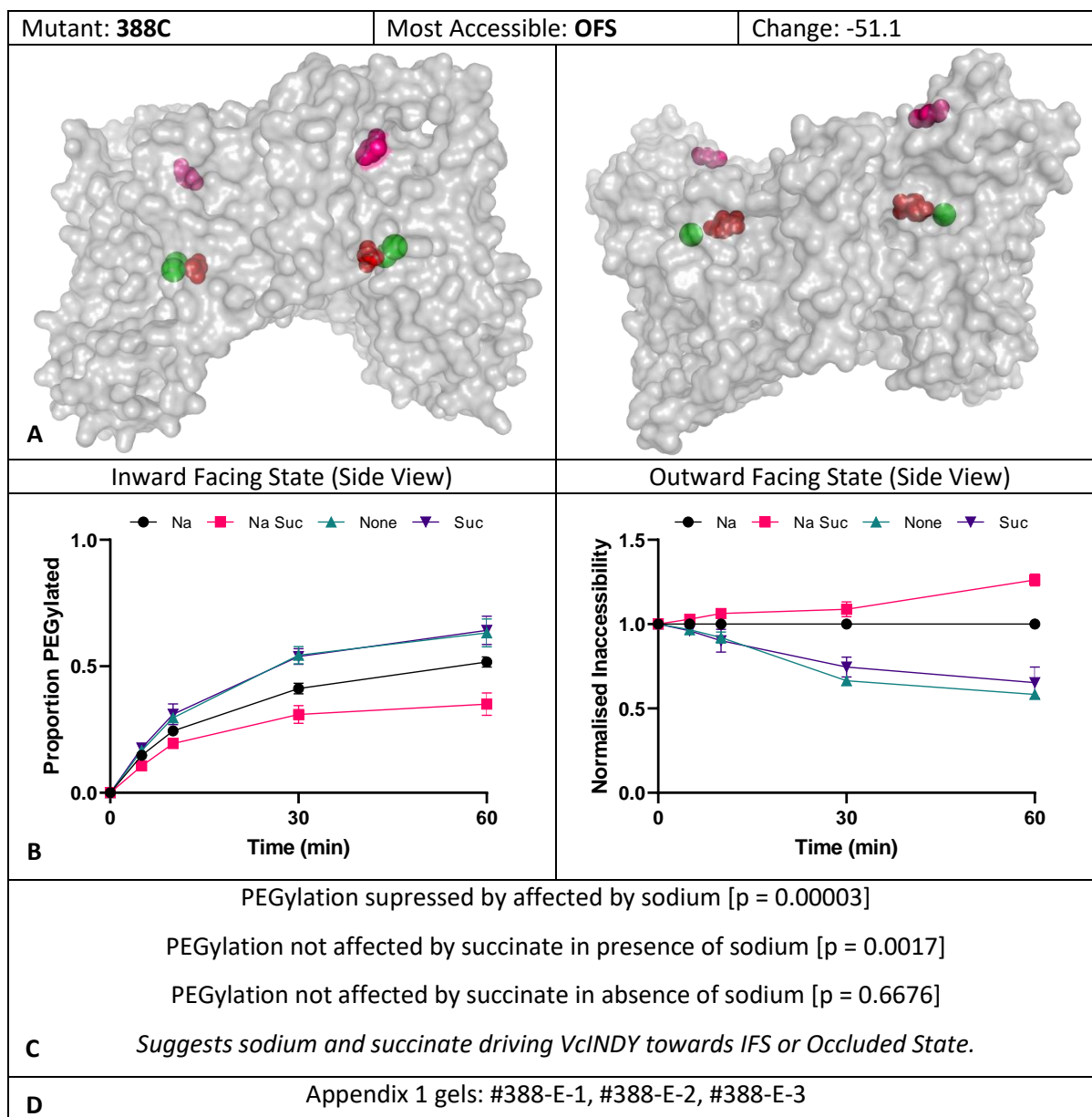


Figure 4.1.3-9 Cysteine Accessibility Profile for VcINDY_{Cysless}V388C. *Title Annotations: Position of the introduced cysteine mutant is indicated, along with a prediction of the conformation in which this residue is most accessible based upon manual structure examination. The computationally estimated relative solvent accessibility change from the Inward-Facing State to the Outward-Facing State, with positive values indicating greater accessibility in the IFS, as predicted by Dr. Vanessa Leone, NIH (Unpublished Data), is also shown. A: Introduced cysteine residue highlighted on the latest inward facing crystal structure [3], and the predicted outward-facing structure [81]. B: Level of PEGylation as a function of time, quantified through densitometry. This is displayed as the average proportion of VcINDY PEGylated at each timepoint, and the relative accessibility metric (discussed in main text). C: Simple t-test results for the effects of substrate addition as monitored through the relative accessibility metric. D: Reference numbers of the associated gels, which can be found in Appendix 1.*

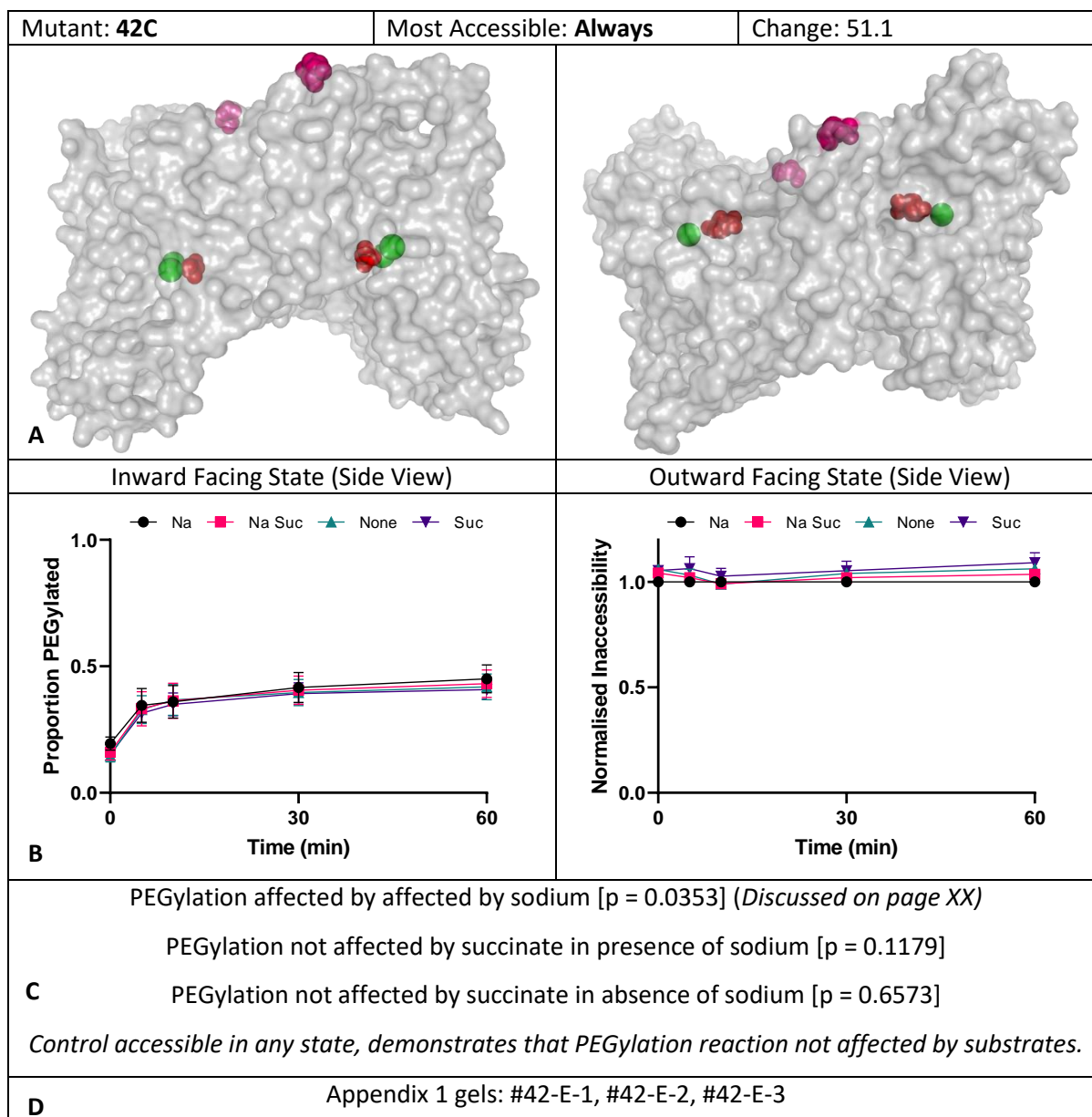


Figure 4.1.3-10 Cysteine Accessibility Profile for VcINDY_{CyslessE42C}. *Title Annotations: Position of the introduced cysteine mutant is indicated, along with a prediction of the conformation in which this residue is most accessible based upon manual structure examination. The computationally estimated relative solvent accessibility change from the Inward-Facing State to the Outward-Facing State, with positive values indicating greater accessibility in the IFS, as predicted by Dr. Vanessa Leone, NIH (Unpublished Data), is also shown. A: Introduced cysteine residue highlighted on the latest inward facing crystal structure [3], and the predicted outward-facing structure [81]. B: Level of PEGylation as a function of time, quantified through densitometry. This is displayed as the average proportion of VcINDY PEGylated at each timepoint, and the relative accessibility metric (discussed in main text). C: Simple t-test results for the effects of substrate addition as monitored through the relative accessibility metric. D: Reference numbers of the associated gels, which can be found in Appendix 1.*

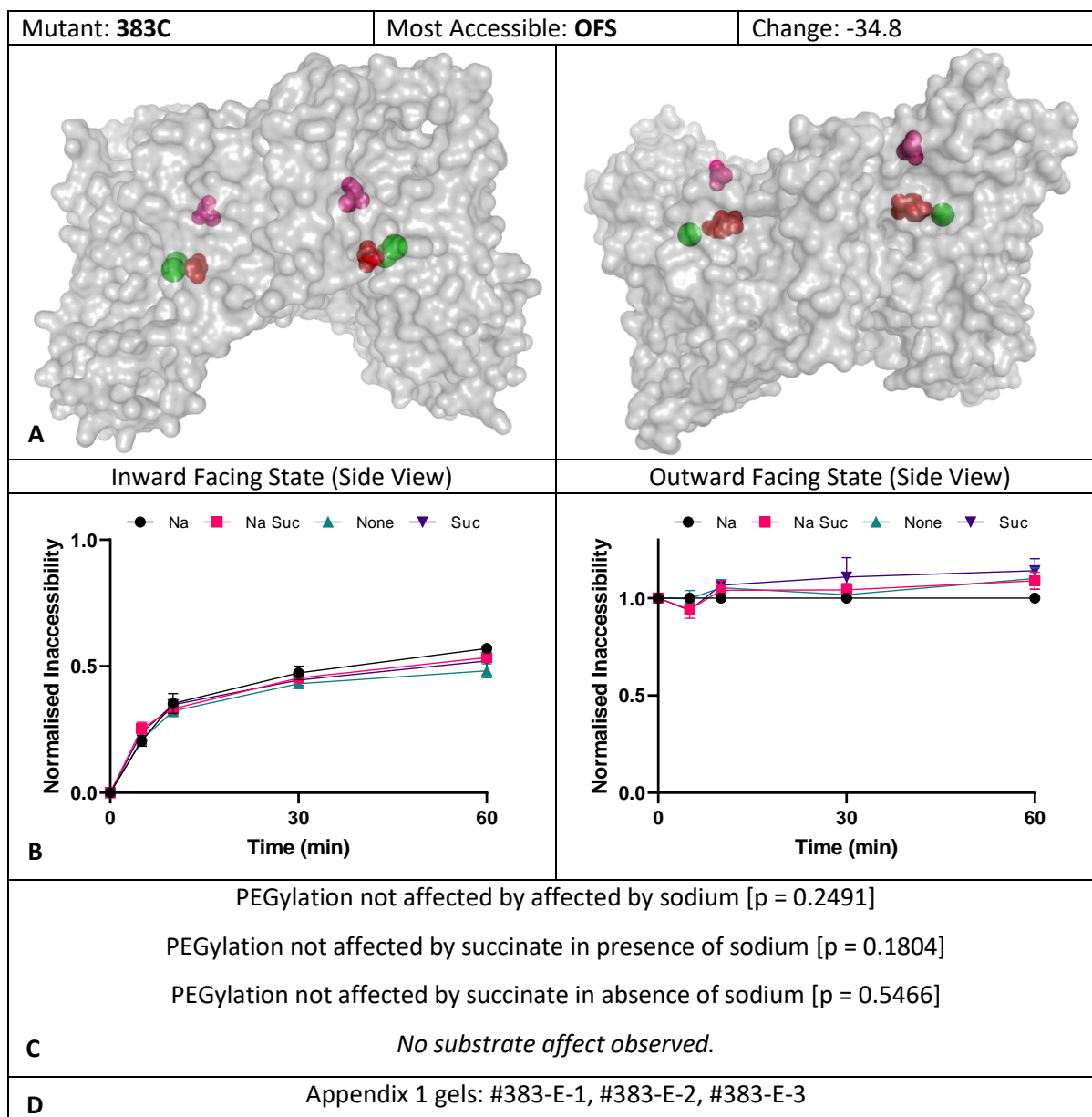


Figure 4.1.3-11 Cysteine Accessibility Profile for VcINDY_{Cysless}A383C. *Title Annotations:* Position of the introduced cysteine mutant is indicated, along with a prediction of the conformation in which this residue is most accessible based upon manual structure examination. The computationally estimated relative solvent accessibility change from the Inward-Facing State to the Outward-Facing State, with positive values indicating greater accessibility in the IFS, as predicted by Dr. Vanessa Leone, NIH (Unpublished Data), is also shown. **A:** Introduced cysteine residue highlighted on the latest inward facing crystal structure [3], and the predicted outward-facing structure [81]. **B:** Level of PEGylation as a function of time, quantified through densitometry. This is displayed as the average proportion of VcINDY PEGylated at each timepoint, and the relative accessibility metric (discussed in main text). **C:** Simple t-test results for the effects of substrate addition as monitored through the relative accessibility metric. **D:** Reference numbers of the associated gels, which can be found in Appendix 1.

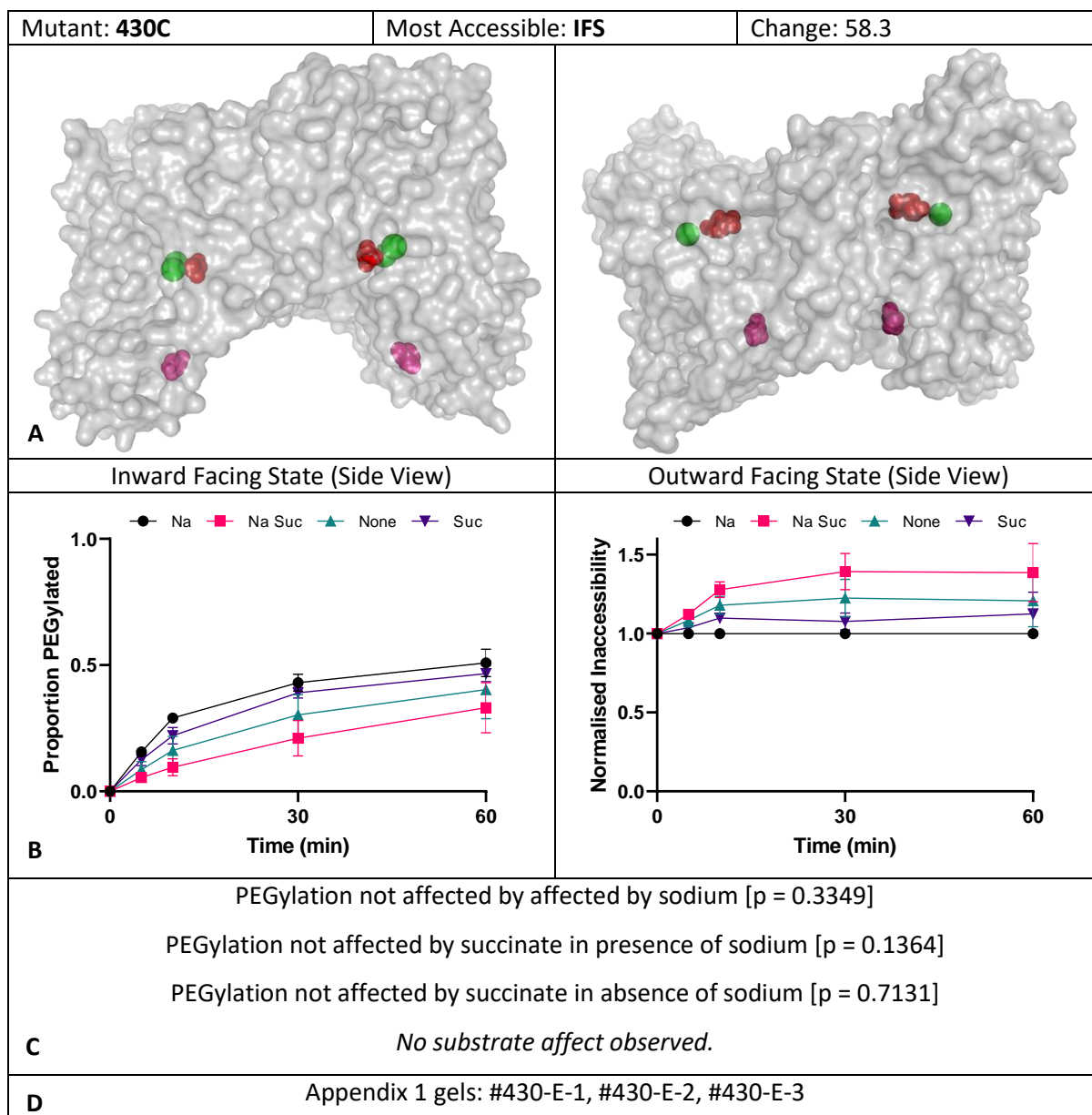


Figure 4.1.3-12 Cysteine Accessibility Profile for VcINDY_{Cysless}S430C. Title Annotations: Position of the introduced cysteine mutant is indicated, along with a prediction of the conformation in which this residue is most accessible based upon manual structure examination. The computationally estimated relative solvent accessibility change from the Inward-Facing State to the Outward-Facing State, with positive values indicating greater accessibility in the IFS, as predicted by Dr. Vanessa Leone, NIH (Unpublished Data), is also shown. **A:** Introduced cysteine residue highlighted on the latest inward facing crystal structure [3], and the predicted outward-facing structure [81]. **B:** Level of PEGylation as a function of time, quantified through densitometry. This is displayed as the average proportion of VcINDY PEGylated at each timepoint, and the relative accessibility metric (discussed in main text). **C:** Simple t-test results for the effects of substrate addition as monitored through the relative accessibility metric. **D:** Reference numbers of the associated gels, which can be found in Appendix 1.

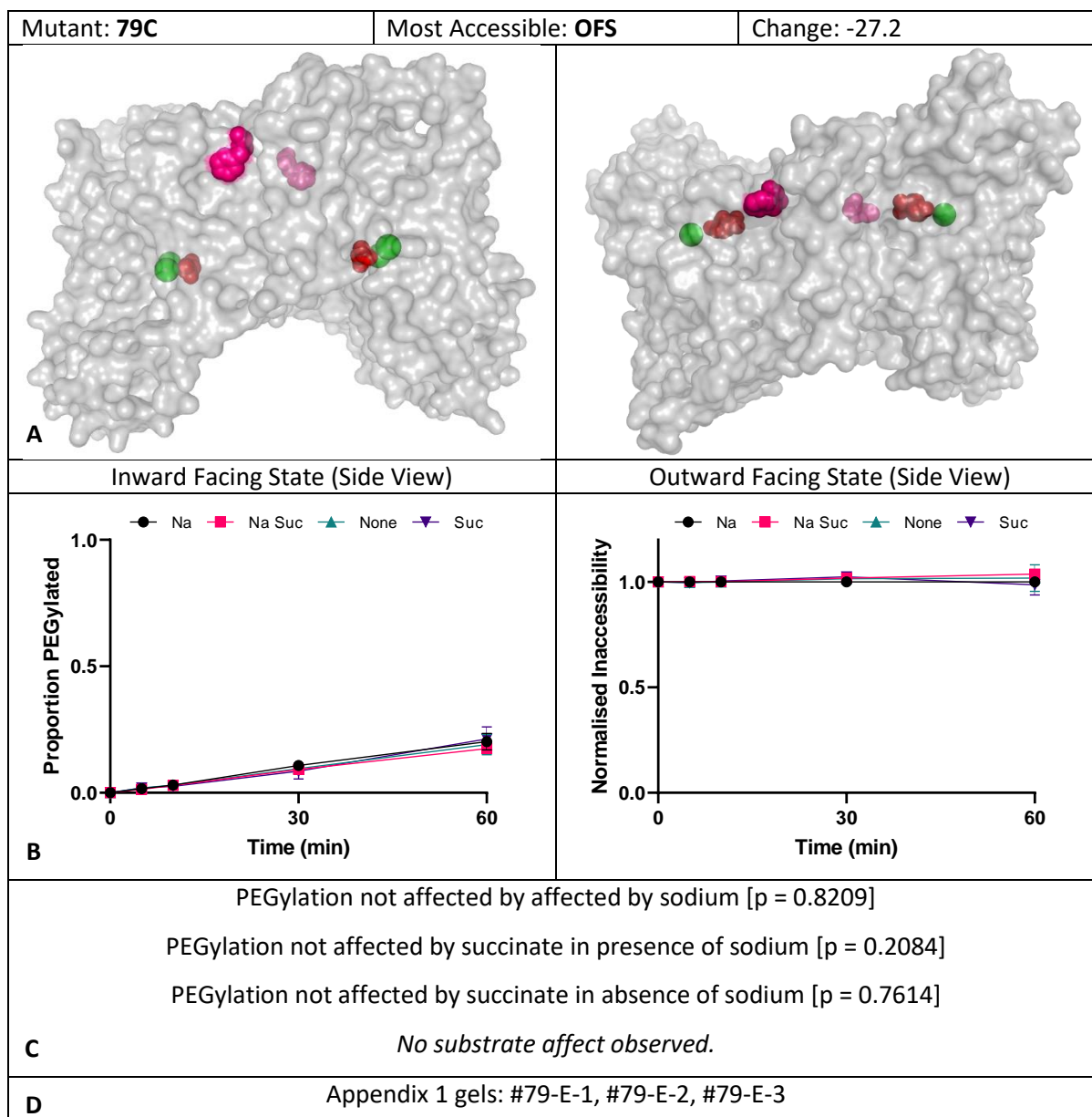


Figure 4.1.3-13 Cysteine Accessibility Profile for VcINDY_{Cysless}F79C. Title Annotations: Position of the introduced cysteine mutant is indicated, along with a prediction of the conformation in which this residue is most accessible based upon manual structure examination. The computationally estimated relative solvent accessibility change from the Inward-Facing State to the Outward-Facing State, with positive values indicating greater accessibility in the IFS, as predicted by Dr. Vanessa Leone, NIH (Unpublished Data), is also shown. **A:** Introduced cysteine residue highlighted on the latest inward facing crystal structure [3], and the predicted outward-facing structure [81]. **B:** Level of PEGylation as a function of time, quantified through densitometry. This is displayed as the average proportion of VcINDY PEGylated at each timepoint, and the relative accessibility metric (discussed in main text). **C:** Simple t-test results for the effects of substrate addition as monitored through the relative accessibility metric. **D:** Reference numbers of the associated gels, which can be found in Appendix 1.

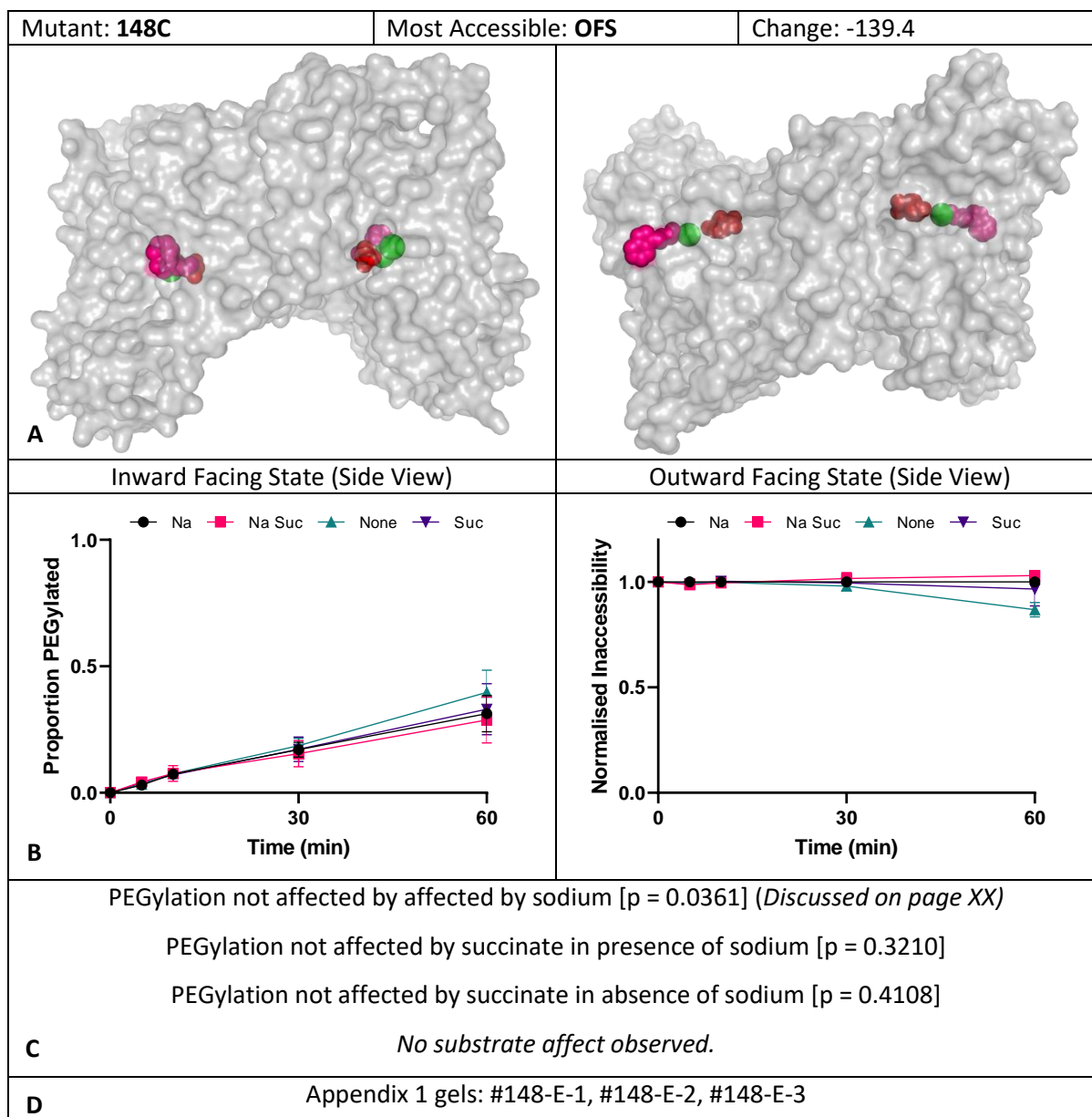


Figure 4.1.3-14 Cysteine Accessibility Profile for VcINDY_{Cysless}W148C. *Title Annotations:* Position of the introduced cysteine mutant is indicated, along with a prediction of the conformation in which this residue is most accessible based upon manual structure examination. The computationally estimated relative solvent accessibility change from the Inward-Facing State to the Outward-Facing State, with positive values indicating greater accessibility in the IFS, as predicted by Dr. Vanessa Leone, NIH (Unpublished Data), is also shown. **A:** Introduced cysteine residue highlighted on the latest inward facing crystal structure [3], and the predicted outward-facing structure [81]. **B:** Level of PEGylation as a function of time, quantified through densitometry. This is displayed as the average proportion of VcINDY PEGylated at each timepoint, and the relative accessibility metric (discussed in main text). **C:** Simple t-test results for the effects of substrate addition as monitored through the relative accessibility metric. **D:** Reference numbers of the associated gels, which can be found in Appendix 1.

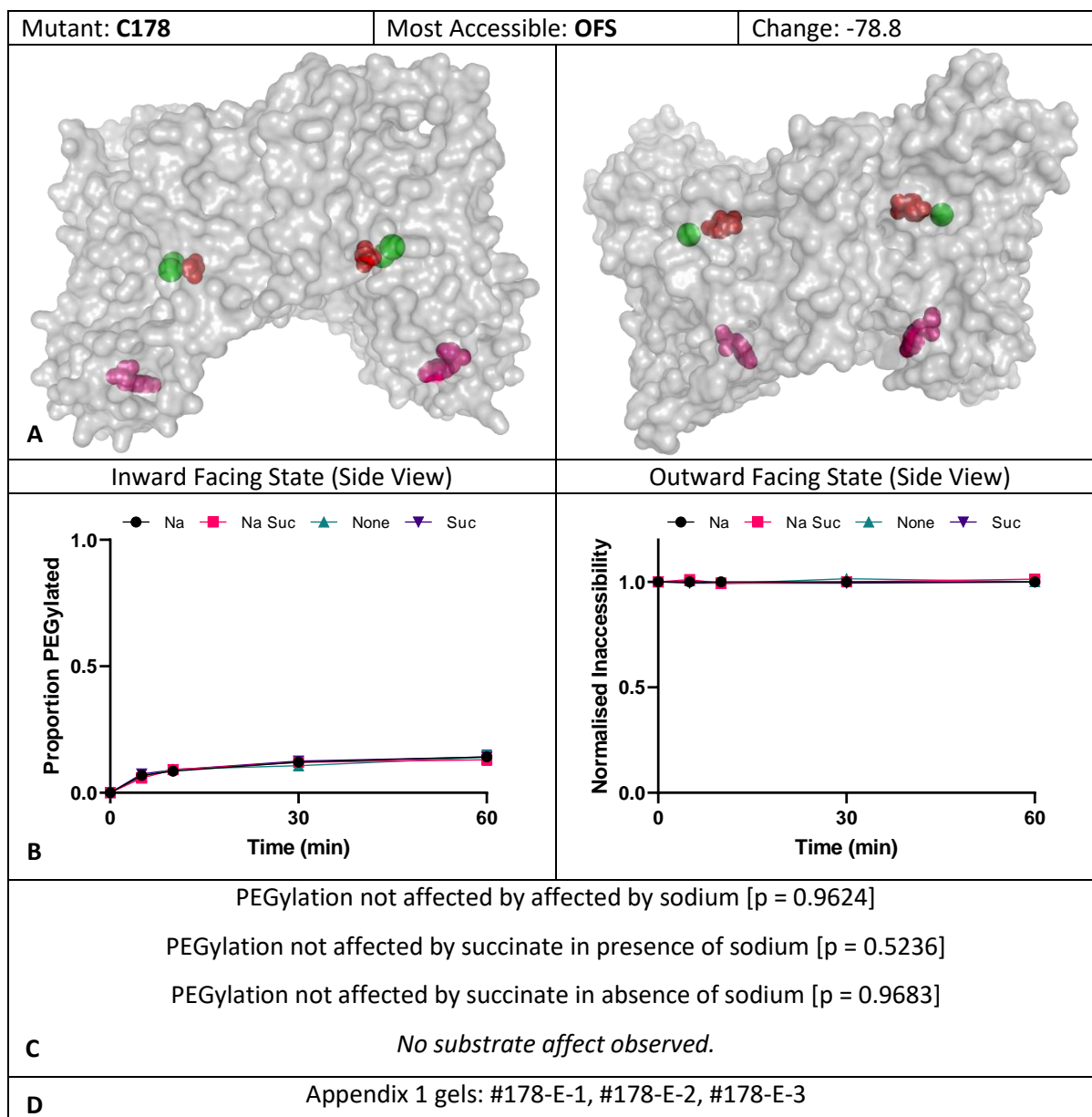


Figure 4.1.3-15 Cysteine Accessibility Profile for VcINDY_{Cysless}Y178C. *Title Annotations:* Position of the introduced cysteine mutant is indicated, along with a prediction of the conformation in which this residue is most accessible based upon manual structure examination. The computationally estimated relative solvent accessibility change from the Inward-Facing State to the Outward-Facing State, with positive values indicating greater accessibility in the IFS, as predicted by Dr. Vanessa Leone, NIH (Unpublished Data), is also shown. **A:** Introduced cysteine residue highlighted on the latest inward facing crystal structure [3], and the predicted outward-facing structure [81]. **B:** Level of PEGylation as a function of time, quantified through densitometry. This is displayed as the average proportion of VcINDY PEGylated at each timepoint, and the relative accessibility metric (discussed in main text). **C:** Simple t-test results for the effects of substrate addition as monitored through the relative accessibility metric. **D:** Reference numbers of the associated gels, which can be found in Appendix 1.

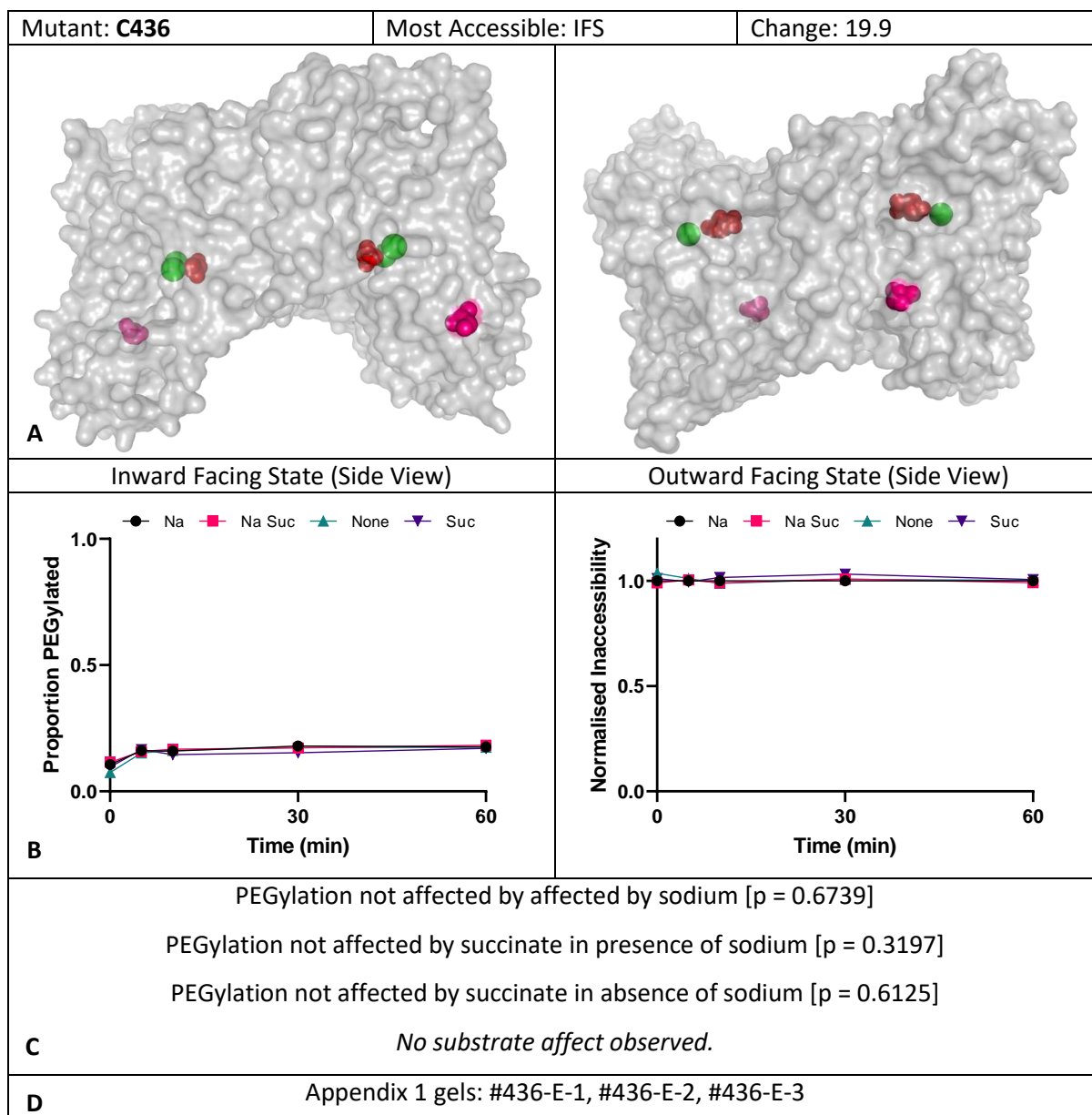


Figure 4.1.3-16 Cysteine Accessibility Profile for VcINDY_{Cysless}S436C. *Title Annotations:* Position of the introduced cysteine mutant is indicated, along with a prediction of the conformation in which this residue is most accessible based upon manual structure examination. The computationally estimated relative solvent accessibility change from the Inward-Facing State to the Outward-Facing State, with positive values indicating greater accessibility in the IFS, as predicted by Dr. Vanessa Leone, NIH (Unpublished Data), is also shown. **A:** Introduced cysteine residue highlighted on the latest inward facing crystal structure [3], and the predicted outward-facing structure [81]. **B:** Level of PEGylation as a function of time, quantified through densitometry. This is displayed as the average proportion of VcINDY PEGylated at each timepoint, and the relative accessibility metric (discussed in main text). **C:** Simple t-test results for the effects of substrate addition as monitored through the relative accessibility metric. **D:** Reference numbers of the associated gels, which can be found in Appendix 1.

First, mutants which do not provide useful information are identified and removed. Of the 15 expressible mutants tested, 4 gave poor levels of PEGylation under all conditions. These 4 mutants (F79C - Figure 4.1.3-13, W148C - Figure 4.1.3-14, Y178C - Figure 4.1.3-15, and S436C - Figure 4.1.3-20) were only able to be clearly labelled with the addition of 1.2 mM mPEG5K, a threefold increase with respect to all other mutants in this study, and showed no clear change in response to the addition of substrates. PEGylation rates were constant for each mutant in all conditions tested. It may be observed that a significant p value was found for VcINDY_{Cysless}W148 when comparing no substrates to sodium only, however as this change is extremely minor and not also present in the change from succinate to succinate and sodium, it may reasonably be assumed this is one of the inevitable false positives associated with the conductance of many t-tests. As such, despite appearing to be accessible in current models, these residues appear to be relatively constitutively inaccessible in the VcINDY micelle. This may be due to either discrepancies between the models and the actual conformations of VcINDY, or due to the detergent micelle itself blocking access to these positions.

Of the residues which were readily labelable, 3 showed no detectible substrate response (E42C - Figure 4.1.3-10, A383C - Figure 4.1.3-11, and S430C - Figure 4.1.3-12). In these cases good levels of PEGylation occurred, however PEGylation rates appeared constant for all conditions examined. It may be noted again that a significant p value was achieved for VcINDY_{Cysless}E42C succinate addition in the presence of sodium, however once again this does not look to be a true impact, and is likely another false positive, as is to be expected. The VcINDY_{Cysless}E42C mutation undergoes some minor predicted accessibility change, however it is largely accessible in both conformations, functioning as a useful control residue, displaying no great substrate impact on the chemical process of labelling. On the other hand, VcINDY_{Cysless}A383C is predicted to be more accessible in the OFS, while VcINDY_{Cysless}S430C is expected to be more accessible in the IFS, yet they show no substrate response. These two positions are reminders that the current model of VcINDY conformational shift is only experimentally verified for large scale movements [81], and the results produced by these residues

are possibly representative of subtle differences between their true locations and current models. Additionally, VcINDY_{Cysless}A383C and VcINDY_{Cysless}S430C showed particularly poor transport, and while they allowed significantly greater succinate uptake than empty liposomes, their exceptionally poor transport may indicate that these mutant proteins are functioning particularly poorly. As such it is possible, and perhaps likely, that the failure of these mutants to demonstrate clear substrate response is simply a failure of these mutants to emulate the behaviour of the wildtype protein.

The remaining 8 mutants in our dataset demonstrated clearly detectable substrate dependent accessibility changes, and will be used for the analysis of substrate induced accessibility changes (T154C - Figure 4.1.3-2, M157C - Figure 4.1.3-3, T177C - Figure 4.1.3-4, A120C - Figure 4.1.3-5, S381C - Figure 4.1.3-6, T215C - Figure 4.1.3-7, L384C - Figure 4.1.3-8, V388C - Figure 4.1.3-9). In all of these cases, the mutants demonstrated clear differences in the rate of PEGylation in the response to the addition of substrates, as confirmed by t-testing carried out upon the Normalised Inaccessibility metric.

In order to determine the impact of substrate addition on VcINDY conformational state, two mutants will be examined in detail; VcINDY_{Cysless}T154C, which is accessible in the inward facing state, and VcINDY_{Cysless}S381C, which is accessible in the outward facing state (Figure 4.1.3-17A).

In the absence of substrates VcINDY_{Cysless}T154C showed rapid PEGylation, reaching 65% after one hour, however the addition of substrates almost completely abolished VcINDY_{Cysless}T154C PEGylation (Figure 4.1.3-17B&C). This indicates that residue 154 is solvent accessible in VcINDY's apo state, but solvent inaccessible in VcINDY's substrate bound state. According to the current two state rigid body model of VcINDY translocation (Figure 1.10.3-1D), this suggests that substrate binding drives VcINDY into the outward facing state.

If this were true position 381, which is solvent accessible in the outward facing state, but not the inward facing state, would be expected to PEGylate more rapidly in the presence of substrates.

Unexpectedly, the inverse is true; VcINDY_{Cysless}S381C PEGylates rapidly in the absence of substrates,

reaching around 50% after one hour, however the addition of substrates once again abolishes PEGylation (Figure 4.1.3-17B&C). This behaviour cannot be explained by the current two state rigid body model of VcINDY movement.

In order to rule out a direct effect of the substrates upon the PEGylation reaction rate, the control mutant VcINDY_{Cysless}E42C, in which the introduced cysteine residue is not predicted to alter accessibility during VcINDY conformational change, is examined. It is seen that substrates have no impact upon PEGylation rates (Figure 4.1.3-17B&C), demonstrating that substrate induced changes in PEGylation rates do indeed result from changes in solvent accessibility.

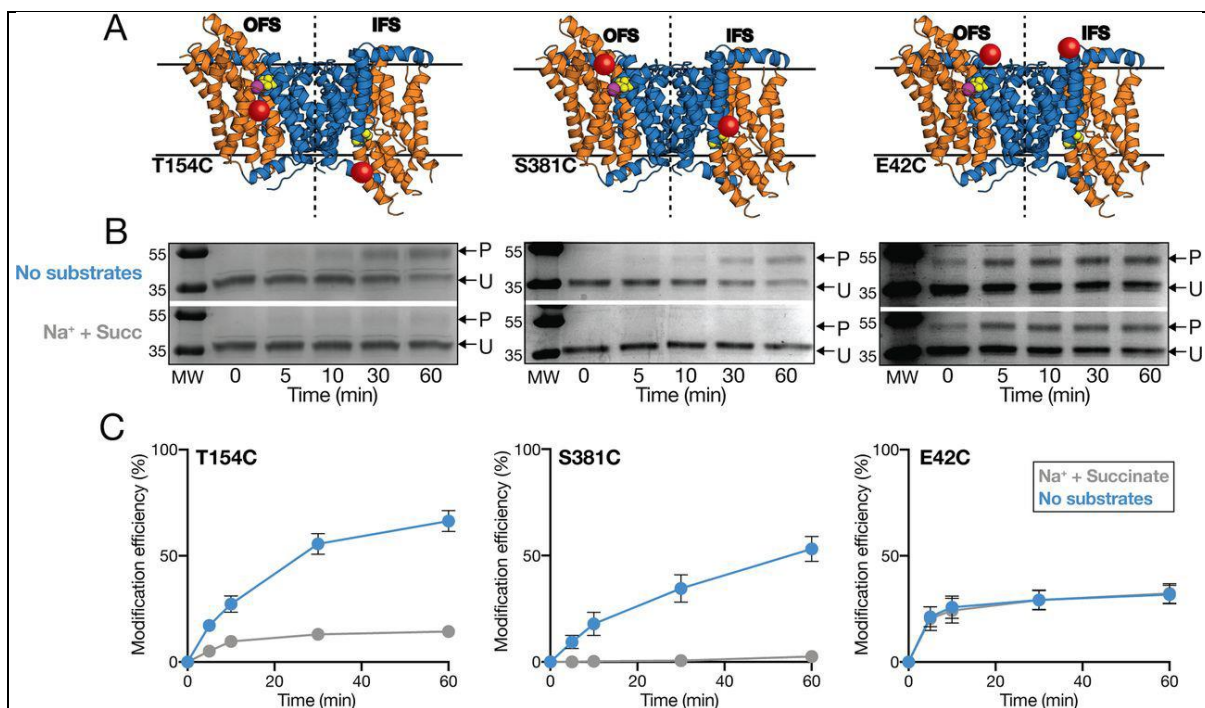


Figure 4.1.3-17 Impact of substrates on the accessibility of key VcINDY residues. Figure taken from Sampson et al 2020

[146], created by Christopher Mulligan. **A:** Hybrid structure showing the predicted outwards facing state (left) known inwards facing state (right) of VcINDY. Orange = Transport domain. Blue = Scaffold domain. Purple = Bound sodium. Yellow = Bound succinate. Red = Location of introduced cysteine residue. **B:** Representative raw PEGylation gels for each cysteine mutant, performed in the absence and presence of substrates. The PEGylated (P) and unPEGylated (U) bands are indicated. **C:** Proportion of each mutant PEGylated over time (Modification Efficiency), in the presence and absence of substrates.

This informs us that the addition of substrates causes VcINDY to favour a previously unobserved conformational state in which both residues 154 and 381 become solvent inaccessible. Examination of six additional residues predicted to change solvent accessibility during VcINDY translocation shows all positions tested to reduce accessibility in response to substrate addition, consistent with the behaviours of 154 and 381 (Figure 4.1.3-18 and Table 4.1.3-1). This further indicates that VcINDY does indeed favour a novel intermediate conformation in response to substrate binding, in which the positions examined become solvent inaccessible either due to the steric effects of the tertiary structure, or the surrounding detergent micelle environment.

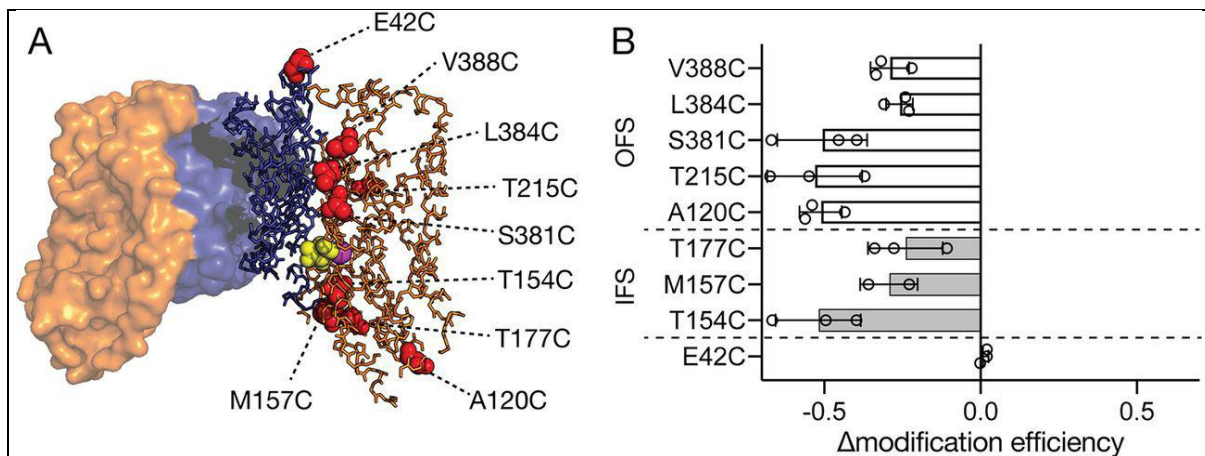


Figure 4.1.3-18 The effects of substrate addition on the accessibility of substrate responsive cysteine positions within

VcINDY. Figure taken from Sampson et al 2020 [146], created by Christopher Mulligan. **A:** Positions of substrate responsive cysteine positions, along with the control position E42C, on the inward facing structure of VcINDY. Orange = Transport domain. Blue = Scaffold domain. Purple = Bound sodium. Yellow = Bound succinate. Red = Location of introduced cysteine residue. **B:** Change in the proportion of each mutant PEGylated after one hour (Modification Efficiency) in response to the addition of substrates. Positive values indicate an increase in PEGylation in response to substrate addition. Negative values indicate a decrease in PEGylation in response to substrate addition. White = Residues predicted to be accessible in the Outward Facing State. Grey = Residues predicted to be accessible in the Inward Facing State. Black = Control residue predicted not to change accessibility in response to substrate addition.

In order to further analyse these results, the impact of sodium and succinate additions upon PEGylation rates can be examined separately. Examining the single cysteine mutants VcINDY_{Cysless}T157C and VcINDY_{Cysless}S381C, shows that the addition of succinate in the absence of sodium does not result in a significant change in cysteine accessibility (Figure 4.1.3-19). In fact, the addition of succinate in the absence of sodium does not result in accessibility changes for any residue tested here (Table 4.1.3-1), demonstrating that sodium must bind first in order for subsequent succinate binding to take place.

The addition of sodium accounts for the entirety of substrate induced accessibility change for VcINDY_{Cysless}S381C (Figure 4.1.3-19B), in stark contrast to VcINDY_{Cysless}T157C for which the addition of succinate in the presence of sodium accounts for the entirety of substrate induced accessibility change (Figure 4.1.3-19A).

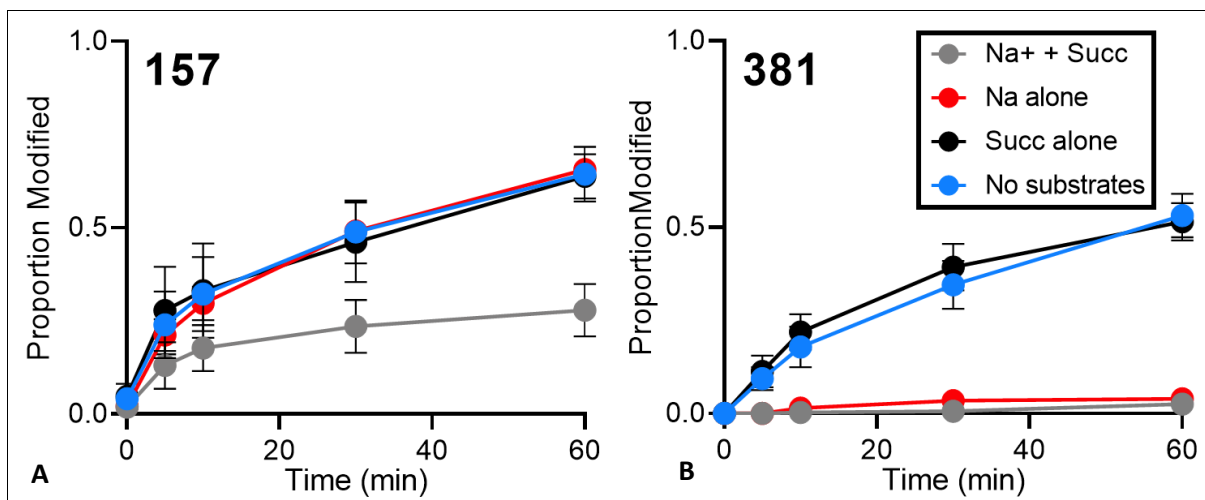


Figure 4.1.3-19 Effects of individual substrates upon the PEGylation rates of specific single cysteine residues. The proportion of VcINDY PEGylated (Modification efficiency) over time is shown. A: VcINDY_{Cysless}T1547C. B: VcINDY_{Cysless}S381C.

Inward or Outward Facing State Accessible	Residue	Sodium Effect?	Succinate Effect in Presence of Sodium?	Succinate Effect in Absence of Sodium?
IFS	154	Supress	Supress	None
IFS	157	None	Supress	None
IFS	177	Supress	None	None
OFS	120	Supress	None	None
OFS	215	Supress	None	None
OFS	381	Supress	None	None
OFS	384	Supress	None	None
OFS	388	Supress	Supress	None

Table 4.1.3-1 Effects of substrate addition on the ability of mPEG5K to label single cysteine mutants at varying positions

within the protein. True effect for the purpose of this table is determined by a t-test carried out upon normalised accessibility values at 60 seconds upon the data shown in Figure 4.1.3-2 to Figure 4.1.3-16. Resultant p values of ≤ 0.05 indicated an effect of substrate addition. Due to the large number of t-tests carried out here, false positive and negative readings are highly possible. As such this table is intended as a quick reference, and any further interrogation of the data should reference the data tables in Figure 4.1.3-2 to Figure 4.1.3-16., where the full datasets are shown. The conformational states in which the residues are predicted to be most accessible based upon manual structural examination are also indicated for reference.

In order to properly assess the differing impacts of sodium and succinate upon residue specific accessibility changes, the proportion of the total substrate derived accessibility change triggered by sodium alone is calculated for each substrate responsive mutant as follows:

$$\text{Sodium Impact} = \frac{[\text{Proportion PEGylated with no substrate}] - [\text{Proportion PEGylated with Sodium}]}{[\text{Proportion PEGylated with no substrate}] - [\text{Proportion PEGylated with both substrates}]}$$

Equation 4.1.3-1 Calculation of the proportion of total substrate induced change in residue accessibility for which sodium is responsible.

This allows sodium and succinate responses to be separated, demonstrating that some residues are more affected by sodium, while others are more affected by succinate (Figure 4.1.3-20A). In particular, VcINDY_{Cysless}M157C, VcINDY_{Cysless}L384C, and VcINDY_{Cysless}V388C show high levels of succinate response compared to the other residues examined. This raises the question; is there a structural basis for the difference in the magnitude of these responses?

Examination of the structure allows these cysteine positions to be divided into three broad categories; hairpin residues with a large succinate response, hairpin residues without a large succinate response, and non-hairpin residues without a large succinate response (Figure 4.1.3-20B). No non-hairpin residues demonstrated large accessibility changes in response to succinate binding, suggesting that any succinate driven changes in VcINDY conformation are largely localised to the hairpin regions. Briefly, these are two pairs of hairpin helices which enter from opposite sides of the membrane, forming much of the binding site (see 1.10 VcINDY Molecular Function and Figure 1.10.3-1A)..

Examining the hairpin regions in more detail allows clear structural differences between succinate sensitive and insensitive hairpin residues to be seen. The two succinate insensitive hairpin residues, T154C and S381C, are located in extreme proximity to sodium binding sites. Examination of VcINDY_{Cysless}T154C and VcINDY_{Cysless}S381C raw PEGylation data (Figure 4.1.3-2 and Figure 4.1.3-6) shows that the binding of sodium massively reduces the accessibility of these residues, reducing PEGylation rates to such an extent that any further effect of succinate would be impossible to detect. This suggests that while these residues may be in a succinate responsive region of the protein, the impact of close proximity sodium binding abolishes their ability to report on any further accessibility changes. The succinate responsive hairpin residues on the other hand, VcINDY_{Cysless}M157C, VcINDY_{Cysless}L384C, and VcINDY_{Cysless}V388C, are located away from the sodium binding sites, allowing them to report on the succinate induced hairpin movements.

As such the three groups of residues can be understood as follows: Residues not located in the hairpins are affected by a general sodium driven conformational shift towards an occluded state which affects much of the transport domain. Residues located on the hairpins in extreme proximity to the sodium binding sites are affected by the change in local environment as sodium enters their proximity. Residues located on the hairpins at least several residues away from the sodium binding are strongly affected by the binding of succinate as a succinate induced conformational shift appears to affect these regions.

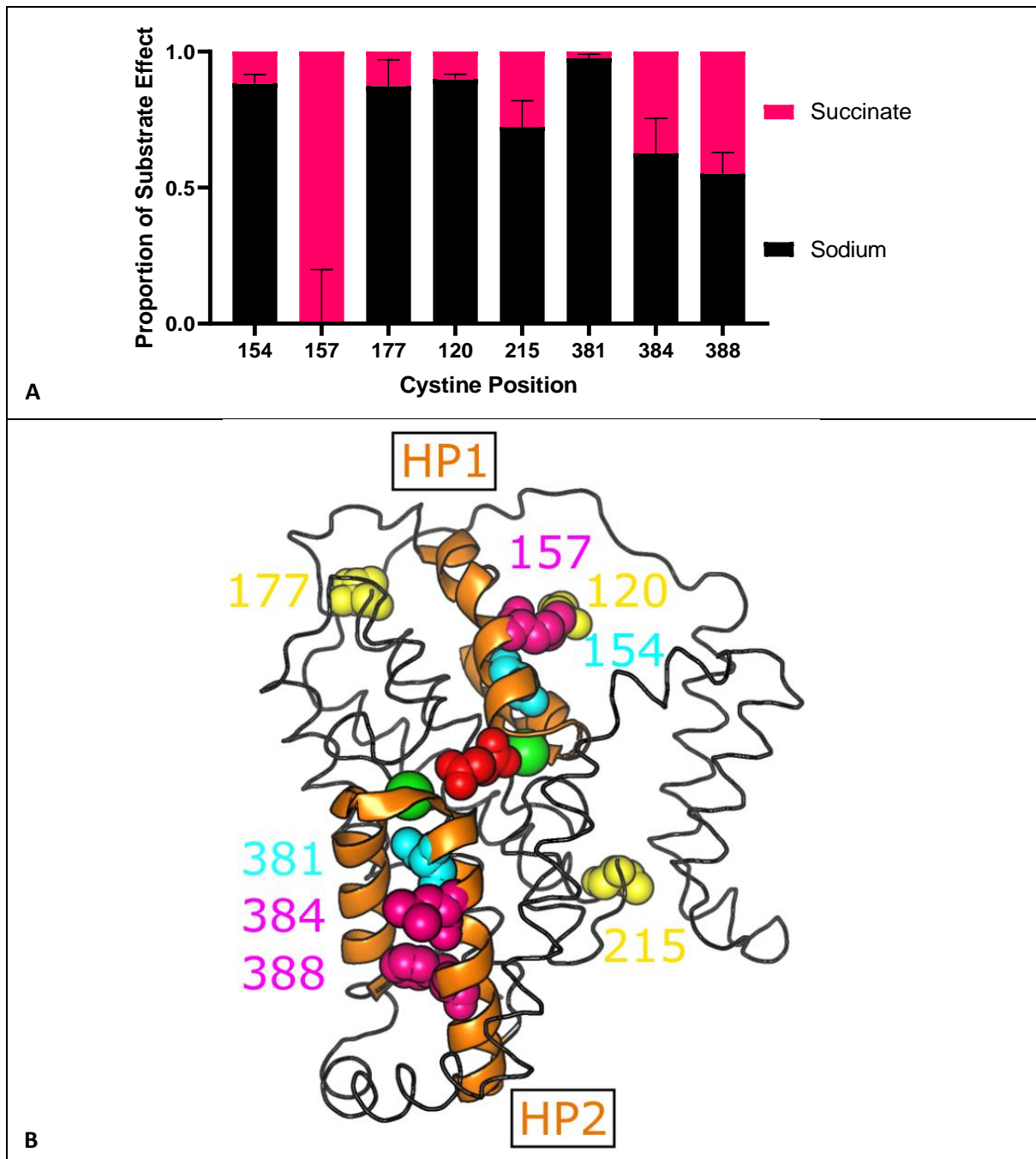


Figure 4.1.3-20 Single cysteine positions and their substrate response in the PEGylation based accessibility assay. A:

Separation of the magnitude of the accessibility change induced by the addition of sodium only and the change induced by the addition of both substrates for each cysteine position, demonstrating differing levels of sensitive to these two substrates. **B:** A single VcINDY transport domain showing the locations of single cysteine mutations for which a substrate dependent change in accessibility was observed. The hairpin regions are shown as cartoons, the general domain backbone is shown as a ribbon, the residues used for single cysteine mutations are shown as spheres, and the substrates are shown as spheres. HP = Hair Pin. The colours are as follows; Orange = Hair pin region. Yellow = Non hair pin residue, succinate insensitive. Pink = Hair pin residue, succinate sensitive. Blue = Hair pin residue, succinate insensitive. Green = Known sodium ion location. Red = Succinate. Based on the crystal structure 5UL7 [3].

Based on the crystal structure 5UL7 [3].

4.1.4 Succinate Induced Accessibility Changes are Replicated by Other Known

Substrates, But Not By Similar Non-substrate Molecules

As our accessibility assays have demonstrated the apparent accessibility of single residues to alter upon the addition of succinate, we tested whether the succinate dependent accessibility changes could be replicated through the addition of other known cationic substrates, and whether non-binding dicarboxylates would cause similar changes through non-specific mechanisms. For this purpose we used a mutant known to provide a clear response to succinate, VcINDY_{Cysless}M157C.

While previous PEGylation assays have been performed as time courses, presenting the reaction at several timepoints, in order to increase the level of throughput in this experiment only the PEGylation after 60 minutes was recorded, allowing multiple samples to be run simultaneously on a single gel and also eradicating much of the batch to batch variation.

Oxalate, the non-binding negative control (see 4.2.4 High Throughput Thermostability Screening Reveals Clear Rules of Substrate Selectivity and 4.4.2 Detergent Solubilised VcINDY is Compatible with MST Binding Affinity Measurements), did not cause a reduction in M157C accessibility, while other dicarboxylates known to interact with VcINDY, fumarate, malate, and oxaloacetate, all resulted in reductions in accessibility similar to succinate (Figure 4.1.4-1). This indicates that the anion derived change in accessibility is specific to interacting dicarboxylates, and is therefore likely a specific response to substrate binding. The difference between the level of accessibility reduction caused by succinate and that caused by alternative dicarboxylates reduces with increasing substrate concentration, suggesting that these alternative substrates may simply bind more weakly than VcINDY. Additionally, citrate showed no clear impact on cysteine accessibility readings despite being known to bind VcINDY in crystallographic studies. Further work in this thesis has suggested that citrate binding is of exceptionally low affinity (see 4.2.4 High Throughput Thermostability Screening Reveals Clear Rules of Substrate Selectivity), and this experiment tested a maximum concentration

of 10 mM citrate, compared to the 50 – 100 mM citrate used in previous crystallographic studies [48][3]. It therefore seems likely that citrate simply does not bind effectively at these concentrations.

This indicates that the effects of succinate upon accessibility measurements are likely the result of specific binding interactions, which can be replicated through the use of alternative substrates.

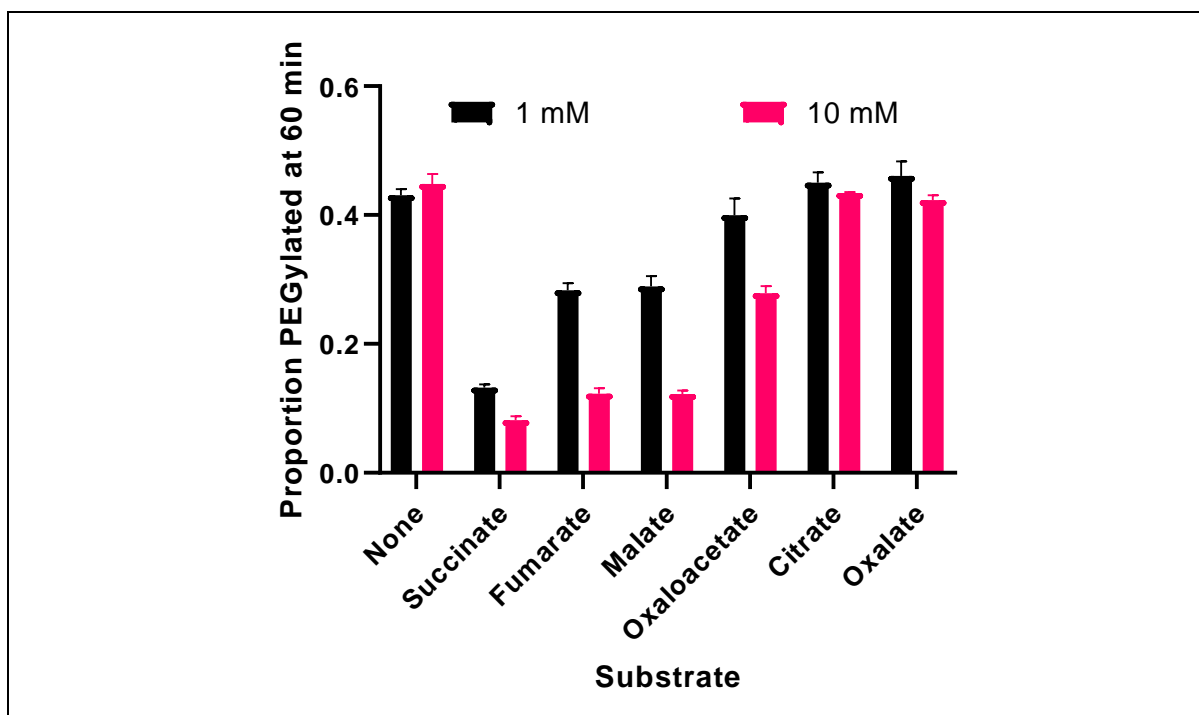


Figure 4.1.4-1 PEGylation of the VcINDY_{Cysless}M157C single cysteine mutant in the presence of varying substrates. The proportion of VcINDY_{Cysless}M157C PEGylated after 60 minutes is shown. VcINDY_{Cysless}M157C PEGylation is known to be anion binding responsive, showing dramatically decreased levels of PEGylation in the presence of succinate. Fumarate, malate, and oxaloacetate are known substrates of VcINDY, here showing an ability to repress PEGylation in a similar manner to succinate. Citrate has been shown to bind in crystallographic studies, however its interaction may be of very low affinity (see main text) and does not result in a suppression of PEGylation under the conditions tested here. Oxalate is a dicarboxylate chemically similar to succinate which is known not to interact with VcINDY, and as such it serves as a control for non-specific interaction. This negative control does not impact the PEGylation rate of VcINDY_{Cysless}M157C.

4.1.5 VcINDY Substrate Induced Accessibility Changes Are Similar Within Both Detergent and Native Lipid Environments

PEGylation experiments have thus far been carried out with detergent solubilised VcINDY, raising the reasonable question as to whether the substrate responses observed are representative of VcINDY *in vivo*. In order to answer this, SMALPs were used. SMALPs are a native lipid nanodisc system, in which membrane proteins are solubilised directly into nanodiscs from the biological membrane, maintaining native lipid interactions [83]. For more information see 3.1 The SMALP Native Lipid Nanodisc System Allows *In Vitro* Examination of VcINDY in a Near Native Environment.

Two mutants were selected for testing in this nanodisc system; VcINDY_{Cysless}120C and VcINDY_{Cysless}157C. These mutants reported on the general sodium response and the specific succinate hairpin response respectively and exclusively, making them ideal testbeds for monitoring whether these substrate responses could be observed in a native lipid system.

Interestingly, both SMALP solubilised mutants were far more resistant to labelling than their detergent solubilised counterparts (Figure 4.1.5-1A & Figure 4.1.5-1B), however once mPEG5K concentrations were increased to compensate for this the characteristic substrate responses were observed. SMALP solubilised VcINDY_{Cysless}A120C showed a reduction in accessibility upon the addition of sodium (Figure 4.1.5-1C), similar to its detergent solubilised form (Figure 4.1.3-5), while SMALP solubilised VcINDY_{Cysless}M157C showed a reduction in accessibility upon the addition of succinate (Figure 4.1.5-1D), also similar to its detergent solubilised form (Figure 4.1.3-3). These results indicate that the substrate responses observed in detergent solubilised VcINDY also occur in a native lipid environment.

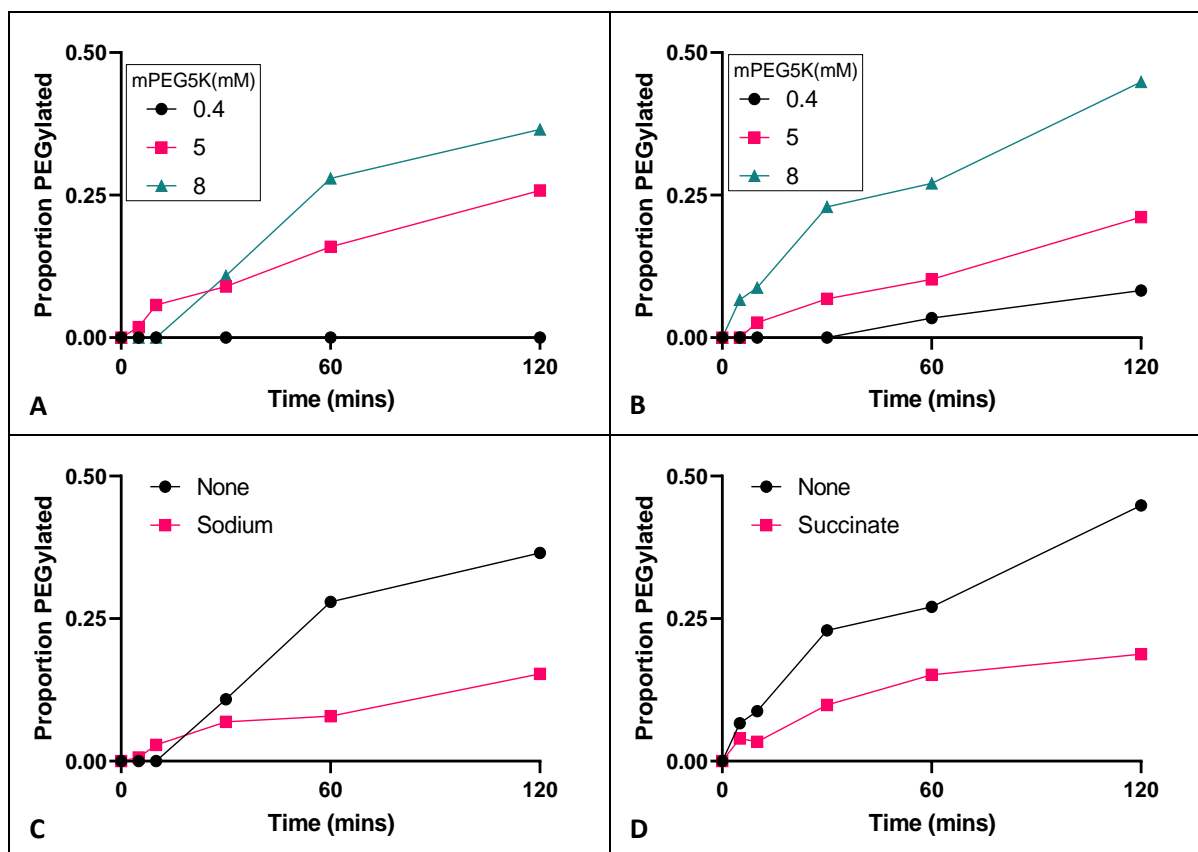


Figure 4.1.5-1 Observation of substrate induced accessibility shifts for SMALP solubilised VcINDY_{Cysless}M157C and

VcINDY_{Cysless}A120C. **A:** Varying concentrations of mPEG5K used for labelling of VcINDY_{Cysless}A120C in the presence of neither substrates. For detergent (DDM) solubilised VcINDY cysteine mutants 0.4 mM mPEG5K was used. **B:** Varying concentrations of mPEG5K for the labelling of VcINDY_{Cysless}M157C in the presence of sodium only. For detergent (DDM) solubilised VcINDY cysteine mutants 0.4 mM mPEG5K was used. **C:** 8 mM mPEG5K labelling of VcINDY_{Cysless}A120C in the presence of either 150 mM sodium or potassium, showing sodium to slow labelling similarly to detergent (DDM) solubilised VcINDY_{Cysless}120C. **D:** 8 mM mPEG5K labelling of VcINDY_{Cysless}157C in the presence or absence of 1 mM succinate, with 150 mM sodium in both cases, showing succinate to slow labelling similarly to detergent (DDM) solubilised VcINDY_{Cysless}157C. Appendix 1 raw data gels: #SMA-120-0.4, #SMA-120-5/8, #SMA-157-E, #SMA-157-PEG, #SMA-157-5.

4.1.6 Chapter Summary

The cysteine accessibility assay has proven to be a useful tool for the examination of VcINDY dynamics.

A major strength of the accessibility assay undertaken here is the range of positions tested, examining 15 functional single cysteine mutants, 13 of which showed good levels of transport, in order to build up a general picture of movement during the transport cycle.

Through examination of this range of positions it has become clear that PEGylation is capable of reporting with high resolution on substrate responses, with positions separated by only a few residues (154 v 157 & 381 v 384) showing dramatically different substrate sensitivities, allowing local conformational changes to be established. Clearly interpreting these local conformational changes is, however, more challenging. The interplay of local conformational changes with the larger domain translocations required for transport, along with the lack of structural understanding of VcINDY's intermediate conformations, makes firm conclusions as to the movements conducted by these residues difficult to establish. This being acknowledged, however, the observation of substrate dependent movements within defined areas of VcINDY's architecture does allow a range of novel conclusions to be reached.

It should be noted that while the bulk of the experiments within this chapter were carried out in detergent solubilised VcINDY, the trials of SMALP solubilised (see 3.1 The SMALP Native Lipid Nanodisc System Allows *In Vitro* Examination of VcINDY in a Near Native Environment)

VcINDY_{Cysless}A120C and VcINDY_{Cysless}M157C, reporters on the sodium and succinate responses respectively, found identical substrate responses to their detergent solubilised counterparts. This indicates that the lessons learnt here are relevant to the lipid embedded VcINDY. While previous literature examining accessibility of residues upon the protease GlpG have indicated lipid dependent dynamic alterations using SMALPs, these differences were modest and did not appear to indicate a general alteration to protein's mechanism [97]. Furthermore, similar cysteine accessibility assays

carried out upon the transporter LacY established identical substrate induced conformational responses to occur whether the protein was contained within a detergent micelle or a lipid bilayer [141]. Thus, the findings presented herein can be reasonably considered biologically relevant.

Firstly, an order of binding is clearly indicated, with succinate only able to influence accessibility through binding in the presence of sodium. This matches well with crystallographic data indicating that the bound succinate molecule blocks movement of the bound sodium ions in and out of the binding pocket [48][3], and with data gathered later in this thesis (see 4.2.3 Details of Cation Interactions are Revealed Through Thermostability Measurements and 4.4.4 Succinate Binding is Dependent upon Prior Low Affinity Sodium Binding). Additionally, previous transport studies upon the human DASS family member hNaDC-1 have suggested this sodium first order of binding based upon the presence of minor sodium only leak currents and the kinetics of succinate transport [147], and similar cysteine accessibility work upon rabbit NaDC-1 has also indicated a sodium first order of binding [148][149], indicating that this ordered binding may be a common feature of the wider DASS family.

This order of binding is also common for sodium coupled secondary active transporters, with examples both within the wider DASS family and beyond [150]. Furthermore, there is clear precedent for the detection of ordered binding through the use of cysteine accessibility assays such as performed herein, as demonstrated by accessibility studies upon the secondary active transporters Tyt1 and NaDC-1, for which a similar sodium first order of binding was determined through cysteine accessibility assays [142][148].

Our picture of this ordered binding process is further developed through the observation that two distinct accessibility shifts result from the addition sodium and succinate. For all substrate responsive cysteine positions examined, the addition of substrates caused a reduction in their accessibility, suggesting that substrate binding moves the protein not into the inward- or outward-facing state, but into an as yet unknown intermediate state. This preference for an intermediate

conformation in the presence of substrates is in good agreement with recent cryo-EM findings for the nanodisc solubilised elevator mechanism transporter Glt_{Ph} , for which structures obtained in the presence of saturating substrates predominantly demonstrated an intermediate occluded state [27].

The proportion of the substrate induced accessibility change stimulated by sodium alone, compared to the addition of sodium and succinate, varied greatly between cysteine positions, indicating two different conformational responses to take place upon the addition of these substrates. This is in good agreement with previous accessibility measurements carried out for the DASS family members NaDC-1 and SdcS. For these transporters the addition of sodium resulted in different accessibility changes than the addition of sodium along with succinate, indicating that these two, distinct, conformational responses are a common feature of DASS family substrate interactions [148][149][151].

It is worthy of note, however, that NaDC-1 accessibility measurements indicated an increase in hairpin residue accessibility in the presence of sodium, and a decrease in hairpin residue accessibility in the presence of both substrates [148][149]. This is in contrast to the two step reduction of accessibility observed here, suggesting either that these two DASS family members differ in the details of their substrate binding process, or that differences in experimental setup are responsible for these differences; for example, the NaDC-1 study was conducted within lipid bilayers with only single sided accessibility measurements conducted while our study examines total accessibility within detergent micelles. Nevertheless, both proteins demonstrate substantial substrate induced changes in accessibility, attesting to conformational responses to substrate binding.

In the case of our VcINDY data, comparison of cysteine positions with the relative impacts of sodium and succinate upon their accessibility allows further conclusions to be drawn. It appears that, with the exception of residues in extreme proximity to the sodium binding sites, the majority of succinate dependent accessibility change is localised to the hairpin regions; regions which have also been

shown to be highly substrate responsive in the DASS family transporter NaDC-1 [148][149], discussed above.

It is a fundamental fact that secondary active transporters of this kind must tightly couple the transport of their substrates in order to prevent leakage. The practical implication of this is that secondary active transporters must be able to translocate freely in the absence of substrates or presence of the full complement of their substrates, but not when only partially loaded. This is well exemplified by the elevator mechanism transporter Glt_{Ph} . Glt_{Ph} uses a sodium gradient to drive aspartate uptake; as such Fluorescence Resonance Energy Transfer (FRET) measurements have demonstrated the sodium only bound state of Glt_{Ph} to be unable to transition between the inward- and outward- facing states, while the fully loaded sodium and aspartate bound state is able to freely make this transition [152].

In the case of VcINDY's sodium-succinate symport system this means that while the *apo* and fully loaded protein must be able to transition freely between inward- and outward-facing states, the sodium only bound state must be unable to undergo this transition. Considering this, substrate binding process can be considered as follows: Initial sodium binding begins movement to an intermediate, partially occluded, state as a locked conformation is formed and the succinate binding site is made ready. Subsequent succinate binding triggers a localised conformational change in the hairpin regions, resulting in a releasing of the conformational lock and triggering transport (see 5.2 The New Model of VcINDY Substrate Transport). It may be hypothesised, therefore, that these hairpins represent the trigger region responsible for tightly coupled ion transport.

This system of hairpin gating has already been observed in a range of other elevator mechanism transporters [15], as exemplified by the sodium coupled elevator mechanism transporter Glt_{Ph} , in which a key hairpin regions opens upon sodium binding [153], and closes over the anion binding site after substrate binding [154][27]. Given that the movements of the VcINDY hairpin observed herein are the product of both the general sodium induced shift towards the intermediate state and hairpin

specific shifts it is impossible to speculate with any certainty as to the exact nature of the hairpin's dynamic cycle in VcINDY beyond what has already been discussed, and the question of how closely the hairpins of VcINDY match the hairpins of Glt_{Ph} in their movements remains open and intriguing.

It may be observed that anionic substrate concentrations of 1 mM and 10 mM were used in these accessibility assays, representing high concentrations in comparison to VcINDY's K_m of $1.0 \pm 0.2 \mu\text{M}$ [73]. This matter of VcINDY substrate binding affinity is examined in detail and properly discussed in

4.4.7 Chapter Summary.

In conclusion, cysteine accessibility assays have established a clear order of substrate binding, demonstrated the presence of previously unknown intermediate conformational states, and revealed a key gating role for VcINDY's hairpin regions similar to that found in other elevator mechanism transporters.

4.2 High Throughput Thermostability Measurements Reveal the Rules of VcINDY

Substrate Binding

4.2.1 Introduction

In the most basic sense, transport can be reduced to cycles of substrate binding, conformational change, and substrate release. Transport proteins are often examined through transport assays, in which the cumulative function of these three transport steps are revealed. Often, however, it is useful to separate these steps so that they can be studied individually, allowing the processes substrate binding and conformational change to be better understood. This is useful as these steps of the transport cycle operate with their own kinetic and functional parameters, which cannot be separated when operating together within transport assays. A binding assay allows the requirements governing the binding of both transportable and non-transportable substrates to be examined, as well as the protein's response to these binding processes. Additionally, in the case of secondary active transporters, which transport multiple substrates, the binding of individual substrates, which does not result usually in transport, may be detected through binding assays. A binding assay would therefore allow the processes of VcINDY's sodium and succinate binding to be understood in detail, along with interactions with alternative substrates.

Development of a binding assay suitable for VcINDY has been previously attempted, testing a scintillation proximity assay (SPA) (C. Mulligan, unpublished work), a filter binding assay with isotopically labelled substrate (C. Mulligan, unpublished work), and a rapid equilibrium dialysis assay (RED) (C. Mulligan, unpublished work). None of these previous attempts detected binding to occur. In light of this, a more indirect approach to detecting VcINDY substrate binding is examined in this chapter; thermostability measurement.

Ligand-protein binding events, and the bonds formed during these events, typically lead to an increase in protein melting temperature (T_m), as defined as the temperature at which the protein

population in is half-folded and half-denatured [155]. This ligand derived increase in melting temperature allows the monitoring of protein thermostability to be used for ligand binding studies.

The use of dyes for monitoring of protein thermostability with the aim of detecting ligand binding was first developed by *Pantoliano et al 2001* [156]. In this original protocol, the environmentally sensitive dyes 1-anilinonaphthalene-8-sulphonic acid (1,8-ANS), 2,6-ANS, 2-(*p*-toluidinyl)-naphthalene-6-sulfonic acid (2,6-TNS), and 5-(4''-dimethylaminophenyl)-2-(4'-phenyl)oxazole) were used. These dyes were known to partition into the hydrophobic, low dielectric constant, environment created by denaturing proteins, resulting in an increase in fluorescence which could be used to monitor protein unfolding. This increase in fluorescence was then measured using 384 well plates mounted in a custom fluorescence reader, allowing for very high throughput melting assays, as exemplified in Figure 4.2.1-1A. This assay went on to become the ThermoFluor® screening tool [157].

Membrane proteins, with their hydrophobic nature and frequent detergent solubilisation, are often incompatible with this hydrophobicity based form of the thermostability assay, producing higher background fluorescence as dyes interact with the readily available hydrophobic environments [158]. An alternative approach, better suited to membrane proteins, is to monitor the accessibility of cysteine residues. Cysteine residues are often found at the helix-helix interaction sites of membrane proteins due to their high packing value and as such are typically non-solvent accessible whilst the protein is correctly folded [159], as is the case for VcINDY (Figure 4.2.1-1B). *Alexandrov et al 2008* proposed the use of N-[4-(7-diethylamino-4-methyl-3-coumarinyl)phenyl]maleimide (CPM), a dye known to dramatically increase fluorescence upon binding to cysteine residues, as an appropriate tool to allow this high throughput binding screen to be used for membrane proteins [160].

A great advantage which comes with the use of the CPM dye in this process is that while CPM's optimal excitation and emission wavelengths are 387 nm and 463 nm respectively [90], the standard filters found within qPCR thermocyclers for the detection of Sybr Green dye are similar

enough that they may be used for the monitoring of this process [90]. The resultant combination of high throughput, low dye requirements, and non-specialised equipment allows for achievable screens with high numbers of substrates, with an exemplar screen having been carried out for a previously uncharacterised transporter by *Majd et al 2018* examining 132 possible interactors in this manner [161].

Principles for estimating substrate binding affinity have been established for this type of thermostability assay [162]. The main difficulty encountered when establishing binding affinity based upon thermostability data is that the observable differences in protein behaviour associated with substrate binding, which may normally be used to establish affinity, are typically only observable at temperatures greatly in excess of physiological conditions, i.e. at the melting temperature. At these raised temperatures, any binding affinity established will not be equivalent to binding affinities occurring at physiological conditions [162]. In order to solve this problem, *Bai et al 2019* have proposed destabilising the protein using chemical denaturants, until melting temperatures are lowered near enough to physiological temperatures for relevant binding affinities to be established [162]. The major drawback of this approach is that there is no guarantee that the denaturants themselves will not interfere with substrate binding interactions. Guanidine Hydrochloride, the denaturant employed by *Bai et al 2019*, for example, may interfere with ionic substrate interactions [162], which VcINDY itself carries out. Due to these complications, while it may be of great interest for alternative proteins, determining binding affinities for VcINDY using this technique is not practical, and any data gained would not be trustworthy.

The CPM thermostability assay, therefore, represents a high throughput, low protein requirement, approach to screening the substrate interactions of VcINDY. It is not, in this case, capable of accurate binding affinity determination, but it *is* capable of providing high quantities of more qualitative information as to VcINDY's substrate interactions.

The current state of knowledge as to VcINDY substrate binding is limited. It is known that three Na⁺ ions are transported for every succinate ion [9], with at least two of these Na⁺ ions appearing to bind before succinate according to current crystal structures [48][3], and the binding of the third Na⁺ ion having not yet been observed structurally. In light of these crystal structures, a hypothesis for ordered binding has been proposed [3]. This hypothesis observes that the binding site contains no charged residues, and instead gains a weak positive charge from surrounding helix dipoles [3], giving it a potentially low affinity for the doubly negatively charged succinate [73]. The binding of Na⁺ ions, however, provides the positive charge required to allow subsequent high affinity succinate binding, thus establishing a clear order of binding (Figure 4.2.1-1C) [3]. It should be cautioned that this model of ordered binding has not been experimentally tested for VcINDY and will be examined in detail in this chapter.

It should be noted that the binding order of the third sodium ion is unclear. As mentioned above, this third ion has not been observed in previous crystal structures, however due to the difficulties involved in identifying sodium ions through crystallography, it is uncertain whether the third sodium is present within these structures, or binds later in the transport cycle. The determination of whether this third sodium ion binds before succinate, or after succinate, will be required in order to fully understand the transport cycle of VcINDY, however it is beyond the scope of this thesis.

Liposome-based transport assays have found Na⁺ to optimally permit VcINDY succinate transport, while Li⁺ only allows succinate transport at a rate far slower than sodium driven transport, and K⁺ does not allow any transport of succinate [73]; a set of ion interactions which will also be examined in this chapter.

Anion interactions have been partially screened using liposome-based transport competition assays, in which potential substrates are tested for their ability to inhibit the transport of radiolabelled succinate. Extended dicarboxylates similar to succinate, such as malate and fumarate, were seen to inhibit radiolabelled succinate transport, suggesting that minor modifications of the four carbon

dicarboxylate were tolerated. Use of the double bond restrained four carbon dicarboxylates fumarate and maleate demonstrated that only the extended conformation fumarate was able to bind, suggesting that the extended conformation adopted by succinate within the binding site was required for binding to occur (Figure 1.10.3-1B). Additionally, the longer chain 5 and 6 carbon dicarboxylates, glutarate and adipate, were also able to inhibit radiosuccinate transport, but not longer chain dicarboxylates [73]. As such it appears that there is a high degree of flexibility in VcINDY's substrate selectivity, whereby a plethora of extended, 4 to 6 carbons long, dicarboxylates are able to bind, although overly long dicarboxylates are rejected. The extent of this anion binding flexibility, however, is currently unclear. A much-extended substrate screen carried out herein will allow the specifics of this substrate selectivity to be determined, and the results of this transport inhibition assay to be better understood.

VcINDY's substrate interactions represent an area in need of further study. While the need for the presence of both substrates before transport occurs has been well established, the order of binding is as of yet only hypothesised, as is the relationship between the cationic and anionic substrates within the binding site. Further to this, while there is enough data to show that flexibility exists in substrate binding, the exact rules and limits of this binding are currently unknown.

A thermal shift assay, specifically the CPM assay, provides the tools required to specifically examine the binding step of the transport cycle, screening a wide range of substrates and conditions in a relatively high throughput manner. While quantitative binding affinities are not determinable in these circumstances, qualitative examination of VcINDY's interacting molecules alone will greatly improve current understanding of the transporter's binding behaviours, and highlight new molecules with potential uses as either state specific stabilisers for future crystal structures, or DASS family inhibitors for future INDY protein drug development.

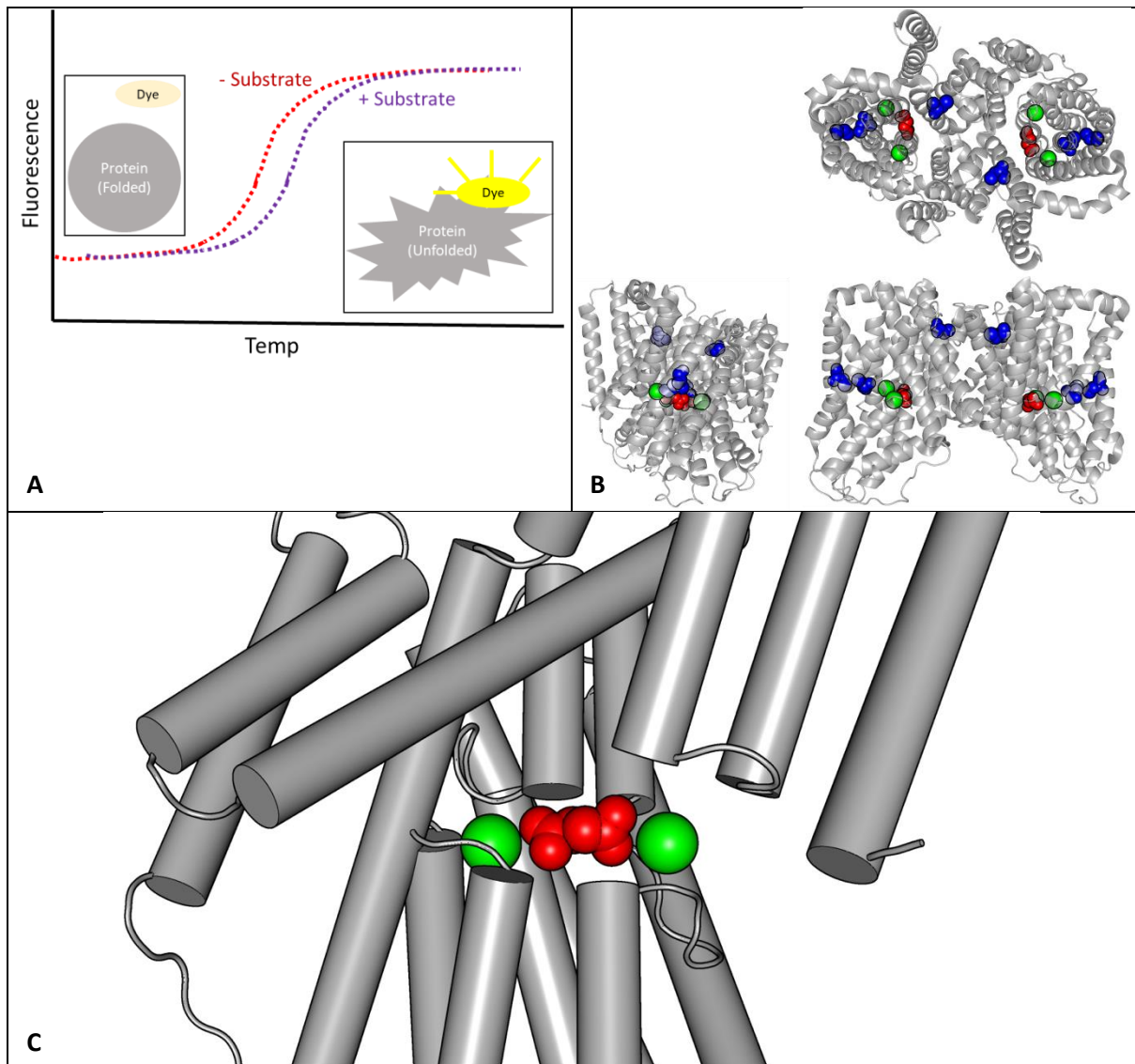


Figure 4.2.1-1 Principle of the CPM based thermostability shift assay. **A:** Illustrative data for a “Thermofluor-style”

experiment. A fluorescence increase is observed with increasing temperature, as the protein undergoes thermal

denaturation leading to dye interactions and enhancement of fluorescence. The addition of substrate leads to protein

stabilisation, resulting in an observable shift in melting temperature. **B:** Locations of cysteine residues within VcINDY.

Cysteine residues can be seen to be contained within the tertiary structure and non-solvent accessible in the native state.

Blue = Cysteine residues. Green = Na⁺ ions. Red = Succinate. PDB ID 5UL7. **C:** Binding pocket of one monomer of VcINDY.

Succinate can be seen to bind in a binding pocket made positive through the interaction of helix dipoles and nearby bound

Na⁺ ions. Alpha helices represented as straight rigid cylinders for clarity. Green = Na⁺ ions. Red = Succinate. Grey cylinders =

α -helices PDB ID 5UL7.

4.2.2 Optimisation and Validation of CPM assay for use with VcINDY

In order to use qPCR thermocycler based CPM thermofluor assays with VcINDY, an initial optimisation experiment was carried out, establishing a suitable CPM dye concentration. All dye concentrations tested resulted in noticeable increases in fluorescence upon heating, indicating that VcINDY thermal denaturation was being detected (Figure 4.2.2-1A). Higher concentrations of dye demonstrated higher levels of fluorescent increase, with 20 $\mu\text{g}/\text{mL}$ providing the highest fluorescent signal.

In order to establish the midpoint of fluorescent increase, i.e. the melting temperature, derivative curves were taken of the fluorescence data (Figure 4.2.2-1B). These derivatives show the highest dye concentration, 20 $\mu\text{g}/\text{mL}$, to provide the clearest melt curve, with the highest signal-to-noise ratio. Melting temperatures determined through this method are unchanged by differing dye concentration at around 52 °C in all cases (Figure 4.2.2-1B-Insert), however analysis of an n=3 dataset indicates that higher dye concentrations provide lower levels of error due to their improved signal-to-noise ratios. Increasing dye concentration from 5 to 10 to 20 $\mu\text{g}/\text{mL}$ reduced apparent standard deviation from 1.24 to 0.47 to 0.0004 °C respectively. As such a CPM concentration of 20 $\mu\text{g}/\text{mL}$ is used throughout this work for DDM solubilised VcINDY.

Now that a suitable dye concentration and a consistent melting temperature had been established, the effect of substrate addition was examined through the addition of 5 mM succinate in the presence of Na^+ (Figure 4.2.2-1C). This 5 mM succinate addition resulted in clear thermostabilisation of VcINDY, increasing its melting temperature from 52.7 ± 0.0 (S.E.) °C to 64.0 ± 0.3 (S.E.) °C, confirming both that this assay is capable of clearly detecting VcINDY's substrate binding, and that succinate binding does indeed provide significant thermostabilisation to VcINDY.

In order to rule out the possibility that non-specific interactions between succinate and VcINDY lead to the observed increase in thermostability, and to demonstrate that specific binding was indeed being detected, oxalate was employed as a negative control. Oxalate is a dicarboxylate similar to

succinate, which is known not to be bound by VcINDY, therefore allowing non-specific and specific interactions to be separated [73]. It is seen that while the addition of 10 mM succinate provided a thermostabilisation of 12.6 ± 1.8 (S.E.) °C, the addition of 10 mM oxalate provided no detectable stabilisation (Figure 4.2.2-1), demonstrating that the observed thermostabilisation is derived from binding interactions, and not non-specific chemical effects. The CPM thermofluor assay can therefore be confidently used as a VcINDY binding assay.

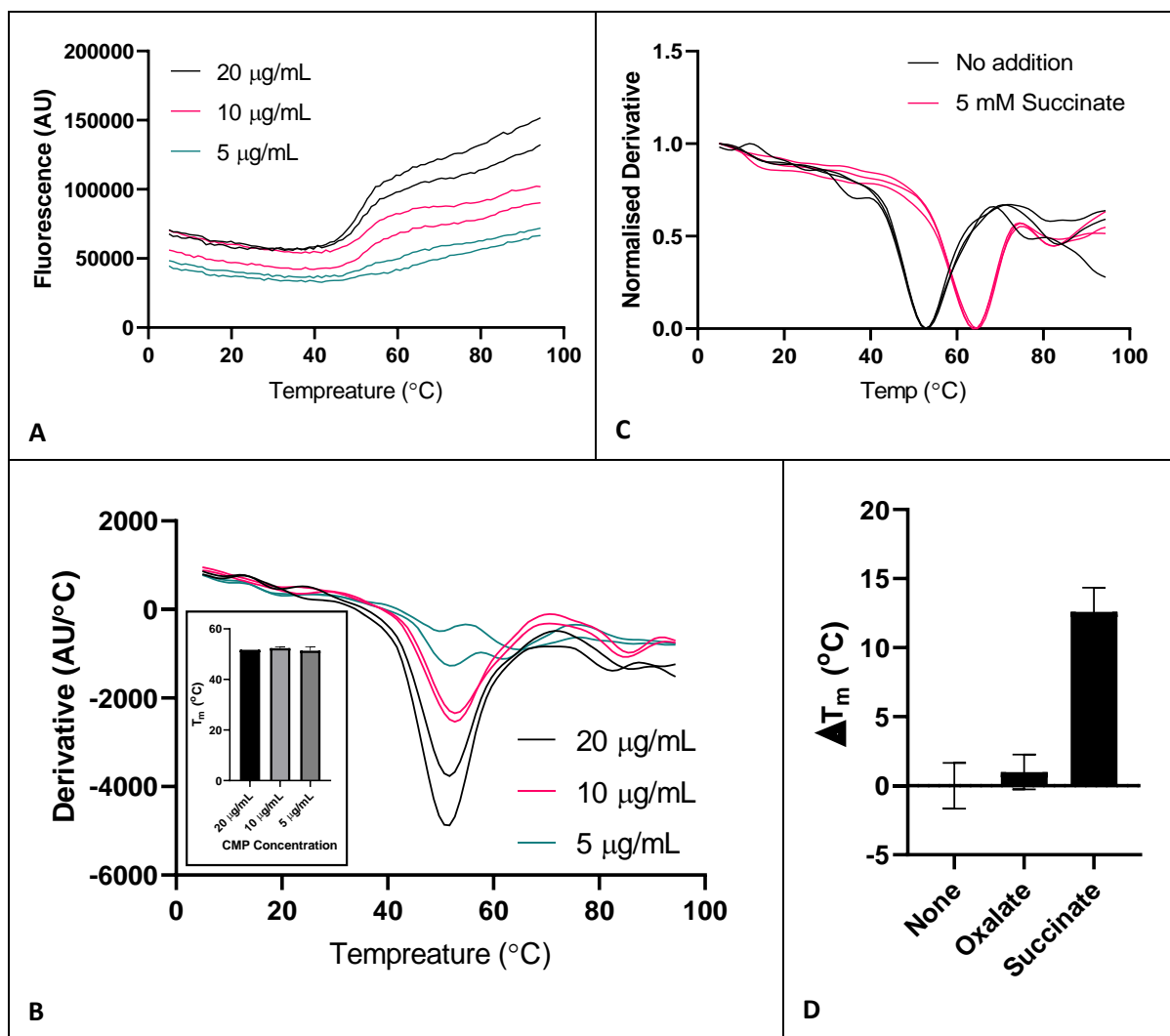


Figure 4.2.2-1 Optimisation of CPM based thermostability measurements for use with VcINDY. A: Raw fluorescent traces for the melting of VcINDY in the presence of varying concentrations of the dye CPM, performed in duplicate. Fluorescent intensity is shown as a function of temperature. **B:** Derivative data for the melting of VcINDY in the presence of varying concentrations of CPM. The rate of change of fluorescence with respect to temperature (dF/dT) is shown with respect to temperature. **B – insert:** Melting temperatures as determined from the data in part B of this figure. T_m is defined as the point of maximal rate of fluorescence change with respect to temperature, which is also the midpoint of fluorescence increase. SE shown. **C:** Effect of the addition of 5mM Succinate in the presence of 50 mM Na^+ on the derivative melt curve. The rate of change of fluorescence with respect to temperature (dF/dT) is shown with respect to temperature. **D:** VcINDY thermostabilisation resulting from the addition of no substrates, 10 mM oxalate, or 10 mM succinate. Standard Deviation is shown. $n = 3$.

4.2.3 Details of Cation Interactions are Revealed Through Thermostability

Measurements

The order of binding, Na⁺ followed by succinate, has been previously proposed but not experimentally verified for VcINDY. In order to verify whether Na⁺ presence supports succinate binding, the difference between the T_m with 5 mM succinate and without succinate, i.e. the level of stabilisation provided by the addition of succinate, was examined for various concentrations of Na⁺ (Figure 4.2.3-1A). Increasing Na⁺ concentration from 0.5 mM to 5 mM to 50 mM resulted in increasing levels of succinate stabilisation, from 2 °C to 4 °C to 7.3 °C, demonstrating a need for sodium presence before succinate binding can occur and supporting a sodium first order of binding.

Curiously, however, increasing the Na⁺ concentration from 50 mM to 500 mM results in a sharp drop in the level of stabilisation provided by succinate, from 7.3 °C to 1.7 °C (Figure 4.2.3-1A). There are two possible explanations for this reduction in succinate stabilisation at high Na⁺ concentrations. The first is that the high concentrations of sodium are facilitating sodium binding to a low affinity, inhibitory, sodium binding site. The second is that the high ionic strength environment created by this high concentration of sodium is disrupting charge interactions which are vital for the binding of succinate, either through electrostatic shielding of the binding site, or coordination of the negatively charged succinate molecule. If the latter possibility is true, and deleterious effects of high sodium concentration are simply due to the high ionic strength environment, then a high concentration of any alternative cation should also lead to a reduction in succinate derived stabilisation. In order to test these possibilities, the effect of sodium binding was separated duly from the effect of a high ionic strength environment through the supplementation of 50 mM Na⁺ with 450 mM of various alternative cations (Figure 4.2.3-1B). Any cation added in excess resulted in a reduction of the stabilisation provided by succinate, indicating that the high ionic strength environment is the source of this effect, whether the interfering ion interactions are occurring between VcINDY and the excess ions, succinate and the excess ions, or both.

Interestingly, the interfering ions suppressed succinate stabilisation to differing extents. The ions with the smallest ionic radii, Li^+ and Na^+ , at 76 pm and 116 pm respectively, resulted in the greatest level of suppression, only allowing succinate stabilisations of around 1.8 °C. The larger ions, K^+ and Rb^+ , at 152 pm and 166 pm respectively, allowed succinate stabilisations of around 3.7 °C. Finally, the largest ion tested, choline, allowed a succinate stabilisation of 7.3 °C, closest to the 11.6 °C stabilisation provided by succinate in the absence of excess interfering ions. Decreasing ion size, therefore, results in increasing levels of suppression of succinate stabilisation in a non-specific, but ion size dependent, manner.

VcINDY optimally transports succinate in the presence of Na^+ , poorly in the presence of Li^+ , and not at all in the presence of K^+ [73]. In order to understand why these similarly charged ions are differently able to facilitate VcINDY succinate transport, the T_m of VcINDY was first established in the presence of 50 mM LiCl, NaCl, and KCl (Figure 4.2.3-1C). Both Li^+ and Na^+ ions were able to stabilise VcINDY to 52.7 °C, compared to the lesser stability of 43.7 °C in the presence of K^+ , indicating that both of the former ions are capable of forming bonds with VcINDY which are not formed by K^+ . This also suggests that the smaller Li^+ ion is able to interact with the Na^+ ion binding sites in a similar manner to Na^+ itself, unlike the larger, likely sterically hindered, K^+ .

The observation that K^+ is unable to bind to VcINDY in the same manner as Na^+ is satisfactory to explain why K^+ is unable to permit succinate binding in a similar manner to Na^+ , however the question is raised of why Li^+ gives such poor transport in comparison to Na^+ , given that both appear equally able to bind to VcINDY. In order to answer this question, the level to which succinate was able to stabilise VcINDY in the presence of 50 mM of each of these ions was examined (Figure 4.2.3-1D). While sodium was able to facilitate the stabilisation of VcINDY by both 1 and 10 mM succinate, by 7.9 °C and 11.3 °C respectively, potassium was unable to facilitate any stabilisation by either 1 or 10 mM succinate. Interestingly lithium facilitated no stabilisation from 1 mM succinate, but was able to facilitate a 3.5 °C stabilisation in the presence of 10 mM succinate.

This demonstrates that while lithium is able to bind to VcINDY in a similar manner to sodium, lithium binding facilitates subsequent succinate binding to a far weaker extent than sodium. Less binding energy is produced from the addition of succinate in the presence of lithium compared to the presence sodium, demonstrating that either lithium bound VcINDY makes less contacts with interacting succinate molecules, or that lithium bound VcINDY binds fewer succinate molecules due to a lower succinate binding affinity.

Only sodium, therefore, interacts with VcINDY in a way which effectively stimulates high levels of succinate binding. Given that both sodium and lithium ions carry the same charge, this suggests that it is not merely the presence of charged cations in the binding pocket which encourages the binding of succinate. Instead, it must be a property more possessed by sodium than lithium; most likely the coordination strength required to induce the correct conformational shift and ready the protein allosterically for succinate binding.

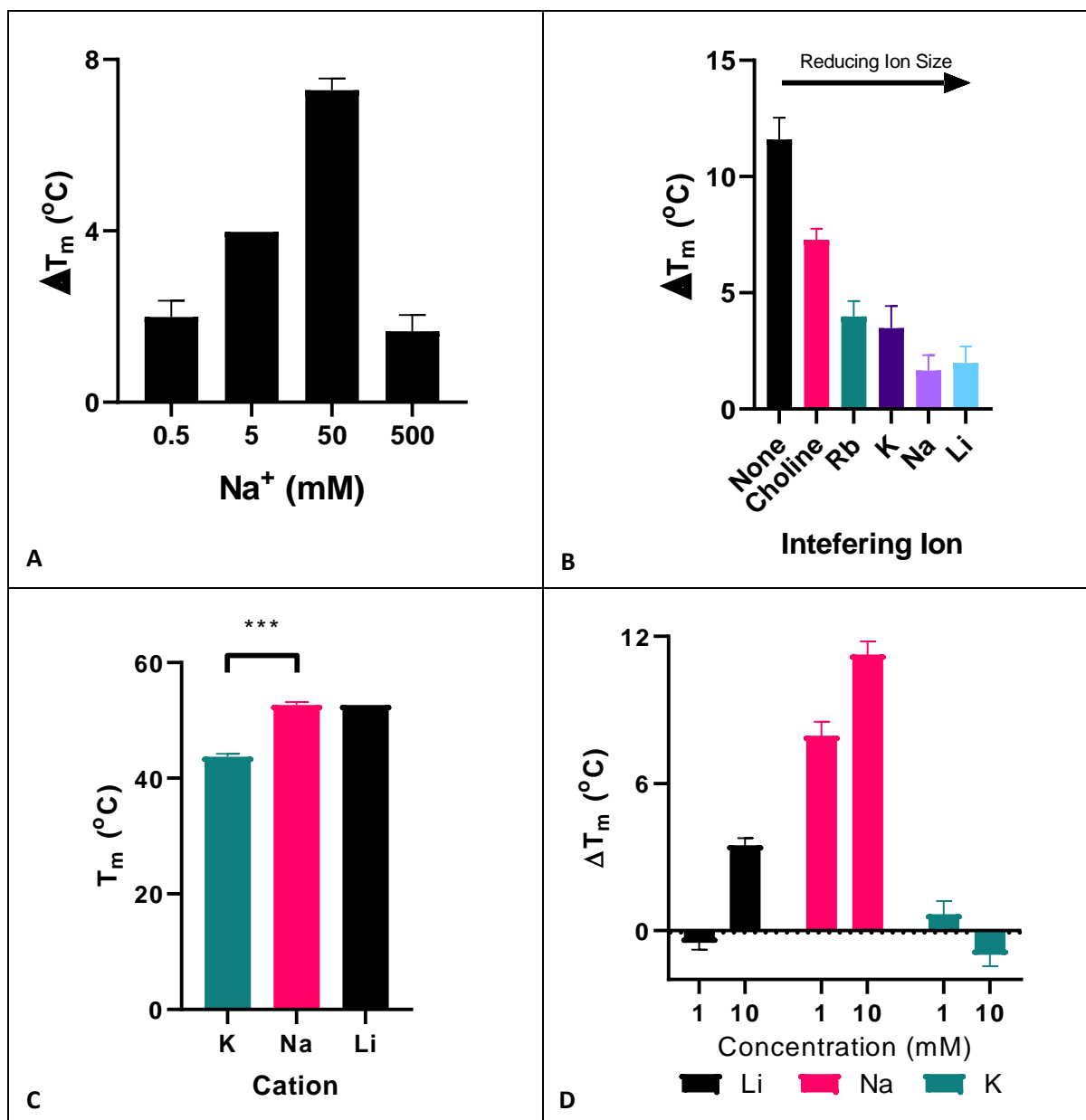


Figure 4.2.3-1 Thermostability based examination of VcINDY cation binding. **A:** Level of stabilisation provided by the addition of 5 mM of succinate in the presence of varying levels of sodium. The difference between the T_m in the absence and presence of 5 mM succinate is shown for each sodium concentration. Ionic strength is maintained through the addition of Choline Chloride, with a 500 mM Cation Chloride concentration maintained throughout. **B:** Level of stabilisation provided by 5 mM succinate in the presence of 50 mM sodium and 450 mM additional “interfering ion”. The difference between the T_m in the absence and presence of 5 mM succinate is shown for each condition. **C:** Thermostability of VcINDY in the presence of 50 mM of each of the indicated cations. **D:** Level of stabilisation provided by the addition of either 1 mM or 10 mM succinate in the presence of 50 mM of the indicated cation. The difference between the T_m in the absence and presence of succinate is shown for each cation.

4.2.4 High Throughput Thermostability Screening Reveals Clear Rules of Substrate

Selectivity

It is well established that standard thermostability assays of this kind cannot be used to determine exact binding affinities due to the changing kinetics at the higher temperatures where melting occurs [155][162], and workarounds to this problem have significant drawbacks [162]. Even so, a suitable substrate concentration to be used in substrate screens needed to be established. In order to determine this concentration, varying concentrations of the known VcINDY substrates succinate, malate, fumarate, and oxaloacetate were tested for thermostabilisation (Figure 4.2.6-1) [73]. No substrate demonstrated significant stabilising effects below 100 μM , with strong stabilisation only occurring in the mM range. As such a substrate concentration of 10 mM was chosen, at which the least stabilising substrate here examined, oxaloacetate, provided a clear stabilisation of 3.1 ± 0.6 (SE) $^{\circ}\text{C}$.

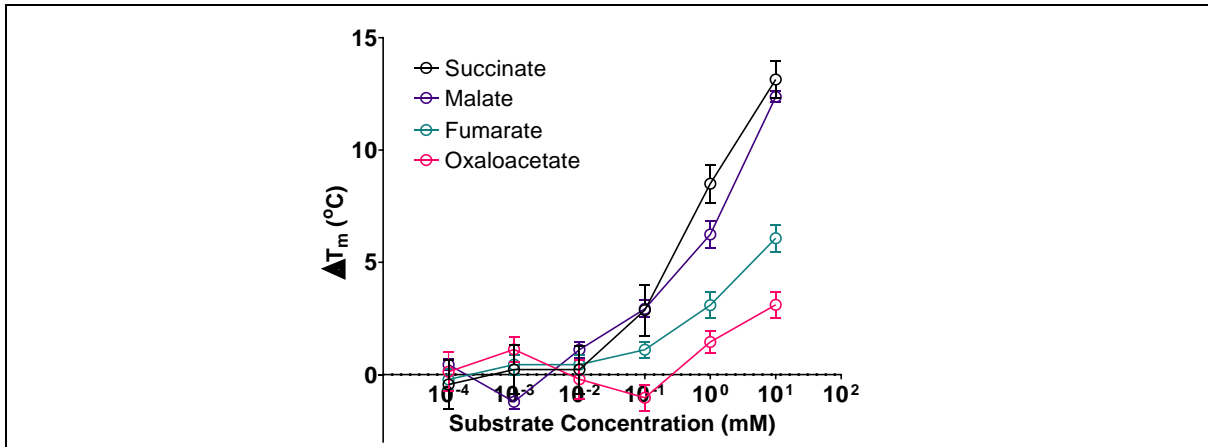


Figure 4.2.4-1 Concentration series of known substrates. The stabilisation of VcINDY provided by four known substrates is shown as a function of their concentration. The difference between the melting temperature of VcINDY without substrate and with substrate is shown.

In order to examine the parameters governing VcINDY-anion interactions, a panel of 72 potential interactors were tested for their ability to stabilise VcINDY, revealing 18 significantly stabilising candidates (Figure 4.2.4-2). The differences between non-stabilising and stabilising molecules from this screen will be examined in detail for the remainder of this section.

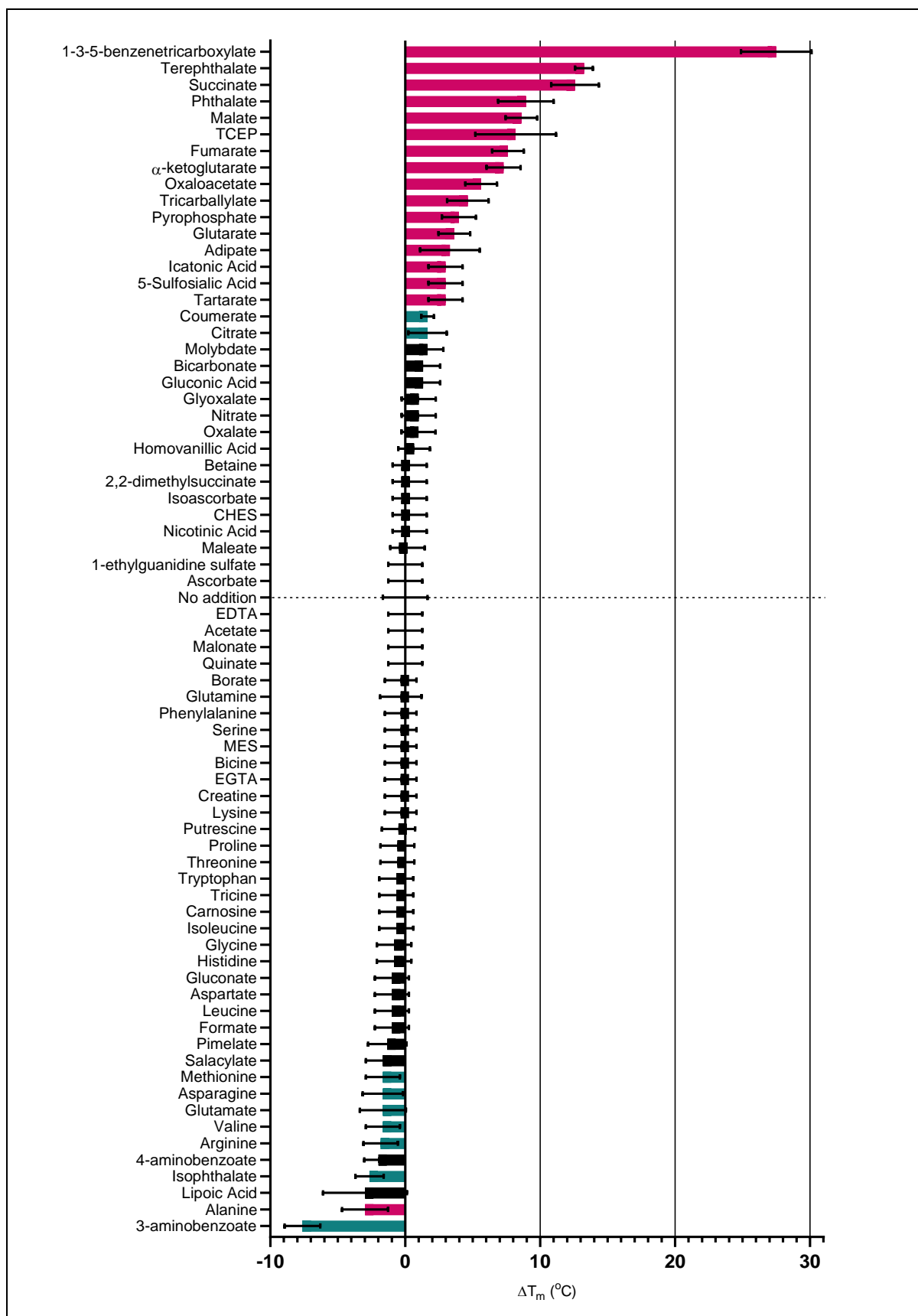


Figure 4.2.4-2 VcINDY thermostability based substrate screening. Stabilisation of VcINDY resulting from the addition of 10 mM of varying potential interactors in the presence of 50 mM Na⁺. Statistical significance deriving from a t-test is shown through colour. Black = no significance. Blue = p ≤ 0.05. Pink = p ≤ 0.001. Standard deviation is shown.

The first feature examined was the effect of varying dicarboxylate chain lengths (Figure 4.2.4-3A). Succinate is a 4 carbon linear dicarboxylate which stabilises VcINDY by around 12 °C at a 10 mM concentration. The larger 5 and 6 carbon dicarboxylates, glutarate and adipate, are able to interact to lesser extents, providing stabilisation of 3.6 °C and 3.3 °C respectively, however further elongation of the carbon chain to the 7 carbon pimelate completely abolishes binding. Dicarboxylates with smaller chain lengths than succinate, the 2 carbon oxalate and the 3 carbon malonate, showed no ability to stabilise VcINDY. These observations can be understood in context of the existing crystal structures; the majority of contacts between VcINDY and succinate take place with succinate's carboxylate groups, interacting with two distinct carboxylate binding regions within the protein. In order to interact with these two regions, the carboxylate groups must be positioned as they are in succinate's extended conformation (Figure 1.10.3-1B). It is likely that the 5 and 6 carbon dicarboxylates can position their carboxylate groups similarly to succinate through adopting bent conformations, and thus satisfy the two carboxylate binding regions. However, longer chain dicarboxylates do not stabilise VcINDY, which is likely caused by steric hindrance preventing the compound from adopting the required pose in the binding site. Dicarboxylates with smaller chain lengths than VcINDY are clearly unable to replicate the carboxylate arrangement of succinate, being unable to bridge the distance between the two dicarboxylate binding regions. These observations allows the formation of a "Molecular Ruler" hypothesis, wherein the ability of molecules to bind to, and stabilise, VcINDY depends on their ability to effectively bridge these two carboxylate binding regions.

The first test of this hypothesis is to examine whether both carboxylates are truly required for binding, through the examination of monocarboxylates. Carbonic acid, gluconic acid, glyoxylic acid, acetic acid, formic acid, bicine, tricine, creatine, and various amino acids were all tested with no binding detected in any case, indicating the essential nature of both of these carboxylate regions for substrate binding (Figure 4.2.4-2).

Next, the phthalic acid isomers were examined. These dicarboxylate isomers feature a rigid central aromatic ring, greatly limiting their conformational flexibility. If the Molecular Ruler hypothesis reflects true binding requirements, then phthalic acid, with its closely positioned carboxylates, should be incapable of binding, while terephthalic or isophthalic acid will likely be able to satisfy the two carboxylate binding regions. This is indeed the case, as phthalic acid is unable to stabilise VcINDY, however both terephthalic and isophthalic acids are capable of stabilising VcINDY, by 13.2 °C and 9.0 °C respectively, despite differently positioned carboxylate groups (Figure 4.2.4-3B), suggesting that there must be some flexibility in this Molecular Ruler system of selectivity.

It is interesting, when discussing the phthalic acids, to note that 1-3-5-benzenetricarboxylate, with three carboxylate groups surrounding the central aromatic ring, provides a huge of stabilisation of around 27°C at 10 mM, far more than the 12 °C provided by succinate (Figure 4.2.4-3B). The explanation for the high level of bond formation between VcINDY and this tricarboxylate is unclear, and allosteric binding cannot be ruled out. This interaction is, however, particularly interesting in the possibilities it raises for future inhibitor design.

Now that the importance of two correctly positioned carboxylate groups for substrate binding has been established, additional modifications to suitable dicarboxylates were examined. Initially, 8 modifications of the 4 carbon succinate were tested (Figure 4.2.4-3C). Consistent with previous crystallographic studies showing succinate to bind VcINDY in an extended conformation [48][3], and the above observations, fumarate, a molecule similar to succinate with the exception of a double bond restricting it to the extended, trans, conformation, was able to stabilise VcINDY by 7.6 °C. Maleate, on the other hand, the cis isomer of fumarate, resembling succinate locked in a bent conformation, showed no ability to stabilise VcINDY, failing to bridge the two carboxylate binding regions (Figure 4.2.4-3C).

Malate and oxaloacetate, resembling succinate with the addition of a hydrophilic hydroxyl or ketone group respectively, are able to stabilise VcINDY by 8.6 °C and 5.6 °C respectively (Figure 4.2.4-3C),

with the binding of these molecules likely facilitated by a substrate conformation similar to that known to be adopted by citrate, in which the additional hydrophilic group is directed out of the binding pocket into the solvent [48][3], likely making contact with surrounding water molecules. Itaconate resembles succinate with the addition of a hydrophobic methylene group, and its binding results in lower levels of VcINDY stabilisation than the hydrophilically modified malate and oxaloacetate, only providing a stabilisation of around 3.0 °C (Figure 4.2.4-3C), likely reflecting the additional methylene group's inability to interact with surrounding water molecules. Furthermore, aspartic acid, resembling succinate with the addition of an amino group is unable to stabilise VcINDY at all (Figure 4.2.4-3C), as the addition of a positively charged group leads to rejection from the positively charged binding site.

Tartrate resembles succinate with the addition of two hydrophilic hydroxyl groups, one more than the single hydroxyl group possessed by malate, and it is only able to stabilise VcINDY by 3.0 °C, forming weaker interactions than malate, which provided 8.6 °C of stabilisation (Figure 4.2.4-3C). It therefore appears that the additional of two chemical groups reduces the ability of dicarboxylates to bind VcINDY, likely due to steric hinderances. This effect is also demonstrated by comparison of 2-2 dimethylsuccinate, resembling succinate with the addition of two hydrophobic methyl groups, with oxaloacetic acid, resembling succinate with the addition of only one hydrophobic methylene group. The two groups upon dimethylsuccinate render this dicarboxylate entirely unable to stabilise VcINDY, while the single group upon oxaloacetate allows a VcINDY stabilisation of 5.6 °C (Figure 4.2.4-3C).

Molecules similar to the 5 carbon glutarate showed similar patterns of binding as molecules similar to the 4 carbon succinate (Figure 4.2.4-3D). Molecules similar to glutarate with additional hydrophilic groups such as the ketone containing α -ketoglutarate and the tricarboxylic tricarballylate acid are once able to bind, stabilising VcINDY by 7.3 °C and 4.6 °C respectively (Figure 4.2.4-3D), presumably binding similarly to malate and oxaloacetate as discussed above. As with molecules

similar to succinate, the presence of multiple additional chemical groups upon molecules similar to glutarate heavily reduce their ability to stabilise VcINDY, as evidenced by citrate. Despite being shown to bind in multiple crystallographic studies, this molecule, similar to glutarate with the additional of both a carboxylate group and a hydroxyl group, can only stabilise VcINDY by around 1.6 °C, much less than α -ketoglutarate and tricarballylate (Figure 4.2.4-3D). Finally, and still consistently with molecules similar to succinate, glutamate, similar to glutarate with the addition of a positively charged amino group, is unable to enter the positively charged binding site of VcINDY, and therefore does not provide any level of stabilisation (Figure 4.2.4-3D).

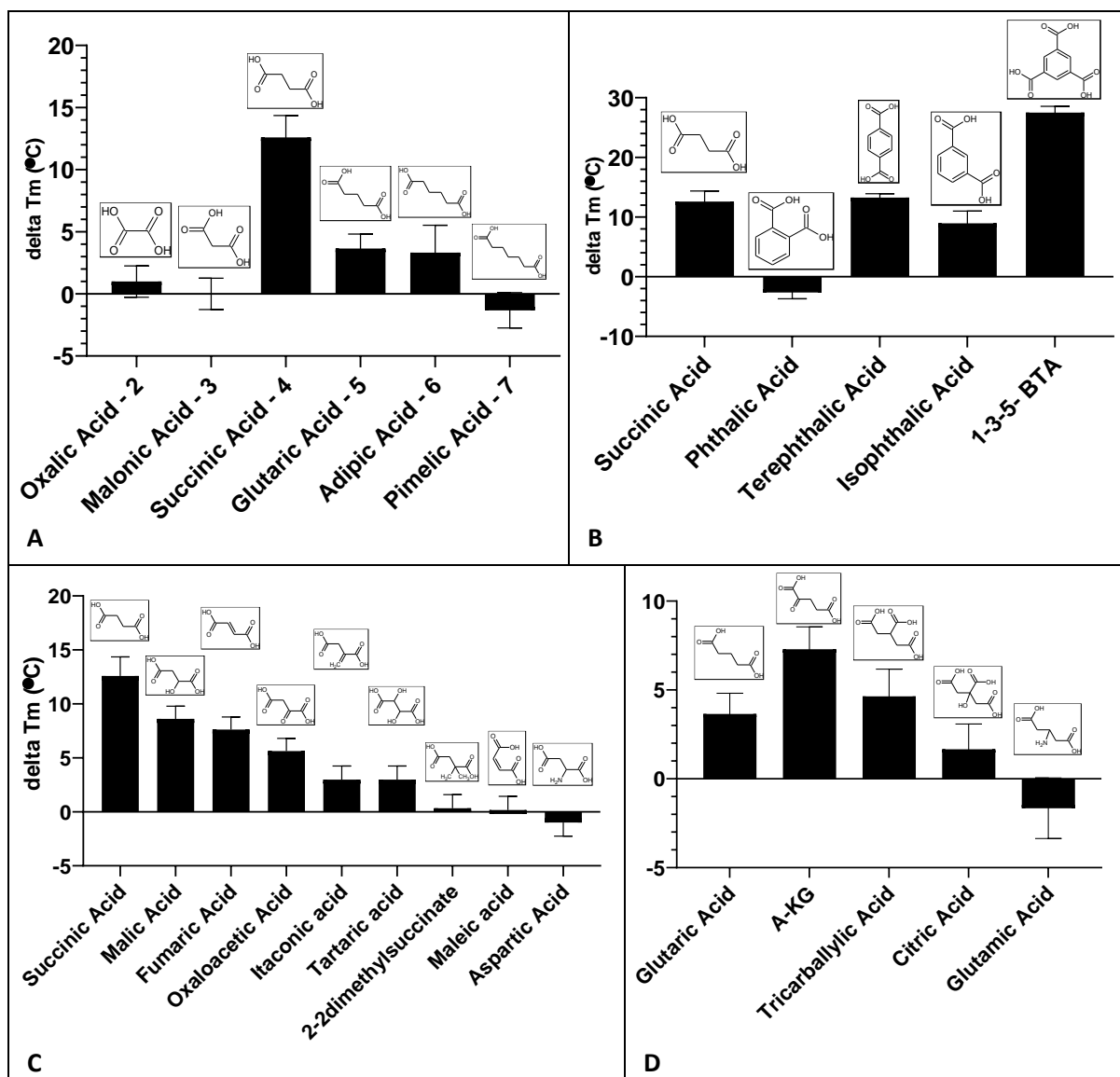


Figure 4.2.4-3 Sub-comparisons of substrate derived VcINDY thermostabilisation. Data taken from Figure 4.2.4-2. A:

Stabilisation of VcINDY resulting from the addition of 10 mM varying chain length linear dicarboxylic acids in the presence

of 50 mM Na⁺. Standard deviation is shown. B: Stabilisation of VcINDY resulting from the addition of 10 mM varying

phthalic acid isomers in the presence of 50 mM Na⁺. Standard deviation is shown. C: Stabilisation of VcINDY resulting from

the addition of 10 mM varying dicarboxylates similar to succinic acid in the presence of 50 mM Na⁺. Standard deviation is

shown. D: Stabilisation of VcINDY resulting from the addition of 10 mM varying dicarboxylates similar to glutaric acid in the

presence of 50 mM Na⁺. Standard deviation is shown.

Tris(2-carboxyethyl)phosphine (TCEP) is worthy of special attention. Initial VcINDY CPM measurements containing TCEP proved difficult to interpret due to interactions between the substrate and the dye. The interaction between TCEP and CPM was linear with respect to temperature (Figure 4.2.4-4A). As such, the linear effect of TCEP CPM interactions could be identified and removed from the dataset, allowing the effect of VcINDY denaturation on fluorescence to be observed normally (Figure 4.2.4-4B). This reveals a clear TCEP induced stabilisation of VcINDY by 8.2 °C (Figure 4.2.4-4C), despite the molecule bearing little similarity to any expected substrate, and other similar large branched carboxylates (EDTA & EGTA) providing no such stabilisation. The mode of binding observed here is unclear, and it is likely that TCEP represents a novel interaction with VcINDY, possibly with an allosteric site. It is worthy of note that previous transport assays by Christopher Mulligan (unpublished data) have demonstrated 5 mM TCEP to significantly inhibit VcINDY transport activity, providing further evidence that this unusual molecule interacts directly with VcINDY.

TCEP is not the only unexpected stabilising interactor, as pyrophosphate, 5-Sulfosalicylic Acid, and p-coumaric acid were also seen to stabilise VcINDY by 4.0 °C, 3.0 °C, and 1.7 °C respectively (Figure 4.2.4-4C). Again, the modes of binding carried out by these novel substrates are currently unclear, and of great interest.

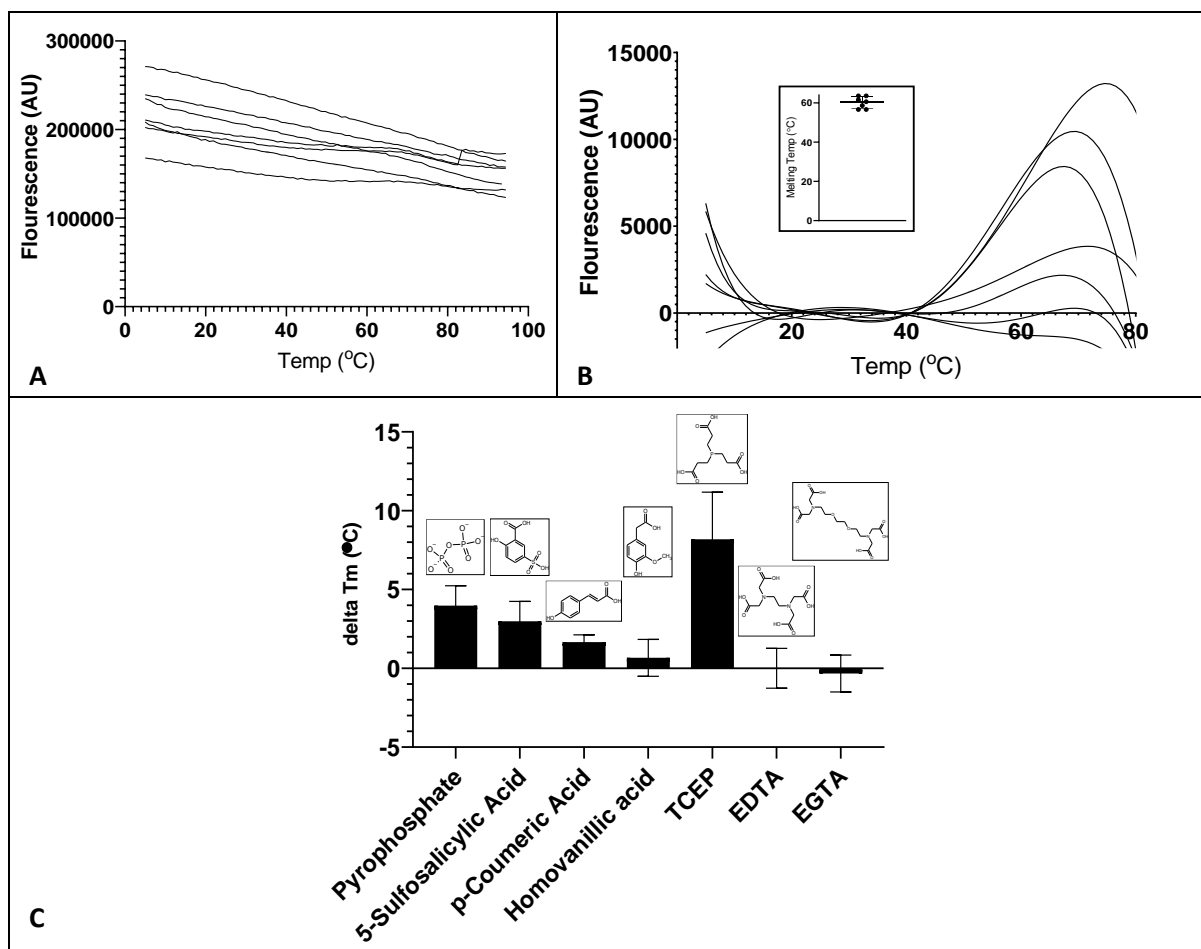


Figure 4.2.4-4 VcINDY thermostability measurements for TCEP and other Miscellaneous substrates. **A:** Raw fluorescence readings for VcINDY thermofluor with the addition of 10 mM TCEP in the presence of 50 mM Na⁺. **B:** Corrected and smoothed fluorescence readings for VcINDY thermofluor with the addition of 10 mM TCEP in the presence of 50 mM Na⁺, removing the linear effect of TCEP upon CPM fluorescence. **B(insert):** Average melting temperature of VcINDY in the presence of 10 mM TCEP and 50 mM Na⁺, as determined from the corrected fluorescence traces shown in figure C: Stabilisation of VcINDY resulting from the addition of 10 mM varying miscellaneous substrates of interest in the presence of 50 mM Na⁺. Standard deviation is shown.

4.2.5 Native Lipid Nanodisc Solubilised VcINDY Shows Extreme Thermostability Along With Substrate Induced Destabilisation

Thus far measurements have been carried out using detergent in solubilised VcINDY, removing native lipid interactions and placing the protein in non-native conditions. This raises the possibility that non-native behaviour, such as a reduction in binding affinity, may be occurring. In order to examine the effects of lipids upon VcINDY, the native lipid nanodisc system known as SMALPs (see 3.1 The SMALP Native Lipid Nanodisc System Allows *In Vitro* Examination of VcINDY in a Near Native Environment) was tested for use with the CPM assay.

Initially VcINDY SMALP thermostability measurements were trialled using the same experimental setup as DDM solubilised VcINDY, in which samples were heated from 5 °C to 95 °C with continuous monitoring of fluorescence in order to establish a melting temperature. These initial attempts were unsuccessful as no clear denaturation derived increase in fluorescence occurred within the temperature range (Figure 4.2.5-1A), only showing what may be a small degree of denaturation around 90°C. Increased dye and protein concentrations were trialled in order to compensate for a possible low signal intensity, however in all conditions tested no clear denaturation derived increase in fluorescence occurred during heating (Figure 4.3.2-3B), suggesting that poor signal strength was not the reason for the failure of this experimental setup to detect SMALP solubilised VcINDY denaturation.

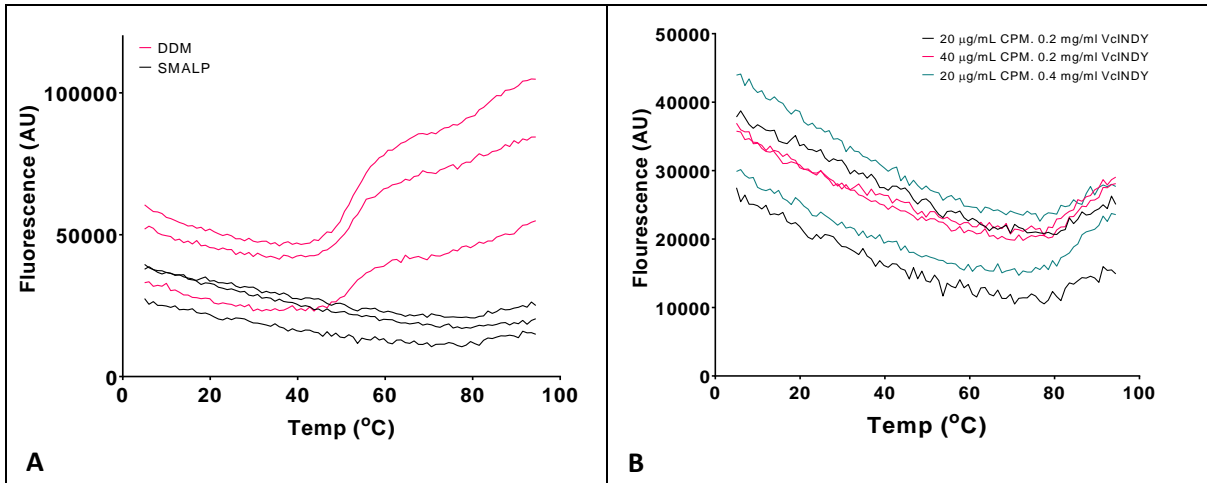


Figure 4.2.5-1 Standard CPM thermofluor examination of SMA solubilised VcINDY. A: Representative raw fluorescence of CPM thermofluor comparing detergent (DDM) solubilised and SMA solubilised VcINDY. Fluorescence is shown as a function of temperature. **B:** Raw fluorescence of CPM thermofluor upon SMA solubilised VcINDY comparing the effects of varying CPM dye and protein concentrations. Fluorescence is shown as a function of temperature.

Given that no clear melting had been observed, two possibilities remained; either SMALP solubilised VcINDY was in some way incompatible with the CPM thermostability assay, or SMALP solubilisation was providing such a huge level of stabilisation compared to detergent solubilisation that complete melting did not occur within the temperature range examined. In order to definitively rule out this latter possibility, SMALP solubilised and DDM solubilised VcINDY samples were held for 12 hours at 40 °C, followed by a further 12 hours at 95 °C (Figure 4.2.5-2A). DDM solubilised VcINDY melted rapidly at 40 °C, with a half-life of around 20 minutes, however, surprisingly, SMALP solubilised VcINDY showed no increase in fluorescence at 40 °C, only beginning to increase in fluorescence at 95 °C, melting with a half-life of around 1.5 hours.

There are two possibilities for the extreme thermostability exhibited by SMALP solubilised VcINDY; either the inclusion of lipids does indeed lead to massive stabilisation of the protein, or the SMA polymer ring surrounding the nanodisc sterically constrains VcINDY, preventing denaturation until the polymer ring itself breaks down. Under this latter possibility the apparent high levels of thermostability exhibited by VcINDY are not a result of biologically relevant stabilisation, but rather an artefact of the polymer system itself.

In order to examine this latter possibility, the thermostability of SMA polymer lipid nanodiscs was examined. Upon solubilisation by SMA, an *E. coli* polar lipids (EPL) solution shows a decrease in optical density, allowing the process of lipid solubilisation by SMA to be followed through monitoring of the average absorbance readings between 300 and 388 nm. SMA solubilised EPL samples were heated at 95°C for varying lengths of time, and the increase in optical density resulting from lipid release from thermally degraded SMA nanodiscs was recorded. SMA's ability to maintain nanodiscs decreased during the course of the 12 hour incubation at 95 °C, as evidenced both by the overall absorbance spectrum beginning to return to its pre-SMA form (Figure 4.2.5-2B), and the average absorbance at 300 – 388 nm rising towards the pre-SMA absorbance levels (Figure 4.2.5-2C). This process was slow, with absorbance readings failing to return to pre-SMA levels even after 12 hours

at 95 °C. As such, while thermal degradation of the SMA polymer does occur at high temperatures, it does not occur at a rate sufficient to explain the behaviour of SMALP solubilised VcINDY under these conditions.

It therefore appears that the VcINDY SMALP thermal denaturation data represents a biologically relevant protein unfolding event, and not polymer breakdown. If this is the case, the addition of succinate, VcINDY's substrate, should result in an increase in VcINDY thermostability. This can be quantified through half-life measurements, in which the time taken for half the protein present to denature is determined. The half-life of SMALP solubilised VcINDY at 95°C was determined by normalising melt curves and recording the time at which fluorescence passed 0.5 (i.e. half of maximum fluorescence) in the presence and absence of 5 mM succinate. The addition of 5 mM succinate significantly reduced the stability of SMALP solubilised VcINDY, lowering the average half-life from 103 minutes to 58 minutes (Figure 4.2.5-2D). While this demonstrated a clear impact derived from the addition of VcINDY's substrate, all previous work with DDM solubilised VcINDY demonstrated the addition of succinate to increase the thermostability of VcINDY. The cause of this difference in behaviour between DDM and SMALP solubilised VcINDY is unclear, raising questions as to the nature of the interactions occurring within the VcINDY SMALP nanodisc.

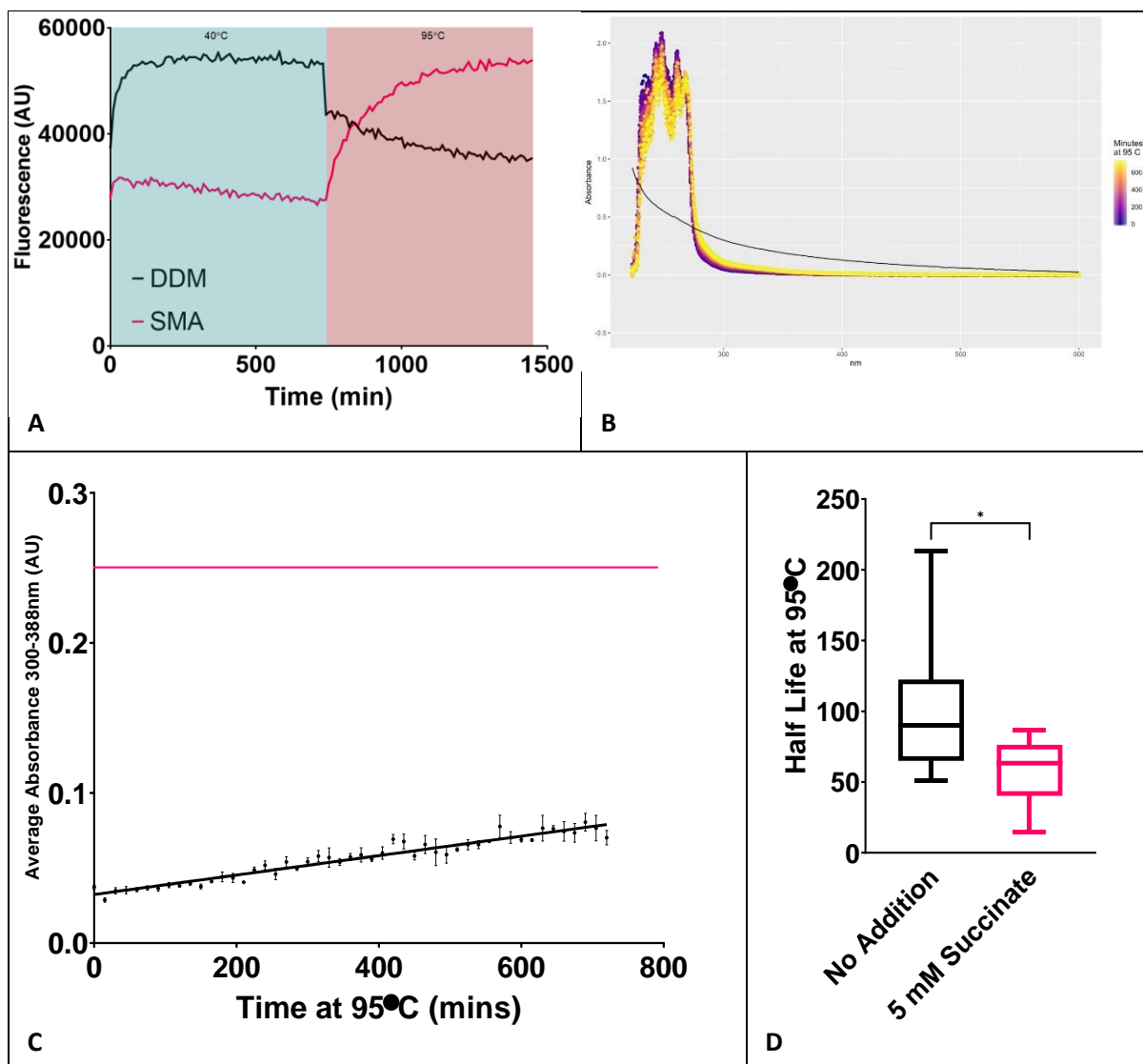


Figure 4.2.5-2 Half-life based CPM thermofluor examination of SMA solubilised VcINDY. **A:** Raw fluorescence for detergent (DDM) solubilised and SMA solubilised VcINDY incubated for 12 hours at 40 °C, followed by 12 hours at 95°C, in the presence of CPM dye. Fluorescence is shown as a function of time. **B:** Effect of thermal degradation on the ability of SMA to solubilise *E. coli* Polar Lipids (EPL). Absorbance of the EPL solution pre-SMA addition, indicating no solubilisation, is shown as a black line. SMALP solubilised EPL solutions were heated to 95 °C for the indicated time before measuring their absorbance. All values were recorded in triplicate and the average plotted. Error bars are not shown for clarity. **C:** Rate of SMALP degradation with heating. Average absorbance values for 300-338nm were taken from part D of this figure, and displayed as a function of time held at 95 °C. Absorbance before the addition of SMA, marking no solubilisation of lipids, is indicated by a pink line. **D:** Half-lives of SMALP solubilised VcINDY in 50 mM sodium and the absence and presence of 5 mM succinate at 95 °C, determined by the time taken by each sample to achieve half maximal fluorescence.

4.2.6 Direct Supplementation of Lipids to Detergent Solubilised VcINDY Results in Poor CPM Thermofluor Output

Due to the difficulties encountered in SMALP-based CPM analysis, lipids were instead directly supplemented to solutions containing detergent (DDM) solubilised VcINDY. In order to test whether this supplementation of lipids was compatible with the CPM thermofluor experiment, simple VcINDY melt experiments were performed in the presence of varying levels of *E. coli* Polar Lipids (EPL) under the same conditions as previous experiments upon DDM solubilised VcINDY, similar to (Figure 4.2.2-1). At EPL concentrations greater than 0.02% w/v the expected VcINDY denaturation derived increase in fluorescence, occurring around 50°C, was not clearly observed. Examination of the change in fluorescence with respect to time derivative traces showed the expected VcINDY melt peak around 50 °C to reduce in intensity with increasing EPL concentrations, while a second peak at around 80 °C increased in intensity with increasing EPL concentrations (Figure 4.2.6-1A).

In order to test whether this inability to observe VcINDY's typical melt peak in the presence of higher EPL concentrations resulted from interactions between the CPM dye and the added lipids, thermofluor assays were carried out with either VcINDY only, EPL only, or VcINDY and EPL together, allowing the effects of these two components to be separated (Figure 4.2.6-1B). EPL only samples showed clear interactions between the lipids and CPM dye to occur at higher temperatures, resulting in high temperature fluorescent increases which do not occur in VcINDY only samples. The combination of EPL and VcINDY shows that increasing concentrations of EPL result in a reduction of VcINDY's melt peak intensity and an increase in the EPL's own melt peak intensity, obscuring VcINDY's melt peak entirely at higher EPL concentrations.

Despite the inability of this assay to report on the effects of high concentrations of EPL, the effects of low concentrations of EPL, ≤ 0.02 % w/v, upon VcINDY thermostability could be examined in the presence and absence of 1 mM succinate (Figure 4.2.6-1C). Increasing EPL concentration from 0.0002 to 0.02 % w/v appeared to increase the level of stabilisation provided by 1 mM succinate

from 7.0 °C to 9.6°C (Figure 4.2.6-1C Insert). This increase is statistically significant, with comparison of the initial and final values yielding a p value of 0.0085, suggesting that the presence of EPL leads to an increased level of VcINDY bond formation upon the addition of succinate, however this experimental approach is clearly problematic. Due to the low signal-to-noise ratio observed in the succinate stabilisation EPL lipid concentration series (Figure 4.2.6-1C), and the high risk that any changes in apparent VcINDY melting temperature are simply caused by direct interactions between EPL and distorting VcINDY's true melting event, the reliability of this data is low.

While the interactions between VcINDY, lipids, and succinate warrant further study, the supplementation of lipids into detergent solubilised VcINDY CPM thermofluor does not represent a reliable system in which these interactions can be examined.

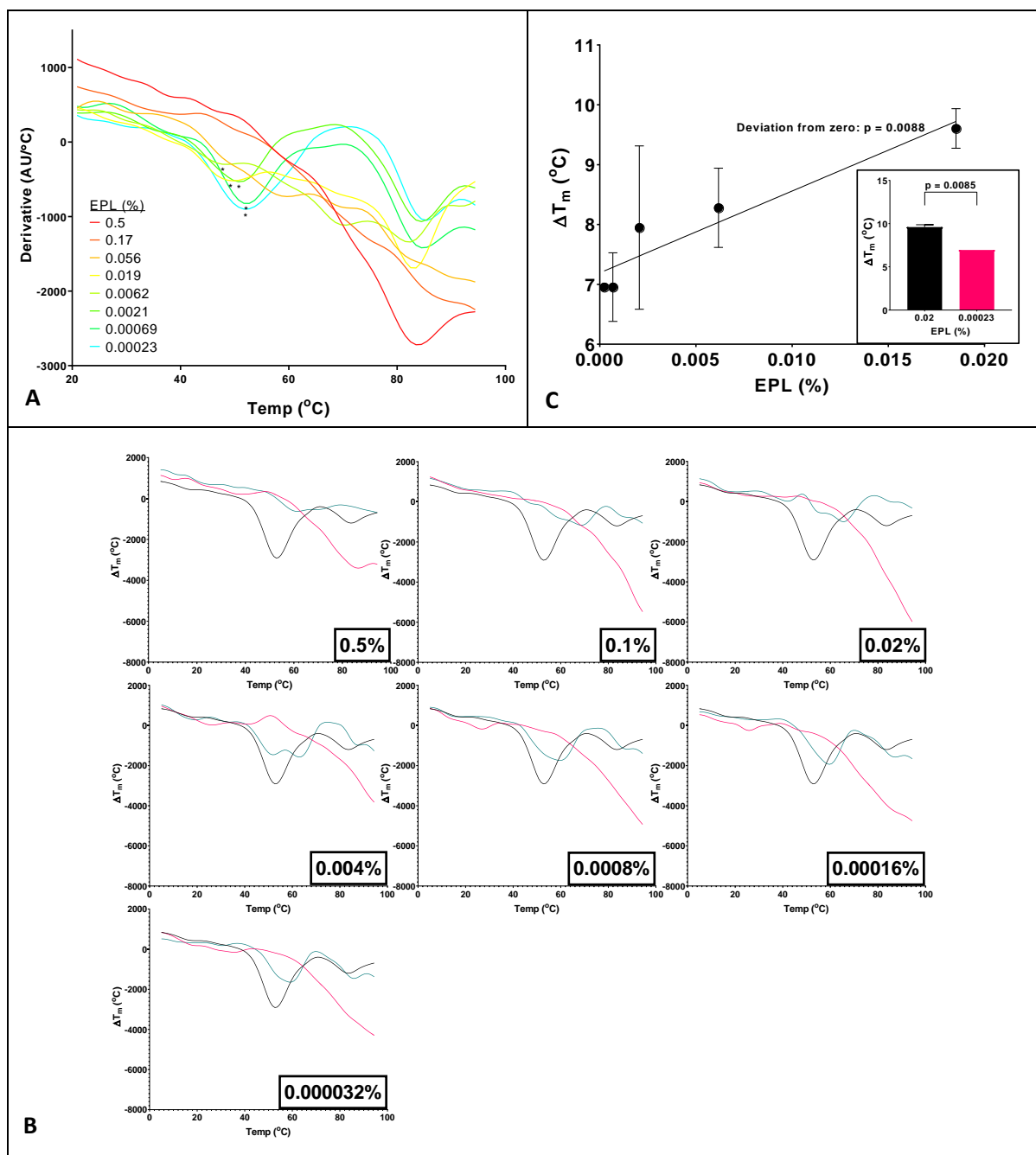


Figure 4.2.6-1 Lipid supplemented CPM thermofluor examination of DDM solubilised VcINDY.

A: CPM thermofluor melting

of VcINDY in the presence of varying concentrations of EPL. The rate of change of fluorescence with respect to temperature

(dF/dT) is shown with respect to temperature. Asterisks indicate the location of probable VcINDY melt peaks. **B:** CPM

thermofluor derivative melt curves for samples consisting of VcINDY only (black), VcINDY + EPL (Green), and EPL only (Pink).

The percentage w/v concentration of EPL is indicated for each graph. The rate of change of fluorescence with respect to

temperature (dF/dT) is shown with respect to temperature. **C:** Stabilisation of VcINDY caused by the addition of 1 mM

Succinate in the presence of various EPL concentrations as estimated through standard CPM thermofluor experiments. **C**

(**insert**): Comparison of extreme values from part C of this figure, showing significantly differing levels of stabilisation

provided by 1 mM Succinate in the presence of differing EPL concentrations.

4.2.7 Chapter Summary

Thermofluor's great strength as a method is its ability to conduct rapid and high throughput screens. This is clearly demonstrated here, as the results of over four hundred individual melting temperature measurements are presented, providing a vast array of thermostability data from which conclusions can be drawn. In addition, much of the further work in this thesis was inspired by observations within this data set.

Firstly, through this process the principles of substrate binding were greatly developed. The necessity for sodium binding before succinate binding was initially demonstrated, confirming the order of binding which has been previously proposed [3], and also observed through PEGylation work. As discussed in 4.1.6 Chapter Summary, previous transport studies upon the human DASS family member hNaDC-1 have suggested this sodium first order of binding based upon the presence of minor sodium only leak currents and the kinetics of succinate transport [147], while cysteine accessibility work upon rabbit NaDC-1 has also indicated a sodium first order of binding [148][149], indicating that this ordered binding may be a common feature of the wider DASS family.

Additionally, a strong influence of ionic strength on succinate binding was observed, with higher concentrations of ions, around 500 mM, suppressing the stabilising effects of succinate addition, suggesting that charged interactions are important for successful anion interactions, as previously proposed for VcINDY based upon its binding site architecture [3].

Vibrio cholerae is found both within saltwater environments and the human gut, meaning that VcINDY will naturally encounter both high and low salt environments. More detailed examination of the impact of salt concentration on VcINDY's ability to bind succinate would be of great interest in future work. This would provide mechanistic insights, identifying the optimal sodium concentration for VcINDY's function, somewhere between 50 and 500 nM, while also providing information on the likely *in vivo* activities of this transporter, as ionic interference appears it largely non-functional within the high salt conditions of seawater.

Cation binding was then further dissected through the use of various mono-cationic candidate ions, through which it was discovered that both sodium and lithium stabilised VcINDY to an identical extent, suggesting comparable binding events to take place, while the larger potassium was not able to stabilise VcINDY; indicating a steric size limit upon cation binding. This maximum size limit represents the first step of VcINDY's cation selectivity. The second step of cation selectivity appears to be a requirement for proper coordination interactions to occur between the cation and VcINDY, indicated by the poor ability of lithium to permit succinate binding despite the effective binding of the cation itself. This is supported by PEGylation data (see 4.1.6 Chapter Summary) indicating that sodium binding induces conformational changes throughout the protein, which must be triggered through these coordination interactions. It appears to be this change which readies the protein for succinate binding, not merely the presence of positively charged ions in proximity to the succinate binding site, as has been previously proposed [3].

Throughout the DASS family, lithium is generally far less able to stimulate substrate transport than sodium. Many family members appear totally unable to utilise this anion, such as animal NaCT homologues and human NaDC3 [163][164], and while others such as *B. licheniformis* SdcF [165], *X. laevis* NaDC-3 [166], and VcINDY [73] are capable of lithium driven transport, it occurs at far lower rates than sodium driven transport. As this preference for sodium over lithium appears to be a common feature of DASS family transporters, it is likely that the principles of cation selectivity exhibited here by VcINDY may be shared by the wider DASS family.

Additionally, the supplementation of lithium to DASS family transporters in the presence of sodium causes either transport inhibition, as for rabbit NaDC1 [167], or transport stimulation, as for human NaDC3 [164]. This lithium supplementation effect varies dramatically between well conserved homologues, with primate NaCTs showing lithium stimulation while other animal NaCTs show lithium inhibition [163], and can be stimulated, reversed or abolished through single point mutations

[168][164][167]. This suggests that small changes in binding site architecture, and therefore substrate binding, are responsible for determining the lithium response.

It has been proposed that lithium causes these changes in transport rates in the presence of sodium through competition with sodium for the cation binding sites, although the number of sites occupied by lithium is unclear. Rabbit NaDC1 lithium supplementation inhibition occurs with a hill coefficient of < 1 suggesting either a lack of cooperativity in lithium supplementation inhibition, or the presence of only one lithium available binding site [169], however the ability of many DASS family transporters to carry out some lithium driven transport, and the ability of *B. licheniformis* SdcF to do so with a hill coefficient of 2.5 [165], suggests that all binding sites must be lithium accessible for many DASS transporters. Here we clearly demonstrate that lithium is capable of stabilising a DASS family transporter as effectively as sodium, indicating that lithium binding is able to provide the same binding energy as sodium, and therefore must occupy the same number of binding sites as sodium. While lithium is unable to stimulate subsequent cationic substrate binding as effectively as sodium, it does appear able to bind to DASS family transporter sodium binding sites similarly to sodium.

As for anion binding, the rules for this process were determined through an extensive 72 substrate screen. Thermofluor based thermostability assays have been previously used for the screening of large numbers of potential transporter substrates, in screens up to twice this size [161], however this chapter represents the first application of this approach to DASS family transporters.

Additionally, the screen carried out herein was designed to allow the precise dissection of the principles of substrate discrimination, achieved through the use many candidate molecules differing from known substrates through only one or two chemical groups. Through use of these substrates, the following principles of VcINDY anion binding were proposed : 1) At least two carboxyl groups must be present in order to interact with the two carboxyl binding regions. 2) These carboxyl groups must be capable of interacting with the two fixed carboxyl binding regions, being positioned similarly to those found upon extended conformation succinate. 3) Additional functional groups which do not

interfere with the placement of the two essential carboxylate regions may be present. These additional groups are best accommodated if they do not introduce a positive charge to the molecule and are either sterically small, or able to be oriented out of the binding pocket so that interactions may be made with solvent molecules.

Accordingly, the two carboxyl binding regions within VcINDY's anion binding site, consisting of the N151 side-chain amide & the T152 side-chain hydroxyl in the first, and the S377 side-chain hydroxyl & the N378 side-chain amide in the second [3], can be considered to form a molecular ruler, with the need to satisfy these two groups of residues acting as VcINDY's primary mode of substrate selectivity. Minimal contacts are made with the non-carboxylate regions of succinate [3], as reflected in the range of dicarboxylates shown herein to be capable of binding to VcINDY, allowing VcINDY to operate with a general selectivity for a range of 4 to 6 carbon dicarboxylates. This mode of selectivity has been shown herein to allow VcINDY to bind 6 Krebs's Cycle intermediates. While it is known that citrate is not transportable, succinate, malate, fumarate, and oxaloacetate have been previously identified as transport substrates [73], indicating that some of the flexibility in dicarboxylate binding results in a flexibility in dicarboxylate transport. The ability to selectively bind multiple members of the Krebs's Cycle is shared by many other members of the DASS family, including the human transporters SLC13A2 / NaDC-1 [36], SLC13A3 / NaDC-3 [37][44], and SLC13A5 / NaCT / mINDY [41]. As such, the combination of firm selectivity for correctly positioned carboxylate groups along with a general tolerance for additional chemical groups may represent an approach evolved to achieve the specific binding of Krebs's Cycle intermediates, which is likely shared by other members of the DASS family.

Additionally, several unexpected molecules were seen to stabilise VcINDY, including TCEP, 5-sulfosalicylic acid, coumarate, and 1-3-5-benzenetricarboxylate, indicating as yet unknown modes of binding to occur. TCEP and 1-3-5-benzenetricarboxylate provided particularly high levels of stabilisation, indicating that they are likely high affinity VcINDY interactors. Both of these molecules

are bulky tricarboxylates, unlike VcINDY's traditional dicarboxylic substrates. Currently the only structurally characterised tricarboxylic VcINDY interactor is citrate, which is seen here to bind weakly to VcINDY. It is therefore likely that TCEP and 1-3-5-benzenetricarboxylate bind to VcINDY in a novel manner, unlike citrate binding. The nature of these strong tricarboxylate binding interactions is currently unclear. Further study of these novel interactors could therefore be of great use to the future design of DASS family inhibitors, and for the trapping of previously unseen conformational states in structural studies.

Beyond these substrate screens, the feasibility of employing CPM thermofluor to study the effects of lipid interactions was examined. The SMALP native lipid nanodisc system (see 3.1.1 Introduction) was trialled as a platform for examining lipid interactions. Thermostability in SMALPs has been previously studied through a range of techniques. These techniques include radioligand binding [107][108], native fluorescence [109], gel based aggregation [101], light scattering [110], circular dichroism [107][103][98], and CPM thermofluor [111]. In all of these examples, SMALPs were more stable than the detergent solubilised protein, although the effects of SMALP solubilisation on substrate interaction were not examined.

As the SMALP system appears to be compatible with CPM thermofluor assays, being shown in previous literature to provide a stabilisation of around 10 °C over a detergent solubilised protein [111], it seems reasonable to assume that any VcINDY melting temperatures gathered through this approach will be reliable. Interestingly, VcINDY SMALPs are ultra-stable, able to withstand hours of near boiling temperatures as measured through both CPM and supported through CD measurements (see 3.1.3 SMALP Solubilised VcINDY Appears Correctly Folded, Monodisperse, and Highly Thermostable), which is not entirely without precedence.

Examination of the extent of SMALP stabilisation observed in previous literature reveals an interesting pattern, with the human proteins A_{2A}R [107], Pgp [111], and hENT1 [108] showing only modest stabilisations of around 10-20 °C in stark contrast to the bacterial transporters KcsA [98],

BmrA [110], and bacterial reaction centres [109], which show far more extreme stabilisations akin to those observed herein for VcINDY. This suggests that, through some currently obscure mechanism, SMALP solubilisation provides far more stability for bacterial proteins than eukaryotic proteins.

Whether this is due to differences in protein-lipid interactions, lipid-SMA interactions, or some other mechanism is a question of great interest, but beyond the scope of this thesis.

The prominent exception to this trend is found in in gel based aggregation assays upon the bacterial LeuT and BmrA [101], revealing SMALP solubilised proteins to be only marginally more stable than their detergent solubilised counterparts, in direct contrast to light scattering measurements for denaturation of the same BmrA protein which indicated SMALP solubilisation to result in extreme stability gains [110]. The former experiment relies on the pelleting of thermally aggregated protein. Experience with GFP-TS in this thesis (see 4.3.2 The Aggregation Based GFP-TS Thermostability Assay Is Compatible With VcINDY) suggests that denaturation and aggregation are not always equivalent processes. Due to this, the light scattering data is to be preferred over the aggregation data when discussing this discrepancy, and the light scattering data is in agreement with the pattern already discussed.

Unlike previous studies of SMALP solubilised protein thermostability, the effect of substrate addition upon thermostability was examined for VcINDY. Unexpectedly, the addition of substrates resulted in a decrease in SMALP solubilised VcINDY thermostability. Substrate derived destabilisation of proteins has been previously observed and may be related to the binding of substrates to the denatured form of the protein [155], however this behaviour was not observed for detergent solubilised VcINDY. As such the causes of this radical differences in substrate response between detergent and SMALP solubilised VcINDY are unclear.

An alternative approach to the examination of the effect of lipids upon this system, simply supplementing EPL into the detergent solubilised reaction mixture proved to be problematic, as high concentrations of lipids both obscured fluorescent signal and directly interacted with the CPM dye.

This is likely due to hydrophobic interactions between the CPM dye and the added lipids leading to increases in fluorescence, as hydrophobic interactions have been previously shown to facilitate increases in CPM fluorescence [170]. While some significant data was gained through this approach, tentatively suggesting that EPL concentrations to increase the level stabilisation provided by succinate, an alternative approach to examining these effects was desirable due to the problematic, low signal-to-noise ratio, nature of this data. As such, the new, lipid compatible, approach to thermostability measurements known as GFP-TS was attempted (see 4.3 Aggregation Based Thermostability Measurements Indicate a Complex Relationship Between Substrate Binding and Lipid Interactions).

CPM thermostability measurements have greatly advanced our model of VcINDY substrate binding, suggesting twofold cation discrimination and flexible anion selectivity based around a molecular ruler principle. It has also provided preliminary data leading to further chapters of this thesis, with potential low binding affinities being addressed through MST (see 4.4 A Thermophoresis Based Binding Assay is Capable of Determining VcINDY's Substrate Binding Affinities) and the obscure lipid interactions being examined through GFP-TS (see 4.3 Aggregation Based Thermostability Measurements Indicate a Complex Relationship Between Substrate Binding and Lipid Interactions).

4.3 Aggregation Based Thermostability Measurements Indicate a Complex

Relationship Between Substrate Binding and Lipid Interactions

4.3.1 Introduction

In light of the incompatibility of CPM thermostability assays with the addition of lipids (see 4.2.6 Direct Supplementation of Lipids to Detergent Solubilised VcINDY Results in Poor CPM Thermofluor Output) another method of examining thermostability is needed. A fully folded and stable protein produces a clear, monodisperse, peak when examined through High Performance Liquid Chromatography (HPLC) Size Exclusion Chromatography (SEC), i.e. it contains one form of the protein molecule, which will elute from the column at a single point in the elution process. Upon protein denaturation this original monodisperse peak is lost, as the protein adopts a range of aberrant denatured and aggregated forms. This behaviour can be used as the basis of an alternative approach to thermostability measurements, as demonstrated by *Mancusso et al 2011* [171], wherein it was observed that a protein's melting temperature could be reliably established by heating samples to varying temperatures for 10 minutes and examining the decrease in the intensity of the native protein's monodisperse HPLC SEC peak, as detected by UV absorbance at 280 nm.

This approach was robust and capable of detecting the stabilisation provided by substrate binding for several membrane proteins, however it was not without limitations. The foremost of these was the need for a large enough quantity of purified protein to provide a clear and unobscured absorbance peak in a HPLC SEC experiment as monitored through 280 nm absorbance measurements. Another limitation was the relatively low throughput nature of the approach, requiring HPLC SEC runs to be individually performed for each condition of interest, imposing time and material cost limits on the scale of screening which could be performed.

The first of these issues, the need for purified protein, was overcome by *Hattori et al 2012* [172]. By linking the protein of interest to the fluorescent protein Green Fluorescent Protein (GFP), it becomes possible to specifically detect the presence of this protein through the observation of GFP's distinct

fluorescent signal. This allows the HPLC SEC elution profile of the GFP-tagged protein to be monitored through in-line fluorescence detection of the GFP-tag even in crude, non-purified, protein mixtures, therefore removing the need to perform protein purification. Through this system, the reduction in peak intensity with respect to temperature can be examined similarly to purified protein samples [172].

Various control measurements of thermostability performed by *Hattori et al 2012* [172], such as the monitoring of denaturation derived changes in intrinsic Tryptophan fluorescence, and the measurement of substrate binding efficiency lost upon denaturation, demonstrated that the addition of a GFP-tag did not greatly affect the thermostability of the tagged protein. This means that thermostability measurements gathered for GFP-tagged proteins were generally equivalent to the thermostability measurements to be expected from the wildtype proteins.

Through the use of these GFP-tagged HPLC SEC based thermostability assays it was not only shown that the substrate derived stabilisation of proteins could be detected, but that the impacts of lipids upon protein thermostability could also be reliably detected, presenting a promising and generally applicable approach to thermostability based lipid interaction analysis. Problems with this approach, however, still remained. The low throughput associated with HPLC SEC based experimentation, and the requirement for a HPLC SEC facility with in-line fluorescence detection makes this approach demanding both in terms of time and equipment.

These remaining obstacles were overcome by *Nji et al 2019*, whereby a new approach named GFP-TS entirely removes the need for a chromatography step [91]. The principle of both previous methods had been the separation of denatured and aggregated protein from the measurable pool of native protein remaining after heating, as achieved by size exclusion chromatography. Alternatively, the aggregation of denatured protein may be encouraged through the addition of the detergent Octyl-beta-Glucoside (β -OG) [91][173], so that denatured protein can be separated from native protein through a centrifugation step, removing the requirement for SEC based separation and

relationship for VcINDY and the wider DASS family, and there is very little current research focused upon the lipid interactions elevator mechanism transporters (see 1.3 The Elevator Mechanism – The Importance of Lipids).

4.3.2 The Aggregation Based GFP-TS Thermostability Assay Is Compatible With VcINDY

GFP-TS can be carried out on both purified and non-purified protein samples. Initially, GFP-tagged VcINDY was examined within non-purified samples, consisting of solubilised cell membranes. In order to determine an appropriate concentration of solubilised membranes to be used for this initial experiment, a range of 100 μ L dilutions of solubilised GFP-VcINDY containing *E. coli* membranes produced through the PASM5052 expression system (see 2.6.1.2 PASM5052 / Lemo21(DE3) Expression) were tested for fluorescent intensity (Figure 4.3.2-1A). Fluorescent intensity increased linearly with respect to membrane concentration, with samples containing at least 1.25 % v/v of the original solubilised membrane solution (originally 50 mL from 3 L of original culture) providing a clear fluorescent signal. In order to provide a high signal strength and therefore maximise signal-to-noise levels, a five-fold dilution of the original solubilised membrane solution was used for GFP-TS experiments.

Using this concentration of detergent solubilised membranes, a standard GFP-TS assay was carried out, in which samples were heated to a range of temperatures in the presence of 1% DDM and 1% β -OG for 10 minutes before centrifugation, resuspension of the resultant pellet in assay buffer, and detection of GFP fluorescence. Clear initial melt data was produced, in which the fluorescence of the supernatant decreased with increasing temperature, while the fluorescence of the pellet increased, indicating VcINDY to be denaturing upon heating and moving into the insoluble portion of the sample (Figure 4.3.2-1B). Above 60 $^{\circ}$ C, however, thermal denaturation of the GFP-tag itself resulted in decreased fluorescence in both the supernatant and the pellet.

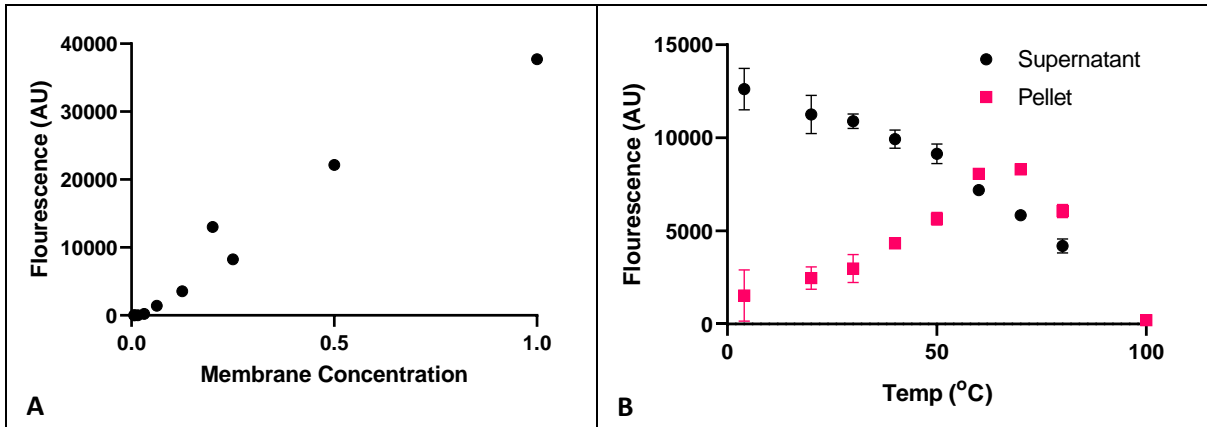


Figure 4.3.2-1 Initial tests of GFP conjugated VcINDY compatibility with GFP-TS. A: Testing the fluorescent intensity of various dilutions of solubilised GFP-VcINDY containing membranes. Membranes were produced from a 3 L batch of *E. coli* grown according to the PASM5052 expression system and diluted to a final volume of 50 mL before further dilution for the measurements presented. **B:** Raw fluorescence readings for VcINDY-GFP over a standard GFP-TS temperature series. Samples were heated for 10 minutes at the indicated temperature, aggregate proteins resulting from thermal denaturation were pelleted through centrifugation, the supernatants were removed, and the pellets resuspended in fresh buffer before fluorescent readings were taken.

The impact of the thermal denaturation of the GFP-tag itself can be monitored by graphing the sum of the fluorescence observed in the supernatant and the pellet, representing the total of the GFP-tagged VcINDY fluorescence at each temperature. This demonstrates that total GFP-fluorescent signal does indeed decay at temperatures above 60°C (Figure 4.3.2-2A). Strangely, total fluorescence appears to vary with respect to temperature at temperatures below 60°C as well, with fluorescence moderately increasing between 30 °C and 60 °C (Figure 4.3.2-2A). The relationship between temperature and fluorescence must be examined before further data analysis is carried out in this chapter. The total fluorescent signals, i.e. the sum of the supernatant and pellet fluorescence readings, from the experiments to be discussed throughout this chapter are gathered and normalised (Figure 4.3.2-2B). It can be seen that this pattern of varying GFP-fluorescence with temperature is reliably observed throughout, with fluorescence initially increasing with respect to temperature until peak fluorescence is reached around 60 °C, before fluorescence drops sharply due to GFP-tag thermal denaturation at higher temperatures, in accordance with GFP's known melting temperature of 76°C [172].

Due to both of these factors, the temperature dependent signal changes and GFP thermal denaturation, fitting a sigmoidal curve to the raw GFP-fluorescence remaining in the supernatant fraction of the sample and assuming major fluorescent changes to derive from the denaturation of the target protein, as in Nji et al 2019 [91], is not necessarily appropriate. Instead, the proportion of fluorescence, and therefore the proportion of GFP-tagged VcINDY, remaining in the supernatant compared to the pellet is calculated for each temperature, allowing the distribution of VcINDY to be determined and temperature based alterations in GFP-fluorescence to be controlled for. Analysing the results gained in (Figure 4.3.2-1B) in this way produces clear sigmoidal melting curves (Figure 4.3.2-2C), as fluorescence transfers from the supernatant to the pellet across the 30 °C to 70 °C temperature range due to VcINDY denaturation. Interestingly fluorescence does not completely transfer from the supernatant to the pellet, plateauing with around 40 % of fluorescence remaining in the supernatant at high temperatures. This is not a sign of problems with the experimental setup

and does not indicate that VcINDY is failing to denature fully during the course of the experiment. If the entirety of the signal were to move from the supernatant to the pellet over the course of the temperature series it would require 100% denaturation of VcINDY, and 100% aggregation of the denatured VcINDY. The plateauing of the curves from 60 °C to 80 °C suggests that denaturation is complete in this range. There is no reason to expect, however, that denatured VcINDY will aggregate and pellet with 100 % efficiency. Indeed, the maximum proportion of fluorescence found in the pellet is 60 %, indicating that 60 % of denatured VcINDY is aggregating and entering the pellet under the conditions tested here.

The applicability of this approach to the examination of VcINDY's thermostability can be confirmed through comparison to the melting behaviour previously observed for VcINDY through the CPM thermofluor approach already discussed (see 4.2.2 Optimisation and Validation of CPM assay for use with VcINDY). The proportion of VcINDY-GFP fluorescence remaining in the supernatant in (Figure 4.3.2-2C) was normalised to the bounds of 0 and 1 and overlaid with CPM thermofluor fluorescence, which was also normalised to the same bounds (Figure 4.3.2-2D). This showed both experiments to produce similar patterns of VcINDY melting; while GFP-TS detected VcINDY denaturation appeared to take place over a broader temperature range than CPM detected VcINDY denaturation, the two methods showed very similar mid points of denaturation, indicating similar melting temperature estimations to be produced by both methods.

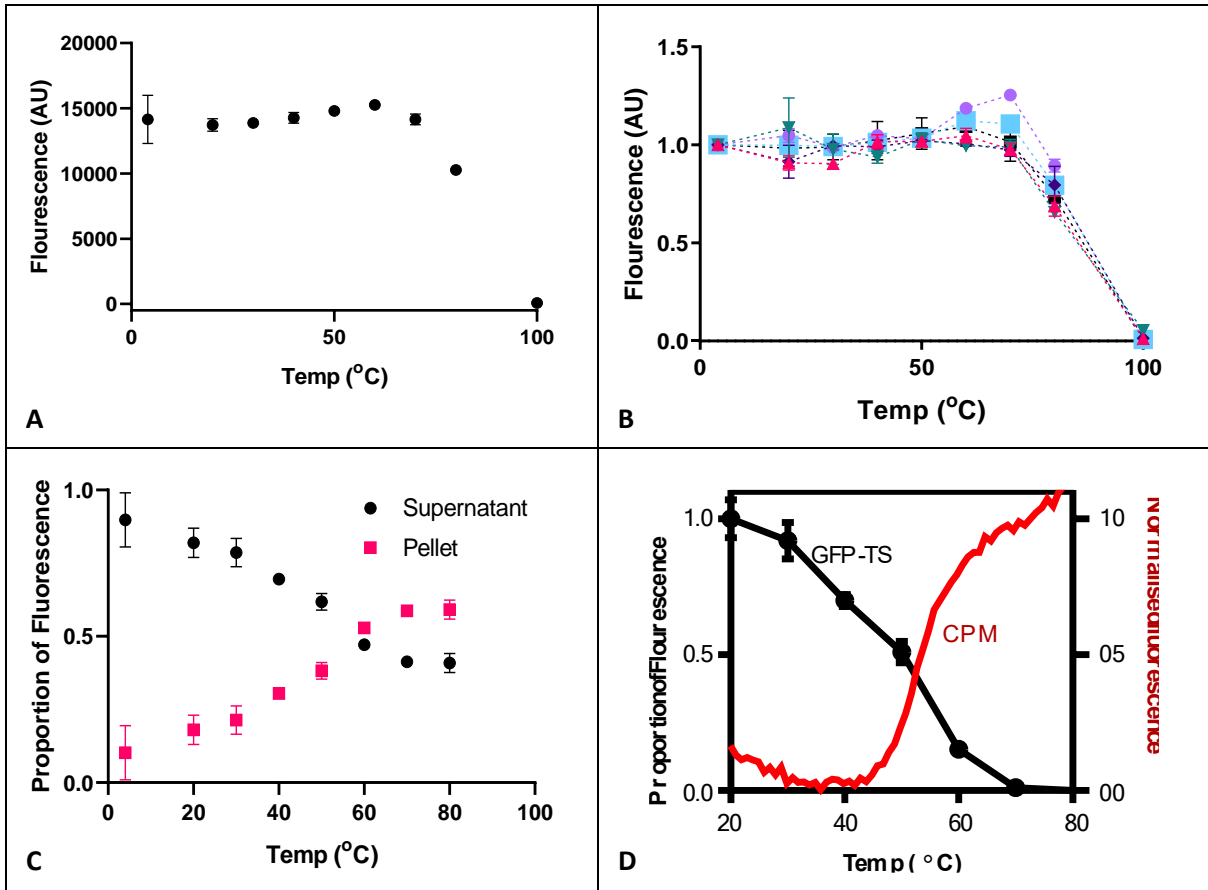


Figure 4.3.2-2 Demonstrating suitability of GFP-TS for VcINDY thermostability determination. **A:** Total fluorescence of supernatant and pellet from the GFP-TS experiment shown in part B of Figure 4.3.2-1. **B:** Total fluorescence of the supernatant and pellet for multiple GFP-TS experiments, showing similar relationships between GFP-fluorescence and heating. **C:** Distribution of GFP-fluorescence between supernatant and pellet for the standard GFP-TS experiment shown in part B of Figure 4.3.2-1. **D:** Comparison of normalised data for supernatant fluorescence from part C of this figure and normalised fluorescence from a CPM thermofluor melting experiment for WT VcINDY. For GFP-TS, VcINDY denaturation is represented by a decrease in supernatant fluorescence proportion from 1 to 0, as displayed on the left axis. For CPM thermofluor, VcINDY denaturation is represented by an increase in fluorescence from 0 to 1, as displayed on the right axis.

This GFP-TS melt curve can be fitted to a sigmoidal function in order to generate an estimate of melting temperature. For maximum control of the fitting process a custom script was written for R, using the nls() function [92]. The simple sigmoidal curve equation used for fitting is shown in Equation 1.

$$b + \frac{a - b}{1 + \frac{tm^s}{c^s}}$$

Equation 4.3.2-1 The sigmoidal dose response equation used for fitting of GFP-TS melt curves. b = initial fluorescence, a = final fluorescence, tm = melting temperature, c = current temperature, s = slope coefficient.

The script is annotated in 7.2 Appendix 2 – R script used for the fitting of GFP-TS data. The programme produced reasonable sigmoidal melt curves which matched the observed data, providing a melting temperature estimate of 50.4 ± 1.0 (SD) °C (Figure 4.3.2-3A). When compared to the CPM estimated melting temperature of 51.7 ± 0.0 (SD) °C, established in **Error! Reference source not found.** through a simple unpaired t-test, a p-value of 0.0979 is achieved, identifying no significant differences between VcINDY melting temperature as determined through these two highly different approaches (Figure 4.3.2-3B). As such, it is reasonable to conclude that these two experimental systems are monitoring the same VcINDY unfolding events.

Now that the applicability of GFP-TS to VcINDY had been demonstrated, the ability of this method to detect substrate induced stabilisation of VcINDY was tested through the addition of succinate. The addition of 5 mM succinate resulted in a stabilisation of the entire melt curve, wherein the GFP signal began to transfer from the supernatant to the pellet only at higher temperatures than in the absence of succinate, although by 80 °C around 60 % of the fluorescence was found in the pellet, indicating total VcINDY denaturation to have occurred, similarly to VcINDY samples tested in the absence of succinate (Figure 4.3.2-3C). Fitting to sigmoidal curves resulted in a melting temperature estimate of 56.8 ± 2.32 (SD) °C, significantly higher than VcINDY's stability of 50.4 ± 1.0 (SD) °C in the absence of substrate (Figure 4.3.2-3D). The observation of this succinate induced stabilisation both

indicates that under the experimental conditions used the protein is able to undertake substrate binding, and that GFP-TS is capable of reporting on this process.

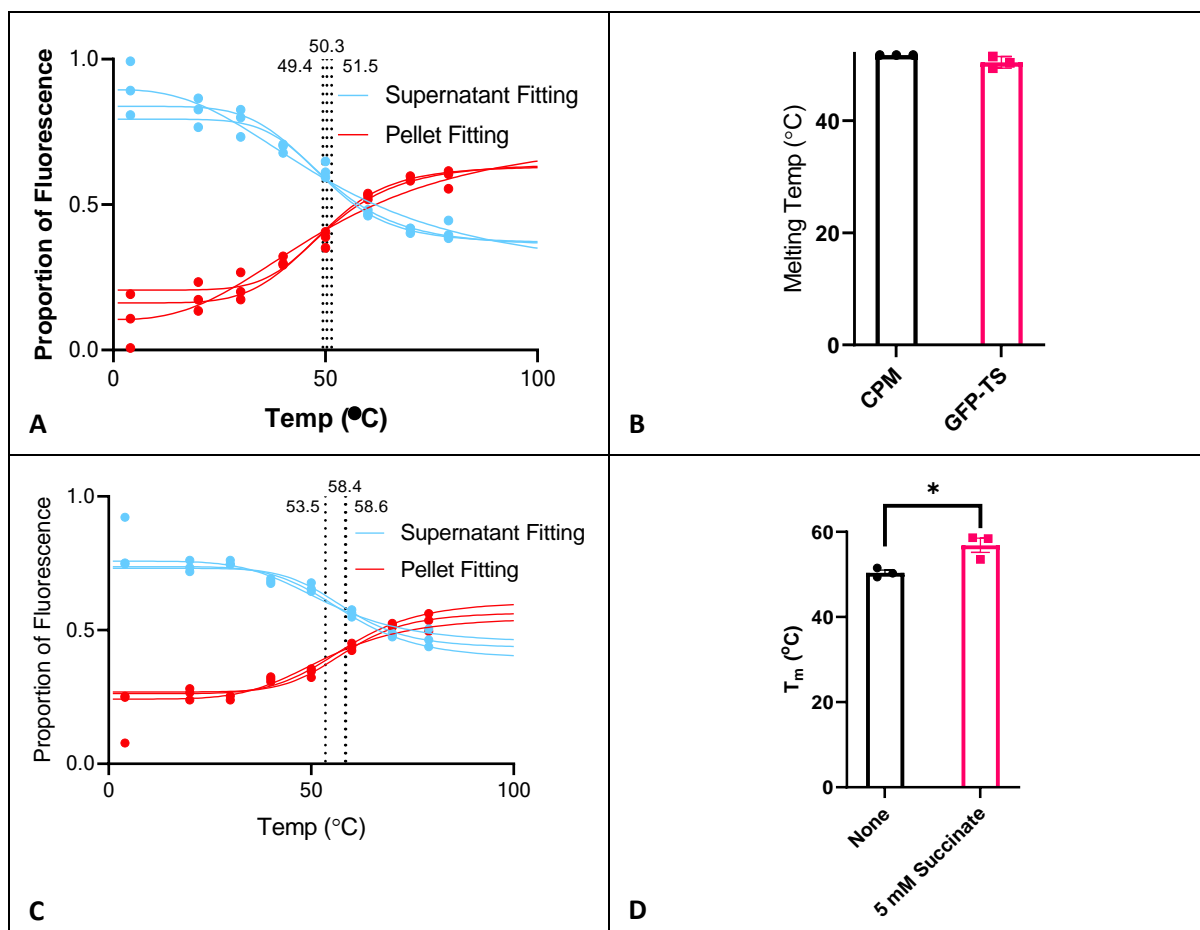


Figure 4.3.2-3 Optimisation and testing of the GFP-TS assay for use with DDM solubilised GFP-VcINDY containing membranes expressed through the PASM5052 expression system. A: Sigmoidal curve fittings for the data in part C of Figure 4.3.2-2 according to Equation 4.3.2-1. Calculated T_m 's are indicated by vertical dotted lines and annotations. **B:** Melting temperature of WT VcINDY as determined by CPM thermofluor and GFP-TS assays, showing no significant difference between the values determined by the two methods, $p = 0.0979$ **C:** GFP-TS melt experiment for GFP-VcINDY in the presence of 5 mM succinate. Experiment was carried out similarly to part B of Figure 4.3.2-1, with the addition of 5 mM succinate. Distribution of GFP-fluorescence between supernatant and pellet is shown. **D:** Melting temperatures determined through GFP-TS for VcINDY in the absence and presence of 5 mM succinate, showing a succinate induced stabilisation ($p = 0.02$).

4.3.3 GFP-TS is Incompatible With Purified VcINDY Samples

Now that this system has been successfully implemented for crude membrane samples, purified GFP-VcINDY was also tested. The initial results showed almost no change in GFP-fluorescent distribution to occur in response to sample heating (Figure 4.3.3-1A), suggesting no aggregation and pelleting of denatured VcINDY to occur. Close examination of the fluorescence data, however, reveals an extremely minor increase in pellet fluorescence to take place in the same temperature range as membrane solubilised samples, with around 10% of GFP-fluorescence moving from the supernatant to the pellet at temperatures above 50 °C. This suggests an extremely poor level of aggregation and pelleting of denatured VcINDY to occur under these condition; i.e. while 60% of denatured VcINDY-GFP is able to be pelleted in solubilised membrane samples, only around 10% of denatured purified VcINDY-GFP is able to be pelleted, leading to an extremely large signal-to-noise ratio and preventing useful interpretation of the data.

One possibility was that a centrifugation force of 18,000 g was not sufficient to pellet VcINDY aggregates. In order to test, this samples were instead pelleted in an ultracentrifuge with a force of 245,000 g, with one attempt examining the total supernatant versus pellet fluorescence, and another examining only the top 100 µL of supernatant from 200 µL samples in order to avoid disturbing tiny or fragile pellets (Figure 4.3.3-1B). In both cases this increase in centrifugation force did not result in a clear melting signal, with no major transfer of GFP-fluorescence from the supernatant to the pellet occurring upon heating, indicating that centrifugation speed was not the solution.

Another possible problem with the aggregation and pelleting of denatured purified GFP-VcINDY was that GFP-VcINDY may be simply unable to form cohesive pellets on its own, and only produced pellets in the solubilised membrane experiments due to co-precipitation with other proteins. In order to test whether this could be simulated in the purified samples, bovine serum albumin (BSA), an unrelated and likely non-interacting protein known to aggregate and precipitate readily within

the temperature range herein examined [174], was added to samples. Samples containing GFP-VcINDY supplemented with varying levels of BSA were heated for 10 minutes at 60°C before centrifugation, and the resulting supernatant fluorescence examined (Figure 4.3.3-1C), showing that while increasing concentrations of BSA resulted in decreasing supernatant fluorescence, similar decreases in supernatant fluorescence could be achieved through the addition of BSA without heating. As such the addition of BSA reduced the GFP-fluorescent signal without encouraging pelleting of denatured VcINDY. It is possible that insufficient BSA was denaturing during the course of the experiment to provide a sufficient aggregate for VcINDY to co-aggregate with, and in a final attempt to solve this issue pre-aggregated 100mg/ml BSA was added to test samples before heating to 60°C for 10 minutes and centrifugation as normal. The resulting supernatant fluorescence readings, 10747 AU for unheated and 11694 AU for heated, indicate that this did not aid VcINDY-GFP aggregation and pelleting as hoped.

Another approach, the use of SMALPs (see 3.1 The SMALP Native Lipid Nanodisc System Allows *In Vitro* Examination of VcINDY in a Near Native Environment) instead of detergent (DDM) solubilised GFP-VcINDY samples was attempted, although this approach also showed no major transfer of GFP-fluorescence from the supernatant to the pellet as a result of heating, both with and without the addition of 1% β -OG (Figure 4.3.3-1D). This failure to observe signal, however, is likely related to the super-stability observed for SMALP solubilised VcINDY samples, as examined in specially designed CPM thermostability studies (see 4.2.5 Native Lipid Nanodisc Solubilised VcINDY Shows Extreme Thermostability Along With Substrate Induced Destabilisation).

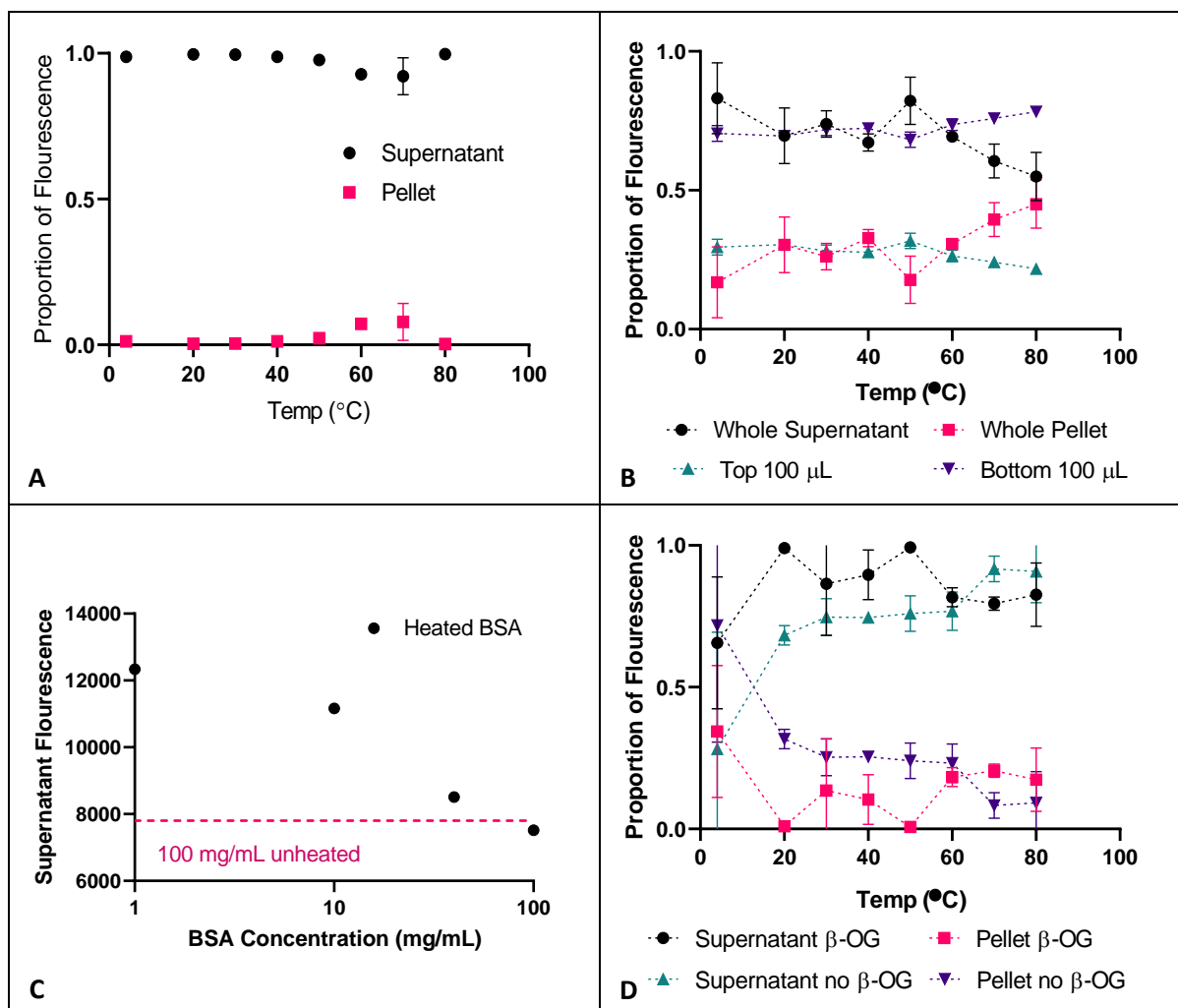


Figure 4.3.3-1 Attempted GFP-TS for purified VcINDY-GFP. **A:** Distribution of GFP-fluorescence between supernatant and pellet over the course of a standard GFP-TS experiment for purified VcINDY-GFP, showing only a minor response to heating. **B:** Distribution of GFP-fluorescence between supernatant and pellet over the course of a modified GFP-TS experiment for purified VcINDY-GFP, in which pelleting of potential aggregates is carried out at 245,000 g, as opposed to the normal force of 18,000 g. This was performed both with the normal process of removing the entire supernatant and comparing this to the resuspended pellet, and through a modified process of removing only the top 100 μ L of a 200 μ L sample, allowing comparison of the upper and lower portion of the solution. **C:** Effect of the addition of BSA to the GFP-TS reaction mixture before heating at 60°C for ten minutes on final supernatant fluorescence. The pink line represents the GFP-fluorescence of a samples containing 100 mg/mL BSA which has not undergone heating, acting as a control for direct BSA suppression of fluorescent signal.presence **D:** Distribution of GFP-fluorescence between supernatant and pellet over the course of a standard GFP-TS experiemnt for native nanodisc (SMALP) solubilised VcINDY-GFP both in the presence and absence of the aggregation encouraging detergent β -OG.

4.3.4 The Effects of Lipids Upon VcINDY-GFP Thermostability Are Altered by the Presence of Succinate

As GFP-TS measurements of VcINDY thermostability are only possible for non-purified membrane solubilised samples. The question becomes, is this condition suitable for the study of lipid interactions? According to rough textbook figures each *E. coli* cell contains 2.59×10^{-14} g of lipids [175]. A 3 L batch of MDA5052 grown Lemo21 cells expressing VcINDY-GFP (see 2.6.1.3 MDA5052 / Lemo21(DE3) Expression) is harvested at a final OD₆₀₀ of 5.2, giving an approximate concentration of 4.16×10^9 cells / mL. This means a final concentration of roughly 0.1 mg/mL of lipids is present in the culture at point of harvest. Through the processes of membrane extraction and solubilisation through DDM treatment, a final volume of 50 mL is reached, and diluted 2.34 fold into this assay, giving a final maximum lipid concentration of approximately 2.5 mg/mL assuming perfect retention of lipids throughout the process and complete solubilisation of lipids by DDM. The true figure can be safely assumed to be far below this theoretical maximum concentration.

In GFP-TS experiments examining the effects of lipid addition to these membrane solubilised samples, 5 mg/mL of lipids of interest were added. This value represents a balance between practical considerations (maximum stock concentrations and the cost of purified lipid samples) and a desire to shift balance of lipids present in the samples sufficiently to alter the environment of VcINDY-GFP in a meaningful way. The proof of whether this was appropriate would of course be in whether clear alterations in VcINDY-GFP thermostability were produced by lipid addition of this kind. Rather than producing entire melt curves for every condition, triplicate samples were heated for ten minutes at VcINDY's known T_m + 5°C before centrifugation and examination as normal. If the addition of a potential interactor resulted in an increase in melting temperature less denaturation would occur, detectable as an increase in supernatant fluorescence compared to the pellet.

Bacterial lipid mixtures (*E. coli* Polar Lipid extract (EPL) & *E. coli* Total Lipid Extract (TLE)), purified eukaryotic lipids (synthetic POPC & SoyPC), and purified bacterial lipids (*E. coli* PE, *E. coli* PG, & *E. coli*

CA) were all tested for their ability to stabilise VcINDY in the presence of 150 mM sodium. For details of these lipids see Table 4.3.4-1. Initial results, examining the effect of lipid addition on the stability of VcINDY-GFP showed a range of effects, immediately validating the levels of lipids used in this experiment (Figure 4.3.4-1A). The majority of lipids added, including both of the *E. coli* lipid extracts and the eukaryotic SoyPC, resulted in significant destabilisations of the protein, which, given the unlikelihood of specific interactions occurring between the bacterial VcINDY and the eukaryotic PC, likely represent non-specific lipid effects; either destabilisation or encouragement of VcINDY aggregation and pelleting. Separation of the *E. coli* lipid mixtures into their major components of PE, PG, and CA, however, allowed specific interactions to be observed. While the addition PE still resulted in a decrease in apparent stability, the addition of CA and PG resulted in substantial increases in VcINDY thermostability, indicating that specific interactions occur between VcINDY and these two lipids under these conditions. As these are both native bacterial lipids, they are likely candidates for native interactions.

In order to test whether any of these lipid interactions affected substrate binding, 8.5 mM succinate was added in the presence of 150 mM sodium and the resulting thermostabilities were measured as before (Figure 4.3.4-1B). Succinate stabilised VcINDY in the presence of no additional lipids as expected, resulting in a higher proportion of GFP-fluorescence remaining in the supernatant, and also provided stabilisation in the presence of EPL, TLC, POPC, SoyPC, and *E. coli* PE. In the presence of *E. coli* PG, however, no succinate derived stabilisation occurred, and in the presence of *E. coli* CA the addition of succinate resulted in a decrease in thermostability.

In order to clarify the extent to which lipids altered succinate's impacts upon VcINDY thermostability, the stabilisation provided by succinate addition in the presence of each lipid mixture was calculated and plotted separately (Figure 4.3.4-1C). In this way it became clear that the eukaryotic POPC and SoyPC did not affect the stabilisation provided by succinate. Interestingly, the *E. coli* lipid mixtures EPL and TLE also did not affect the level of stabilisation provided by succinate

addition, despite their three principle components all altering the level of stabilisation provided by succinate when added individually. PE greatly increased the level of stabilisation provided by succinate addition, while CA addition caused succinate addition to result in a destabilisation of the VcINDY, and PG addition entirely abolished any effect of succinate addition on VcINDY thermostability. The impact of substrate upon VcINDY thermostability is therefore radically changed through the addition of lipids.

Lipid(s)	Composition		Description	Supplier
EPL – <i>E. coli</i> Polar Lipid extract	Component	% wt/wt	A non-quality-controlled extract of the polar lipids present in log phase <i>E. coli</i> grown in Kornberg Minimal Media at 37°C.	Avanti (100600)
	PE	67.0		
	PG	23.2		
	CA	9.8		
	Unknown	0		
TLE – <i>E. coli</i> Total Lipid Extract	Component	% wt/wt	A non-quality-controlled extract of the total lipids present in <i>E. coli</i> cells grown and harvested as above, containing many unknown native plasma membrane constituents.	Avanti (100500)
	PE	57.5		
	PG	15.1		
	CA	9.8		
	Unknown	17.6		
POPC – 1-palmitoyl-2-oleoyl-glycero-3-phosphocholine	>99% purity 1-palmitoyl-2-oleoyl-glycero-3-phosphocholine		A synthetically generated 16:0-18:1 PC representing the phosphocholine lipids found in eukaryotic, but not prokaryotic, cells.	Avanti (850457)
SoyPC – L- α -phosphatidylcholine	Component	wt/wt%	Phosphocoline extract from soybeans containing PCs of varying molecular weights and saturation levels, representing this class of lipids exclusive to eukaryotic cells.	Avanti (840054)
	PC	97.2		
	Lyso PC	2.8		

<i>E. coli</i> PG – L- α - <i>phosphatidylglycerol</i>	>99% purity L- α - phosphatidylglycerol	Phosphatidylglycerols extracted from <i>E. coli</i> membranes consisting of PGs of varying molecular weights and saturation levels.	Avanti (841188)
<i>E. coli</i> PE – L- α - phosphatidylethanolamine	>99% purity L- α - phosphatidylethanolamine	Phosphatidylethanolamines extracted from <i>E. coli</i> membranes consisting of PEs of varying molecular weights and saturation levels.	Avanti (840027)
<i>E. coli</i> CA – cardiolipin	>99% purity cardiolipin	Cardiolipin extracted from <i>E. coli</i> membranes consisting of CAs of varying molecular weights and saturation levels.	Avanti (841199)

Table 4.3.4-1 Lipid preparations used in the GFP-TS lipid screening experiment. A description of their components is given, along with the product number for the solutions used.

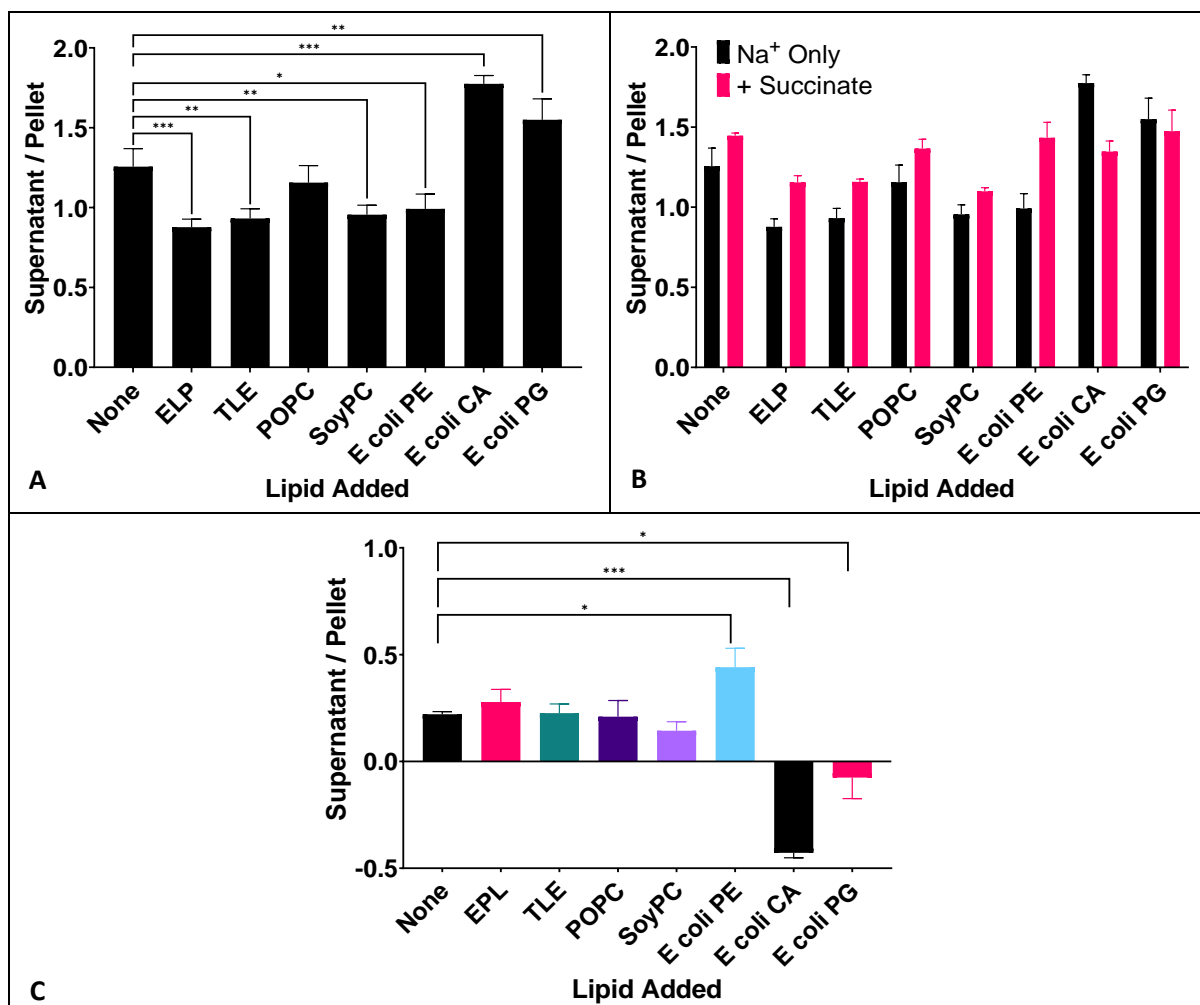


Figure 4.3.4-1 The impact of lipids on VcINDY thermostability and succinate interactions. **A:** Effect of the addition of 5 mg/mL of various lipids on thermostability of detergent solubilised VcINDY-GFP. Samples were heated to $T_m + 5$ °C for ten minutes before centrifugation and analysis as normal. Supernatant fluorescence was divided by pellet fluorescence to show differences in stability, with higher ratios indicating higher levels of stability. **B:** Effect of the addition of 5 mg/mL of various lipids in the presence and absence of 8.5 mM succinate, with values determined as in part A of this figure. **C:** Difference in thermostability resulting from the addition of 8.5 mM succinate in the presence of 5 mg/mL of the indicated lipids, based upon the data in part B of this figure. Abbreviations: EPL = *E. coli* Polar Lipid Extract. TLE = *E. coli* Total Lipid Extract. POPC = 1-palmitoyl-2-oleoyl-glycero-3-phosphocholine. SoyPC = L- α -phosphatidylcholine. *E. coli* PG = L- α -phosphatidylglycerol. *E. coli* PE = L- α -phosphatidylethanolamine. *E. coli* CA = cardiolipin. * = $p \leq 0.05$, ** = $p \leq 0.01$, *** = $p \leq 0.001$

4.3.5 Chapter Summary

GFP-TS thermostability analysis provided less precise thermostability estimates than CPM thermofluor thermostability analysis, but was effective where CPM thermofluor analysis was not; in the examination of complex solutions containing high concentrations of lipids. As such, novel and interesting data was made available.

GFP-TS did not allow analysis of purified VcINDY due to the poor aggregation of denatured VcINDY in the absence of other membrane components, and while multiple approaches were trialled to overcome this problem, none were successful. It is unclear why denatured VcINDY is only able to be aggregated and pelleted in the presence of other membrane components, however it is likely that these components allow co-aggregation to occur and encourage the formation of a clear pellet upon centrifugation. As such, GFP-TS examination of VcINDY thermostability took place in dilute solubilised membrane solutions.

The approach to GFP-TS data analysis performed here was improved from the originally proposed approach of Nji et al 2018 [91], in which changes in raw supernatant fluorescence were considered to directly reflect the level of the protein which had not yet undergone thermal denaturation. Here, the proportions of GFP-fluorescence in the supernatant and pellet were compared instead of absolute fluorescence, allowing for the fitting of melt curves not influenced by the thermal decay of GFP fluorescence, which begins to occur around 70 °C and thus would skew examination of VcINDY's 52°C melting temperature. Through this method, the GFP-TS determined VcINDY melting temperature was indistinguishable from that determined through CPM-thermofluor. This refinement of the GFP-TS data analysis process is likely to be of general use to future experimental work upon any protein used in GFP-TS.

Examination of the relationship between VcINDY, lipids, and substrate revealed a surprisingly complex network of interactions. While the non-bacterial lipids POPC and SoyPC, along with the *E. coli* lipid mixtures EPL and TLE, had no clear impact on VcINDY behaviour, the purified *E. coli* lipids

PE, CA, and PG substantially effected both VcINDY's thermostability, and VcINDY's substrate interactions. Substrate free VcINDY was seen to be selectively stabilised by CA, with the addition of succinate abolishing this interaction and leading to a net reduction in VcINDY thermostability. Similarly, PE appeared to selectively stabilise the succinate bound state of VcINDY, but not the succinate free state, causing the binding of succinate to result in a far higher level of stabilisation than in the absence of lipids. Finally, PG appeared to stabilise the substrate free state to a similar extent to succinate, and addition of succinate in the presence of PG did not lead to any change in VcINDY thermostability. It is unclear whether this is due to PG preventing succinate interaction, or the binding of succinate displacing PG similarly to CA, leading to no net change in VcINDY thermostability during the succinate binding process.

This data suggests a dynamic relationship to exist between VcINDY, lipids, and substrates, in which the binding of substrate radically alters VcINDY's lipid interactions. This raises an intriguing possibility; that lipids may be exchanged throughout the transport cycle in response to substrate binding and release. Upon binding to succinate, VcINDY appears to switch from CA and PG binding to PE binding, suggesting that succinate binding may encourage the dissociation of the former lipids and the binding of the later lipid. It has not yet been shown that such exchanges occur under native conditions, however this speculative dynamic lipid model may form the basis of future studies upon VcINDY lipid interactions.

This model of dynamic lipid interactions is in good agreement with previous observations made in this thesis, wherein the addition of succinate resulted in the destabilisation of SMALP solubilised VcINDY. These VcINDY native lipid nanodiscs were formed in the absence of succinate, and therefore likely contain lipids which interact with VcINDY's succinate free form. Upon the addition of succinate, the protein-lipid interactions within these nanodiscs are disrupted, leading to the observed reduction in thermostability.

Previous studies of elevator mechanism transporter lipid interactions are rare. Structural studies have detected densities likely to represent lipids in a range of elevator mechanism transporters, either between the dimerization domains as in CitS [80], or between the transport and scaffold domains, as in ASCT2, NapA, and EAAT1 [21][176][25]. Intriguingly, a large hydrophobic also cavity exists between the dimerization domains of VcINDY [48][3], hinting at the presence of a structural lipid similar to CitS. These appear to represent structural lipids, aiding in dimerization and the maintenance of domain contacts, and while they are highly important for proper protein function, with ASCT2 and EAAT2 both demonstrating increased transport rates in the presence of added cholesterol [21][22], they have not been shown to behave in a dynamic manner or respond to the addition of substrates.

Previous propositions of dynamic lipid interactions for elevator mechanism transporters are highly tentative, and confined to the SLC1 family. The transporter ASCT2 has been structurally solved to reveal a lipid interaction with the HP1 region which will require relocation in order for transport to occur [23], while Glt_{Ph} molecular dynamics have proposed the transient entry of lipids into the transport-scaffold domain interface to stabilise an unlocked conformation [177], and cryo EM structures have observed energetically costly bilayer deformations to occur during the transport cycle of Glt_{Ph} [27]. All of these observations suggest that the interactions between lipid and transporter must alter throughout the transport cycle of these SLC1 family members, possibly similar to what has been observed herein for VcINDY. It may therefore be speculated that dynamic lipid interactions may be a general feature of elevator mechanism transport, however far more work will be required before this can be confidently stated.

GFP-TS thermostability assays have therefore been successful in their examination of VcINDY-lipid interactions, demonstrating the presence of a complex, dynamic, relationship between VcINDY, lipids, and substrate. While the details and mechanisms behind this relationship are currently unclear, the preliminary data gathered here may form the basis of much future research.

4.4 A Thermophoresis Based Binding Assay is Capable of Determining VcINDY's

Substrate Binding Affinities

4.4.1 Introduction

As discussed previously (see 4.2.1 Introduction), transport in the most basic sense consists of cycles of substrate binding, translocation, and release. Typical measurements of substrate transport report on an arcane combination of these three processes, and do not allow a precise understanding of these individual steps to be gained. In order to properly understand the process of substrate binding, and thus gain a fuller understanding of the interactions between transporter and substrates, a binding assay is required.

In 4.2 High Throughput Thermostability Measurements Reveal the Rules of VcINDY Substrate Binding, a binding assay suitable for substrate screening was employed to great effect, and in 4.3 Aggregation Based Thermostability Measurements Indicate a Complex Relationship Between Substrate Binding and Lipid Interactions, a less precise but more robust binding assay elucidated complex, previously unexpected, relationships between lipids and substrates. These approaches to the examination of binding, however, share severe limitations.

Both CPM thermofluor and GFP-TS are thermostability based techniques, detecting substrate binding through increases in thermostability. A major caveat of this approach is that the dynamics of protein-substrate interactions are being observed at a range of elevated, non-biological, temperatures. As such, any pseudo-binding affinities which may be observed through increasing substrate concentration and examining the resultant melting temperature are not equivalent to the binding affinities which occur under physiological conditions [155][162]. Lowering of the melting temperature to biologically relevant ranges through the use of chaotropic salts can correct for this problem, however the chaotropic salts themselves may interfere with charged based binding, as is performed by VcINDY [162].

So, while binding has already been examined, one key detail remains elusive: affinity. It appears, based on the concentration of succinate required to generate a thermostability shift (Figure 4.2.4-1) and cause a change in residue accessibility (Figure 4.1.2-1B) that succinate binding affinity is in the millimolar range, although no confident value has yet been established.

Thermophoresis is a well understood process by which large molecules migrate away from areas of heat in solution [178]. Importantly, the rate of migration away from the area of heat is dependent upon the nature of the molecule and its interface with the solvent, meaning that changes in factors such as size, charge, and solvation entropy result in detectable changes in the rate of migration. This fact was exploited by *Baaske et al 2010* [179] for the development of a precise binding assay, in which the binding of a fluorescently labelled aptamer to the protein thrombin was effectively measured by applying a heating laser to a solution contained in glass capillary tubing and measuring the dispersal of the labelled aptamer molecules through the depletion of their signal at the point of heating [179]. This system, in which a heating laser was used alongside a fluorescent tag in order to observe the movement of fluorescently charged molecules, is unchanged in the current methodologies of Microscale Thermophoresis (MST)[180].

To our knowledge MST has not been previously used to examine a DASS family transporter, or any elevator mechanism transporter, and as such it is not certain that VcINDY will be compatible with this approach. If possible, an examination of succinate binding affinities in varying salt conditions, along with examination of sodium affinities, would be of great interest. Additionally, the use of lipid nanodisc systems will allow examination of the lipid dependence of substrate binding affinity.

4.4.2 Detergent Solubilised VcINDY is Compatible with MST Binding Affinity

Measurements

For the MST examination of VcINDY, a Nanotemper Monolith NT.115 system was used. This system could be used in two main ways: A his-tag specific fluorescent label could be used to allow detection of protein movements, or alternatively intrinsic protein fluorescence could be followed through the use of a GFP-tagged construct.

Both approaches had potential advantages and shortcomings; the his-tag specific dye was relatively expensive, and required proteins to be kept for thirty minutes at room temperature for labelling to occur, risking the denaturation of unstable protein samples. GFP-tagging, on the other hand, necessitated the anchoring of the protein of interest to the large globular GFP, with potentially adverse effects on function. Accordingly, both approaches were trialled.

A proper and critical examination of data analysis for VcINDY MST shall follow the presentation here of his-labelled and GFP-labelled data. This ordering is taken due to the need to demonstrate some functional use of the assay and to select a detection method before presenting the finer details of data analysis.

The addition of a range of succinate concentrations in the presence of 150 mM Na for 250 nM his-labelled VcINDY produced a clear reduction in ΔF_{norm} at succinate concentrations greater than 1 mM, representing an increase in the rate of movement of labelled VcINDY away from the point of heating (discussed below) (Figure 4.4.2-1A). The addition of the non-binding negative control dicarboxylate, oxalate, did not result in any major change to the ΔF_{norm} at any concentration. This indicates that the change in VcINDY thermophoresis rates in response to succinate addition are caused by the binding of succinate to VcINDY, and not by non-specific effects deriving from dicarboxylate addition. Fitting of the effects of succinate addition upon VcINDY ΔF_{norm} to a sigmoidal dose-response curve (discussed below) indicates a K_d of roughly 4.3 mM, in agreement with the mM affinity anticipated, although due to the lack of clear plateauing of F_{norm} at higher

succinate concentrations there are high levels of uncertainty in this fitting, with the 95% CI ranging from 1.8 to 11.1 mM. Regardless, this preliminary data shows VcINDY to be amenable to this form of study.

Attempting this approach with GFP-labelled VcINDY still resulted in a detectable succinate induced change in VcINDY ΔF_{norm} , however changes in ΔF_{norm} values did not occur until succinate concentrations of around 10 mM, demonstrating a lower succinate affinity than his-tag-labelled VcINDY samples (Figure 4.4.2-1B). The cause of this label derived affinity difference is unclear, although the bulky GFP label appears to reduce affinity to such an extent that saturation of the succinate binding curve is not achievable within the limits of succinate solubility, with no clear saturation observed at 150 mM, therefore making it difficult to fit to a sigmoidal model with accuracy. As such the GFP-tagging approach is unsuitable for use with VcINDY.

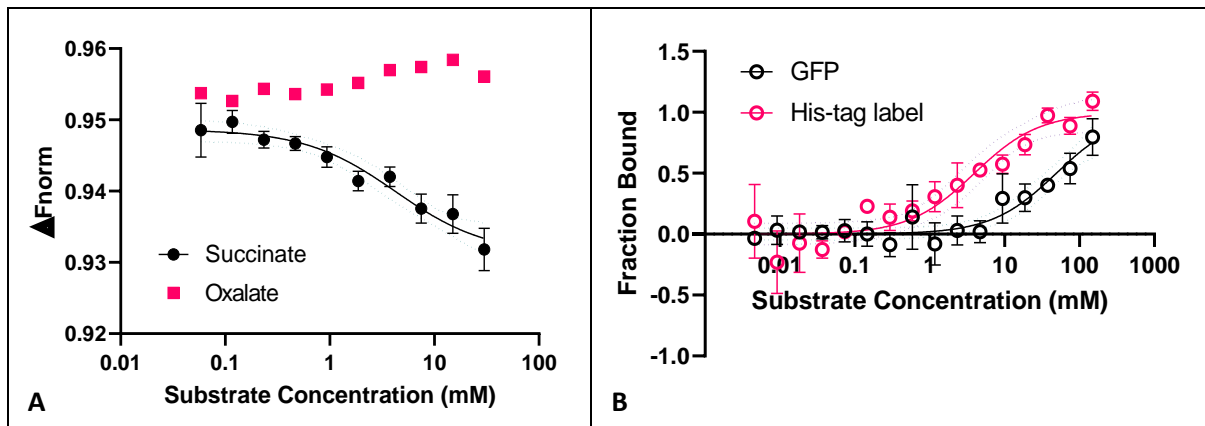


Figure 4.4.2-1 Demonstration of the compatibility of MST with VcINDY. A: MST examination of VcINDY substrate binding.

ΔF_{norm} , representing level of thermophoresis based depletion of VcINDY from the path of the heating laser over time, is shown with respect to substrate concentration. Succinate addition results in an increase in the rate of thermophoresis, and is fitted to a sigmoidal dose response curve with standard error shown, producing a K_d value of 4.3 mM. The addition of the non-binding dicarboxylate, oxalate, does not result in a clear alteration of ΔF_{norm} , and as such was not fitted to a dose-response curve. **B:** The fraction of VcINDY bound to succinate as determined for GFP-tagged VcINDY, and VcINDY fluorescently labelled using a his-tag specific dye. Fraction bound is determined through normalisation of ΔF_{norm} data such that pre binding $\Delta F_{norm} = 0$, substrate saturated $\Delta F_{norm} = 1$. The 95 % C. I. of sigmoidal dose-response curve fittings are shown.

4.4.3 Careful Analysis of VcINDY MST Data is Required In Order To Provide Reliable K_d estimates

The first quality control needed is confirmation that VcINDY is not adhering to the capillary walls, which would alter the concentrations of VcINDY available for substrate binding in unpredictable ways and lead to misleading MST results. This is easily checked by observing the fluorescent signal produced with respect to its position across the capillary; an adhering protein would show two fluorescent peaks at the capillary inner walls, while a non-adhering protein would show a single peak at the centre of the capillary. Luckily, this single central peak was observed, indicating no adhesion to capillary walls, and example traces from 10 representative capillary scans are presented (Figure 4.4.3-1).

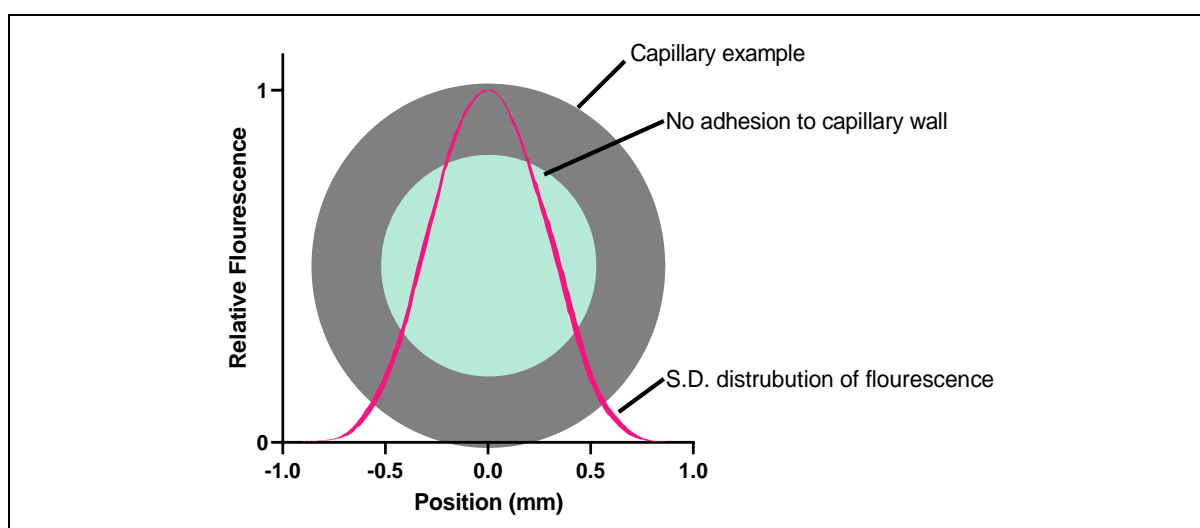


Figure 4.4.3-1 Capillary scans showing the distribution of fluorescence with respect to position across the capillary tube.

No adherence of fluorescent particles to the capillary walls is seen to occur. The S.D. limits of 10 representative runs are shown as exemplar data, although similar results were gathered for every condition tested.

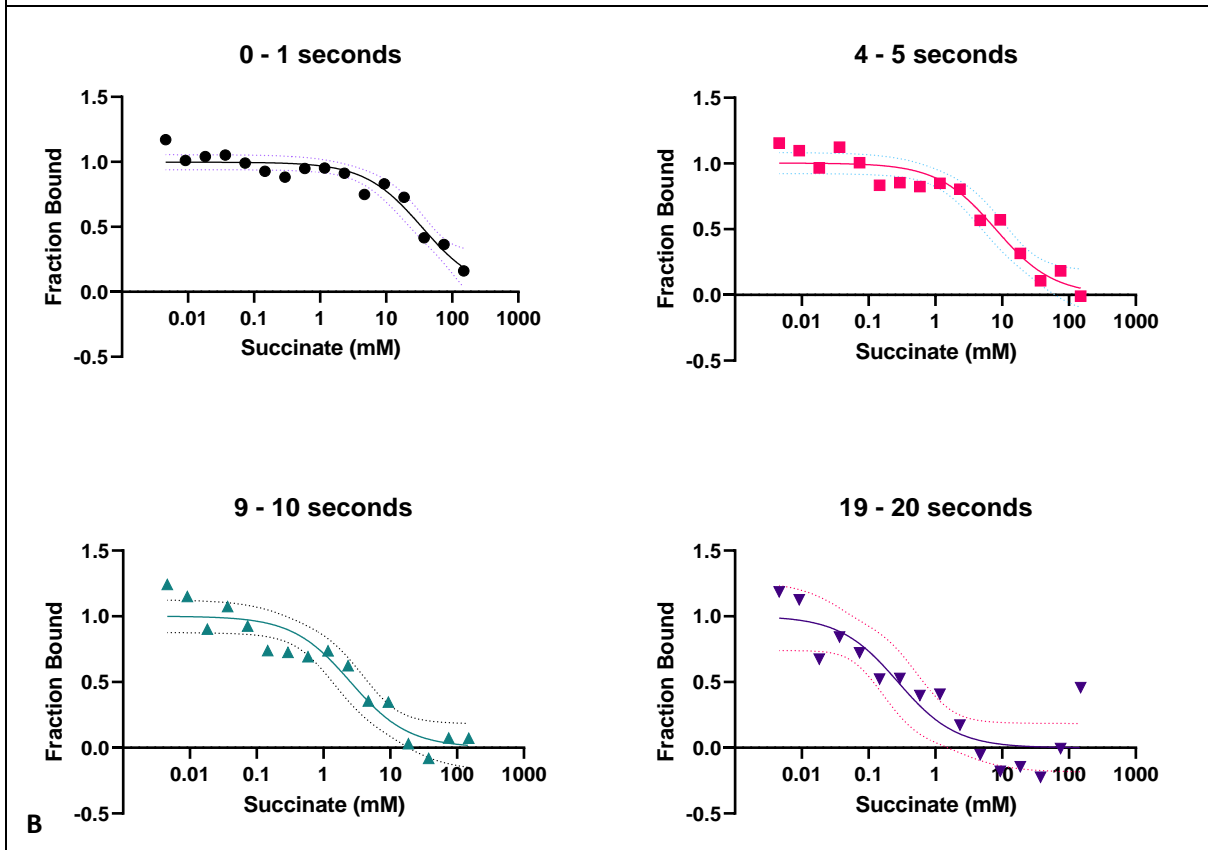
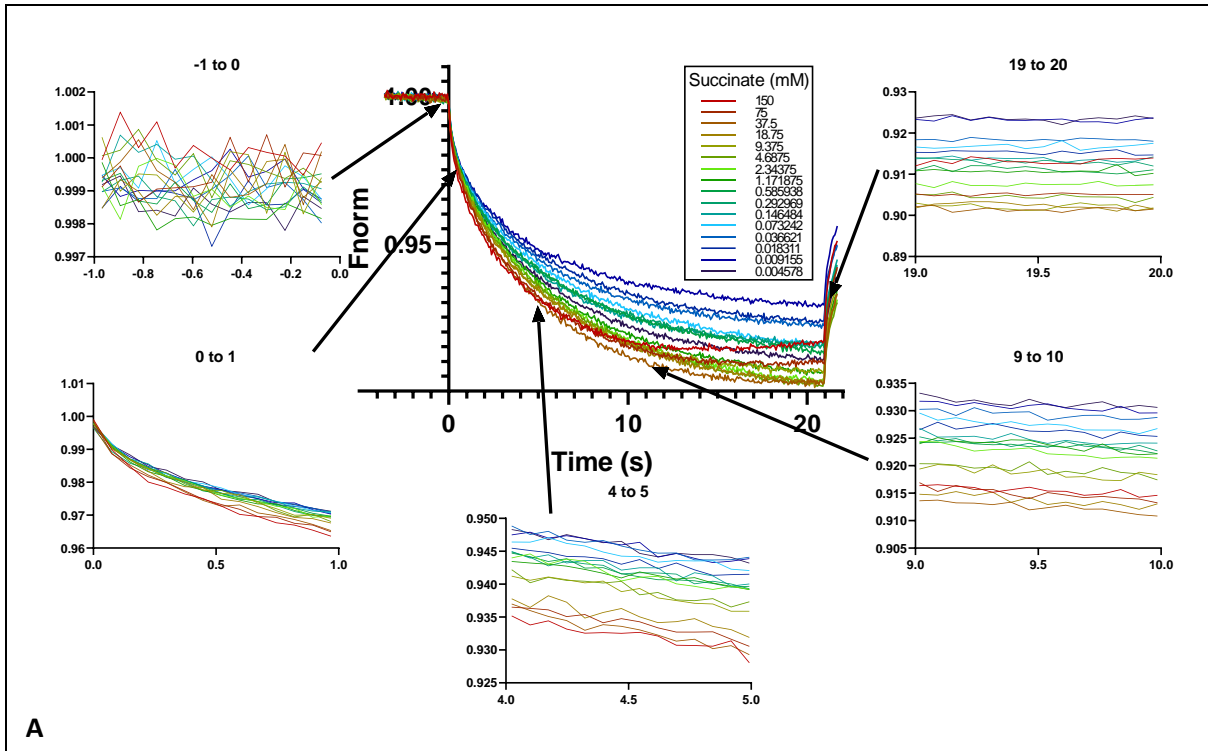
Raw MST data is normalised fluorescence (F_{norm}) with respect to time since heating laser activation, allowing the rate of depletion of fluorescent particles from the path of the hearing laser to be observed (Figure 4.4.3-2A). In order to convert this into values representative of the labelled molecule's thermophoresis rate, the ΔF_{norm} value must be determined; i.e. the change in normalised fluorescence. This value is typically determined as the normalised difference between

fluorescence pre-thermophoresis, and a chosen averaged timespan after (defaulting to 4-5 seconds in Nanotemper's MO.Affinity Analysis software unless overridden through expert mode analysis – n.b. in this project MST data analysis is carried out manually in order to minimise reliance on “black box software”) [181].

It should be briefly noted that the first moments after the activation of the laser are known as the T-Jump, during which the sudden temperature change results in sudden fluorescence changes distinct from true thermophoresis [181]. This T-jump value can be used for fitting binding curves alone, as in the 0-1 timepoint below, included in the thermophoresis measurement, or removed from the dataset by taking the initial fluorescence readings at around 0 to 1 seconds, instead of -1 to 0 seconds [181]. In this case, as the t-jump change in fluorescence reduced fluorescence similarly to true thermophoresis movement, it is included in thermophoresis measurements and not discussed beyond this point.

The baseline, pre-thermophoresis, fluorescent level was taken at -1 to 0 s, where 0 marks the activation of the heating laser. In order to establish suitable parameters for the determination of ΔF_{norm} , the level of fluorescence remaining at various post-heating laser activation timepoints compared to initial fluorescence was examined. These timepoints were 0 to 1 s, 4 to 5 s, 9 to 10 s, and 19 to 20 s (Figure 4.4.3-2A). The varying ΔF_{norm} values generated through these approaches were plotted with respect to succinate concentration (Figure 4.4.3-2B). Interestingly, different choices of timepoints for the determination of ΔF_{norm} appear to result in substantially different binding curves. F_{norm} readings taken later in the thermophoresis process resulted in ΔF_{norm} values which reduced at lower succinate concentrations than ΔF_{norm} values derived from F_{norm} readings taken earlier in the thermophoresis process, despite all analysis being carried out on the same dataset. These putative ΔF_{norm} values were fitted to a sigmoidal dose-response curve (Figure 4.4.3-2B), and their apparent K_d values determined (Figure 4.4.3-2C). Curiously, a clear negative correlation exists between the time point chosen and the apparent K_d determined; 0 to 1 s resulted

in a K_d of 35 ± 14.2 (S.E.) mM, 4 to 5 s in 7.9 ± 2.7 (S.E.) mM, 9 to 10 s in 2.5 ± 1 (S.E.) mM, and 19 to 20 mM in 0.27 ± 0.2 (S.E.) mM. Choosing a timepoint for the determination of ΔF_{norm} must, therefore, be done with care. Late readings risk thermal denaturation aggregation of the protein, visible in the upward trends of some fluorescent curves after prolonged heating (Figure 4.4.3-2A), and as such these later values should be largely avoided. The 0-1 seconds read takes place before the thermophoresis curves representing different succinate concentrations have properly separated, therefore providing poor signal resolution. This leaves the 4 to 5 s and 9 to 10 s timepoints as candidates. Both of these are similar, suggesting K_d s of around 7.9 ± 2.7 (S.E.) and 2.5 ± 1 (S.E.) mM respectively. As such the more commonly used 4 to 5 s (see 4.4.7 Chapter Summary) shall be used for analysis throughout this chapter. This consistency shall allow comparisons of different conditions to be made with confidence.



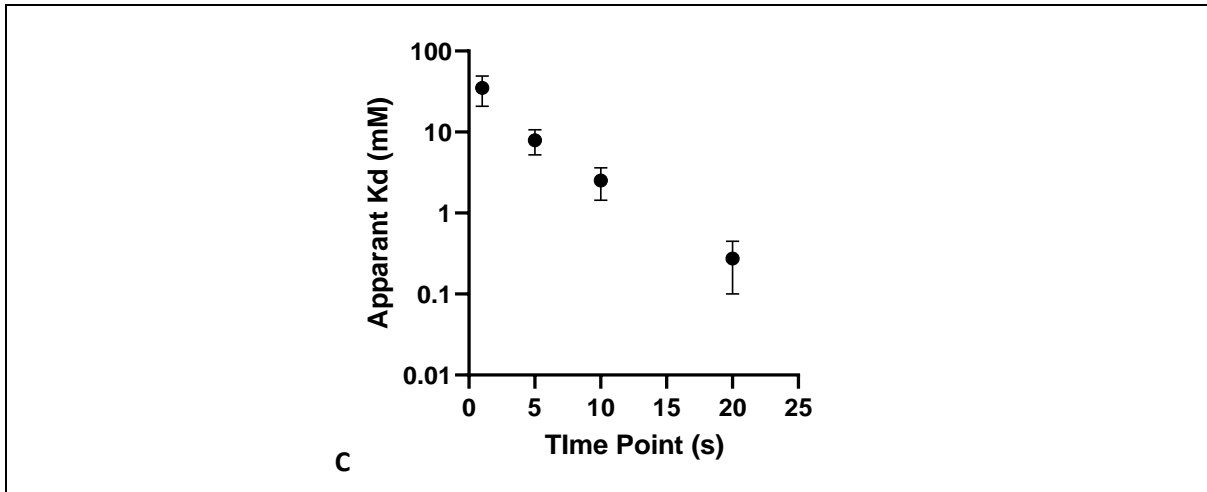


Figure 4.4.3-2 Optimisation of MST for detection of VcINDY succinate binding. **A:** MST readings of F_{norm} for his-tag labelled VcINDY in the presence of increasing concentrations of succinate. One second extracts are shown indicating the regions of the graph which will be averaged for calculation of ΔF_{norm} values in part E of this figure. **B:** ΔF_{norm} binding curves derived from the data in part D of this figure, representing the proportion of initial fluorescence remaining at the time indicated with respect to succinate concentration. Datasets are fitted to sigmoidal dose-response curves with standard error shown. All graphs shown here are produced from the same initial dataset, shown in part D of this figure. **C:** The estimated K_d of succinate binding produced from the fittings shown in part E of this figure, against the time point chosen for calculation of ΔF_{norm} .

4.4.4 Succinate Binding is Dependent upon Prior Low Affinity Sodium Binding

Now that the assay is proven to work, succinate affinity could finally be established definitively. In order to do this, succinate titrations were carried out at a range of sodium concentrations (Figure 4.4.4-1A). Interestingly, experiments carried out with 150 mM, 300 mM, and 600 mM NaCl showed dramatic decreases in ΔF_{norm} at succinate concentrations over 1 mM, however experiments carried out with 10 mM and 75 mM NaCl showed no succinate derived reduction in ΔF_{norm} , and exhibited lower ΔF_{norm} values at low succinate concentrations than their high sodium counterparts.

As already discussed, MST relies on a change in the nature of the protein upon substrate binding, be it conformation, charge, etc, which results in a change in the rate of movement of the molecule through the solution away from a source of heat. This can be used to determine when binding occurs as the protein moves from one state to another in a relatively simplistic two state system (bound and unbound). Here, we to observe what appear to be three states. These are, conveniently, interchangeable upon the increase in the concentration of a single substrate, allowing their likely substrate binding states to be discussed (Figure 4.4.4-1B). Firstly, an increase in sodium concentration moves the protein from the apo to the sodium bound state, resulting in an increase in ΔF_{norm} . Secondly, a subsequent increase in succinate concentration moves the protein from the sodium bound state to the fully loaded state, resulting in a decrease in ΔF_{norm} .

Initial conclusions can be drawn from high sodium concentration experiments. Examining this data in more detail, there is some variation in behaviour between higher sodium concentration experiments, with increasing salt levels appearing to produce slightly lower affinity binding curves (Figure 4.4.4-1C), whereby 150 mM NaCl results in a K_d of 3.9 ± 1.4 (S.E.) mM, and 600 mM NaCl results in a K_d of 8.6 ± 1.6 (S.E.) mM, supporting CPM thermofluor data indicating high ionic strength solutions to interfere with succinate binding (see 4.2.3 Details of Cation Interactions are Revealed Through Thermostability Measurements). The determined K_d s for succinate binding are, however, in the expected millimolar range. As the most physiologically representative condition, the 3.9 ± 1.4

(S.E.) mM succinate K_d recorded in the presence of 150 mM sodium shall be taken as the canonical reading.

At low concentrations of sodium, 10 mM and 75 mM, succinate addition does not appear to cause the characteristic drop in ΔF_{norm} observed at higher sodium concentrations, instead resulting only in a modest rise of ΔF_{norm} (Figure 4.4.4-1D), as previously observed for an oxalate negative control (Figure 4.4.2-1A), indicating a lack of apparent succinate binding. This supports the various observations in this thesis suggesting a strict order of binding to occur, requiring the binding of sodium before succinate (see 4.1.6 Chapter Summary and 4.2.7 Chapter Summary).

While there is a clear thermophoretic difference between low and high sodium concentration in the absence of succinate, in which high sodium concentrations result in higher ΔF_{norm} values, the addition of succinate abolishes this sodium derived difference, with succinate reducing the ΔF_{norm} value of high sodium concentration V_{cINDY} to values similar to low sodium concentration V_{cINDY} (Figure 4.4.4-1A). As such, while the sodium only bound V_{cINDY} is thermophoretically distinct, the *apo* and fully loaded states appear similar, suggesting a similarity between V_{cINDY} molecules under these two conditions. The fully loaded and *apo* V_{cINDY} molecules are capable of translocation between inward and outward facing states, in contrast to the conformationally locked sodium only bound molecules, so it may be speculated that this difference in dynamism is behind the changing thermophoretic responses observed.

Looking further into this sodium dependent change, the data can be replotted as ΔF_{norm} with respect to sodium concentration for varying succinate concentrations. Due to the already discussed suppression of the sodium shift in V_{cINDY} thermophoresis rates caused by succinate addition, high succinate (150 to 18.75 mM) conditions resulted in no clear effect of sodium on ΔF_{norm} values. The addition of sodium in the presence of extremely low, non-binding, succinate concentrations (below 0.05 mM, around 100 fold lower than the estimated succinate K_d), however, resulted in a clear sodium induced increase in ΔF_{norm} (Figure 4.4.4-1F). When fitted to sigmoidal dose-response

curves, the addition of sodium produced a highly consistent K_d of 140.5 ± 0.80 (S.E.) mM, as averaged across all conditions. Further examination of the sodium binding affinity under these conditions is warranted, especially through the use of a higher number of concentrations. Unfortunately, due to the COVID-19 pandemic, the follow up experiment could not be performed, and this preliminary data shall have to be used.

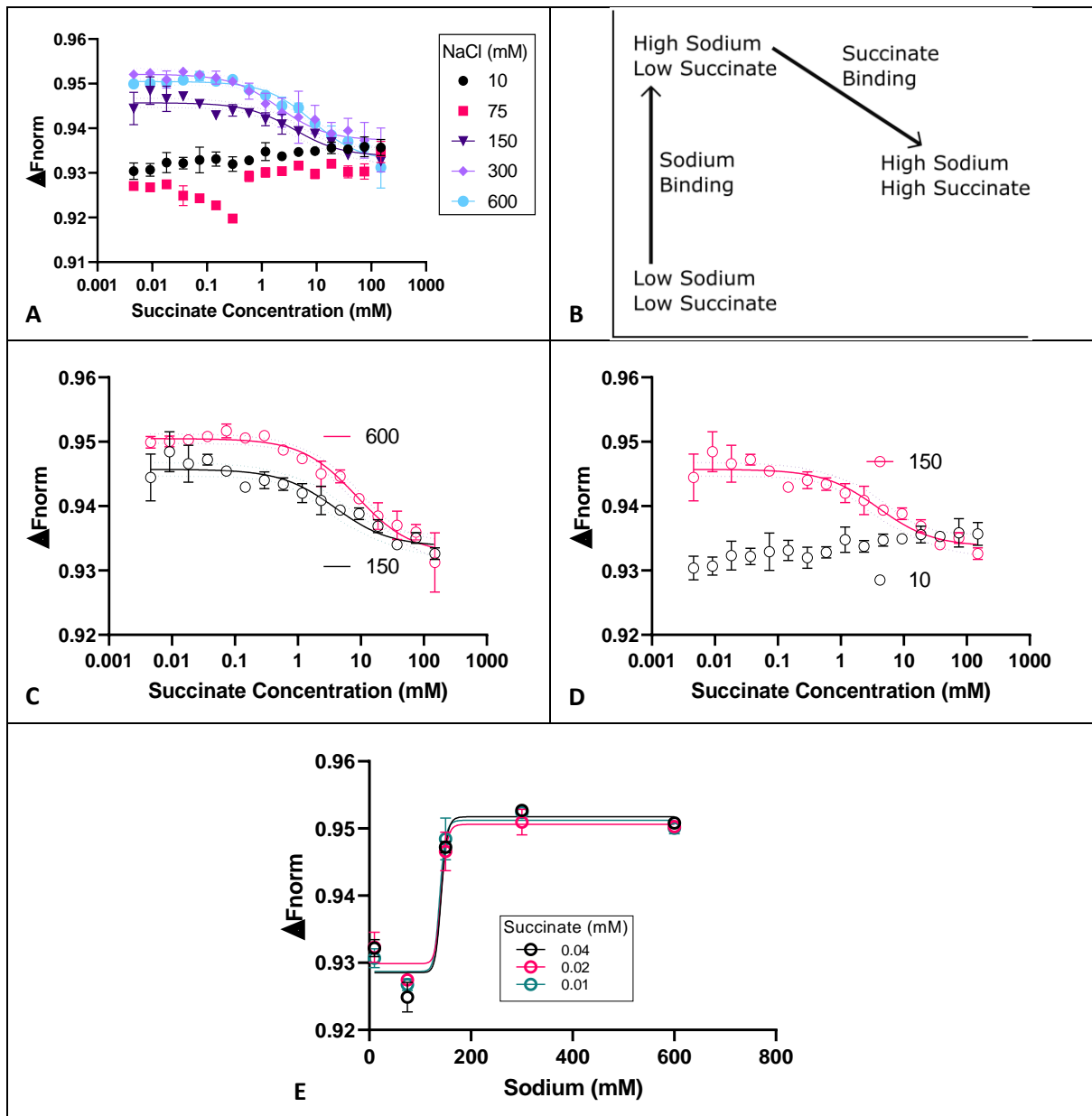


Figure 4.4.4-1 MST readings covering range of sodium and succinate concentrations for his-tag labelled detergent

solubilised VcINDY. A: Succinate concentration series in the presence of varying sodium concentrations, fitted to sigmoidal dose-response curves with 95% C. I. shown. B: Schematic representation of the three distinct MST movement rates observed in part A of this diagram, showing the likely binding events which cause transition between them. C: Succinate concentration series in the presence of high concentrations of sodium, fitted to sigmoidal dose-response curves with 95% C. I. shown. Data taken from part A of this figure. D: Succinate concentration series in the presence of high and low concentrations of sodium, fitted to sigmoidal dose-response curves with 95% C.I. shown. Data taken from part A of this figure. E: Sodium concentration series in the presence of non-binding concentrations of succinate, where the effect of sodium addition produces a clear shift in thermophoresis rates, fitted to sigmoidal dose response curves.

4.4.5 Preliminary MST Examination of Nanodisc Solubilised VcINDY Indicated Similar Substrate Affinities to Detergent Solubilised VcINDY

Given that the MST experiments thus far have been performed upon detergent (DDM) solubilised VcINDY, it is possible to question the applicability of these measurements to the function of VcINDY under native, lipid environment, conditions. One route to addressing this question was the creation of lipid nanodisc solubilised VcINDY, with the aim of allowing the quantification of VcINDY binding affinities in the presence of controlled lipid environments. Unfortunately, due to the COVID-19 pandemic, only preliminary trials of TLE based nanodiscs had been conducted.

A succinate titration of TLE containing VcINDY nanodiscs resulted in a ΔF_{norm} change of around + 3.5 A. U.; a small change compared to the approximate change of - 11.8 A. U. observed for detergent solubilised VcINDY (Figure 4.4.5-1). Fitting of this nanodisc based succinate response to a sigmoidal dose-response curve yields a K_d of 25 ± 16 (S.E.) mM, compared to detergent solubilised VcINDY's $3.9 \pm$ (S.E.) 1.3 mM, giving a p value of 0.38, therefore detecting no significant difference between the succinate affinity of detergent and TLE nanodisc solubilised is observed here.

While this analysis is certainly preliminary, with more work required to improve the resolution of VcINDY nanodisc based MST, it indicates that VcINDY likely possess a mM range K_d even when reconstituted into a TLE nanodisc environment. As such, the mM range succinate affinities observed for detergent solubilised VcINDY are likely biologically relevant based upon our current data.

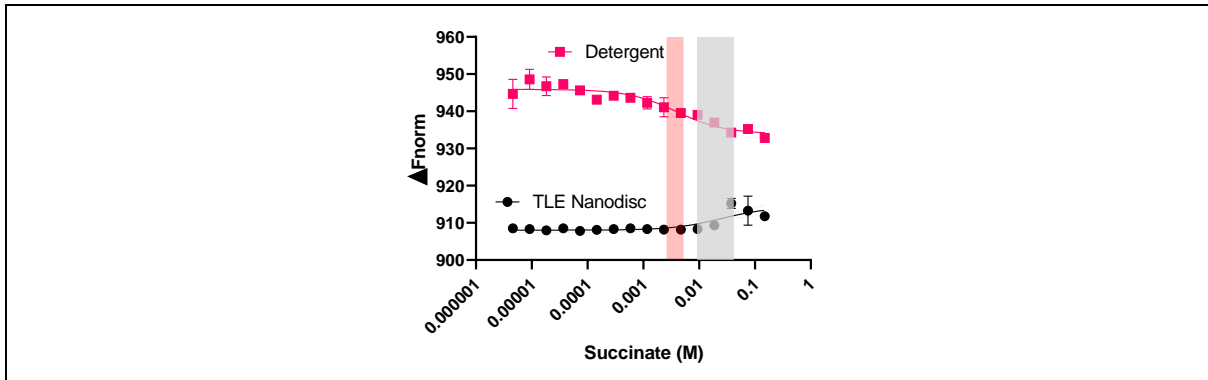


Figure 4.4.5-1 MST binding analysis of detergent and nanodisc solubilised VcINDY. Sigmoidal dose-response curve fitted succinate concentration series for VcINDY solubilised using either DDM detergent or TLE lipid MSP1E3D1 nanodiscs are shown, in the presence of 150 mM sodium. The approximate range of VcINDY's K_d (± 1 S.D.) is marked for each conditions. No significant difference is seen.

4.4.6 Preliminary MST Examination of SMALP Solubilised VcINDY Indicates that the SMALP System May be Capable of Isolating Transient Lipid Environments

SMALPs are another nanodisc system which allow the solubilisation of VcINDY in a detergent free lipid environment, as introduced in 3.1 The SMALP Native Lipid Nanodisc System Allows *In Vitro* Examination of VcINDY in a Near Native Environment. Given the ability of SMALPs to solubilise proteins in the presence of their surrounding lipids, an interesting possibility is raised. VcINDY has already been demonstrated to change lipid preference in response to substrate presence *in vitro* (see 4.3.4 The Effects of Lipids Upon VcINDY-GFP Thermostability Are Altered by the Presence of Succinate). If these changes in lipid preference result in changes in lipid interactions *in vivo*, it is possible that SMALPs may be able to isolate these changing lipid environments. Through the use of MST, the behaviour of VcINDY SMALPs, produced under differing substrate conditions, can be compared.

In order to examine this possibility, 2:1 SMA purifications were carried out in three conditions; sodium only, in which the normal sodium based buffers were used, potassium only, in which sodium was substituted for potassium in all buffers from the point of cell pellet resuspension, and succinate, in which all buffers were supplemented by 20 mM succinate pH 7 from the point of cell pellet resuspension. Any difference in the behaviour of these three SMALPs would indicate that different lipid environments were being extracted.

These differently prepared VcINDY SMALPs were then examined using MST. A succinate titration was carried out in the presence of 150 mM sodium (Figure 4.4.6-1). Intriguingly, the only SMALP type which showed any clear response to succinate addition was those purified in the presence of sodium and succinate. The implications of this observation are twofold. First, the presence of substrate during the process of SMALP solubilisation causes SMALPs with differing properties to be produced. This suggests that a change in lipid environment is indeed being isolated by the SMALP system. Second, as only SMALPs created in the presence of succinate are capable of thermophoretically

responding to the addition of succinate, it appears that VcINDY requires the presence of its succinate binding favoured lipid environment in order to successfully bind succinate and undergo the change in conformation or dynamics which results in a measurable change in thermophoretic state.

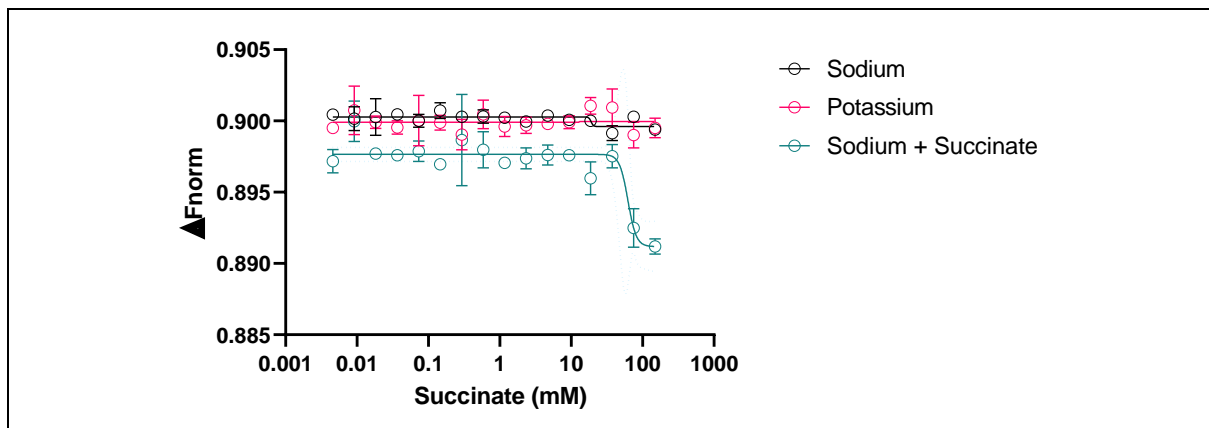


Figure 4.4.6-1 MST results, showing the effect of varying succinate concentration in the presence of 150 mM sodium on VcINDY (2:1) SMALPs. VcINDY containing membranes were harvested, solubilised into SMALPs, and purified in the presence of either sodium, potassium, or sodium and succinate. Attempted fittings of sigmoidal dose-response curves are shown, with 95 % C. I. indicated for the sodium + succinate purified SMALP samples.

4.4.7 Chapter Summary

MST has been successfully employed in the study of VcINDY, elucidating previously unknown binding affinities, and supporting a model of ordered substrate binding. It was observed that both his-tag specific fluorescent labelling and GFP-tagging were viable approaches to detecting VcINDY movements in MST experiments, however succinate affinity was observed to be dramatically lower for GFP-tagged VcINDY. It therefore appears that the addition of a large protein tag to the dynamic structure of VcINDY in some way impairs native function and substrate binding, thus making the his-tag specific dye labelling approach preferable.

Succinate binding resulted in clear changes to the rate of movement of VcINDY under the influence of a heating laser, although the conversion of these movements into definitive binding affinities required careful analysis. It was seen that the time chosen to record post-thermophoresis fluorescence correlated strongly with the K_d concluded. While the consistent use of a 4 to 5 s timeframe in this work prevented this effect from causing issues, significant questions are raised as to the power of MST to report of true and replicable binding affinities. A brief survey of the literature reveals that out of ten papers reporting MST based binding affinities, one reads at 3.7 seconds [182], one at five seconds [183], two at thirty seconds [179][180], one at thirty five seconds [181], while five do not clearly indicate the time used [184][185][186][187][188]. Of these papers, only one states that the K_d for their protein is not significantly influenced by choice of thermophoresis time [183]. Clearly the choice of timeframe is an important parameter which merits greater recognition and control in MST studies.

Once suitable parameters were determined, the use of MST added swiftly to our understanding of VcINDY, providing two binding parameters. First, a succinate binding K_d of 3.9 ± 1.4 (S.E.) mM was established, in great agreement with the mM affinity suggested by other techniques presented in this thesis. Second, a low sodium affinity K_d of 140 ± 0.80 (S.E.) mM was observed which may represent the sodium binding step necessary for the subsequent binding of succinate, however more

detailed experimentation will be required in order to provide a higher confidence binding affinity for this binding event.

It is uncertain which sodium binding event is observed here, as it is known that VcINDY transports three sodium ions per succinate [9]. It is known that the binding of at least two sodium ions is required for succinate binding to take place [48][3], however the binding order of the final ion is unclear. As such the sodium binding event observed here can only be interpreted as the binding of the lowest affinity sodium ion which is required to facilitate subsequent succinate binding. Notably, study of the elevator mechanism transporter Glt_{Ph} has indicated this transporter to pose a sodium binding K_d of 120 mM in the absence of substrate, and 25 mM in the presence of substrate [150]; similar values to the 140 mM K_d herein determined for VcINDY sodium binding. Further study will be required in order to understand the exact nature of the interactions between VcINDY's substrates.

VcINDY's succinate K_d was determined to be 3.9 ± 1.4 (S.E.) mM, which represents weak binding in comparison to VcINDY's succinate transport K_m of 1 μM [73]. For comparison, the elevator mechanism transporter Glt_{Ph} possesses transport K_m of approximately 120 nM [189][190], approximately tenfold lower than VcINDY, but the substrate binding K_d is 2.6 nM under high sodium concentrations [150], similar to the conditions used herein, approximately 1.5 millionfold lower than VcINDY. Furthermore, Glt_{Ph} possesses a K_d lower than its K_m , whilst VcINDY possesses a K_d far higher than its K_m , suggesting fundamental differences between the mechanisms of these two commonly compared elevator mechanism transporters.

As this succinate binding affinity was determined primarily using detergent solubilised VcINDY, it is possible that it is non-representative of VcINDY's *in vivo* binding affinity. Preliminary work examining the binding affinity of VcINDY in MSP-based nanodiscs suggests that a similar binding affinity is demonstrated by VcINDY in both detergent and lipid environments. Nevertheless, further work will be required to confidently determine the binding affinity of VcINDY in a lipid environment, and to

confirm whether the low binding affinities observed herein are truly representative of *in vivo* VcINDY behaviour.

The reason for the drastically higher K_d than K_m in VcINDY transport is unclear, and transporters possessing higher K_d values than K_m are uncommon. One example of this kinetic arrangement is found in the transporter CaiT, which possesses an apparent K_d of 2 – 3 mM and a K_m of 40 – 80 μ M [191], with this arrangement likely resulting from the presence of multiple substrate binding sites [191]. In the case of VcINDY it is possible that competing interactions with the inwards and outwards facing binding sites upon detergent solubilised VcINDY contribute to the apparent low substrate affinity, however more work will be required to fully understand the reason for VcINDY's substrate affinity, with the study of oriented VcINDY molecules likely to greatly expand our understanding of this subject (see 5.3.2 Binding Site Deconvolution).

Unfortunately, due to the COVID-19 shutdown further planned work could not be carried out. This includes further examination of the sodium binding process. The data presented herein is sufficient to allow a reasonable estimation of sodium binding affinity, however a more dedicated set of sodium focused experiments would allow improved confidence and accuracy. Increasing the number of sodium concentrations tested would initially provide clearer binding curves. Further experiments would be performed in solutions ionically balanced through the addition of potassium or choline. Initial work examining sodium and potassium ionically balanced solutions faced difficulties, likely due to the impact of high ionic strength solutions on VcINDY function, and is not included herein (see 4.2.3 Details of Cation Interactions are Revealed Through Thermostability Measurements).

Additionally, if the work with MSP1E3D1 nanodiscs containing varying compositions provided little useful results, it would have been simple to supplement detergent solubilised VcINDY with lipids in a manner similar to the GFP-TS work carried out in this thesis (see 4.3.4 The Effects of Lipids Upon VcINDY-GFP Thermostability Are Altered by the Presence of Succinate) and observe any possible lipid interactions in this manner, possibly allowing lipid K_d s to be established.

MST has proved a potentially powerful tool for the examination of the SMALP nanodisc system, and work carried out herein has provided compelling preliminary evidence that the SMALP nanodisc system may be capable of isolating mechanistically important transient lipid environments. VcINDY has already been observed in this thesis to alter lipid interactions in response to substrate presence (see 4.3.4 The Effects of Lipids Upon VcINDY-GFP Thermostability Are Altered by the Presence of Succinate). VcINDY containing SMALPs, prepared in the absence and presence of substrates, demonstrated clearly distinct thermophoretic behaviour, with only VcINDY SMALPs purified in the presence of both sodium and succinate showing succinate inducible changes to thermophoretic rate. This clearly suggests that SMALP solubilisation is able to isolate the different transient lipid environments created by VcINDY throughout its transport cycle. Far more work, including both further MST experimentation, and direct identification of SMALP solubilised lipids, through either Mass Spectrometry or Nuclear Magnetic Resonance, will be required to fully explore and understand this system.

In this chapter, MST has been successfully applied to VcINDY, allowing the determination of VcINDY's sodium and succinate binding affinities for the first time. It has also allowed novel observations of the behaviour of the SMALP nanodisc system. This technique has great potential for the future study of VcINDY, and the work presented herein will form the basis of a great deal of future research.

5 DISCUSSION

This thesis has applied a wide range of biochemical and biophysical techniques to VcINDY, each providing different insights as to the function of this transport protein, which this discussion shall integrate in the context of pre-existing literature in order to form a new, much extended, proposed model for the dynamic cycle of VcINDY substrate transport.

5.1 The methods, and their unique perspectives

5.1.1 Cysteine Accessibility Assays

Cysteine accessibility assays provided clear, single residue resolution, readings of local conformational changes occurring throughout the transport cycle. Through the use of these assays the effects of substrate binding upon the solvent accessibility of specific residues was recorded with good resolution, allowing clear differences to be observed between positions only several residues apart. This allowed conclusions to be drawn for both global protein function, and local dynamic contributions to the transport cycle.

In brief, our data suggested that substrates drove the protein into a previously unobserved occluded state, with this process separable into two distinct steps. First, sodium binding drives a global conformational change towards the occluded state, affecting both residues in extreme proximity to the binding sites, and residues distal to the binding sites. Secondly, succinate addition drives an additional conformational change only in the presence of sodium, demonstrating clear ordered binding, similar to that observed in other elevator transporters and detected through similar accessibility assays [150][142]. This additional conformational change is exclusive to the hairpin regions (HP1 & HP2), indicating that these hairpins undergo dramatic and specific movement in response to succinate in a regulatory gating motion similar to that found upon other elevator mechanism transporters, suggesting a Two Gate elevator mechanism [15]. Given that basic transporter theory states that the sodium only bound state must be unable to undergo transition from the inward-facing to the outward-facing state, this succinate induced change is a good candidate for the trigger movement, which allows translocation to take place. As such, using this

approach, high resolution positional information has elucidated orders of binding, general conformational changes, separable substrate effects, the number of gating regions involved in transport, and provided a promising candidate for the exact region responsible for triggering the translocation of the fully loaded protein.

5.1.2 CPM-based Thermoflour

Thermoflour-based thermostability assays provided a platform for high-throughput examination of VcINDY ligand binding. Through this approach, simple interrogations of the effects of varying buffering conditions were carried out alongside rapid substrate screening. This was perhaps the most productive single technique within this thesis, with the results from over 400 samples included in the final results. Through substrate screening many novel interactors were identified, and the comparison of similar molecules allowed the principle requirements for interaction with VcINDY to be determined.

Cation discrimination was found to be a two-step process. Initially, steric selectivity prevents atoms larger than sodium from interacting with the binding sites, however once binding as achieved only sodium is capable of effectively preparing the protein for succinate binding, a process seen in cysteine accessibility assays to involve significant conformational change. It is likely that correct coordination interactions must occur in order to trigger the allosteric process, which is only achievable with an ion of the correct coordination strength, i.e. sodium.

Anion discrimination was found to primarily revolve around a molecular ruler principle. Two carboxyl binding regions, known to interact with both citrate and succinate must be satisfied in order for binding to occur [48][3]. As such any molecule with these groups positioned too close together or too far apart to bridge this gap is unable to bind, along with any molecule lacking these two groups.

Interacting dicarboxylates may possess moderate additional sidechains. It is likely that these sidechains are oriented out the binding pocket similarly to citrate [48][3]. Multiple side chains make

this sterically difficult, disrupting binding. The addition of any sidechains which introduce a positive charge into the weakly positive binding pocket results in substrate rejection.

These anion requirements have been observed in multiple cases, showing remarkable consistency and reliability as predictors of substrate binning.

Further to this high-resolution deconstruction of VcINDY's substrate binding requirements, high throughput screening has shed light upon many more aspects of VcINDY's behaviour, revealing an unusually low substrate affinity, hyper-stability of VcINDY when solubilised in SMALPs, a reduction of SMALP thermostability upon substrate addition, and significant impacts of lipids upon substrate binding.

5.1.3 GFP-TS Thermostability

GFP-TS-based thermostability observations took over where CPM-based thermostability measurements could not go; into complex solutions containing anything more than a trace amount of lipids, allowing the elucidation of processes not otherwise detectible. Through this approach, a complex lipid-substrate relationship was discovered, indicating that while CA and PG interact with the sodium bound protein, the addition of succinate dramatically reduces these interactions and instead allows interaction with PE to take place. These results indicate a complex relationship between substrates and lipids previously unknown for this type of transporter, raising fundamental questions as to the level of active lipid involvement throughout the transport cycles of elevator mechanism transporters.

5.1.4 MST Affinity Assays

MST-based affinity measurements allowed for the precise examination of binding, resulting in the first determination of VcINDY's elusive binding affinities. After careful analysis of the data, a succinate binding affinity of 3.9 ± 1.4 (S.E.) mM was confidently established, confirming many earlier indications that this transporter was of unusually low affinity.

Further to this, preliminary examinations of sodium binding allowed the K_d of the lowest affinity sodium binding event required for the subsequent binding of succinate to be estimated as around 140 ± 0.80 (S.E.) mM.

5.1.5 SMALP Solubilisation

SMALP solubilisation provided an alternate approach to the study of this enigmatic protein; a system through which it could be readily examined in its native lipid environment, providing invaluable insights to this project. While SMALPs largely confirmed the suitability of detergent solubilised VcINDY for use in cysteine accessibility assays, elsewhere they provided far more unexpected results. The thermostability of SMALPs, as examined through CPM thermoflour, provided the first indication of a major lipid role in VcINDY's transport cycle, leading directly to the implementation of the GFP-TS system and the discoveries made through that approach.

Furthermore, VcINDY SMALPs were observed to behave differently in MST assays depending whether substrates were present or absent at the point of nanodisc formation. Only VcINDY SMALPs initially formed in the presence of both sodium and succinate showed any change in thermophoretic rate under a succinate titration, suggesting that SMALPs may be able to capture the differing lipid contacts made by VcINDY throughout its transport cycle.

5.1.6 MSP Nanodiscs

Nanodisc solubilised VcINDY was, unfortunately, not fully optimised in time to greatly impact this project, although the ability to define the lipids present in this system provides the basis for extensive future work of great interest. The creation of functional VcINDY nanodiscs, the first nanodiscs to be produced in this laboratory, is itself a significant achievement.

Even at the current stage they have provided MST binding data, demonstrating their functional nature and confirming that detergent based binding affinities are largely representative of the true affinities exhibited by this protein in a lipid environment.

Through the use of these methods we are therefore able to build a broad and detailed model of VcINDY and its interactions with substrates, accounting for dynamics, the intricacies of substrate binding, binding affinities, and the interplay of lipids with substrates.

5.2 The New Model of VcINDY Substrate Transport

The current understanding of VcINDY transport is discussed in 1.10.3 Transport. To summarise; each VcINDY monomer is known to bind three sodium ions and one succinate [9], with two of these ions located below the succinate in the binding pocket [48][3], although no ordered binding has previously been experimentally verified. Substitution of sodium for lithium is known to permit slight transport rates, indicating a degree of cation flexibility [73]. The tricarboxylate citrate is able to bind in place of succinate [48][3], while dicarboxylates, specifically fumarate, malate, and oxaloacetate, can be transported [73], showing flexibility to also occur in anion binding.

With suitable substrates bound, VcINDY conducts transport through elevator like rigid body movement of the transport domains, translocating the binding site across the membrane [81].

Two crystallographic studies have produced models of the inward-facing-state [48][3], and computational modelling has allowed prediction of the appearance of the outward-facing-state [81], illustrating the current two state model of transport.

Further details, such as the specifics of substrate discrimination, the existence of intermediate states, local conformational changes, and lipid interactions were previously unknown.

Combining the knowledge gained throughout this body of work, a new, greatly expanded, transport cycle model can be proposed (Figure 5.2.5-1). This will be discussed beginning with sodium binding to the outward facing state.

5.2.1 Cation Binding

Sodium binding must precede succinate binding, in keeping with crystal structure based predictions [48][3], a rule manifesting throughout this thesis as the absolute requirement of sodium presence for any succinate based binding effects to be observed. This includes, without exception or omission, the results of 15 single cysteine accessibility assays, multiple CPM dye-based thermostability assays,

and thermophoresis based binding assays. Microscale thermophoresis allowed the K_d for the sodium binding event to be estimated as 140.5 ± 0.80 (S.E.) mM.

During this cation binding step there are two distinct modes of discrimination. The first appears to be steric, with thermostability assays finding that while sodium and lithium can bind to VcINDY, stabilising the protein to an identical extent, potassium cannot bind, putting the maximum ion size somewhere between 0.1 and 0.14 nm.

The second is likely based on the coordination strength of the ion. A combination of evidence from thermostability and accessibility assays suggests that as sodium binds, the protein undergoes significant conformational changes, entering an occluded hairpin open conformation which is receptive to succinate binding. While ions such as lithium are able to interact, their inability to effectively induce this conformational change results in very weak succinate binding potential, as observed in thermostability assays.

This is in good agreement with previous transport data [73], and provides a clear molecular explanation for behaviours previously observed.

This sodium binding step, in addition to readying the protein for succinate binding must also prevent transition between the inward and outward facing states in order to prevent sodium leakage.

5.2.2 Anion Binding

Once sodium binding has taken place, anion binding is possible. In keeping with previous transport inhibition work [73], dicarboxylates similar to succinate are observed to bind, however a far greater resolution of this binding flexibility was established herein.

Anion discrimination is largely based upon a Molecular Ruler principle. Based on existing crystal structures, the majority of succinate binding interactions are performed by two carboxyl binding regions, consisting of residues N151 and T152 in the first, S377 and N378 in the second [48][3].

Successful interaction with these regions is critical for successful binding, with molecules unable to

present two carboxyl regions approximately 3.8 nm apart unable to effectively bind VcINDY, as observed in extensive thermostability based substrate screens.

The binding of succinate was observed to take place with a K_d of 3.9 ± 1.4 (S.E.) mM, as measured through thermophoresis binding assays in detergent, and similarly confirmed in nanodiscs containing *E. coli* total lipid extract lipids. The binding of succinate, or similar suitable substrate, has several effects upon the protein. It is possible that one of these is to trigger the exchange of interacting lipids from preferentially phosphatidylglycerol and cardiolipins to phosphatidylethanolamines, observed in aggregation based thermostability assays and supported by native lipid nanodisc based work. Another is to cause the movement of hairpin loops to closed, inaccessible, conformations as detected through accessibility assays. With these two induced changes the protein is able to undergo translocation.

This presents two possible triggers for translocation. Under the Hairpin Trigger model, the hairpin regions are the major regulators of translocation. According to this model, sodium binding induces the occluded hairpin open state, which is sterically unable to undergo translocation. Upon binding of succinate, these hairpin regions move to the closed positions, removing the blockage to translocation and triggering coupled transport.

Under the Lipid Lock model, the roll of lipid interactions is of greater importance. The rigid body movement of transport domains through the membrane necessitates complex interactions with the surrounding lipids, allowing them a potential regulatory role. The sodium bound protein interacts preferentially with PG and CA, which may stabilise the conformation of VcINDY and are unable to facilitate the rigid body translocation. Upon succinate binding, the PG and CA interactions are exchanged for PE interactions, which may fundamentally alter the relationship between VcINDY and the surrounding membrane, facilitating the movement of the transport domain through the lipid environment. In this way it is possible that substrate driven changes in lipid interactions may allow control of the transport cycle.

These two models are both plausible based upon current data for VcINDY dynamics, and it is possible that both contain an element of truth. Examination and testing of these would form the basis of further research of interest.

5.2.3 Substrate Release

As VcINDY is a secondary active transporter, using gradient energy to drive transport, substrates are likely released through a reversal of their binding process; i.e. release of succinate and relaxing of the hairpin regions, followed by release of sodium and exit from the occluded state.

It has been proposed that substrate release from the inward facing state of Glt_{Ph} is triggered by the lower sodium concentration found in the cytoplasm compared to the periplasm, encouraging sodium dissociation, and therefore driving substrate release into the cell [13]. It is likely that a similar process may encourage the release of VcINDY's substrates once transported into the cell.

5.2.4 Predictions of apo state behaviour

In order to carry out transport, it is necessary that the apo state must be able to transition between inward and outward facing conformations relatively freely. The nature of this movement is currently not well elucidated, although predictions can be made.

The apo state of the binding site must first be considered. In this regard, comparisons to other elevator mechanism transporters are of use. In some elevator mechanism transporters, such as Glt_{Ph} and Glt_{Pk}, the apo state is maintained through the orientation of charged binding residues so that they balance one another, with an arginine acting as a substitute substrate [79][78]. In others, such as CitS, the charged residues of the binding site are instead satisfied through hydration, interacting with polar water molecules [80]. VcINDY is unusual in that it does not possess charged residues in its binding site (see 1.10.2 Substrate Binding) and as such the stabilisation of the binding site is expected to be a less demanding process than that of the Glt_P or Cit binding sites. It can therefore be proposed that the mild route of binding site hydration would be sufficient in this case [3].

Next, the mode of apo state translocation must be considered. Two potential translocation locks have been discussed above, in the Hairpin Trigger and Lipid Lock models. The apo state would have to be able to unlock translocation similarly to the fully loaded state, and as such, depending on the truth behind these proposed models, this may require the hairpins to be capable of closing with no substrates present, and the lipid exchange to PE lipids to occur.

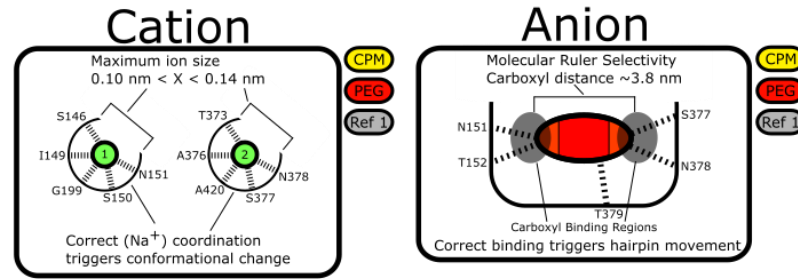
5.2.5 VcINDY Transport Mechanism Classification

As discussed in 1.10.3 Transport, the form of elevator mechanism transport carried out by VcINDY was previously unknown. Herein it has been observed that both hairpin regions move significantly in response to binding, suggesting that VcINDY is a Fixed Barrier Two Gate transporter. This is consistent with the positioning of VcINDY's binding site at the interface between the scaffold and transport domains; a common architectural feature shared by all known elevator mechanism transporters of this type [15].

VcINDY Transport Cycle

A schematic diagram showing the newly extended transport cycle of VcINDY, incorporating data derived from multiple experimental approaches. Some obscure steps remain, and in these cases speculation is used. It is hoped that future work may address the remaining unknowns of the cycle, and continue to improve upon the current level of detail.

- PEG Cystine Accessibility Assays
- CPM Fluorescent Thermostability Assays
- GFP Aggregation Thermostability Assays
- MST Thermophoresis Binding Assays
- SMA SMA based native lipid nanodiscs
- MSP MSP based nanodiscs
- Ref 1 Nie et al 2017
- Ref 2 Mulligan et al 2014



Sodium binding precedes succinate binding ● ● ●

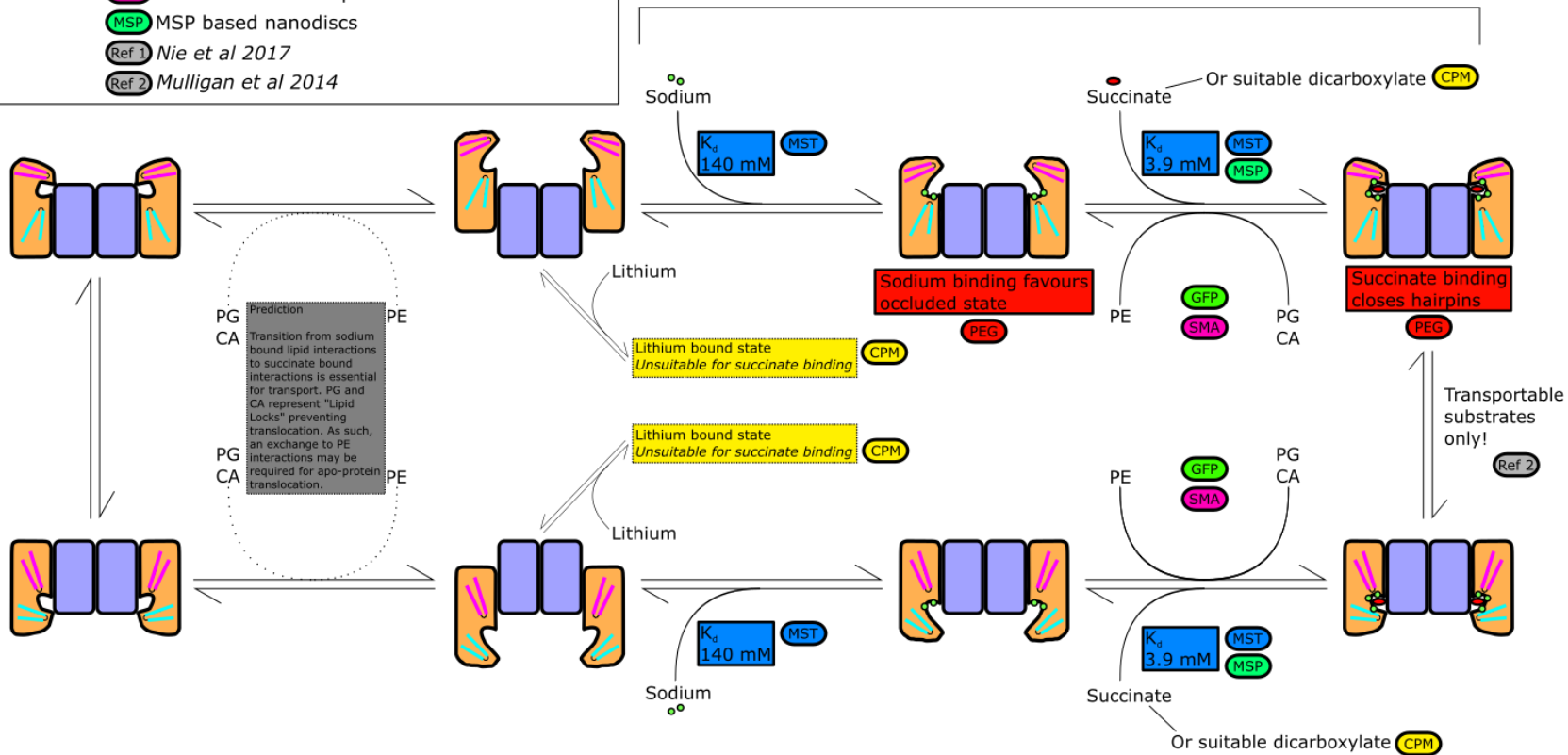


Figure 5.2.5-1 Proposed updated transport cycle for VcINDY, showing which chapters of this thesis provide supporting information for each step. Hairpin regions are shown as pink and light blue rectangles. The binding of at least two sodium ions to apo-VcINDY occurs with a K_d of 145 ± 0.80 (S.E.) mM, resulting in the movement of VcINDY to a partially occluded state, with open hairpin gating regions. This occluded, hairpin open, state, is primed for succinate binding. While lithium may bind in place of sodium, lithium binding does not result in a similar readying for subsequent succinate binding. Succinate, or another suitable dicarboxylate, binds to the already sodium bound state of VcINDY with a K_d of 3.9 ± 1.4 (S.E.) mM, resulting in the closure of hairpin gating regions, and an apparent shift in VcINDY's lipid binding preferences from PG and CA to PE. VcINDY is now ready for binding site translocation across the membrane, as achieved through rigid body movements of the transport domains. After translocation is complete, the bound substrates are released in reverse order. Succinate is released, resulting in an opening of the hairpin gating regions, and a change of lipid interactions from PE to PG and CA. Next, sodium ions are released, allowing movement of the protein out of the occluded state. It is unknown at the present time whether an exchange of lipid interactions from PG and CA to PE is required for translocation of the binding site across to the membrane to occur in the apo form of the protein, however the lipid exchange is speculatively proposed here in order to complete the transport cycle model. Abbreviations: PE = phosphatidylethanolamine. PG = phosphatidylglycerol. CA = cardiolipins.

5.3 Unknowns and Future Work

5.3.1 Apo State and Unloaded Translocation

As already discussed above as part of the proposed transport cycle, unloaded VcINDY has not yet been structurally observed or modelled. While some predictions are above made based upon binding site architecture and the behaviour of comparable transporters, these require experimental verification.

Furthermore, a combination of accessibility assays and thermostability assays carried out within this thesis demonstrated that sodium binding is required before the binding site becomes capable of succinate binding. As such it would be of interest to examine whether the non-sodium bound binding site is capable of interacting with any small molecules. Conducting screening similar to the CPM thermoflour assay conducted herein with sodium replaced by either the non-interacting potassium or the poorly interacting lithium could allow for the identification of *apo*-VcINDY binders. This could both provide information on the *apo* state of VcINDY's binding site, and inform the design of VcINDY apo state binding inhibitors.

5.3.2 Binding Site Deconvolution

There are still many major uncertainties surrounding VcINDY and its transport cycle.

The current work takes place largely within nanodiscs and detergent micelles, and as such both the intracellular and extracellular faces are equally accessible. Accordingly, any data gathered is representative of substrate interaction with both of these binding sites.

In some elevator mechanism transporters, these sites can differ greatly in behaviour while appearing similar. A prime and well-studied example of this are the inwards and outwards facing binding sites in GlTPh, in which the binding site is contained within the transport domain for inward, outward, and predicted transitional conformations [192][13][193]. Even with this binding site conservation, the properties of the inward- and outward-facing binding sites are highly divergent. While

measurements of Gl_{Tph} aspartate affinity have found this substrate to bind equally well to the inward-facing and outward-facing binding site [194], measurements of transport inhibition (K_i) by a range of compounds has identified clear differences between the two binding sites [195]. For example the compound L-TFB-TBOA inhibits aspartate transport 132 fold more effectively from the outward-facing-binding site than the inward-facing binding site, indicating clear variations in relative selectivities and inhibitor affinities of these two binding sites [195]. Another example is CitS, in which the substrate makes the vast majority of its binding contacts with the transport domain, but does carry out slight interactions with the adjacent scaffold domain in the outward facing binding site, and possibly during translocation [196]. In this case, substrate interactions vary greatly between inwards and outwards facing crystal structures [196].

As such, it is seen that even in relatively unchanging elevator mechanism binding sites the nature of substrate interaction changes between the inward and outward facing state. VcINDY is structurally distinct from these examples in that the observed outwards facing binding site includes interactions with both the transport and scaffold domains [48][3], necessitating new interactions to be formed with alternate residues in the inwards facing conformation [81]. Therefore, in a type of system where subtle differences greatly impact the behaviour of the inwards and outwards facing binding sites, VcINDY shows unsubtle, large scale, differences in these sites. It is overwhelmingly probable that these two sites possess differing properties, and that the data gathered herein relating to binding, while exceedingly useful for our understanding of VcINDY, represents a combination of the action of these two binding sites which must be deconvoluted in future work.

There are two main possible approaches to deconvoluting the behaviour of VcINDY's two binding sites. The first is to lock the protein into desired conformations through the cross linking of strategically located cysteine pairs, allowing the examination of each binding site's properties individually. This approach to locking VcINDY has already been demonstrated in previous literature [81], demonstrating that oriented forms of VcINDY may be readily generated for analysis.

The second is to use cysteine targeting modifications which are known to deactivate the protein. These modifications could be in the form of disruptive cross links or the introduction of inhibitory groups. The important aspect of this approach is to ensure the cross links are accessible on either the intracellular or extracellular side of the membrane only. Once reconstituted into proteoliposomes, VcINDY is oriented in both directions. If a non-membrane permeable cysteine targeting agent is added to the inside or outside of the proteoliposome, this will deactivate only one orientation of VcINDY, i.e. the orientation with the accessible deactivating cysteine target sites, leaving the other orientation active. This general technique has been proven effective in the deconvolution of GltPh binding sites [26][195], making it a promising approach for VcINDY study.

5.3.3 Lipid Interaction Exploration

In this thesis, a dynamic and complex role of lipids was discovered. To this authors knowledge this is the first indication of dynamic interactions between substrates and lipids for an elevator type transporter, however far more work is required to properly understand this aspect of transport. For example, the full cycle of lipid interactions needs to be examined, the effects on transport need to be explored, the effects on binding affinity need to be quantified, and the interactions need to be examined in more detail than simply PE, PG, CA, etc, given the wide range of lipid molecules included in each umbrella group.

To date there has been very little experimental examination of the relationship between lipids and elevator function due to the difficulties involved in investigating these interactions. What little there has been is insufficient to allow us to make predictions for VcINDY, but sufficient to hint at further complexities (see 1.3 The Elevator Mechanism – The Importance of Lipids). Examinations of GltPh in liposomal transport assays have shown the level of methylation upon PE lipids to clearly alter transport rates [26], while cryo-EM examination of nanodiscs has observed conformationally dependent deformations of the lipid bilayer as inwards facing protomers induce clear distortions [27]. Tantalisingly, the bilayer deformations caused by a movement to the inward facing state incurs

an energetic cost of around 6 – 7 kcal/mol per protomer [28], a cost which appears affordable if driven by substrate binding energy [29]. Substrate binding in Glt_{Ph} must, therefore impact lipid interactions. Tantalisingly, molecular dynamic simulations of VcINDY have suggested a bilayer deformation to occur as a result of translocation in this transporter as well [27], suggesting a similar process to occur, although no energetic costs for VcINDY bilayer deformation have yet been calculated. Given the apparently dynamic lipid interactions which appear to occur during Glt_{Ph} and VcINDY transport, representatives of the SLC1 and DASS families, it is worth speculating whether this manner of lipid interaction may be a common feature of elevator mechanism transport. Far more work, both upon these two transporters and other elevator mechanism transporters, will be required to understand whether this is the case.

So while there is exciting evidence that the lipid observations made herein for VcINDY indicate a generally dynamic relationship between elevator mechanism transporters and their lipid environments, the details of these relationships are unclear for all relevant proteins.

Not only is more research on this topic of great interest for VcINDY, further research could allow VcINDY to lead the way in our understanding of elevator mechanism transporter lipid interactions in general.

This thesis has developed effective VcINDY native lipid nanodiscs, capable of isolating various lipid environments, along with functional MSP based VcINDY nanodiscs. These are known to be compatible with binding affinity determination through MST and conformational dynamics monitoring through cysteine accessibility assays. Additionally, these nanodiscs are ready to be trialled with the VcINDY compatible thermostability assays of CD, CPM thermoflour, and GFP-TS.

For cases in which detergent solubilisation is preferred, the effectiveness of supplementing detergent solubilised VcINDY with lipids has been demonstrated and is compatible with both the GFP-TS thermostability the MST binding affinity assay.

As such, the toolbox provided to future researchers wishing to examine the relationships between VcINDY and lipids is vast. It should be entirely achievable to further analyse lipid preferences throughout VcINDY's transport cycle, while also examining the effects of various lipids upon VcINDY's behaviour as detected through binding affinities, binding specificities, and conformational changes. Even the determination of lipid binding affinities through carefully designed MST experiments is not an unachievable goal given the tools provided by this project.

5.3.4 *Vibrio cholerae* Pathobiology

The sequence of VcINDY used here, and in referenced works, originates from the *Vibrio Cholerae* pathogenic strain N16961 [197]. Given the recombinant use of this protein as a DASS family representative, this biological context is easily overlooked. The role of VcINDY in pathobiology is discussed in 1.9 INDY Proteins – *Vibrio cholerae*, however to summarise drastically, VcINDY appears to be downregulated during infection to prevent depletion of host succinate, which would otherwise lead to increased host lipolysis and host death [74]. The downregulation of VcINDY during infection appears to be evolutionarily conserved, and is likely important in allowing sufficient host survival for the spread of the bacteria [74].

Given that VcINDY is only downregulated threefold in this process, it is interesting to speculate whether further suppression of VcINDY function through targeted inhibitor treatment would further increase host survival. In this work the principles behind VcINDY substrate interactions have been established and novel interacting small molecules have been identified. Using this information to develop potent VcINDY inhibitors, which may reduce the lethality of *Vibrio Cholerae*, infections is therefore a research avenue of great interest.

5.3.5 Concluding Remarks

This project has revolved around the development, optimisation, and application of a range of techniques to the study of VcINDY. Some of these approaches have allowed rapid advancements in our understanding of this DASS family transporter, resulting in the formation of a new, and more detailed, model of VcINDY substrate transport.

It is remarkable to consider that the first publication demonstrating VcINDY to operate through an elevator mechanism emerged in 2016 [81], merely a year before this project began. Now, in 2020 there are multiple publications being developed based upon the data contained herein, each expanding the transport cycle. From hairpin triggers, to ionic coordination discrimination, to an active role of lipids in the transport cycle; many discoveries have been made.

Far more discoveries are still to be made, however. Some of the approaches in this thesis, such as nanodisc solubilisation and MST assays have barely been explored, leaving a great deal of clear experimental work ahead. In addition to these techniques, a grand array of questions have been raised in this thesis, from the differing properties of VcINDY's binding sites to the extent of the role of lipids in the transport cycle.

VcINDY is the most well understood member of the DASS family, although it far less studied than Glt_{Ph} , the model member of the SLC1 family of elevator mechanism transporters. As elevator mechanism transporters continue to be studied it will be interesting to see how this class of transporters continues to diversify, and whether the current gate and barrier classifications, which allowed prediction of VcINDY's own gating mechanism, will continue to be sufficient.

Finally, it will be fascinating to observe whether the potential of mINDY as a therapeutic target will be fulfilled, providing us with cures to type 2 diabetes and obesity. While the ethical production and implementation of a drug which, while of great potential for the treatment of age related diseases, can be taken in substitution of exercise and in protection from an indulgent diet, represents

dilemma for those differently qualified to myself, it is certainly exciting that the creation of such a drug may be possible.

6 BIBLIOGRAPHY

- 1 Bullen, K. E., de Robin, G. Q. and Peter Mitchell, B. D. (1957) A GENERAL THEORY OF MEMBRANE TRANSPORT FROM STUDIES OF BACTERIA. Katz, S., Bull. Seism. Soc. Amer, 3 Press.
- 2 Zhou, Y., Morais-Cabral, J. H., Kaufman, A. and Mackinnon, R. (2001) Chemistry of ion coordination and hydration revealed by a K⁺ channel-Fab complex at 2.0 Å resolution. Nature, Nature Publishing Group **414**, 43–48.
- 3 Nie, R., Stark, S., Symersky, J., Kaplan, R. S. and Lu, M. (2017) Structure and function of the divalent anion/Na⁺ symporter from *Vibrio cholerae* and a humanized variant. Nat. Commun., Nature Publishing Group **8**, 15009.
- 4 Deng, D., Xu, C., Sun, P., Wu, J., Yan, C., Hu, M. and Yan, N. (2014) Crystal structure of the human glucose transporter GLUT1. Nature, Nature Publishing Group **510**, 121–125.
- 5 Nyblom, M., Poulsen, H., Gourdon, P., Reinhard, L., Andersson, M., Lindahl, E., Fedosova, N. and Nissen, P. (2013) Crystal structure of Na⁺, K⁺-ATPase in the Na⁺-bound state. Science (80-.), American Association for the Advancement of Science **342**, 123–127.
- 6 Matulef, K., Annen, A. W., Nix, J. C. and Valiyaveetil, F. I. (2016) Individual Ion Binding Sites in the K⁺ Channel Play Distinct Roles in C-type Inactivation and in Recovery from Inactivation. Structure, Cell Press **24**, 750–761.
- 7 Holman, G. D. (2020, June 26) Structure, function and regulation of mammalian glucose transporters of the SLC2 family. Pflugers Arch. Eur. J. Physiol., Springer.
- 8 Vergara-Jaque, A., Fenollar-Ferrer, C., Kaufmann, D. and Forrest, L. R. (2015) Repeat-swap homology modeling of secondary active transporters: Updated protocol and prediction of elevator-type mechanisms. Front. Pharmacol. **6**, 183.

- 9 Fitzgerald, G. A., Mulligan, C. and Mindell, J. A. (2017) A general method for determining secondary active transporter substrate stoichiometry. *Elife* **6**.
- 10 Accardi, A. and Picollo, A. (2010, August 1) CLC channels and transporters: Proteins with borderline personalities. *Biochim. Biophys. Acta - Biomembr.*, Elsevier.
- 11 Drew, D. and Boudker, O. (2016) Shared Molecular Mechanisms of Membrane Transporters. *Annu. Rev. Biochem.*, Annual Reviews **85**, 543–572.
- 12 Ryan, R. M., Mitrovic, A. D. and Vandenberg, R. J. (2004) The chloride permeation pathway of a glutamate transporter and its proximity to the glutamate translocation pathway. *J. Biol. Chem.*, American Society for Biochemistry and Molecular Biology **279**, 20742–20751.
- 13 Reyes, N., Ginter, C. and Boudker, O. (2009) Transport mechanism of a bacterial homologue of glutamate transporters. *Nature*, Nature Publishing Group **462**, 880–885.
- 14 Dechancie, J., Shrivastava, I. H. and Bahar, I. (2011) The mechanism of substrate release by the aspartate transporter Glt Ph: Insights from simulations. *Mol. Biosyst.*, Royal Society of Chemistry **7**, 832–842.
- 15 Garaeva, A. A. and Slotboom, D. J. (2020) Elevator-type mechanisms of membrane transport. *Biochem. Soc. Trans.*, Portland Press Ltd.
- 16 Ji, Y., Postis, V. L. G., Wang, Y., Bartlam, M. and Goldman, A. (2016) Transport mechanism of a glutamate transporter homologue GltPh. *Biochem. Soc. Trans.* **44**, 898–904.
- 17 Riederer, E. A. and Valiyaveetil, F. I. (2019) Investigation of the allosteric coupling mechanism in a glutamate transporter homolog via unnatural amino acid mutagenesis. *Proc. Natl. Acad. Sci. U. S. A.*, National Academy of Sciences **116**, 15939–15946.
- 18 Hirschi, M., Johnson, Z. L. and Lee, S. Y. (2017) Visualizing multistep elevator-like transitions of a nucleoside transporter. *Nature*, Nature Publishing Group **545**, 66–70.

- 19 Hu, N. J., Iwata, S., Cameron, A. D. and Drew, D. (2011) Crystal structure of a bacterial homologue of the bile acid sodium symporter ASBT. *Nature* **478**, 408–411.
- 20 Zhou, X., Levin, E. J., Pan, Y., McCoy, J. G., Sharma, R., Kloss, B., Bruni, R., Quick, M. and Zhou, M. (2014) Structural basis of the alternating-access mechanism in a bile acid transporter. *Nature*, Nature Publishing Group **505**, 569–573.
- 21 Garaeva, A. A., Oostergetel, G. T., Gati, C., Guskov, A., Paulino, C. and Slotboom, D. J. (2018) Cryo-EM structure of the human neutral amino acid transporter ASCT2. *Nat. Struct. Mol. Biol.*, Nature Publishing Group **25**, 515–521.
- 22 Butchbach, M. E. R., Tian, G., Guo, H. and Lin, C. L. G. (2004) Association of excitatory amino acid transporters, especially EAAT2, with cholesterol-rich lipid raft microdomains: Importance for excitatory amino acid transporter localization and function. *J. Biol. Chem.*, American Society for Biochemistry and Molecular Biology **279**, 34388–34396.
- 23 Garaeva, A. A., Guskov, A., Slotboom, D. J. and Paulino, C. (2019) A one-gate elevator mechanism for the human neutral amino acid transporter ASCT2. *Nat. Commun.*, Nature Publishing Group **10**, 1–8.
- 24 Yu, X., Plotnikova, O., Bonin, P. D., Subashi, T. A., McLellan, T. J., Dumlao, D., Che, Y., Dong, Y., Y., Carpenter, E. P., West, G. M., et al. (2019) Cryo-EM structures of the human glutamine transporter SLC1a5 (ASCT2) in the outward-facing conformation. *Elife*, eLife Sciences Publications Ltd **8**.
- 25 Canul-Tec, J. C., Assal, R., Cirri, E., Legrand, P., Brier, S., Chamot-Rooke, J. and Reyes, N. (2017) Structure and allosteric inhibition of excitatory amino acid transporter 1. *Nature*, Nature Publishing Group **544**, 446–451.
- 26 McIlwain, B. C., Vandenberg, R. J. and Ryan, R. M. (2015) Transport rates of a glutamate transporter homologue are influenced by the lipid bilayer. *J. Biol. Chem.* **290**, 9780–9788.

- 27 Arkhipova, V., Guskov, A. and Slotboom, D. J. (2020) Structural ensemble of a glutamate transporter homologue in lipid nanodisc environment. *Nat. Commun., Nature Research* **11**, 1–9.
- 28 Zhou, W., Fiorin, G., Anselmi, C., Karimi-Varzaneh, H. A., Poblete, H., Forrest, L. R. and Faraldo-Gómez, J. D. (2019) Large-scale state-dependent membrane remodeling by a transporter protein. *Elife, eLife Sciences Publications Ltd* **8**.
- 29 Heinzlmann, G., Baştuğ, T. and Kuyucak, S. (2011) Free energy simulations of ligand binding to the aspartate transporter Glt Ph. *Biophys. J., Cell Press* **101**, 2380–2388.
- 30 Prakash, S., Cooper, G., Singhi, S. and Saier, M. H. (2003) The ion transporter superfamily. *Biochim. Biophys. Acta - Biomembr., Elsevier* **1618**, 79–92.
- 31 Pajor, A. M. (2014, January 10) Sodium-coupled dicarboxylate and citrate transporters from the SLC13 family. *Pflugers Arch. Eur. J. Physiol., Springer*.
- 32 Knauf, F., Rogina, B., Jiang, Z., Aronson, P. S. and Helfand, S. L. (2002) Functional characterization and immunolocalization of the transporter encoded by the life-extending gene *Indy*. *Proc. Natl. Acad. Sci., National Academy of Sciences* **99**, 14315–14319.
- 33 Inoue, K., Fei, Y. J., Huang, W., Zhuang, L., Chen, Z. and Ganapathy, V. (2002) Functional identity of *Drosophila melanogaster Indy* as a cation-independent, electroneutral transporter for tricarboxylic acid-cycle intermediates. *Biochem. J., Portland Press* **367**, 313–319.
- 34 Knauf, F., Mohebbi, N., Teichert, C., Herold, D., Rogina, B., Helfand, S., Gollasch, M., Luft, F. C. and Aronson, P. S. (2006) The life-extending gene *Indy* encodes an exchanger for Krebs-cycle intermediates. *Biochem. J., Portland Press* **397**, 25–29.
- 35 BuschSB, A. E., WaldeggerS, S., HerzerS, T., Bibedl, J., Markovichl, D., Murefl, H. and LangS, F. (1994) Electrogenic Cotransport of Na⁺ and Sulfate in *Xenopus* Oocytes Expressing the Cloned Na⁺/SO₄ Transport Protein. *ASBMB*.

- 36 Pajor, A. M. (1996) Molecular cloning and functional expression of a sodium-dicarboxylate cotransporter from human kidney. *Am. J. Physiol., Am J Physiol* **270**.
- 37 Burckhardt, B. C., Lorenz, J., Kobbe, C. and Burckhardt, G. (2005) Substrate specificity of the human renal sodium dicarboxylate cotransporter, hNaDC-3, under voltage-clamp conditions. *Am. J. Physiol. Physiol., American Physiological Society* **288**, F792–F799.
- 38 Markovich, D., Regeer, R. R., Kunzelmann, K. and Dawson, P. A. (2005) Functional characterization and genomic organization of the human Na⁺-sulfate cotransporter hNaS2 gene (SLC13A4). *Biochem. Biophys. Res. Commun., Academic Press Inc.* **326**, 729–734.
- 39 Gopal, E., Miyauchi, S., Martin, P. M., Ananth, S., Srinivas, S. R., Smith, S. B., Prasad, P. D. and Ganapathy, V. (2007) Expression and functional features of NaCT, a sodium-coupled citrate transporter, in human and rat livers and cell lines. *Am. J. Physiol. Liver Physiol., American Physiological Society* **292**, G402–G408.
- 40 Inoue, K., Zhuang, L. and Ganapathy, V. (2002) Human Na⁺-coupled citrate transporter: Primary structure, genomic organization, and transport function. *Biochem. Biophys. Res. Commun., Academic Press* **299**, 465–471.
- 41 Zwart, R., Peeva, P. M., Rong, J. X. and Sher, E. (2015) Electrophysiological characterization of human and mouse sodium-dependent citrate transporters (NaCT/SLC13A5) reveal species differences with respect to substrate sensitivity and cation dependence. *J. Pharmacol. Exp. Ther., American Society for Pharmacology and Experimental Therapy* **355**, 247–254.
- 42 Uhlén, M., Fagerberg, L., Hallström, B. M., Lindskog, C., Oksvold, P., Mardinoglu, A., Sivertsson, Å., Kampf, C., Sjöstedt, E., Asplund, A., et al. (2015) Tissue-based map of the human proteome. *Science (80-.), American Association for the Advancement of Science* **347**.
- 43 Markovich, D. and Murer, H. (2004, February 12) The SLC13 gene family of sodium sulphate/carboxylate cotransporters. *Pflugers Arch. Eur. J. Physiol., Springer*.

- 44 Dewulf, J. P., Wiame, E., Dorboz, I., Elmaleh-Bergès, M., Imbard, A., Dumitriu, D., Rak, M., Bourillon, A., Helaers, R., Malla, A., et al. (2019) SLC13A3 variants cause acute reversible leukoencephalopathy and α -ketoglutarate accumulation. *Ann. Neurol.*, John Wiley and Sons Inc. **85**, 385–395.
- 45 Birkenfeld, A. L., Lee, H. Y., Guebre-Egziabher, F., Alves, T. C., Jurczak, M. J., Jornayvaz, F. R., Zhang, D., Hsiao, J. J., Martin-Montalvo, A., Fischer-Rosinsky, A., et al. (2011) Deletion of the mammalian INDY homolog mimics aspects of dietary restriction and protects against adiposity and insulin resistance in mice. *Cell Metab.* **14**, 184–195.
- 46 Markovich, D. (2014, January 6) Na⁺-sulfate cotransporter SLC13A1. *Pflugers Arch. Eur. J. Physiol.*, Springer.
- 47 Rakoczy, J., Zhang, Z., Bowling, F. G., Dawson, P. A. and Simmons, D. G. (2015, November 1) Loss of the sulfate transporter Slc13a4 in placenta causes severe fetal abnormalities and death in mice. *Cell Res.*, Nature Publishing Group.
- 48 Mancusso, R., Gregorio, G. G., Liu, Q. and Wang, D. N. (2012) Structure and mechanism of a bacterial sodium-dependent dicarboxylate transporter. *Nature*, NIH Public Access **491**, 622–626.
- 49 Boynton, S. and Tully, T. (1992) *latheo*, a new gene involved in associative learning and memory in *Drosophila melanogaster*, identified from P element mutagenesis. *Genetics* **131**.
- 50 Rogina, B., Reenan, R. A., Nilsen, S. P. and Helfand, S. L. (2000) Extended Life-Span Conferred by Cotransporter Gene Mutations in *Drosophila*. *Science (80-)*. **290**, 2137–2140.
- 51 Lin, Y. J., Seroude, L. and Benzer, S. (1998) Extended life-span and stress resistance in the *Drosophila* mutant *methuselah*. *Science (80-)*, American Association for the Advancement of Science **282**, 943–946.
- 52 Araújo, A. R., Reis, M., Rocha, H., Aguiar, B., Morales-Hojas, R., Macedo-Ribeiro, S., Fonseca,

- N. A., Reboiro-Jato, D., Reboiro-Jato, M., Fdez-Riverola, F., et al. (2013) The *Drosophila melanogaster* methuselah Gene: A Novel Gene with Ancient Functions. *PLoS One, Public Library of Science* **8**.
- 53 Gimenez, L. E. D., Ghildyal, P., Fischer, K. E., Hu, H., Ja, W. W., Eaton, B. A., Wu, Y., Austad, S. N. and Ranjan, R. (2013) Modulation of methuselah expression targeted to *Drosophila* insulin-producing cells extends life and enhances oxidative stress resistance. *Aging Cell, Aging Cell* **12**, 121–129.
- 54 Fei, Y. J., Inoue, K. and Ganapathy, V. (2003) Structural and functional characteristics of two sodium-coupled dicarboxylate transporters (ceNaDC1 and ceNaDC2) from *Caenorhabditis elegans* and their relevance to life span. *J. Biol. Chem., American Society for Biochemistry and Molecular Biology* **278**, 6136–6144.
- 55 Fei, Y.-J., Liu, J.-C., Inoue, K., Zhuang, L., Miyake, K., Miyauchi, S. and Ganapathy, V. (2004) Relevance of NAC-2, an Na⁺-coupled citrate transporter, to life span, body size and fat content in *Caenorhabditis elegans*. *Biochem. J.* **379**, 191–8.
- 56 Toivonen, J. M., Walker, G. A., Martinez-Diaz, P., Bjedov, I., Driège, Y., Jacobs, H. T., Gems, D. and Partridge, L. (2007) No influence of Indy on lifespan in *Drosophila* after correction for genetic and cytoplasmic background effects. *PLoS Genet., Public Library of Science* **3**, 0973–0983.
- 57 Wang, P. Y. P.-Y., Neretti, N., Whitaker, R., Hosier, S., Chang, C., Lu, D., Rogina, B. and Helfand, S. L. (2009) Long-lived Indy and calorie restriction interact to extend life span. *Proc. Natl. Acad. Sci., National Academy of Sciences* **106**, 9262–9267.
- 58 Rogina, B. and Helfand, S. L. (2013) Indy Mutations and *Drosophila* Longevity. *Front. Genet., Frontiers Media SA* **4**, 47.
- 59 von Loeffelholz, C., Lieske, S., Neuschäfer-Rube, F., Willmes, D. M., Raschzok, N., Sauer, I. M.,

- König, J., Fromm, M. F., Horn, P., Chatzigeorgiou, A., et al. (2017) The human longevity gene homolog INDY and interleukin-6 interact in hepatic lipid metabolism. *Hepatology* **66**, 616–630.
- 60 Li, Z., Li, D., Choi, E. Y., Lapidus, R., Zhang, L., Huang, S. M., Shapiro, P. and Wang, H. (2017) Silencing of solute carrier family 13 member 5 disrupts energy homeostasis and inhibits proliferation of human hepatocarcinoma cells. *J. Biol. Chem.*
- 61 Huard, K., Brown, J., Jones, J. C., Cabral, S., Futatsugi, K., Gorgoglione, M., Lanba, A., Vera, N. B., Zhu, Y., Yan, Q., et al. (2015) Discovery and characterization of novel inhibitors of the sodium-coupled citrate transporter (NaCT or SLC13A5). *Sci. Rep.*, Nature Publishing Group **5**, 1–13.
- 62 Nishimura, M., Suzuki, S., Satoh, T. and Naito, S. (2009) Tissue-Specific mRNA Expression Profiles of Human Solute Carrier 35 Transporters. *Drug Metab. Pharmacokinet.*, The Japanese Society for the Study of Xenobiotics **24**, 91–99.
- 63 Takeda, I., Stretch, C., Barnaby, P., Bhatnager, K., Rankin, K., Fub, H., Weljie, A., Jha, N. and Slupsky, C. (2009) Understanding the human salivary metabolome. *NMR Biomed.* **22**, 577–584.
- 64 Inoue, K., Fei, Y. J., Zhuang, L., Gopal, E., Miyauchi, S. and Ganapathy, V. (2004) Functional features and genomic organization of mouse NaCT, a sodium-coupled transporter for tricarboxylic acid cycle intermediates. *Biochem. J.*, Portland Press Ltd **378**, 949–957.
- 65 Gnoni, G. V., Priore, P., Geelen, M. J. H. and Siculella, L. (2009) The mitochondrial citrate carrier: Metabolic role and regulation of its activity and expression. *IUBMB Life*, John Wiley & Sons, Ltd **61**, 987–994.
- 66 Rogers, R. P. and Rogina, B. (2015) The role of INDY in metabolism, health and longevity. *Front. Genet.*, Frontiers Media SA.

- 67 Willmes, D. M. and Birkenfeld, A. L. (2013) The role of Indy in metabolic regulation. *Comput. Struct. Biotechnol. J., Research Network of Computational and Structural Biotechnology* **6**, e201303020.
- 68 Shimomura, I., Bashmakov, Y. and Horton, J. D. (1999) Increased levels of nuclear SREBP-1c associated with fatty livers in two mouse models of diabetes mellitus. *J. Biol. Chem., American Society for Biochemistry and Molecular Biology* **274**, 30028–30032.
- 69 Zhang, Z., Liu, H. and Liu, J. (2019, October 1) Akt activation: A potential strategy to ameliorate insulin resistance. *Diabetes Res. Clin. Pract., Elsevier Ireland Ltd.*
- 70 Kanehisa, M., Furumichi, M., Tanabe, M., Sato, Y. and Morishima, K. (2016) KEGG: new perspectives on genomes, pathways, diseases and drugs. *Nucleic Acids Res.* **45**, 353–361.
- 71 Sugimoto, M., Ikeda, S., Niigata, K., Tomita, M., Sato, H. and Soga, T. (2012) MMMDB: Mouse multiple tissue metabolome database. *Nucleic Acids Res.* **40**.
- 72 Samuel, V. T. and Shulman, G. I. (2012, March 2) Mechanisms for insulin resistance: Common threads and missing links. *Cell, Cell Press.*
- 73 Mulligan, C., Fitzgerald, G. A., Wang, D.-N. and Mindell, J. A. (2014) Functional characterization of a Na⁺-dependent dicarboxylate transporter from *Vibrio cholerae*. *J. Gen. Physiol.* **143**, 745–759.
- 74 Kamareddine, L., Wong, A. C. N., Vanhove, A. S., Hang, S., Purdy, A. E., Kierek-Pearson, K., Asara, J. M., Ali, A., Morris, J. G., Watnick, P. I., et al. (2018) Activation of *Vibrio cholerae* quorum sensing promotes survival of an arthropod host. *Nat Microbiol, NIH Public Access* **3**, 243–252.
- 75 Ball, A. S., Chaparian, R. R. and van Kessel, J. C. (2017) Quorum sensing gene regulation by LuxR/HapR master regulators in vibrios. *J. Bacteriol., American Society for Microbiology.*

- 76 Vergara-Jaque, A., Fenollar-Ferrer, C., Mulligan, C., Mindell, J. A. and Forrest, L. R. (2015) Family resemblances: A common fold for some dimeric ion-coupled secondary transporters. *J. Gen. Physiol.*, Rockefeller University Press **146**, 423–434.
- 77 Rives, M. L., Shaw, M., Zhu, B., Hinke, S. A. and Wickenden, A. D. (2016) State-dependent allosteric inhibition of the human SLC13A5 citrate transporter by hydroxysuccinic acids, PF-06649298 and PF-06761281. *Mol. Pharmacol.*, American Society for Pharmacology and Experimental Therapy **90**, 766–774.
- 78 Verdon, G., Oh, S. C., Serio, R. and Boudker, O. (2014) Coupled ion binding and structural transitions along the transport cycle of glutamate transporters. *Elife*, eLife Sciences Publications Ltd **2014**.
- 79 Jensen, S., Guskov, A., Rempel, S., Hänel, I. and Slotboom, D. J. (2013) Crystal structure of a substrate-free aspartate transporter. *Nat. Struct. Mol. Biol.*, Nature Publishing Group **20**, 1224–1227.
- 80 Kim, J. W., Kim, S. S., Kim, S. S., Lee, H., Lee, J.-O. O. and Jin, M. S. (2017) Structural insights into the elevator-like mechanism of the sodium/citrate symporter CitS. *Sci. Rep.*, Nature Publishing Group **7**.
- 81 Mulligan, C., Fenollar-Ferrer, C., Fitzgerald, G. A., Vergara-Jaque, A., Kaufmann, D., Li, Y., Forrest, L. R. and Mindell, J. A. (2016) The bacterial dicarboxylate transporter VcINDY uses a two-domain elevator-type mechanism. *Nat. Struct. Mol. Biol.* **23**, 256–263.
- 82 Lee, C., Kang, H. J., Hjelm, A., Qureshi, A. A., Nji, E., Choudhury, H., Beis, K., De Gier, J. W. and Drew, D. (2014) MemStar: A one-shot *Escherichia coli*-based approach for high-level bacterial membrane protein production. *FEBS Lett.* **588**, 3761–3769.
- 83 Lee, S. C., Knowles, T. J., Postis, V. L. G., Jamshad, M., Parslow, R. A., Lin, Y. P., Goldman, A., Sridhar, P., Overduin, M., Muench, S. P., et al. (2016) A method for detergent-free isolation of

- membrane proteins in their local lipid environment. *Nat. Protoc.*, Nature Publishing Group **11**, 1149–1162.
- 84 Kopf, A. H., Koorengevel, M. C., van Walree, C. A., Dafforn, T. R. and Killian, J. A. (2019) A simple and convenient method for the hydrolysis of styrene-maleic anhydride copolymers to styrene-maleic acid copolymers. *Chem. Phys. Lipids*, Elsevier Ireland Ltd **218**, 85–90.
- 85 Studier, F. W. (2005) Protein production by auto-induction in high density shaking cultures. *Protein Expr. Purif.* **41**, 207–234.
- 86 Kapust, R. B., Tózsér, J., Fox, J. D., Anderson, D. E., Cherry, S., Copeland, T. D. and Waugh, D. S. (2001) Tobacco etch virus protease: Mechanism of autolysis and rational design of stable mutants with wild-type catalytic proficiency. *Protein Eng.*, Oxford University Press **14**, 993–1000.
- 87 Denisov, I. G., Baas, B. J., Grinkova, Y. V. and Sligar, S. G. (2007) Cooperativity in cytochrome P450 3A4: Linkages in substrate binding, spin state, uncoupling, and product formation. *J. Biol. Chem.*, American Society for Biochemistry and Molecular Biology **282**, 7066–7076.
- 88 Artimo, P., Jonnalagedda, M., Arnold, K., Baratin, D., Csardi, G., de Castro, E., Duvaud, S., Flegel, V., Fortier, A., Gasteiger, E., et al. (2012) ExPASy: SIB bioinformatics resource portal. *Nucleic Acids Res.* **40**, W597-603.
- 89 Schneider, C. A., Rasband, W. S. and Eliceiri, K. W. (2012) NIH Image to ImageJ: 25 years of image analysis. *Nat. Methods* **9**, 671–675.
- 90 Crichton, P. G., Lee, Y., Ruprecht, J. J., Cerson, E., Thangaratnarajah, C., King, M. S. and Kunji, E. R. S. (2015) Trends in thermostability provide information on the nature of substrate, inhibitor, and lipid interactions with mitochondrial carriers. *J. Biol. Chem.*, American Society for Biochemistry and Molecular Biology **290**, 8206–17.
- 91 Nji, E., Chatzikyriakidou, Y., Landreh, M. and Drew, D. (2018) An engineered thermal-shift

- screen reveals specific lipid preferences of eukaryotic and prokaryotic membrane proteins. *Nat. Commun.* **9**.
- 92 R Core Team. (2017) R: A Language and Environment for Statistical Computing, Vienna, Austria.
- 93 Xue, M., Cheng, L., Faustino, I., Guo, W. and Marrink, S. J. (2018) Molecular Mechanism of Lipid Nanodisk Formation by Styrene-Maleic Acid Copolymers. *Biophys. J.* **115**, 494–502.
- 94 Tonge, S. (2005) Composition for use in the solubilisation of hydrophobic active agents. UK Patent GB2426703A, United Kingdom.
- 95 Tonge, S. and HARPER, A. (2006) Solubilised peptide or protein formulations using molecular assemblies comprising a surfactant and a lipid. UK Patent GB2464393, United Kingdom.
- 96 Teo, A. C. K., Lee, S. C., Pollock, N. L., Stroud, Z., Hall, S., Thakker, A., Pitt, A. R., Dafforn, T. R., Spickett, C. M. and Roper, D. I. (2019) Analysis of SMALP co-extracted phospholipids shows distinct membrane environments for three classes of bacterial membrane protein. *Sci. Rep.*
- 97 Reading, E., Hall, Z., Martens, C., Haghighi, T., Findlay, H., Ahdash, Z., Politis, A. and Booth, P. J. (2017) Interrogating Membrane Protein Conformational Dynamics within Native Lipid Compositions. *Angew. Chemie Int. Ed., Wiley-VCH Verlag* **56**, 15654–15657.
- 98 Dörr, J. M., Koorengevel, M. C., Schäfer, M., Prokofyev, A. V., Scheidelaar, S., van der Crujisen, E. A. W. W., Dafforn, T. R., Baldus, M. and Killian, J. A. (2014) Detergent-free isolation, characterization, and functional reconstitution of a tetrameric K⁺ channel: The power of native nanodiscs. *Proc. Natl. Acad. Sci., National Academy of Sciences* **111**, 18607–18612.
- 99 Cuevas Arenas, R., Klingler, J., Vargas, C. and Keller, S. (2016) Influence of lipid bilayer properties on nanodisc formation mediated by styrene/maleic acid copolymers. *Nanoscale, Royal Society of Chemistry* **8**, 15016–15026.

- 100 Simon, K. S., Pollock, N. L. and Lee, S. C. (2018) Membrane protein nanoparticles: the shape of things to come. *Biochem. Soc. Trans.* **46**, 1495–1504.
- 101 Gulamhussein, A. A., Meah, D., Soja, D. D., Fenner, S., Saidani, Z., Akram, A., Lallie, S., Mathews, A., Painter, C., Liddar, M. K., et al. (2019) Examining the stability of membrane proteins within SMALPs. *Eur. Polym. J.* **112**, 120–125.
- 102 Oluwole, A. O., Danielczak, B., Meister, A., Babalola, J. O., Vargas, C. and Keller, S. (2017) Solubilization of Membrane Proteins into Functional Lipid-Bilayer Nanodiscs Using a Diisobutylene/Maleic Acid Copolymer. *Angew. Chemie - Int. Ed., Wiley-VCH Verlag* **56**, 1919–1924.
- 103 Knowles, T. J., Finka, R., Smith, C., Lin, Y.-P. P., Dafforn, T. and Overduin, M. (2009) Membrane proteins solubilized intact in lipid containing nanoparticles bounded by styrene maleic acid copolymer. *J. Am. Chem. Soc.* **131**, 7484–7485.
- 104 Broecker, J., Eger, B. T. and Ernst, O. P. (2017) Crystallogensis of Membrane Proteins Mediated by Polymer-Bounded Lipid Nanodiscs. *Structure, Cell Press* **25**, 384–392.
- 105 Parmar, M., Rawson, S., Scarff, C. A., Goldman, A., Dafforn, T. R., Muench, S. P. and Postis, V. L. G. (2018) Using a SMALP platform to determine a sub-nm single particle cryo-EM membrane protein structure. *Biochim. Biophys. Acta - Biomembr., Elsevier B.V.* **1860**, 378–383.
- 106 Smirnova, I. A., Sjöstrand, D., Li, F., Björck, M., Schäfer, J., Östbye, H., Högbom, M., von Ballmoos, C., Lander, G. C., Ädelroth, P., et al. (2016) Isolation of yeast complex IV in native lipid nanodiscs. *Biochim. Biophys. Acta - Biomembr., Elsevier B.V.* **1858**, 2984–2992.
- 107 Jamshad, M., Charlton, J., Lin, Y., Routledge, S. J., Bawa, Z., Knowles, T. J., Overduin, M., Dekker, N., Dafforn, T. R., Bill, R. M., et al. (2015) G-protein coupled receptor solubilization and purification for biophysical analysis and functional studies, in the total absence of

- detergent. *Biosci. Rep.* **35**, 1–10.
- 108 Rehan, S., Paavilainen, V. O. and Jaakola, V. P. (2017) Functional reconstitution of human equilibrative nucleoside transporter-1 into styrene maleic acid co-polymer lipid particles. *Biochim. Biophys. Acta - Biomembr.*, Elsevier B.V. **1859**, 1059–1065.
- 109 Swainsbury, D. J. K., Scheidelaar, S., Van Grondelle, R., Killian, J. A. and Jones, M. R. (2014) Bacterial reaction centers purified with styrene maleic acid copolymer retain native membrane functional properties and display enhanced stability. *Angew. Chemie - Int. Ed.* **53**, 11803–11807.
- 110 Morrison, K. A., Akram, A., Mathews, A., Khan, Z. A., Patel, J. H., Zhou, C., Hardy, D. J., Moore-Kelly, C., Patel, R., Odiba, V., et al. (2016) Membrane protein extraction and purification using styrene-maleic acid (SMA) copolymer: effect of variations in polymer structure. *Biochem. J.*, Portland Press Limited **473**, 4349–4360.
- 111 Gulati, S., Jamshad, M., Knowles, T. J., Morrison, K. A., Downing, R., Cant, N., Collins, R., Koenderink, J. B., Ford, R. C., Overduin, M., et al. (2014) Detergent-free purification of ABC (ATP-binding-cassette) transporters. *Biochem. J.* **461**, 269–278.
- 112 Pollock, N. L., Rai, M., Simon, K. S., Hesketh, S. J., Teo, A. C. K., Parmar, M., Sridhar, P., Collins, R., Lee, S. C., Stroud, Z. N., et al. (2019) SMA-PAGE: A new method to examine complexes of membrane proteins using SMALP nano-encapsulation and native gel electrophoresis. *Biochim. Biophys. Acta - Biomembr.*, Elsevier B.V. **1861**, 1437–1445.
- 113 Swainsbury, D. J. K., Scheidelaar, S., Foster, N., van Grondelle, R., Killian, J. A. and Jones, M. R. (2017) The effectiveness of styrene-maleic acid (SMA) copolymers for solubilisation of integral membrane proteins from SMA-accessible and SMA-resistant membranes. *Biochim. Biophys. Acta - Biomembr.*, Elsevier B.V. **1859**, 2133–2143.
- 114 Pollock, N. L., Lee, S. C., Patel, J. H., Gulamhussein, A. A. and Rothnie, A. J. (2018) Structure

- and function of membrane proteins encapsulated in a polymer-bound lipid bilayer. *Biochim. Biophys. Acta - Biomembr.*, Elsevier **1860**, 809–817.
- 115 Postis, V., Rawson, S., Mitchell, J. K., Lee, S. C., Parslow, R. A., Dafforn, T. R., Baldwin, S. A. and Muench, S. P. (2015) The use of SMALPs as a novel membrane protein scaffold for structure study by negative stain electron microscopy. *Biochim. Biophys. Acta - Biomembr.*, Elsevier B.V. **1848**, 496–501.
- 116 Logez, C., Damian, M., Legros, C., Dupré, C., Guéry, M., Mary, S., Wagner, R., M’Kadmi, C., Nosjean, O., Fould, B., et al. (2016) Detergent-free Isolation of Functional G Protein-Coupled Receptors into Nanometric Lipid Particles. *Biochemistry*, American Chemical Society **55**, 38–48.
- 117 Bersch, B., Dörr, J. M., Hessel, A., Killian, J. A. and Schanda, P. (2017) Proton-Detected Solid-State NMR Spectroscopy of a Zinc Diffusion Facilitator Protein in Native Nanodiscs. *Angew. Chemie Int. Ed.*, Wiley-Blackwell **56**, 2508–2512.
- 118 Georgila, K., Vyrla, D. and Drakos, E. (2019, August 1) Apolipoprotein A-I (ApoA-I), immunity, inflammation and cancer. *Cancers (Basel)*., MDPI AG.
- 119 Brouillette, C. G., Jones, J. L., Ng, T. C., Kercret, H., Chung, B. H. and Segrest, J. P. (1984) Structural Studies of Apolipoprotein A-I/Phosphatidylcholine Recombinants by High-Field Proton NMR, Nondenaturing Gradient Gel Electrophoresis, and Electron Microscopy. *Biochemistry*, American Chemical Society **23**, 359–367.
- 120 Denisov, I. G. and Sligar, S. G. (2017) Nanodiscs in Membrane Biochemistry and Biophysics. *Chem. Rev.*, American Chemical Society **117**, 4669–4713.
- 121 Bayburt, T. H., Grinkova, Y. V. and Sligar, S. G. (2002) Self-Assembly of Discoidal Phospholipid Bilayer Nanoparticles with Membrane Scaffold Proteins. *Nano Lett.*, American Chemical Society **2**, 853–856.

- 122 Denisov, I. G., Grinkova, Y. V., Lazarides, A. A. and Sligar, S. G. (2004) Directed Self-Assembly of Monodisperse Phospholipid Bilayer Nanodiscs with Controlled Size. *J. Am. Chem. Soc.*, American Chemical Society **126**, 3477–3487.
- 123 Tropea, J. E., Cherry, S. and Waugh, D. S. (2009) Expression and purification of soluble His6-tagged TEV protease. *Methods Mol. Biol.*, Humana Press **498**, 297–307.
- 124 Kapust, R. B. and Waugh, D. S. (1999) Escherichia coli maltose-binding protein is uncommonly effective at promoting the solubility of polypeptides to which it is fused. *Protein Sci.*, Wiley **8**, 1668–1674.
- 125 Baas, B. J., Denisov, I. G. and Sligar, S. G. (2004) Homotropic cooperativity of monomeric cytochrome P450 3A4 in a nanoscale native bilayer environment. In *Archives of Biochemistry and Biophysics*, pp 218–228, Academic Press.
- 126 Inagaki, S., Ghirlando, R. and Grisshammer, R. Biophysical characterization of membrane proteins in nanodiscs. *Methods*, pp 287–300, Academic Press Inc.
- 127 Erickson, H. P. (2009) Size and shape of protein molecules at the nanometer level determined by sedimentation, gel filtration, and electron microscopy. *Biol. Proced. Online*, BioMed Central.
- 128 Her, C., Filoti, D. I., McLean, M. A., Sligar, S. G., Alexander Ross, J. B., Steele, H. and Laue, T. M. (2016) The Charge Properties of Phospholipid Nanodiscs. *Biophys. J.*, Biophysical Society **111**, 989–998.
- 129 Inagaki, S. and Ghirlando, R. (2017) Nanodisc characterization by analytical ultracentrifugation. *Nanotechnol. Rev.*
- 130 Graziano, V., Miller, L. and Yang, L. (2018) Interpretation of solution scattering data from lipid nanodiscs: *J. Appl. Crystallogr.* **51**, 157–166.

- 131 Brüne, D., Andrade-Navarro, M. A. and Mier, P. (2018) Proteome-wide comparison between the amino acid composition of domains and linkers. *BMC Res. Notes*, BioMed Central Ltd. **11**, 117.
- 132 Marino, S. M. and Gladyshev, V. N. (2010) Cysteine Function Governs Its Conservation and Degeneration and Restricts Its Utilization on Protein Surfaces. *J. Mol. Biol.*, Academic Press **404**, 902–916.
- 133 Bak, D. W., Bechtel, T. J., Falco, J. A. and Weerapana, E. (2019, February 1) Cysteine reactivity across the subcellular universe. *Curr. Opin. Chem. Biol.*, Elsevier Ltd.
- 134 Pace, N. J. and Weerapana, E. (2013) Diverse functional roles of reactive cysteines. *ACS Chem. Biol.*, American Chemical Society **8**, 283–296.
- 135 Gunnoo, S. B. and Madder, A. (2016) Chemical Protein Modification through Cysteine. *ChemBioChem*, Wiley-VCH Verlag **17**, 529–553.
- 136 McKay, C. S. and Finn, M. G. (2014, September 18) Click chemistry in complex mixtures: Bioorthogonal bioconjugation. *Chem. Biol.*, Elsevier Ltd.
- 137 Hett, E. C., Xu, H., Geoghegan, K. F., Gopalsamy, A., Kyne, R. E., Menard, C. A., Narayanan, A., Parikh, M. D., Liu, S., Roberts, L., et al. (2015) Rational targeting of active-site tyrosine residues using sulfonyl fluoride probes. *ACS Chem. Biol.*, American Chemical Society **10**, 1094–1098.
- 138 Koniev, O. and Wagner, A. (2015) Developments and recent advancements in the field of endogenous amino acid selective bond forming reactions for bioconjugation. *Chem. Soc. Rev.*, Royal Society of Chemistry **44**, 5495–5551.
- 139 Jiang, X., Nie, Y. and Kaback, H. R. (2011) Site-directed alkylation studies with LacY provide evidence for the alternating access model of transport. *Biochemistry*, American Chemical Society **50**, 1634–1640.

- 140 Kaback, H. R., Dunten, R., Frillingos, S., Venkatesan, P., Kwaw, I., Zhang, W. and Ermolova, N. (2007) Site-directed alkylation and the alternating access model for LacY. *Proc. Natl. Acad. Sci. U. S. A., National Academy of Sciences* **104**, 491–494.
- 141 Nie, Y. and Kaback, H. R. (2010) Sugar binding induces the same global conformational change in purified LacY as in the native bacterial membrane. *Proc. Natl. Acad. Sci. U. S. A., National Academy of Sciences* **107**, 9903–9908.
- 142 Quick, M., Yano, H., Goldberg, N. R., Duan, L., Beuming, T., Shi, L., Weinstein, H. and Javitch, J. A. (2006) State-dependent conformations of the translocation pathway in the tyrosine transporter Tyt1, a novel neurotransmitter:sodium symporter from *Fusobacterium nucleatum*. *J. Biol. Chem., American Society for Biochemistry and Molecular Biology* **281**, 26444–26454.
- 143 Forrest, L. R., Zhang, Y. W., Jacobs, M. T., Gesmonde, J., Xie, L., Honig, B. H. and Rudnick, G. (2008) Mechanism for alternating access in neurotransmitter transporters. *Proc. Natl. Acad. Sci. U. S. A., National Academy of Sciences* **105**, 10338–10343.
- 144 Zhang, Y. W., Tavoulari, S., Sinning, S., Aleksandrova, A. A., Forrest, L. R. and Rudnick, G. (2018) Structural elements required for coupling ion and substrate transport in the neurotransmitter transporter homolog LeuT. *Proc. Natl. Acad. Sci. U. S. A., National Academy of Sciences* **115**, E8854–E8862.
- 145 Ziegler, C. (Biochemist). (2017) A Structure-Function Toolbox for Membrane Transporter and Channels.
- 146 Sampson, C. D. D., Stewart, M. J., Mindell, J. A. and Mulligan, C. (2020) Solvent accessibility changes in a na1-dependent C4-dicarboxylate transporter suggest differential substrate effects in a multistep mechanism. *J. Biol. Chem., American Society for Biochemistry and Molecular Biology Inc.* **295**, 18524–18538.

- 147 Yao, X. and Pajor, A. M. (2000) The transport properties of the human renal Na⁺-dicarboxylate cotransporter under voltage-clamp conditions. *Am. J. Physiol. - Ren. Physiol.*, American Physiological Society **279**.
- 148 Pajor, A. M. and Randolph, K. M. (2005) Conformationally sensitive residues in extracellular loop 5 of the Na⁺/dicarboxylate co-transporter. *J. Biol. Chem.*, American Society for Biochemistry and Molecular Biology **280**, 18728–18735.
- 149 Pajor, A. M. (2001) Conformationally Sensitive Residues in Transmembrane Domain 9 of the Na⁺/dicarboxylate Co-transporter. *J. Biol. Chem.*, American Society for Biochemistry and Molecular Biology **276**, 29961–29968.
- 150 Hänel, I., Jensen, S., Wunnicke, D. and Slotboom, D. J. (2015) Low affinity and slow Na⁺ binding precedes high affinity aspartate binding in the secondary-active transporter GltPh. *J. Biol. Chem.* **290**, 15962–15972.
- 151 Joshi, A. D. and Pajor, A. M. (2009) Identification of conformationally sensitive amino acids in the Na⁺/dicarboxylate symporter (SdcS). *Biochemistry*, American Chemical Society **48**, 3017–3024.
- 152 Erkens, G. B., Hänel, I., Goudsmits, J. M. H., Slotboom, D. J. and Van Oijen, A. M. (2013) Unsynchronised subunit motion in single trimeric sodium-coupled aspartate transporters. *Nature*, Nature Publishing Group **502**, 119–123.
- 153 Focke, P. J., Moenne-Loccoz, P. and Larsson, H. P. (2011) Opposite Movement of the External Gate of a Glutamate Transporter Homolog upon Binding Cotransported Sodium Compared with Substrate. *J. Neurosci.*, Society for Neuroscience **31**, 6255–6262.
- 154 Boudker, O., Ryan, R. M., Yernool, D., Shimamoto, K. and Gouaux, E. (2007) Coupling substrate and ion binding to extracellular gate of a sodium-dependent aspartate transporter. *Nature*, Nature Publishing Group **445**, 387–393.

- 155 Cimperman, P., Barauskiene, L., Jachimovičiute, S., Jachno, J., Torresan, J., Michailoviene, V., Matuliene, J., Sereikaite, J., Bumelis, V. and Matulis, D. (2008) A quantitative model of thermal stabilization and destabilization of proteins by ligands. *Biophys. J., Elsevier* **95**, 3222–3231.
- 156 Pantoliano, M. W., Petrella, E. C., Kwasnoski, J. D., Lobanov, V. S., Myslik, J., Graf, E., Asel, E., Springer, B. A., Lane, P. and Salemme, F. R. (2001) High-Density Miniaturized Thermal Shift Assays as a General Strategy for Drug Discovery. *J. Biomol. Screen.* **6**, 429–440.
- 157 Cummings, M. D., Farnum, M. A. and Nelen, M. I. (2006) Universal screening methods and applications of ThermoFluor®. *J. Biomol. Screen.* **11**, 854–863.
- 158 Yeh, A. P., McMillan, A. and Stowell, M. H. B. (2006) Rapid and simple protein-stability screens: Application to membrane proteins. *Acta Crystallogr. Sect. D Biol. Crystallogr.* **62**, 451–457.
- 159 Eilers, M., Patel, A. B., Liu, W. and Smith, S. O. (2002) Comparison of helix interactions in membrane and soluble α -bundle proteins. *Biophys. J., Biophysical Society* **82**, 2720–2736.
- 160 Alexandrov, A. I., Mileni, M., Chien, E. Y. T., Hanson, M. A. and Stevens, R. C. (2008) Microscale Fluorescent Thermal Stability Assay for Membrane Proteins. *Structure* **16**, 351–359.
- 161 Majd, H., King, M. S., Palmer, S. M., Smith, A. C., Elbourne, L. D., Paulsen, I. T., Sharples, D., Henderson, P. J. and Kunji, E. R. R. S. (2018) Screening of candidate substrates and coupling ions of transporters by thermostability shift assays. *Elife, Cold Spring Harbor Laboratory* **7**, 367805.
- 162 Bai, N., Roder, H., Dickson, A. and Karanicolas, J. (2019) Isothermal Analysis of ThermoFluor Data can readily provide Quantitative Binding Affinities. *Sci. Rep., Springer US* **9**, 1–15.
- 163 Gopal, E., Babu, E., Ramachandran, S., Bhutia, Y. D., Prasad, P. D. and Ganapathy, V. (2015)

- Species-Specific Influence of Lithium on the Activity of SLC13A5 (NaCT): Lithium-Induced Activation Is Specific for the Transporter in Primates s. J. Pharmacol. Exp. Ther. J Pharmacol Exp Ther **353**, 17–26.
- 164 Schlessinger, A., Sun, N. N., Colas, C. and Pajor, A. M. (2014) Determinants of substrate and cation transport in the human Na⁺/dicarboxylate cotransporter NaDC3. J. Biol. Chem., American Society for Biochemistry and Molecular Biology Inc. **289**, 16998–17008.
- 165 Pajor, A. M., Sun, N. N. and Leung, A. (2013) Functional characterization of SdcF from *Bacillus licheniformis*, a homolog of the SLC13 Na⁺/dicarboxylate transporters. J. Membr. Biol. **246**, 705–715.
- 166 Oshiro, N. and Pajor, A. M. (2005) Functional characterization of high-affinity Na⁺ /dicarboxylate cotransporter found in *Xenopus laevis* kidney and heart. Am. J. Physiol. Physiol., American Physiological Society **289**, C1159–C1168.
- 167 Colas, C., Schlessinger, A. and Pajor, A. M. (2017) Mapping Functionally Important Residues in the Na⁺/Dicarboxylate Cotransporter, NaDC1. Biochemistry, American Chemical Society **56**, 4432–4441.
- 168 Pajor, A. M. and Sun, N. N. (2010) Single nucleotide polymorphisms in the human Na⁺-dicarboxylate cotransporter affect transport activity and protein expression. Am. J. Physiol. - Ren. Physiol., American Physiological Society **299**, F704.
- 169 Pajor, A. M., Hirayama, B. A. and Loo, D. D. F. (1998) Sodium and lithium interactions with the Na⁺/dicarboxylate cotransporter. J. Biol. Chem., American Society for Biochemistry and Molecular Biology **273**, 18923–18929.
- 170 Wang, Z., Ye, C., Zhang, X. and Wei, Y. (2015) Cysteine residue is not essential for CPM protein thermal-stability assay. Anal. Bioanal. Chem., Springer Verlag **407**, 3683–3691.
- 171 Mancusso, R., Karpowich, N. K., Czyzewski, B. K. and Wang, D. N. (2011) Simple screening

- method for improving membrane protein thermostability. *Methods* **55**, 324–329.
- 172 Hattori, M., Hibbs, R. E. and Gouaux, E. (2012) A fluorescence-detection size-exclusion chromatography-based thermostability assay for membrane protein precrystallization screening. *Structure* **20**, 1293–1299.
- 173 Sonoda, Y., Newstead, S., Hu, N. J., Alguet, Y., Nji, E., Beis, K., Yashiro, S., Lee, C., Leung, J., Cameron, A. D., et al. (2011) Benchmarking membrane protein detergent stability for improving throughput of high-resolution x-ray structures. *Structure* **19**, 17–25.
- 174 Militello, V., Vetri, V. and Leone, M. (2003) Conformational changes involved in thermal aggregation processes of bovine serum albumin. *Biophys. Chem., Elsevier* **105**, 133–141.
- 175 Milo, R., Jorgensen, P., Moran, U., Weber, G. and Springer, M. (2009) BioNumbers The database of key numbers in molecular and cell biology. *Nucleic Acids Res.* **38**.
- 176 Coincon, M., Uzdavinyis, P., Nji, E., Dotson, D. L., Winkelmann, I., Abdul-Hussein, S., Cameron, A. D., Beckstein, O. and Drew, D. (2016) Crystal structures reveal the molecular basis of ion translocation in sodium/proton antiporters. *Nat. Struct. Mol. Biol., Nature Publishing Group* **23**, 248–255.
- 177 Akyuz, N., Georgieva, E. R., Zhou, Z., Stolzenberg, S., Cuendet, M. A., Khelashvili, G., Altman, R. B., Terry, D. S., Freed, J. H., Weinstein, H., et al. (2015) Transport domain unlocking sets the uptake rate of an aspartate transporter. *Nature, Nature Publishing Group* **518**, 68–73.
- 178 Duhr, S. and Braun, D. (2006) Why molecules move along a temperature gradient. *Proc. Natl. Acad. Sci. U. S. A., National Academy of Sciences* **103**, 19678–19682.
- 179 Baaske, P., Wienken, C. J., Reineck, P., Duhr, S. and Braun, D. (2010) Optical thermophoresis for quantifying the buffer dependence of aptamer binding. *Angew. Chemie - Int. Ed., John Wiley & Sons, Ltd* **49**, 2238–2241.

- 180 Jerabek-Willemsen, M., Wienken, C. J., Braun, D., Baaske, P. and Duhr, S. (2011, August 1) Molecular interaction studies using microscale thermophoresis. *Assay Drug Dev. Technol.*, Mary Ann Liebert, Inc. 140 Huguenot Street, 3rd Floor New Rochelle, NY 10801 USA .
- 181 Scheuermann, T. H., Padrick, S. B., Gardner, K. H. and Brautigam, C. A. (2016) On the acquisition and analysis of microscale thermophoresis data. *Anal. Biochem.*, Academic Press Inc. **496**, 79–93.
- 182 Lippok, S., Seidel, S. A. I., Duhr, S., Uhland, K., Holthoff, H. P., Jenne, D. and Braun, D. (2012) Direct detection of antibody concentration and affinity in human serum using microscale thermophoresis. *Anal. Chem.*, American Chemical Society **84**, 3523–3530.
- 183 Linke, P., Amaning, K., Maschberger, M., Vallee, F., Steier, V., Baaske, P., Duhr, S., Breitsprecher, D. and Rak, A. (2016) An Automated Microscale Thermophoresis Screening Approach for Fragment-Based Lead Discovery. *J. Biomol. Screen.*, SAGE Publications Inc. **21**, 414–21.
- 184 Entzian, C. and Schubert, T. (2016) Studying small molecule-aptamer interactions using MicroScale Thermophoresis (MST). *Methods*, Academic Press Inc. **97**, 27–34.
- 185 Mao, Y., Yu, L., Yang, R., Qu, L. B. and Harrington, P. D. B. (2015) A novel method for the study of molecular interaction by using microscale thermophoresis. *Talanta*, Elsevier B.V. **132**, 894–901.
- 186 Moon, M. H., Hilimire, T. A., Sanders, A. M. and Schneekloth, J. S. (2018) Measuring RNA-Ligand Interactions with Microscale Thermophoresis. *Biochemistry*, American Chemical Society **57**, 4638–4643.
- 187 Liu, Y., Liu, N., Ma, X., Li, X., Ma, J., Li, Y., Zhou, Z. and Gao, Z. (2015) Highly specific detection of thrombin using an aptamer-based suspension array and the interaction analysis via microscale thermophoresis. *Analyst*, Royal Society of Chemistry **140**, 2762–2770.

- 188 Zhang, W., Duhr, S., Baaske, P. and Laue, E. (2014) Microscale thermophoresis for the assessment of nuclear protein-binding affinities. In *Methods in Molecular Biology*, pp 269–276, Humana Press Inc.
- 189 Ryan, R. M., Compton, E. L. R. and Mindell, J. A. (2009) Functional characterization of a Na⁺-dependent aspartate transporter from *Pyrococcus horikoshii*. *J. Biol. Chem.*, American Society for Biochemistry and Molecular Biology **284**, 17540–8.
- 190 Mulligan, C. and Mindell, J. A. (2013) Mechanism of transport modulation by an extracellular loop in an Archaeal Excitatory Amino Acid Transporter (EAAT) Homolog. *J. Biol. Chem.*, JBC Papers in Press **288**, 35266–35276.
- 191 Schulze, S., Köster, S., Geldmacher, U., Terwisscha Van Scheltinga, A. C. and Kühlbrandt, W. (2010) Structural basis of Na⁺-independent and cooperative substrate/product antiport in CaiT. *Nature*, Nature Publishing Group **467**, 233–236.
- 192 Yernool, D., Boudker, O., Jin, Y. and Gouaux, E. (2004, October 14) Structure of a glutamate transporter homologue from *Pyrococcus horikoshii*. *Nature*, Nature Publishing Group.
- 193 Stolzenberg, S., Khelashvili, G. and Weinstein, H. (2012) Structural intermediates in a model of the substrate translocation path of the bacterial glutamate transporter homologue GltPh. *J. Phys. Chem. B* **116**, 5372–5383.
- 194 Reyes, N., Oh, S. and Boudker, O. (2013) Binding thermodynamics of a glutamate transporter homolog. *Nat. Struct. Mol. Biol.*, NIH Public Access **20**, 634–640.
- 195 McIlwain, B. C., Vandenberg, R. J. and Ryan, R. M. (2016) Characterization of the Inward- and Outward-Facing Substrate Binding Sites of the Prokaryotic Aspartate Transporter, GltPh. *Biochemistry*, American Chemical Society **55**, 6801–6810.
- 196 Wöhlert, D., Grötzinger, M. J., Kühlbrandt, W. and Yildiz, Ö. (2015) Mechanism of Na⁽⁺⁾-dependent citrate transport from the structure of an asymmetrical CitS dimer. *Elife* **4**,

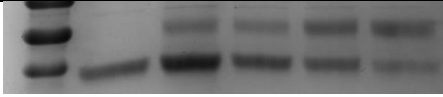
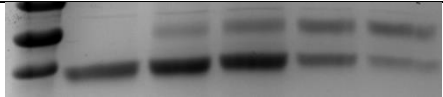
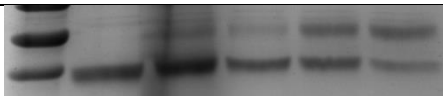
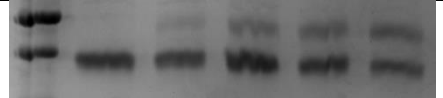
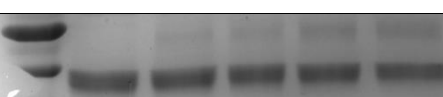

e09375.

- 197 Heidelberg, J. F., Elsen, J. A., Nelson, W. C., Clayton, R. A., Gwinn, M. L., Dodson, R. J., Haft, D. H., Hickey, E. K., Peterson, J. D., Umayam, L., et al. (2000) DNA sequence of both chromosomes of the cholera pathogen *Vibrio cholerae*. *Nature*, Nature Publishing Group **406**, 477–483.

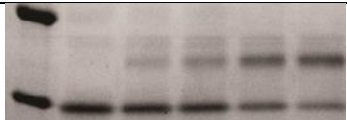
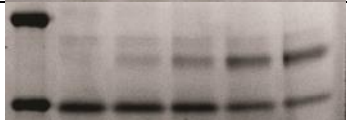
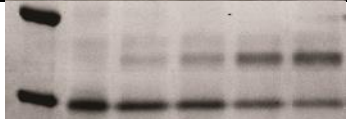

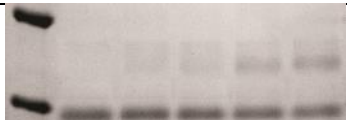

7 APPENDICES

7.1 Appendix 1 – Raw PEGylation Data

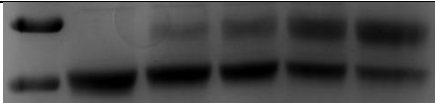


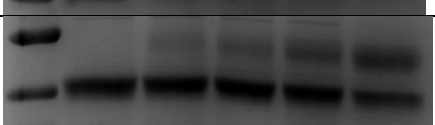
#157-R-1 157C Succinate Range, 150 mM Sodium

Succinate (μM)	M157C
0	
1	
10	
100	
500	
1000	

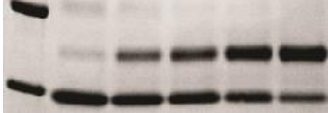
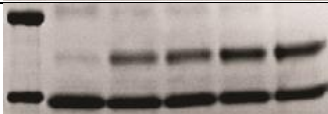
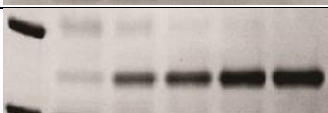
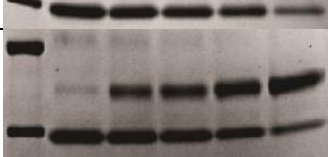
#157-R-2-Chris

Succinate (μM)	M157C
0	
1	
10	
100	
500	
1000	

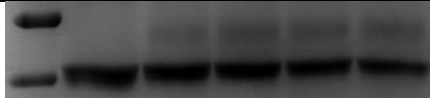



#157-E-1

Succinate (mM)	Na (mM)	K (mM)	
0	150	0	
1000	150	0	
0	0	150	
1000	0	150	

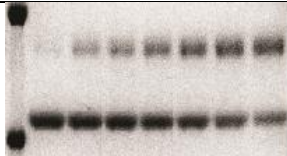
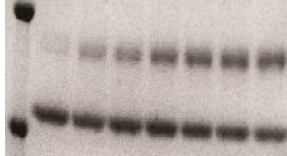

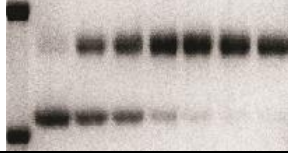
#157-E-2-Chris

Succinate (mM)	Na (mM)	K (mM)	
0	150	0	
1000	150	0	
0	0	150	
1000	0	150	

#120-E-1

Succinate (mM)	Na (mM)	K (mM)	
0	150	0	
1000	150	0	
0	0	150	
1000	0	150	

#120-E-2-Chris

Succinate (mM)	Na (mM)	K (mM)	
0	150	0	
1000	150	0	
0	0	150	
1000	0	150	

#154-E-1 – n.b. the gel highlighted in red represents an anomalous run, and is not analysed

Succinate (mM)	Na (mM)	K (mM)	
0	150	0	
1000	150	0	
0	0	150	
1000	0	150	

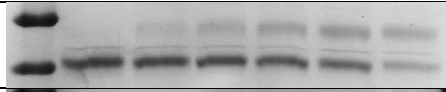
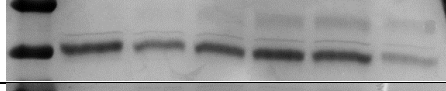
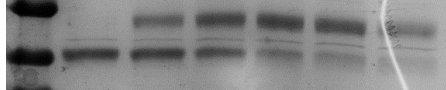
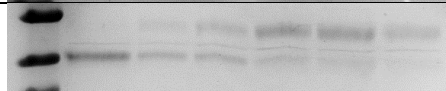
#154-E-2

Succinate (mM)	Na (mM)	K (mM)	
0	150	0	
1000	150	0	
0	0	150	
1000	0	150	

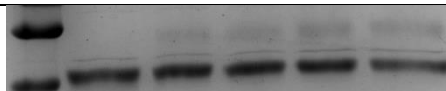
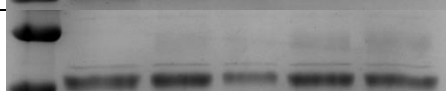
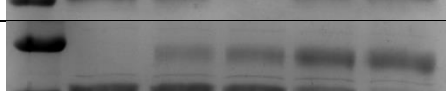

#154-E-3

Succinate (mM)	Na (mM)	K (mM)	
0	150	0	
1000	150	0	
0	0	150	
1000	0	150	

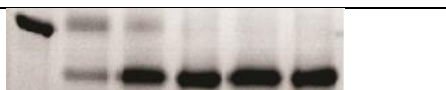

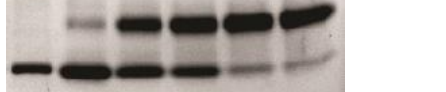
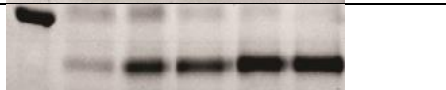
#215-E-1

Succinate (mM)	Na (mM)	K (mM)	
0	150	0	
1000	150	0	
0	0	150	
1000	0	150	

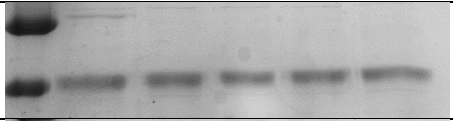
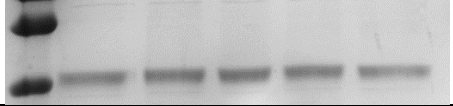
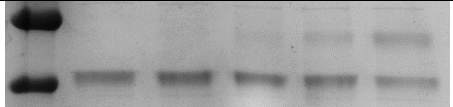

#215-E-2

Succinate (mM)	Na (mM)	K (mM)	
0	150	0	
1000	150	0	
0	0	150	
1000	0	150	

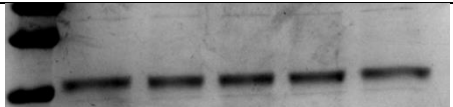
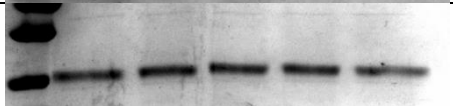
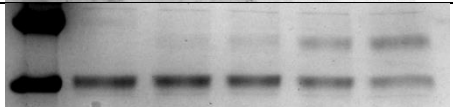
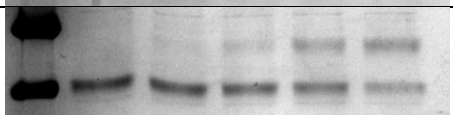
#215-E-3-Chris

Succinate (mM)	Na (mM)	K (mM)	
0	150	0	
1000	150	0	
0	0	150	
1000	0	150	

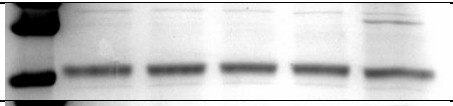
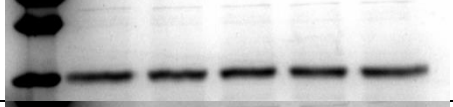
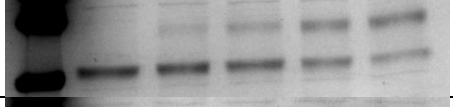
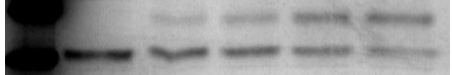
#381-E-1

Succinate (mM)	Na (mM)	K (mM)	
0	150	0	
1000	150	0	
0	0	150	
1000	0	150	

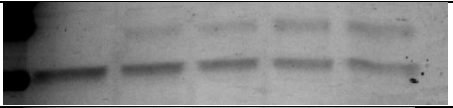
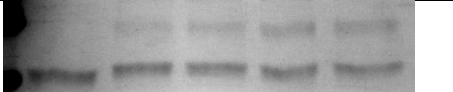
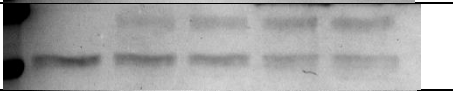

#381-E-2

Succinate (mM)	Na (mM)	K (mM)	
0	150	0	
1000	150	0	
0	0	150	
1000	0	150	

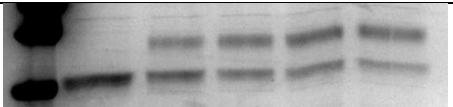
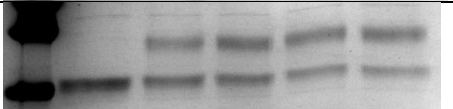
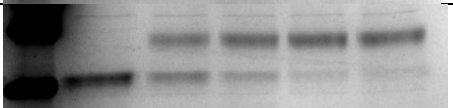
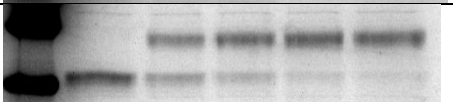
#381-E-3

Succinate (mM)	Na (mM)	K (mM)	
0	150	0	
1000	150	0	
0	0	150	
1000	0	150	

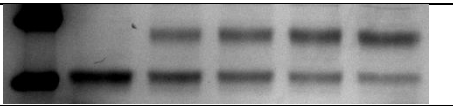
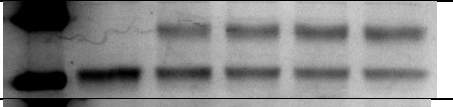

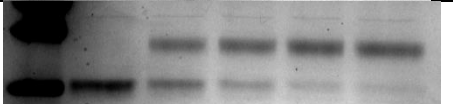
#384-E-1

Succinate (mM)	Na (mM)	K (mM)	
0	150	0	
1000	150	0	
0	0	150	
1000	0	150	

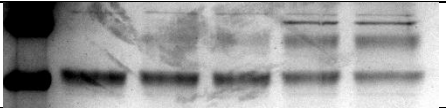
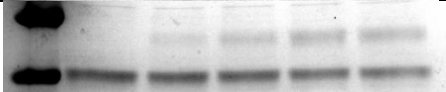
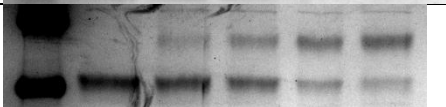
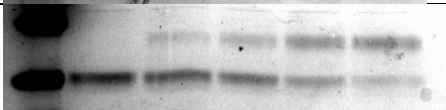
#384-E-2

Succinate (mM)	Na (mM)	K (mM)	
0	150	0	
1000	150	0	
0	0	150	
1000	0	150	

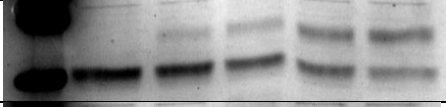
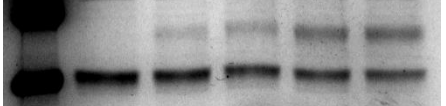
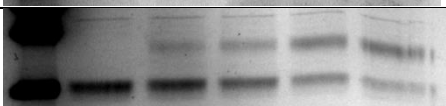
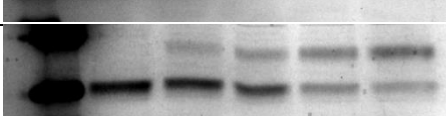
#384-E-3

Succinate (mM)	Na (mM)	K (mM)	
0	150	0	
1000	150	0	
0	0	150	
1000	0	150	

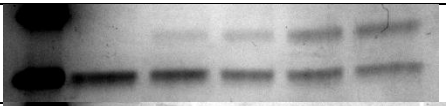
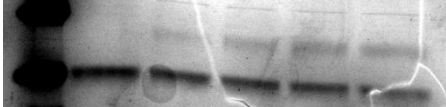
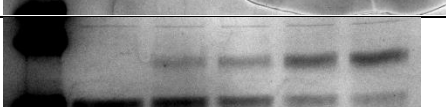
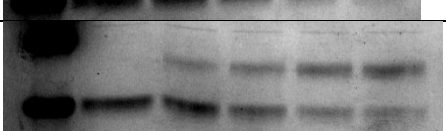
#388-E-1

Succinate (mM)	Na (mM)	K (mM)	
0	150	0	
1000	150	0	
0	0	150	
1000	0	150	

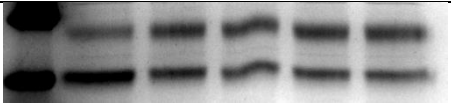
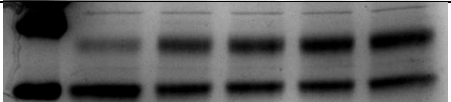
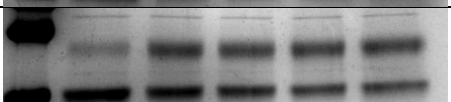
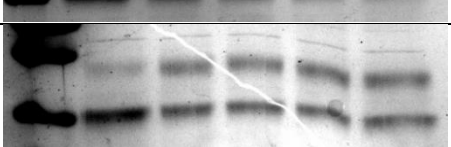
#388-E-2

Succinate (mM)	Na (mM)	K (mM)	
0	150	0	
1000	150	0	
0	0	150	
1000	0	150	

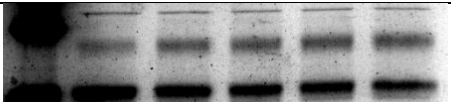
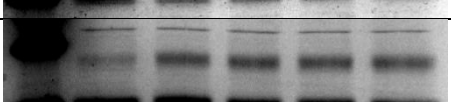
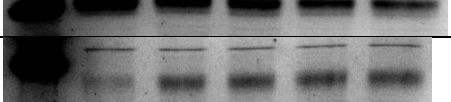
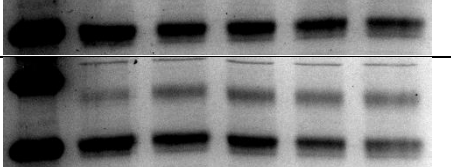
#388-E-3

Succinate (mM)	Na (mM)	K (mM)	
0	150	0	
1000	150	0	
0	0	150	
1000	0	150	

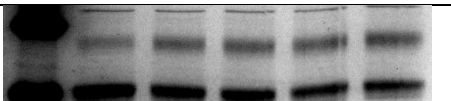
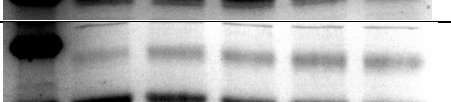
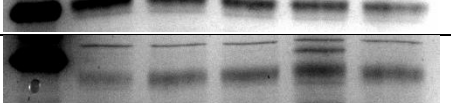
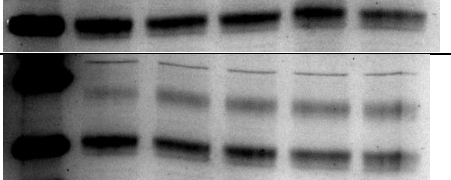
#42-E-1

Succinate (mM)	Na (mM)	K (mM)	
0	150	0	
1000	150	0	
0	0	150	
1000	0	150	

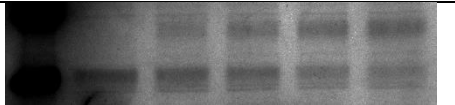
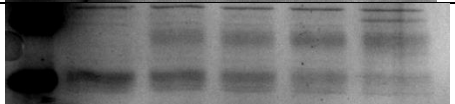
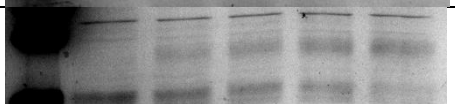
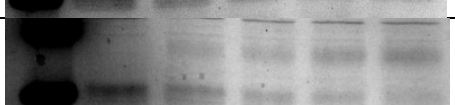
#42-E-2

Succinate (mM)	Na (mM)	K (mM)	
0	150	0	
1000	150	0	
0	0	150	
1000	0	150	

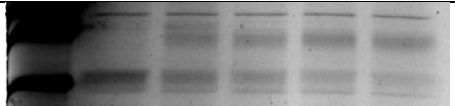
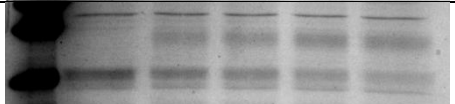
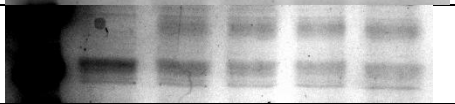
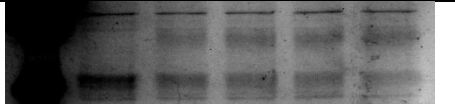
#42-E-3

Succinate (mM)	Na (mM)	K (mM)	
0	150	0	
1000	150	0	
0	0	150	
1000	0	150	

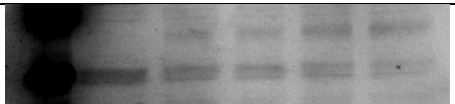



#383-E-1

Succinate (mM)	Na (mM)	K (mM)	
0	150	0	
1000	150	0	
0	0	150	
1000	0	150	

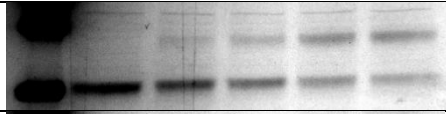
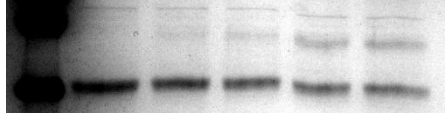
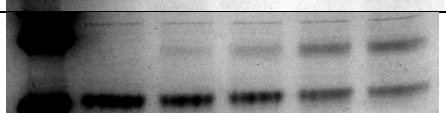
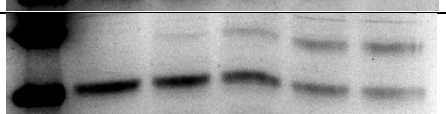
#383-E-2

Succinate (mM)	Na (mM)	K (mM)	
0	150	0	
1000	150	0	
0	0	150	
1000	0	150	

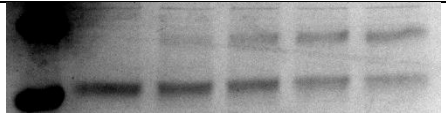
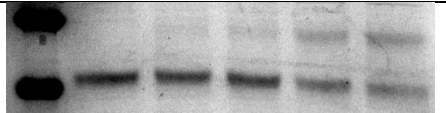
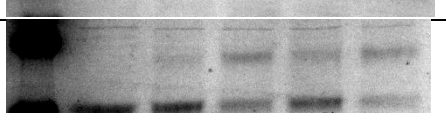
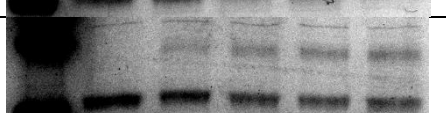
#383-E-3

Succinate (mM)	Na (mM)	K (mM)	
0	150	0	
1000	150	0	
0	0	150	
1000	0	150	

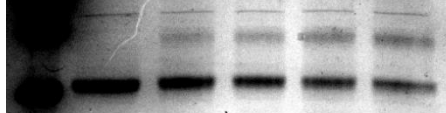
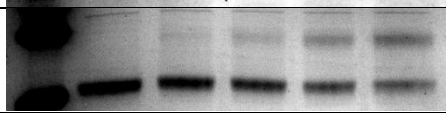
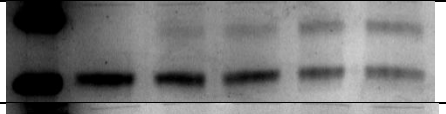
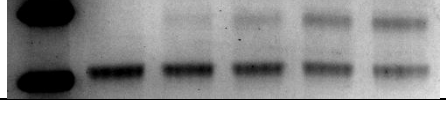
#430-E-1

Succinate (mM)	Na (mM)	K (mM)	
0	150	0	
1000	150	0	
0	0	150	
1000	0	150	

#430-E-2

Succinate (mM)	Na (mM)	K (mM)	
0	150	0	
1000	150	0	
0	0	150	
1000	0	150	

#430-E-3

Succinate (mM)	Na (mM)	K (mM)	
0	150	0	
1000	150	0	
0	0	150	
1000	0	150	

#79-E-1-H

Succinate (mM)	Na (mM)	K (mM)	
0	150	0	
1000	150	0	
0	0	150	
1000	0	150	

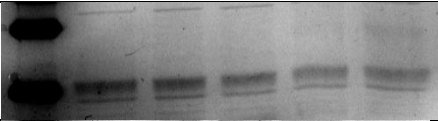
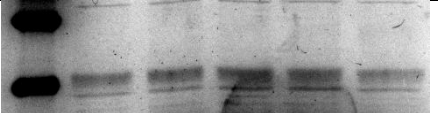
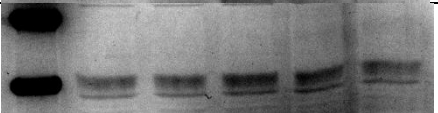
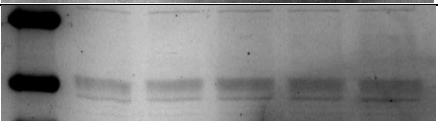
#79-E-2-H

Succinate (mM)	Na (mM)	K (mM)	
0	150	0	
1000	150	0	
0	0	150	
1000	0	150	

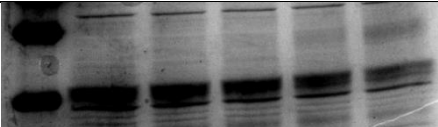

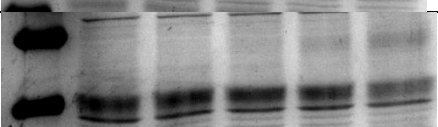
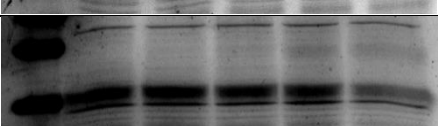
#79-E-3-H

Succinate (mM)	Na (mM)	K (mM)	
0	150	0	
1000	150	0	
0	0	150	
1000	0	150	

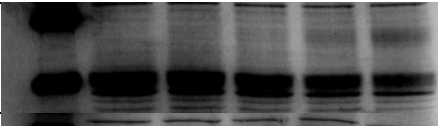
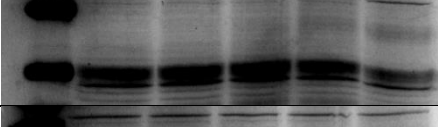
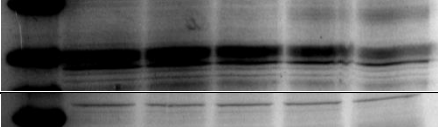
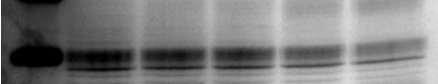
#148-E-1-H

Succinate (mM)	Na (mM)	K (mM)	
0	150	0	
1000	150	0	
0	0	150	
1000	0	150	

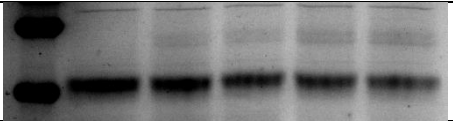
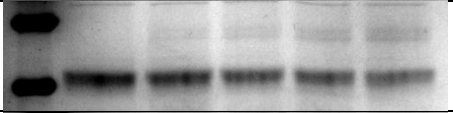
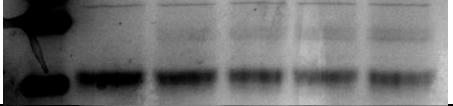
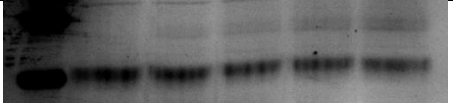
#148-E-2-H

Succinate (mM)	Na (mM)	K (mM)	
0	150	0	
1000	150	0	
0	0	150	
1000	0	150	

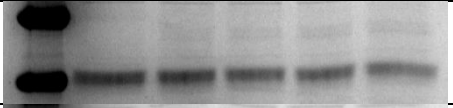
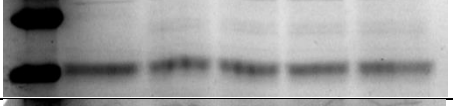
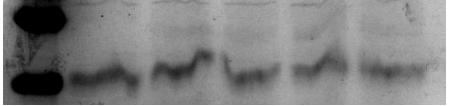
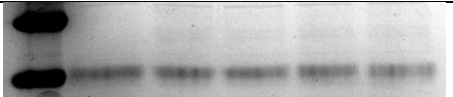
#148-E-3-H

Succinate (mM)	Na (mM)	K (mM)	
0	150	0	
1000	150	0	
0	0	150	
1000	0	150	

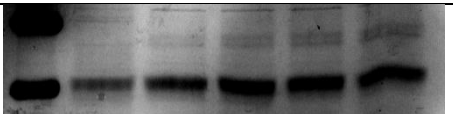
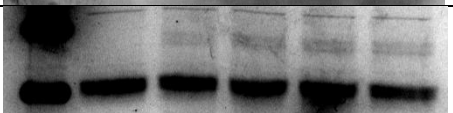
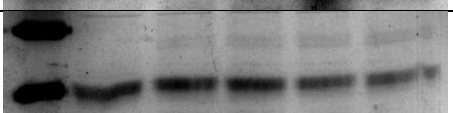
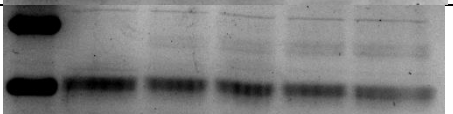
#178-E-1-H

Succinate (mM)	Na (mM)	K (mM)	
0	150	0	
1000	150	0	
0	0	150	
1000	0	150	

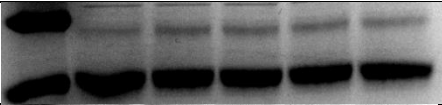
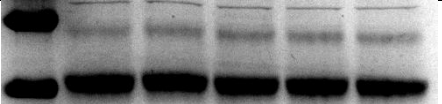
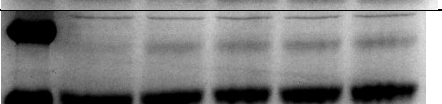
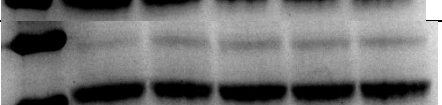
#178-E-2-H

Succinate (mM)	Na (mM)	K (mM)	
0	150	0	
1000	150	0	
0	0	150	
1000	0	150	

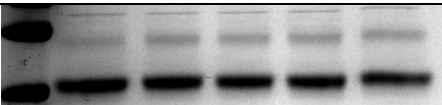
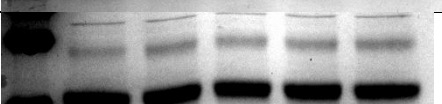
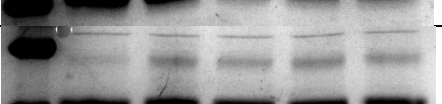
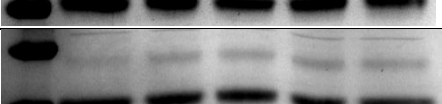
#178-E-3-H

Succinate (mM)	Na (mM)	K (mM)	
0	150	0	
1000	150	0	
0	0	150	
1000	0	150	

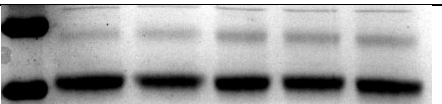
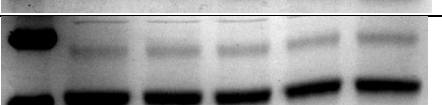

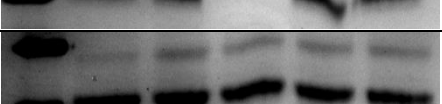
#436-E-1-H

Succinate (mM)	Na (mM)	K (mM)	
0	150	0	
1000	150	0	
0	0	150	
1000	0	150	

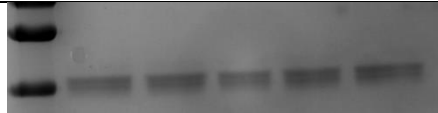


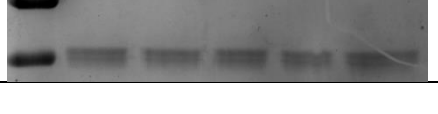
#436-E-2-H

Succinate (mM)	Na (mM)	K (mM)	
0	150	0	
1000	150	0	
0	0	150	
1000	0	150	

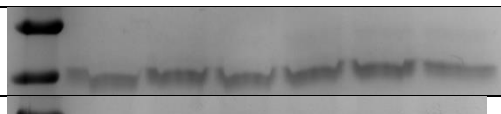
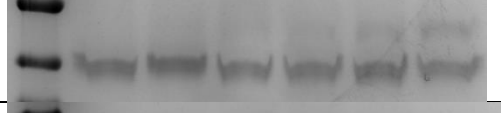

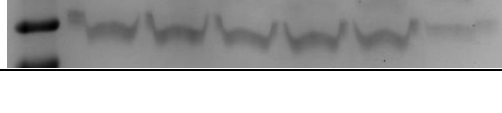
#436-E-3-H

Succinate (mM)	Na (mM)	K (mM)	
0	150	0	
1000	150	0	
0	0	150	
1000	0	150	



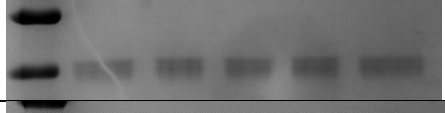
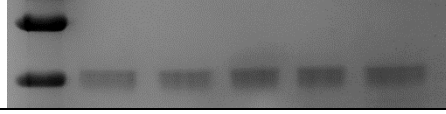
#SMA-120-0.4

Succinate (mM)	Na (mM)	K (mM)	
0	150	0	
1000	150	0	
0	0	150	
1000	0	150	

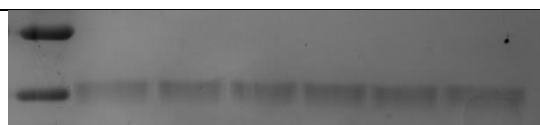
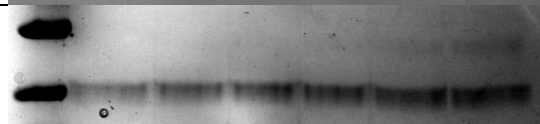
#SMA-120-5/8

mPEG5K (mM)	Na (mM)	K (mM)	
5	150	0	
5		150	
8	150	0	
8	0	150	


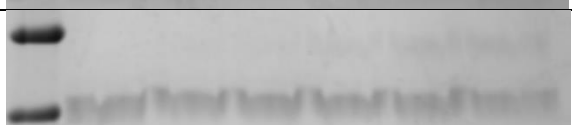
#SMA-157-E

Succinate (mM)	Na (mM)	K (mM)	
0	150	0	
1000	150	0	
0	0	150	
1000	0	150	

#SMA-157-PEG

mPEG5K (mM)	
0.4	
2	

#SMA-157-5

Succinate (mM)	Na (mM)	K (mM)	
0	150	0	
1000	150	0	

7.2 Appendix 2 – R script used for the fitting of GFP-TS data

R script for the fitting of sigmoidal dose response curves to GFP-TS data through the least squares method, allowing accurate estimation of melting temperature. The below script graphically displays fittings as they are calculated and outputs final values at the end, showing calculated fitting values, melting temperatures, average melt temperature, and melt temperature standard deviation.


```

SupProAll <- read.csv("SupProAll.csv") #Open file for 3 replicates
NowSupPro <- SupProAll #Set all replicates as working dataset

fitmodel <- nls(y ~ b + (a - b)/(1 + ((tm^s)/(x^s))),
start=list(a=0.4,b=0.9,s=3,tm=60), data = SupProAll, trace = TRUE)
#Fit data to sigmoidal equation using arbitrary start values
a <- coef(fitmodel)[1] #Extract end value
b <- coef(fitmodel)[2] #Extract start value
s <- coef(fitmodel)[3] #Extract slope coefficient
tm <- coef(fitmodel)[4] #Extract melt temperature
rtm <- round(tm, 1) #Define value for rounded melting temperature

plot(SupProAll, xlab="Temp (°C)", ylab="Relative Fluorescence")
#Plot dataset
c <- seq(0,80,0.1)
lines(c,b + (a - b)/(1 + ((tm^s)/(c^s)))) #Plot calculated model
abline(v= tm, lty=2) #Mark melting temperature
text(tm+10, 0.9, labels = "Tm =")
text(tm+14.1, 0.9, labels = rtm)
text(tm+17, 0.9, labels = "°C") #Annotate melting temperature

CatWhole <- c("tm together","a","b","s","tm")
Values <- c(tm,a,b,s,tm)
outputWhole <- data.frame(CatWhole, Values)
output1 #Save and output calculated Tm and fitting values

SupPro1 <- read.csv("SupPro1.csv")
SupPro2 <- read.csv("SupPro2.csv")
SupPro3 <- read.csv("SupPro3.csv") #Open individual replicates

```

```

NowSupPro <- SupPro1 #Set first replicate as working dataset

fitmodel <- nls(y ~ b + (a - b)/(1 + ((tm^s)/(x^s))),
start=list(a=0.2,b=0.9,s=3,tm=70), data = NowSupPro, trace = TRUE)
a <- coef(fitmodel)[1]
b <- coef(fitmodel)[2]
s <- coef(fitmodel)[3]
tm <- coef(fitmodel)[4]
rtm <- round(tm, 1) #Fit model and extract values as before

plot(NowSupPro, xlab="Temp (°C)", ylab="Relitive Flourescence",
ylim = c(0,1))
c <- seq(0,80,0.1)
lines(c,b + (a - b)/(1 + ((tm^s)/(c^s))))
abline(v= tm, lty=2)
text(tm+10, 0.9, labels = "Tm =")
text(tm+14.1, 0.9, labels = rtm)
text(tm+17, 0.9, labels = "°C") #Plot and annotate as before
tm1 <- tm #Save melting temperature for initial replicate
tm1 #Display melting temperature for initial replicate

Cat1 <- c("tm together","a","b","s","tm")
Values <- c(tm,a,b,s,tm)
output1 <- data.frame(Cat1, Values)
output1 #Save and output calculated Tm and fitting values

NowSupPro <- SupPro2 #Set second replicate as working dataset

fitmodel <- nls(y ~ b + (a - b)/(1 + ((tm^s)/(x^s))),
start=list(a=0.4,b=0.9,s=3,tm=60), data = NowSupPro, trace = TRUE)
a <- coef(fitmodel)[1]
b <- coef(fitmodel)[2]
s <- coef(fitmodel)[3]
tm <- coef(fitmodel)[4]
rtm <- round(tm, 1) #Fit model and extract values as before

```

```

plot(NowSupPro, xlab="Temp (°C)", ylab="Relitive Flourescence",
ylim = c(0,1))
c <- seq(0,80,0.1)
lines(c,b + (a - b)/(1 + ((tm^s)/(c^s))))
abline(v= tm, lty=2)
text(tm+10, 0.9, labels = "Tm =")
text(tm+14.1, 0.9, labels = rtm)
text(tm+17, 0.9, labels = "°C") #Plot and annotate as before
tm2 <- tm #Save melting temperature for second replicate
tm2 #Display melting temperature for second replicate

Cat2 <- c("tm together","a","b","s","tm")
Values <- c(tm,a,b,s,tm)
output2 <- data.frame(Cat2, Values)
output2 #Save and output calculated Tm and fitting values

NowSupPro <- SupPro3 #Set third replicate as working dataset

fitmodel <- nls(y ~ b + (a - b)/(1 + ((tm^s)/(x^s))),
start=list(a=0.4,b=0.9,s=3,tm=50), data = NowSupPro, trace = TRUE)
a <- coef(fitmodel)[1]
b <- coef(fitmodel)[2]
s <- coef(fitmodel)[3]
tm <- coef(fitmodel)[4]
rtm <- round(tm, 1) #Fit model and extract values as before

```

```

plot(NowSupPro, xlab="Temp (°C)", ylab="Relitive Flourescence",
ylim = c(0,1))
c <- seq(0,80,0.1)
lines(c,b + (a - b)/(1 + ((tm^s)/(c^s))))
abline(v= tm, lty=2)
text(tm+10, 0.9, labels = "Tm =")
text(tm+14.1, 0.9, labels = rtm)
text(tm+17, 0.9, labels = "°C") #Plot and annotate as before
tm3 <- tm #Save melting temperature for third replicate
tm3 #Display melting temperature for third replicate

Cat3 <- c("tm together","a","b","s","tm")
Values <- c(tm,a,b,s,tm)
output3 <- data.frame(Cat3, Values)
output3 #Save and output calculated Tm and fitting values

NowSupPro <- SupProAll #Set all replicates as working dataset

fitmodel <- nls(y ~ b + (a - b)/(1 + ((tm^s)/(x^s))),
start=list(a=0.4,b=0.9,s=3,tm=60), data = NowSupPro, trace = TRUE)
a <- coef(fitmodel)[1]
b <- coef(fitmodel)[2]
s <- coef(fitmodel)[3]
tm <- coef(fitmodel)[4]
rtm <- round(tm, 1) #Fit model and extract values as before

plot(NowSupPro, xlab="Temp (°C)", ylab="Relitive Flourescence",
ylim = c(0,1))
c <- seq(0,80,0.1)
lines(c,b + (a - b)/(1 + ((tm^s)/(c^s)))) #Plot and annotate all

```

```

tmA <- mean(c(tm1,tm2,tm3))
tmA
rtmA <- round(tmA, 1)
tmSD <- sd(c(tm1,tm2,tm3))
tmSD
rtmSD <- round(tmSD, 1) #Calculate average melt temp, with std dev

abline(v= tmA, lty=2) #Mark average melt temp on graph
text(tm+2, 0.9, labels= paste("Tm =",rtmA,"+/-",rtmC)) #Show values
catagories <-c("tm1","tm2","tm3","Average","SD","a","b","s","tm")
Values <- c(tm1,tm2,tm3,tmA,tmSD,a,b,s,tm)
output <- data.frame(catagories, Values)

outputWhole
output1
output2
output3 #Output results of individual fittings
output #Output summary of melting temperatures and fit values

```